Electronic Thesis and Dissertation Repository

6-17-2021 9:30 AM

Cationic Boron Formazanate Complexes

Benjamin D. Katzman, *The University of Western Ontario*

Supervisor: Gilroy, Joseph B., *The University of Western Ontario*
A thesis submitted in partial fulfillment of the requirements for the Master of Science degree in Chemistry
© Benjamin D. Katzman 2021

Follow this and additional works at: https://ir.lib.uwo.ca/etd

Part of the Chemistry Commons

Abstract

This thesis describes the synthesis and characterization of various three- and four-coordinate cationic and dicationic boron complexes supported by formazanate ($[R^1$-N-N=C(Ph)-N=N-$R^5]^-$ ligands. The first chapter provides a review of various three-coordinate and cationic boron complexes and related applications. Chapter two examines the effect of several variations (*i.e.,* charge, coordination number and boron-bound substituents) on the electronic structure of cationic boron formazanate complexes. Absorption spectroscopy measurements reveal that the wavelengths, intensities, and type of the first electronic transitions in cationic boron complexes can be modulated by these structural variations. Chapter three exploits the electron deficiency of a borenium cation supported by a N_2O^{2-} formazanate ligand. Excellent Lewis acidity is demonstrated using the Gutmann-Beckett method. Further, a drastic decrease in the LUMO energy is observed upon introduction of cationic boron, compared to related neutral complexes. Together, this work demonstrates the utility of these cationic boron formazanates in the design of molecular materials.

Keywords

Main-group chemistry, borenium cations, three-coordinate boron, cationic boron, dicationic boron, formazanate ligands, absorption and emission spectroscopy, redox chemistry, Lewis acidity, cyclic voltammetry, electronic structure modulation.

Summary for Lay Audience

Designing boron-containing molecules can be challenging, especially if the boron atom has fewer than four bonds with other atoms. This violates a fundamental bonding principle in chemistry, the octet rule, which requires atoms to make a net total of four bonds, containing a total of eight electrons. Boron is often used in its three-coordinate mode (three bonds) as it is in a state of electron deficiency, meaning it can act as an acceptor of electrons. This property is exploited in the design of materials such as organic light emitting diodes (OLEDs), which can be found in your LED TV, providing a vivid and attractive display. The electron acceptor property can also be used in sensing, where the electron deficient boron atom can make a bond with anions (*e.g.,* fluoride ions), which can be detected using different spectroscopic techniques. This work presents a set of *cationic* ('positively charged') boron complexes, supported by a nitrogen-rich ligand (formazanate). Imposing a positive charge increases the electron deficiency and allows for a wider use of applications with an increased performance. The challenge when using cationic boron is their propensity to bind with water and other electron donating molecules because of the electron deficiency. Cationic boron can be difficult to successfully make in a lab, but is typically done by removing a weakly bound halogen (*i.e.,* fluorine or chlorine) from boron. The research performed in this thesis examines how changing the chemical environment around boron will affect its properties. We also examine a strongly electron deficient boron complex (very reactive) and gain a qualitative and quantitative understanding of its properties. The work provides a platform and guidelines for the design of electron deficient cationic boron complexes with desired properties for use in material applications.

Co-Authorship Statement

The work described in this thesis contains contributions from the author as well as co-workers Dr. Ryan R. Maar, Ms. Daniela Capello, Dr. Paul B. Boyle, Prof. Viktor N. Staroverov, and Prof. Joe B. Gilroy. The contributions of each are described below.

Chapter 1 was written by the author and edited by Prof. Gilroy.

Chapter 2 described the synthesis of cationic boron formazanate dyes and modulation of their electronic structure. The synthesis and characterization were carried out predominantly by the author. Dr. Maar initially synthesized **2.8**, **2.9** and **2.10**$^+$, which were later resynthesized by the author. Dr. Maar and Dr. Boyle collected and refined all X-ray crystallographic data. Prof. Staroverov performed all computational analyses. The chapter was written by the author and edited by Prof. Gilroy.

Chapter 3 describes a new series of highly Lewis acidic, fluorescent, and redox-active borenium cations. The author conducted the synthesis and characterization of all compounds. Ms. Daniela Capello assisted with cyclic voltammetry experiments. Dr. Maar assisted with reaction methodology and participated in thoughtful discussions. Dr. Boyle collected and refined all X-ray crystallographic data. Prof. Staroverov performed all computational analyses. The chapter was written by the author and edited by Prof. Gilroy.

Chapter 4 was written by the author and edited by Prof. Gilroy.

Acknowledgments

There are so many who deserve thanks for helping get me to where I am today. First, I want to thank my supervisor Prof. Joe Gilroy. I have had a long journey as a member of the Gilroy group – first as a volunteer, then 4491 student and finally a graduate student. I am incredibly lucky to have worked with such an intelligent and fantastic supervisor. Joe has always been supportive of me and has helped me improve both as a chemist and a professional. It was a privilege to work with you.

Of course, I must give thanks to the current members of the Gilroy group. Jas, Daniela, Francis, Mike, and Alex have made coming to the lab every day full of fun and laughter. I will miss the daily lab shenanigans with all of you. The long days, nights and weekends would not have been the same without such a great group. I must give a personal thank you to former group member Dr. Ryan Maar. Ryan has been my mentor since my first day in the Gilroy lab, and has taught me essentially all that I know about synthetic chemistry. Despite his departure from the lab, he has always remained eager to help. I was very lucky to work with such a talented chemist.

Thank you to the faculty of the chemistry department for an amazing undergraduate and graduate education. In addition, I want to thank the incredible support staff – Mat, Aneta, Paul, Doug and Haidy, who were always incredibly helpful to me while conducting my projects.

I would like to thank my examining committee, Prof. Workentin, Prof. Corrigan, and Prof. Zhang for taking the time to read and review my thesis.

Finally, I want to thank my closest friends and family for all their support over the years. Thank you to my parents, Jeff and Davida as well as my sister Rebecca for their non-stop help and encouragement. To the boys of 19 fek, I appreciate all of you listening to me talk chemistry non-stop and occasionally pretending to care. If you thought me complaining about the brutality of analytical labs was annoying, you should hear about cationic boron. Thank you to Lauren for always being supportive despite my long days/nights and generally ridiculous schedule. You were always there for me no matter the time, day, or place. I truly appreciate all the love you all have given me over the years.

Table of Contents

List of Tables

List of Figures

List of Schemes

List of Appendices

List of Abbreviations

°	Degrees
°C	Degrees Celsius
Å	Angstrom
a	Crystallographic Lattice Constant – Unit Cell Length
Ar	Aryl
ATR	Attenuated Total Reflectance
a.u.	Arbitrary Units
b	Crystallographic Lattice Constant – Unit Cell Length
BF	Boron-fluoride
c	Crystallographic Lattice Constant – Unit Cell Length
ca.	Circa
cm	Centimeter
cm^{-1}	Wavenumber
CV	Cyclic Voltammogram
d	Doublet
dd	Doublet of Doublets
D-A	Donor-Acceptor
DABCO	1,4-diazabicyclo[2.2.2]octane
Dipp	2,6-diisopropylphenyl
DFT	Density Functional Theory
DMAP	4-dimethylaminopyridine

E_g	Energy of Band Gap
E_{LUMO}	Energy of LUMO
E_{HOMO}	Energy of HOMO
E_{ox1}	First oxidation potential
E_{red1}	First reduction potential
E_{red2}	Second reduction potential
EI	Electron-impact Ionization
ESI	Electrospray Ionization
Et	Ethyl
Et_3PO	Triethylphosphine oxide
equiv.	Equivalent
Fc	Ferrocene
Fc^+	Ferrocenium
FLP	Frustrated Lewis Pair
FT-IR	Fourier-transform Infrared
g	Gram
GB	Gutmann-Beckett
GOF	Goodness of Fit
h	Hours
HOMO	Highest Occupied Molecular Orbital

IR	Infrared
ISC	Intersystem Crossing
J	NMR Coupling Constant
LA	Lewis Acid
LB	Lewis Base
LDA	Lithium diisopropylamide
LUMO	Lowest Unoccupied Molecular Orbital
m	Multiplet
M	Molar
max	Maximum
Me	Methyl
Mes	Mesityl
mg	Milligram
MHz	Megahertz
min	Minutes
mL	Milliliter
mM	Millimolar
mol	Mole
mmol	Millimole
M.p.	Melting Point

NHC	N-heterocyclic Carbene
nm	Nanometer
NMR	Nuclear Magnetic Resonance
OTf	Triflate
Ph	Phenyl
ppm	Parts Per Million
p-tol	*Para*-tolyl
q	Quartet
R_1	Confidence Factor Observed Data
R_f	Retention Factor
s	Singlet
t	Triplet
T	Temperature
TDDFT	Time-dependent Density Functional Theory
tBu	*tert*-butyl
THF	Tetrahydrofuran
UV-vis	Ultraviolet-visible
V	Volts
V	Volume
Z	Formula Unit

α	Crystallographic Lattice Constant – Unit Cell Angle
β	Crystallographic Lattice Constant – Unit Cell Angle
γ	Crystallographic Lattice Constant – Unit Cell Angle
λ_{max}	Wavelength of Maximum Absorbance
λ_{em}	Wavelength of Maximum Emission
υ_{ST}	Stokes Shift
Φ_F	Fluorescence Quantum Yield
δ	Chemical Shift

Chapter 1

1 Introduction

Main-group complexes containing boron have found application due to their unique structure, bonding and reactivity that they offer.[1] The inherent electron deficiency of low-coordinate boron, often paired with π-conjugated organic frameworks, has resulted in a vast library of complexes that can be incorporated into optoelectronic devices and materials. Boron chemists in the 21st century are constantly searching for methods to design new complexes, with a focus on either increasing electron deficiency or extending π-conjugation to create superior materials with attractive electronic properties. A challenging, but unique strategy is to incorporate cationic boron atoms into organic scaffolds to achieve these goals. This approach has transformed the modern approach and has challenged researchers to devise methods to isolate and stabilize cationic boron complexes for desired applications. Recent advances are highlighted below.

1.1 Three-Coordinate Boron

One of the most recognizable features of the periodic table is the "zigzag" staircase that spans several p block (main-group) elements. Several elements intersect with this staircase, and they typically contain characteristics of both metals and non-metals. The position of an element on the periodic table will typically provide insight into its reactivity, stability, and bonding in complexes. At the top of this staircase lies boron, a group 13 element that has only three valence electrons. Boron is one of the few first row elements that can violate the octet rule and form stable complexes with only three (or fewer) bonds. The octet rule states that atoms must have eight electrons in their valence shell, but it is possible for boron to only have six electrons.[2] Under these low valent conditions, boron has an empty p orbital that can typically participate in π-conjugation when paired with aromatic frameworks (Figure 1.1) and can act as a strong Lewis acid or electron acceptor under certain conditions.[3, 4] These distinctive features pave the way for design and exploration of boron-containing complexes that can be used in catalysis, sensory technology or optoelectronic devices.
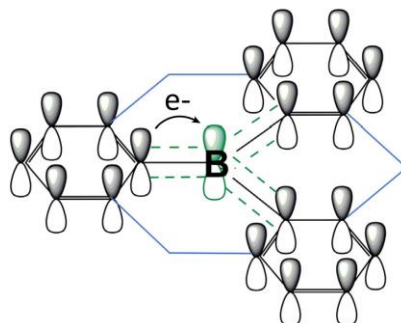
Figure 1.1. Aromatic π-conjugation utilizing boron's empty p orbital. Image reproduced from Ref. 3 with permission.

Boron is often combined with organic fragments to modulate the energies of the highest occupied molecular orbital (HOMO) and lowest unoccupied molecular orbital (LUMO) and to design materials with lowered band gaps. The empty p orbital can overlap with adjacent π systems or heteroatoms, which can lead to a strong π-acceptor effect as a result of p-π* conjugation.[5, 6] The p-π* interaction in a conjugated organic system often results in reduction of the LUMO energy, as the molecular orbital can be extended over large parts (if not all) of the molecule. This phenomenon leads to smaller HOMO-LUMO gaps, bathochromic shifts in absorption maxima and a less negative redox potential.[4, 7-9] This effect was exemplified by the Yamaguchi group, who compared several anthracene substituted boron centered complexes. Upon increasing the number of aromatic units, more effective π-conjugation results due to the capability of boron to participate in the π system. There is a gradual reduction in the energy of absorption maxima from **1.1** to **1.2** to **1.3**, and a corresponding increase in reduction potential of these systems (Table 1). This increase in π-conjugation lowers the energy level of the LUMO, and the continuous addition of aromatic units continues to narrow the HOMO-LUMO gap.[10] Further studies have been performed to confirm these properties computationally.[11, 12]

1.1   **1.2**   **1.3**
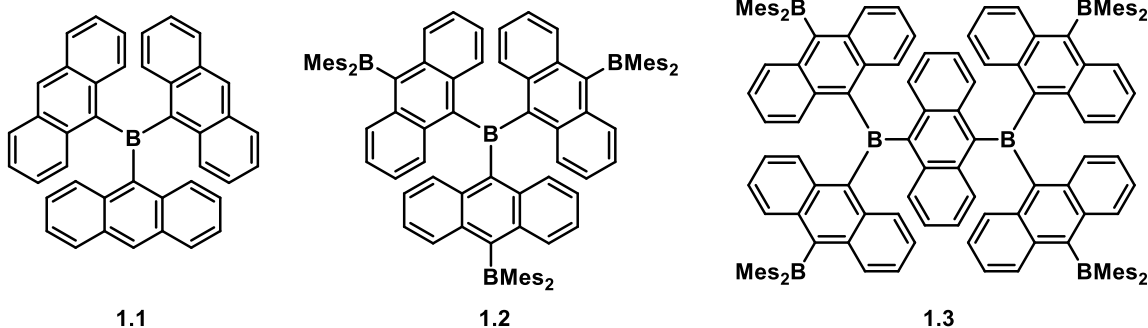
Table 1.1. Spectroscopic and electrochemical data for **1.1**, **1.2** and **1.3**.

Compound	λ_{max} (nm)	E_{red1} (V)
1.1	470	−1.86
1.2	524	−1.71
1.3	535	−1.56

Three-coordinate boron finds much application in catalytic reactions and transformations,[13, 14] with a progressively increasing reach in Frustrated Lewis Pair (FLP) chemistry. FLP's were first reported by the Stephan group in 2006,[15] and have revolutionized the chemical approach to small molecule activation.[16] FLPs are compounds containing, or a mixture of a Lewis acid and base that cannot form an adduct due to steric hindrance.[17] The first example reported by the Stephan group was a unimolecular FLP, which could reversibly activate and split dihydrogen (Scheme 1.1). **1.4** contains a Lewis acidic boron and a Lewis basic phosphorous atom, both surrounded by sterically demanding ligands. Using an FLP for this transformation bypasses the common use of toxic and expensive transition metal catalysts and replaces the process with a more safe and efficient method.[18]
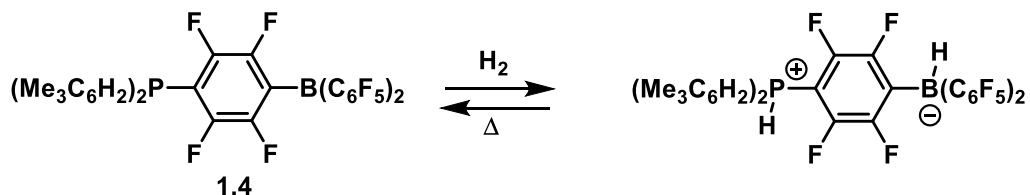
Scheme 1.1. Reversible activation of dihydrogen using a FLP.[15]

The scope of boron FLP chemistry has expanded drastically over the last decade, including many examples of small molecule activation,[19, 20] including CO,[21] CO_2,[22] and NO_2[23] without the use of transition metals.

Stimuli-responsive materials are frequently engineered, and take advantage of boron's empty p orbital as well.[24] Careful creation of complexes can allow for a system to respond to a variety of stimuli that will cause boron to exist in its *displaced* (three-coordinate) or *bound* (four-coordinate) state (Scheme 1.2). The *displaced* and *bound* state are expected to have drastically different electronic structures, and in turn, different properties. The stimuli that promote the fluxionality could be light, heat, pH or a ligand, which may or may not be tethered to the framework.[25]
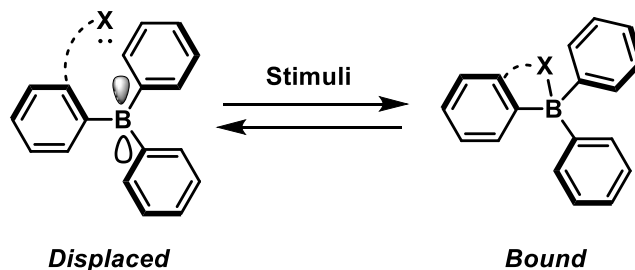
Scheme 1.2. Stimuli-promoted fluxionality between three-coordinate "displaced" state and four-coordinate "bound state."

The Murata group reported a thermochromic responsive sensor, exhibiting differing coordination modes depending on the temperature of the solution (Figure 1.2).[26] The molecular scaffold was designed such that the Lewis basic nitrogen atom is in close proximity to form an adduct with the Lewis acidic boron atom under certain conditions. This fluxionality was monitored via UV-vis spectroscopy, and different electronic structures and corresponding properties were expected due to the difference between a three- and four- coordinate boron center. At lower temperature (−40 °C), coordination was not observed (**1.5**), and the solution appeared blue. At higher temperatures (100 °C), an adduct is formed, giving a brown-yellow solution (**1.6**).

Figure 1.2. Temperature dependent fluxionality of B-N bonding. Image insets reproduced from Ref. 26 with permission.

Boron chemistry has expanded beyond small molecules, and into the realm of π-conjugated organic polymers. Three-coordinate boranes are an attractive addition to conjugated polymers as the boron atoms can act as excellent electron acceptors. In a polymer, if multiple boron centers are separated by a π-conjugated system, there should be an extension of conjugation via boron's p orbital (Figure 1.3a).[8, 27-29] The Jäkle group has contributed greatly to this field of study, and recently described an example utilizing a novel conjugated donor-acceptor (D-A) conjugated polymer.[30] Electron deficient borane units were combined with electron rich dithienogermane donor moieties to afford π-conjugated polymers (**1.7**). The polymer D-A interaction was verified by significant bathochromic shifts in optical spectra compared to the monomer. The system was solvatochromic, suggesting intramolecular charge transfer in the excited state, consequently resulting in emission maxima >650 nm in polar solvents. This D-A polymeric design lays a foundation for use of such systems and related species for fluorescence imaging and optoelectronic applications (*e.g.*, photovoltaic or non-linear optical materials).
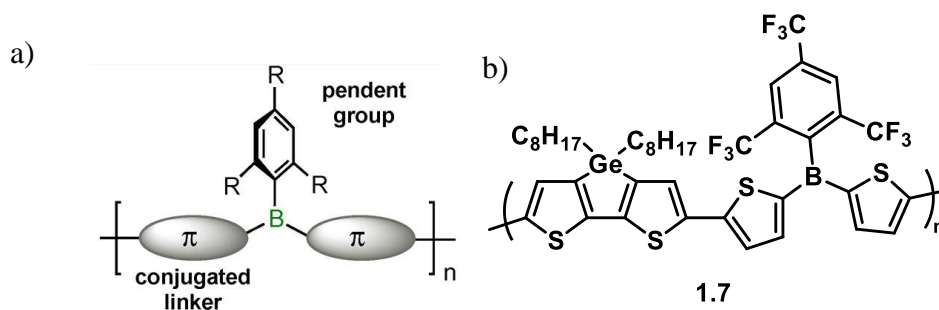
Figure 1.3. a) π-conjugation with multiple boron atoms utilizing aromatic spacers. Image reproduced from Ref. 29 with permission. b) D-A polymer with potential use in optoelectronic devices.[30]

Organic light emitting diode (OLED) displays for visual technology are competing with the traditional liquid crystal displays (LCD) that have long dominated the market. Unlike LCDs, OLEDs are emissive, offering advantages such as true black state, creating a more vivid contrast, offering a more realistic depiction to the viewer. Figure 1.4a is an illustration of a non-boron containing OLED display[31, 32] Triarylboranes are frequently incorporated into OLED devices due to their attractive photophysical (strong fluorescence) and electron accepting properties.[33, 34] The Wang group synthesized **1.8**, a D-A organoborane capable of acting both as a blue emitter and for electron transport, and as such is termed a bifunctional molecule.[35] Solvatochromism, combined with evidence that the HOMO is dominated by the orbitals surrounding the amino group, while the LUMO is dominated by the π system surrounding boron's empty p orbital suggest charge transfer character upon excitation.[36] **1.8** boasts an emission quantum yield of up to 0.95 in solution and 0.31 in the solid state. Devices were fabricated, and electron transport capabilities of **1.8** were demonstrated, and the reasoning is hypothesized to be a result of the three-coordinate electron acceptor unit combined with an electron rich amino center to transport the holes.
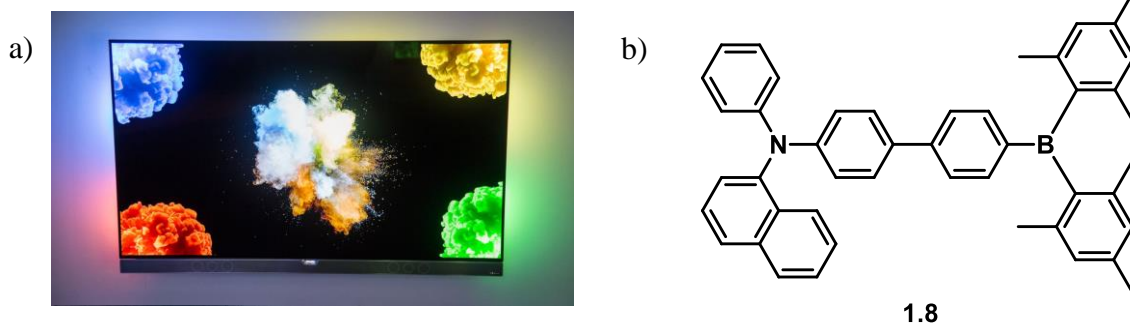
Figure 1.4. a) General representation of an OLED display.[37] b) D-A organoborane with potential use in OLED technology.[35]

1.2 Lewis Acidity of Boron Complexes

Amongst the most fundamental concepts in chemistry comes the various theories of chemical bonding. Intramolecular bonding is divided into three broad types including ionic, covalent, and metallic. Although they largely simplify the interactions, these models provide the basis of how researchers understand atomic bonding. A frequently encountered type of covalent bond in main-group chemistry is the coordinate covalent (or dative) bond. This interaction is fundamental to the Lewis theory of bonding,[38] which models the bond between a Lewis acid (LA) and a Lewis base (LB). A LA is the acceptor, and contains an empty orbital capable of accepting an electron pair. A LB is the donor, and contains a non-bonding pair of electrons capable of donating into an acceptor orbital of another species. Together, a LA-LB adduct can be formed. Ammonia borane is the simplest B-N bonding interaction, and is a fundamental example of such adduct (Figure 1.5). By convention, a dative interaction is drawn with the arrow tail beginning at the donor atom, extending the tip until the acceptor atom.
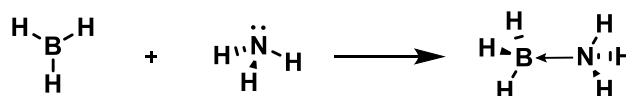
Figure 1.5. Dative bond between a LA (BH_3) and LB (NH_3).

LAs vary greatly in acceptor strength, thus there are several methods used to quantitatively assess Lewis acidity. A majority of experimental methods rely on the reaction of the LA with a LB probe, and use NMR spectroscopic chemical shifts to evaluate the acidity. The most common experimental method is the Gutmann-Beckett (GB) test.[39, 40] The LA is combined with triethylphosphine oxide (Et_3PO) and a $^{31}P\{^1H\}$ NMR spectrum is then obtained (often in CD_2Cl_2) (Scheme 1.3).
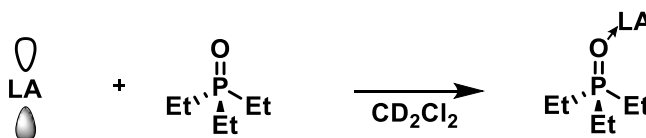
Scheme 1.3. Reaction between LA and triethylphosphine oxide to determine $^{31}P\{^1H\}$ NMR shift.

The $^{31}P\{^1H\}$ NMR chemical shift of the adduct is used to compute an "Acceptor Number" (AN), where a larger acceptor number represents greater Lewis acidity. The AN can be calculated using equation (**1**). It is derived by arbitrarily setting the AN of hexanes with Et_3PO to be 0, and the Et_3PO-$SbCl_5$ adduct set to 100.

$$AN = 2.21(\delta_{adduct} - 41) \tag{1}$$

Many researchers use these values as an aid to predict reactivity, and to give clues on methods to enhance the Lewis acidity. A compilation of several common boron Lewis acids and their known acceptor numbers are shown in Figure 1.6.[41]
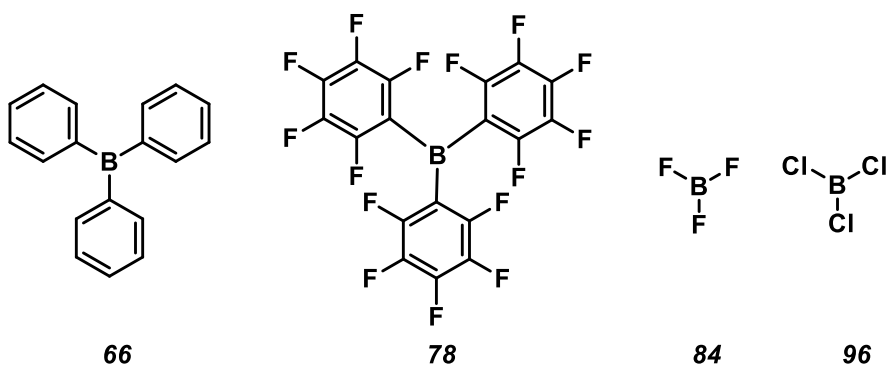
Figure 1.6. Several common Lewis acids. Italicized values represent the GB Acceptor Number.

Another method to experimentally probe Lewis acidity is Childs' method.[42] In this experiment, the Lewis acid analyte is combined with crotonaldehyde. The Lewis acidity is derived using ^1H NMR spectroscopy, and the chemical shift of H^3 upon binding of the LA to the carbonyl oxygen is measured (Scheme 1.4). The chemical shift difference in relation to the naked crotonaldehyde is then determined. The convention is to compare this value to that of boron tribromide (BBr_3) and determine the "Relative acidity," where BBr_3 is arbitrarily set to 1.0. The GB method is often preferred over Childs' method for boron chemistry due to the stronger Lewis basicity of triethylphosphine oxide towards boranes, and consequently Childs' method is used less in practice.[43]
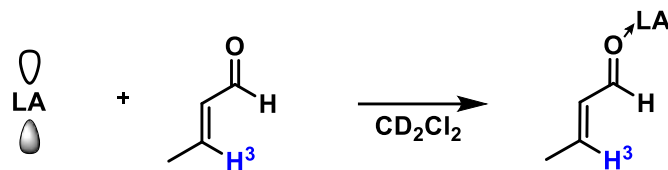
Scheme 1.4. Reaction between LA and crotonaldehyde to determine H^3 ^{1}H NMR shift**.**

A method recently developed by the Caputo and Baumgartner groups uses fluorescence as a probe for quantification.[44, 45] The researchers designed a scaffold that mimics the GB phosphine oxide donor (**1.9**), and relies on the generation of fluorescent Lewis acid-base adducts (Scheme 1.5). A method using fluorescence is desirable due to low detection limits and the potential to visually observe large differences in luminescence, corresponding to differences in Lewis acidity. Coordination of a LA should further polarize the P=O bond, increasing electronegativity of oxygen and decreasing the LUMO energy. This electronic structure change gives rise to a bathochromic ('red') shift in fluorescence of the adducts.
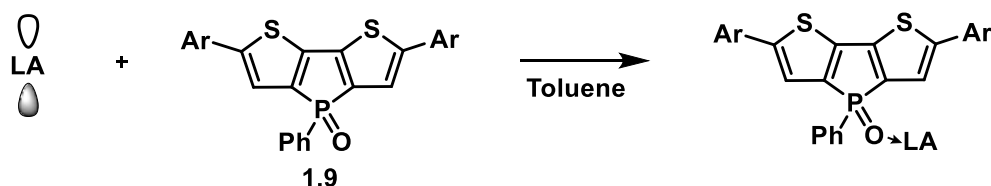
Scheme 1.5. Reaction between LA and phosphine oxide to determine shift in emission wavelength.

The researchers generated an experimental LA scale, using arbitrary Lewis Acid Units (LAU) to quantify the differences between the measured Lewis acids. A systematic evaluation of some of the most common LAs was performed, and the results for neutral, three-coordinate boranes are provided in Figure 1.7.
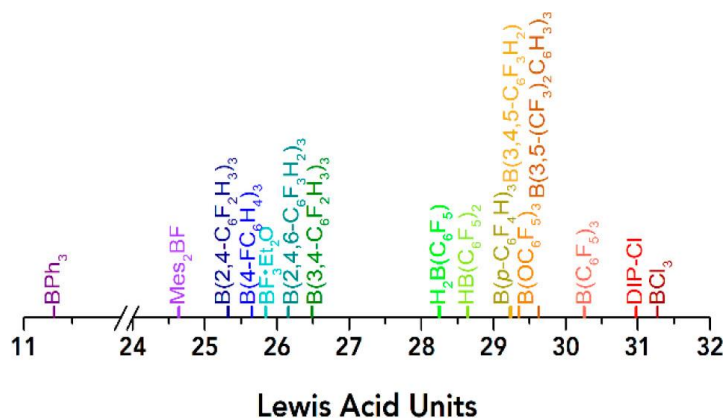
Figure 1.7. Scale of several boron-based Lewis acids using the fluorescence method. Image reproduced from Ref. 44 with permission.

In general, three coordinate boranes are excellent Lewis acids, but enhancing their inherent electron deficiency is targeted as a path towards the advancement of many boron-based materials.[46] The acidity is a result of the electronically unsaturated boron center with an empty p orbital. There are two methods often used to increase the Lewis acidity in boron containing complexes. The first is to install electron withdrawing groups (e.g. fluorination) on substituents surrounding boron. Tris(pentalfuorophenyl)borane (**1.10**) was first reported in 1964,[47] and is now a commercially available LA often used to remove anionic ligands from metal centres[48] and as a catalyst for olefin polymerization.[49] These applications are made possible by the added Lewis acidity offered by the fluorination when compared to triphenylborane. While continuously increasing the number of fluorinated aromatic groups[50, 51] is an effective strategy,[52] the steric crowding caused by these groups will eventually reduce the utility of these complexes (**1.11** and **1.12**).

1.10   **1.11**   **1.12**
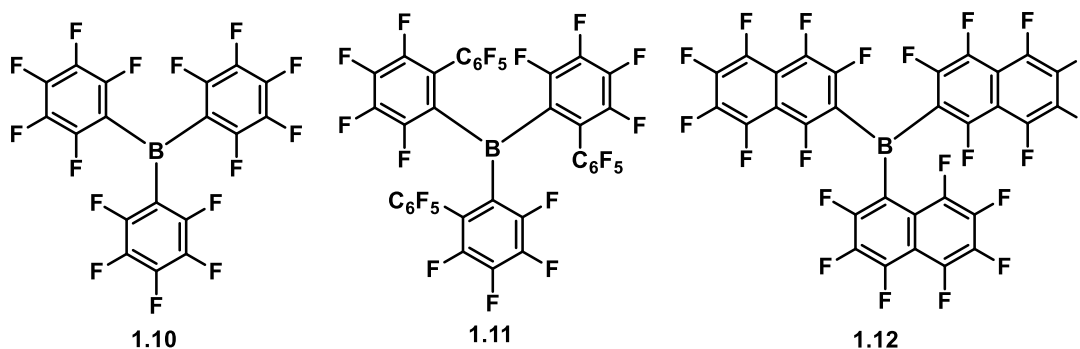
Using anti-aromatic heterocyclic scaffolds, such as boroles, is a common method to improve Lewis acidity.[53] Boroles are five membered, anti-aromatic B-C heterocyclic rings (**1.13**). The anti-aromaticity ensures the empty p orbital is isolated from π-conjugation, increasing the deficiency. The acidity offered by boroles typically make them extremely sensitive to air and moisture,[54, 55] limiting their practical use without the incorporation of large and bulky substituents. The Braunschweig group has made significant advances developing the chemistry of boroles,[56-58] and recently introduced **1.14** and **1.15**,[59] boroles with a bulky 2,4,6-tris(trifluoromethyl)phenyl group as the boron bound substituent. This design combines the ideology of fluorination with the method of utilizing anti-aromatic boroles to enhance the Lewis acidity.

1.13 **1.14** **1.15**
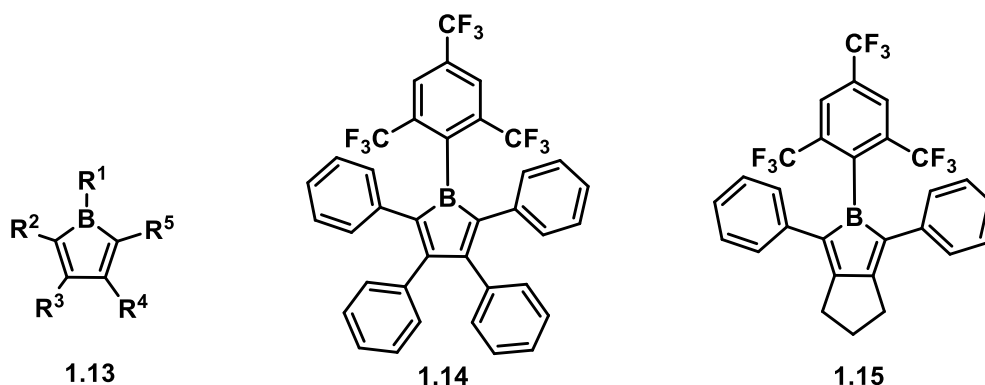
1.3 Cationic Boron

An alternative, non-traditional approach to enhance Lewis acidity and acceptor capability is to impose a positive charge on boron. The positive charge will alter the electronic structure, enhance the p-π* interactions (if available) and further lower LUMO energies.[60-62] Accordingly, the HOMO-LUMO gap will decrease, allowing electrons to mobilize between molecular orbitals with lower excitation energies. Neutral boron can have three or four bonds, with a minimum of three anionic donor ligands. Cationic boron has a maximum of two anionic donor ligands, and can be two, three or four coordinate, termed *borinium*, *borenium* or *boronium* respectively (Figure 1.8). Reactivity of these compounds increases as coordination number decreases.[62, 63]
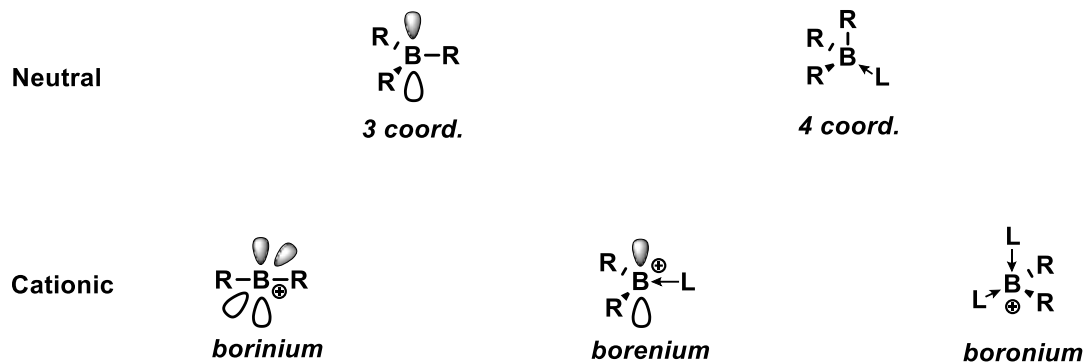
Figure 1.8. Hypothetical representations of neutral and cationic boron. R denotes an anionic ligand. L is a neutral two-electron donor ligand.

There are few reported examples of borinium cations, and consequently their properties are underexplored. This can reasonably be attributed to their instability and difficulty offered in attempts to isolate and handle them. The Gessner group isolated **1.16$^+$**, a borinium cation with "ylide" stabilization.[64] The species was prepared via hydride abstraction, using [Ph$_3$C][B(C$_6$F$_5$)$_4$], as the trityl (Ph$_3$C$^+$) cation has strong affinity for hydride.[65] The reactivity of **1.16$^+$** was probed by reaction with Lewis bases, such as 4-dimethylaminopyridine (DMAP), dimethylformamide (DMF) and *N*-methyl-2-pyrrolidone (NMP) to form adducts. **1.16$^+$** exhibited fluoride ion affinity when reacted with KF, demonstrating its capability to act as a fluoride sensor. Finally, its potential use in catalysis was discovered as the addition *p*-nitroaniline results in N-H bond activation across the B-C bond, and cleavage of both ylide substituents (Scheme 1.6).
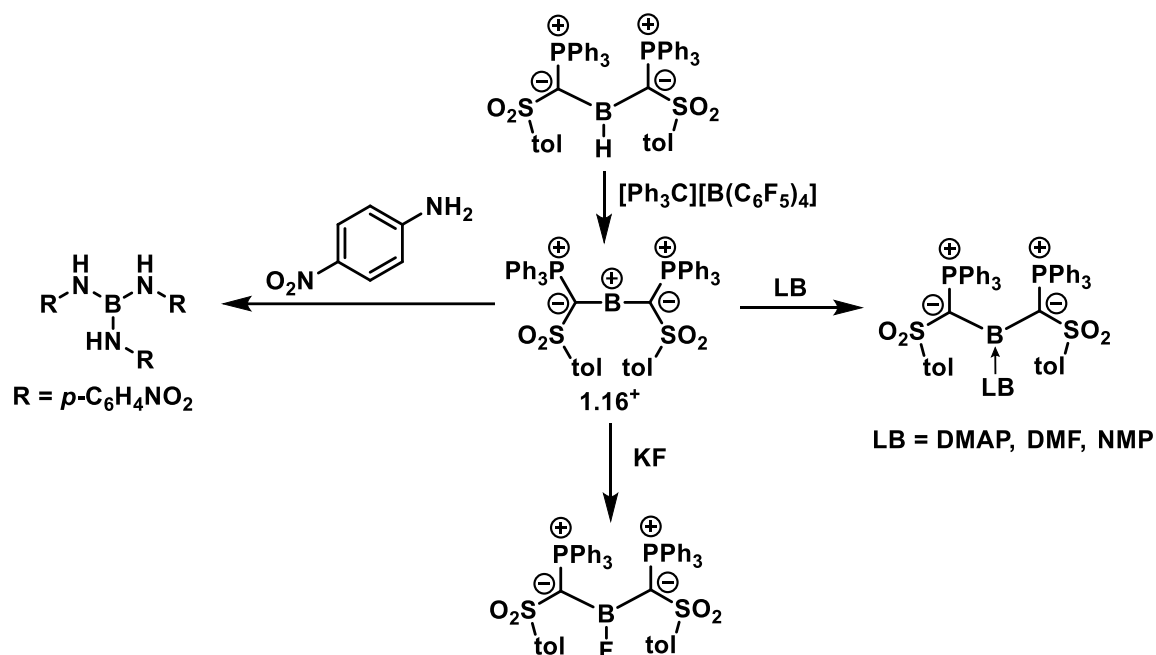
Scheme 1.6. Reactivity and applications of **1.16⁺**, as a fluoride detector, electron acceptor for LA-LB adducts and catalyst for N-H bond activation.

The Chiu group stabilized a borinium cation with a η^5-coordinated 1,2,3,4,5-pentamethylcyclopentadienyl (Cp*) and a mesityl (Mes) group.[66] **1.17⁺** was prepared with an excess of MesLi added to Cp*BCl₂, followed by a metathesis reaction with Li[B(C₆F₅)₄] (Scheme 1.7). Borinium cation **1.17⁺** exhibited ambient stability, mirroring stability expected for higher valent cations. **1.17⁺** demonstrated exceptional Lewis acidity, with an acceptor number of 104.5 on the GB acidity scale (**1.18⁺**). This value is larger than many commercial potent Lewis acids, such as BCF (AN = 78). The combination of unprecedented stability and Lewis acid potency allowed for use in the catalytic reduction of ketones.
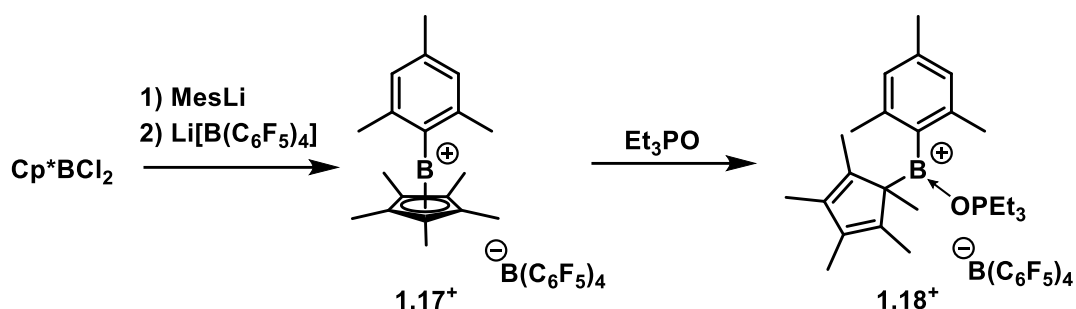
Scheme 1.7. Synthesis of **1.17⁺** and determination of Lewis acidity using triethylphosphine oxide.

Borenium cations are more stable than divalent borinium cations, but more reactive than boronium cations. This balance allows for a wider range of applications.[67] The Bourissou group isolated an intramolecular phosphine stabilized borenium cation (**1.19⁺**), prepared via bromide abstraction with AgNTf₂ (NTf₂⁻ = bistriflimide) (Scheme 1.8).[68] The steric bulk provided by the -Mes group allows for use of the borenium center in FLP chemistry, upon addition of tBu₃P. Under these conditions, this pair can activate and split H₂, resulting in **1.20** and a phosphonium salt. Further studies with **1.19⁺** resulted in an unusual *syn* 1,2 carboration upon reaction with 3-hexyne, resulting in a cleavage of the B-Mes bond, producing **1.21⁺**. This is demonstrative of the vast possibilities of the reactions involving borenium cations in carboration reactions.
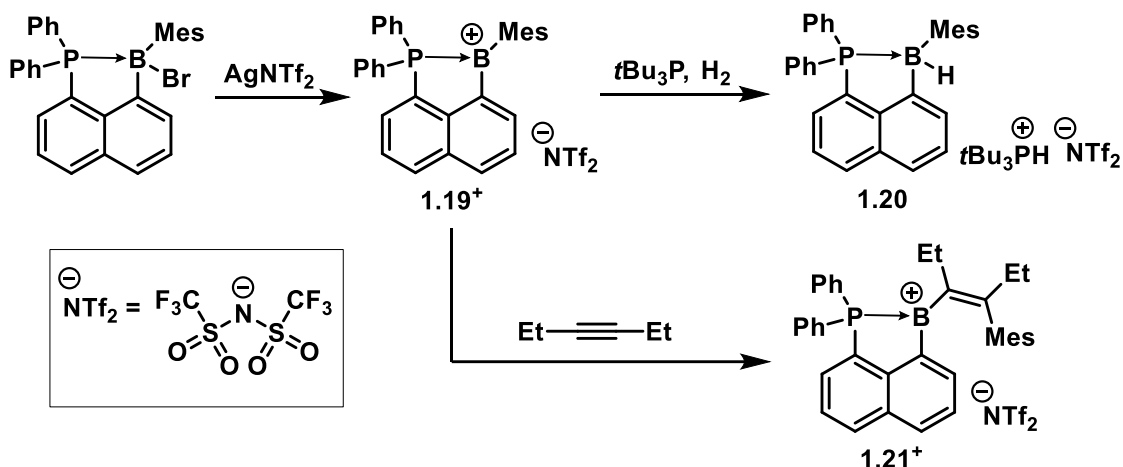
Scheme 1.8. Synthesis of **1.19⁺** and use in FLP chemistry and carboration.

The first reported NHC stabilized borefluorenium heterocycles were recently reported by the Gilliard group.[69] The methoxy substituted cation **1.22⁺** appeared red in a CH_2Cl_2 solution, but colourless when dissolved in THF. After much investigation, the authors determined that THF could coordinate and form a boronium cation (**1.23⁺**), changing the electronic structure and colour in solution. Interestingly, upon heating to 40 °C, the solution regained its red colour, indicating that the THF molecule had dissociated (Scheme 1.9). This phenomenon was rationalized by calculating frontier molecular orbitals of the three-coordinate borenium and the four-coordinate boronium cation. In the borenium complex, the empty p orbital stabilizes the LUMO, changing the electronic structure and lowering the energy of absorption (Figure 1.9a). This is not observed in the boronium case as boron's coordination sphere is saturated with four bonds. This complex provides a fundamental design for a thermochromic sensor (Figure 1.9b), where the B-O bonding can be modulated by adjusting the temperature, and observing the colour of solution.
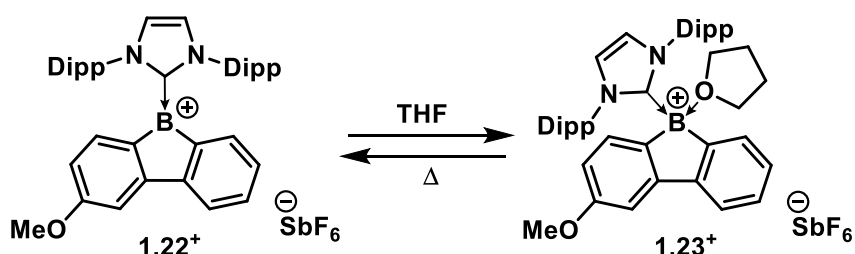
Scheme 1.9. Reversible coordination of THF to **1.22⁺**.
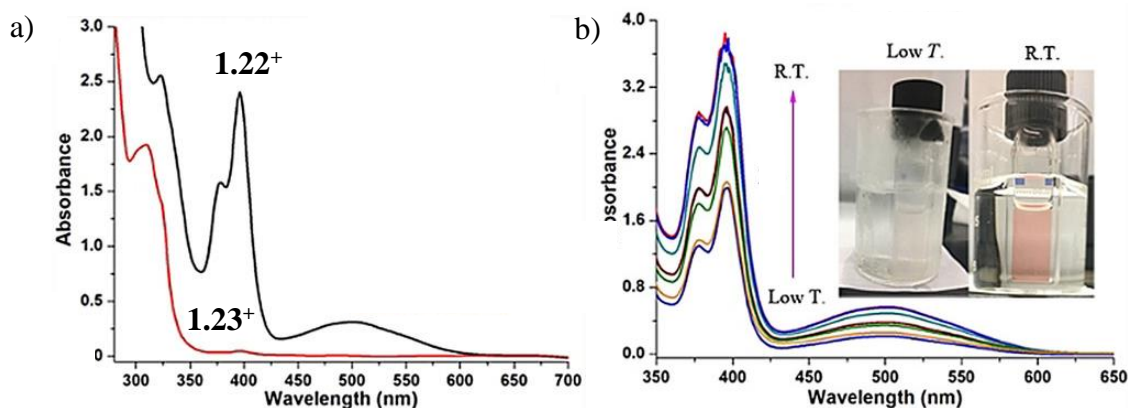
Figure 1.9. a) UV-vis spectrum of **1.22⁺** and **1.23⁺**. b) UV-vis spectrum representing thermochromic character. Image reproduced from Ref. 69 with permission.

The Stephan group synthesized a borenium cation used for dihydrogen activation in FLP chemistry.[70] **1.25**$^+$ was prepared via hydride abstraction, and is stabilized by a bulky 9-borabicyclo[3.3.1]nonane (9-BBN) substituent (Scheme 1.10). When *t*-butylphosphine (*t*Bu$_3$P) is added to the mixture, a FLP is formed as both the Lewis acidic boron and Lewis basic phosphorous are sterically congested. This FLP can activate and split dihydrogen and was capable of catalytically hydrogenating enamines and imines.
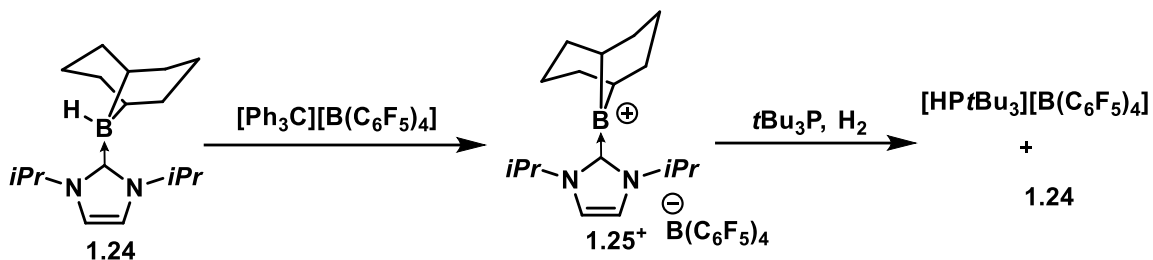
Scheme 1.10. Preparation and FLP chemistry of **1.25**$^+$.

While three-coordinate borenium cations have many possible applications, four coordinate boronium cations are more common throughout the literature, largely because of their stability when compared to other boron cations. However, the absence of an empty p orbital limits application in the same realm as borinium and borenium cations.

Boronium cations can be a potential precursor for the isolation of stable neutral radicals. When combined with organic fragments, the cationic nature of these complexes typically offers lower LUMO energy levels than four-coordinate neutral species, allowing for a more facile reduction. The Piers group isolated **1.26**$^+$ using halide abstraction with AgBF$_4$, followed by addition of a chelating donor ligand, 2,2'-dipyridyl (Scheme 1.11).[71] The first (single electron) reduction potential was −1.45 V, prompting the researchers to treat the cation with KC$_8$, which allowed them to successfully isolate **1.27**$^•$, a neutral radical. A combination of EPR and DFT calculations determined that a large amount of spin density lies on the boron center, with delocalization over the 2,2'-dipyridyl ligand contributing to the stability.
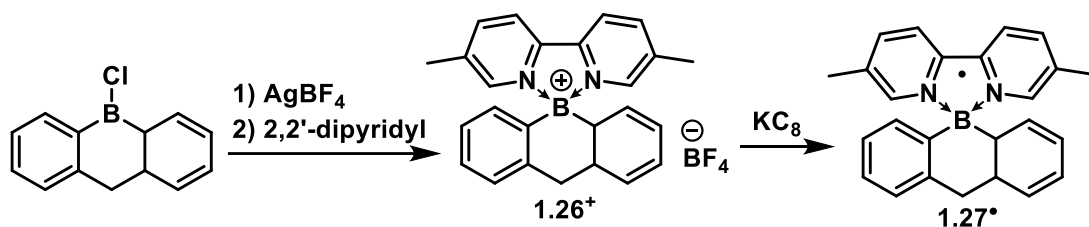
Scheme 1.11. Preparation of boronium cation **1.26⁺** and neutral radical **1.27•**.

Organoboron complexes are frequently encountered in anion sensing, with a majority devoted towards the detection of fluoride ions due to their importance in health but also potential toxicity at high doses.[72] The Gabbaï group has been on the forefront of developing boron-containing complexes for fluoride ion capture, and has expanded the reach to include cationic boron complexes.[73] Boron difluoride dipyrromethene (BODIPY) compounds (**1.29**) are amongst the most well-known fluorescent boron complexes. The researchers designed a boronium cation (**1.28⁺**), where the DMAP ligand can be displaced. Upon reaction with a fluoride source (*i.e.,* TBAF), fluoride replaces DMAP to form **1.29** (Figure 1.10a), which resembles a BODIPY and drastically enhances the fluorescence intensity (Figure 1.10b). The DMAP ligand can be displaced due to the high affinity and strength of a B-F bond. This system acts as a "turn-on" fluorescence sensor in the presence of fluoride ions, which can be used as a probe in anion sensory applications.
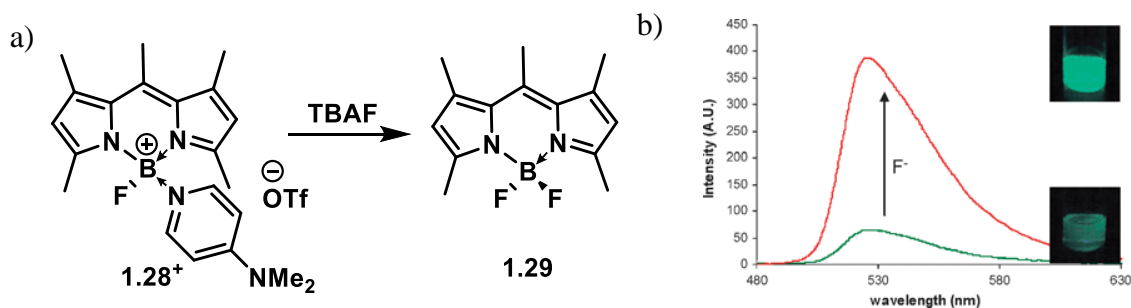
Figure 1.10. a) Displacement of DMAP ligand to form BODIPY. b) Emission spectrum upon addition of fluoride. Image reproduced from Ref. 73 with permission

1.3.1 Dicationic Boron

Although the focus of the cationic boron discussions is on monocations, there have been several reports of dicationic boron,[74] which can also exist as either two (**1.30²⁺**),[75] three (**1.31²⁺**) [76] or four-coordinate (**1.32²⁺**) (Figure 1.11).[77]
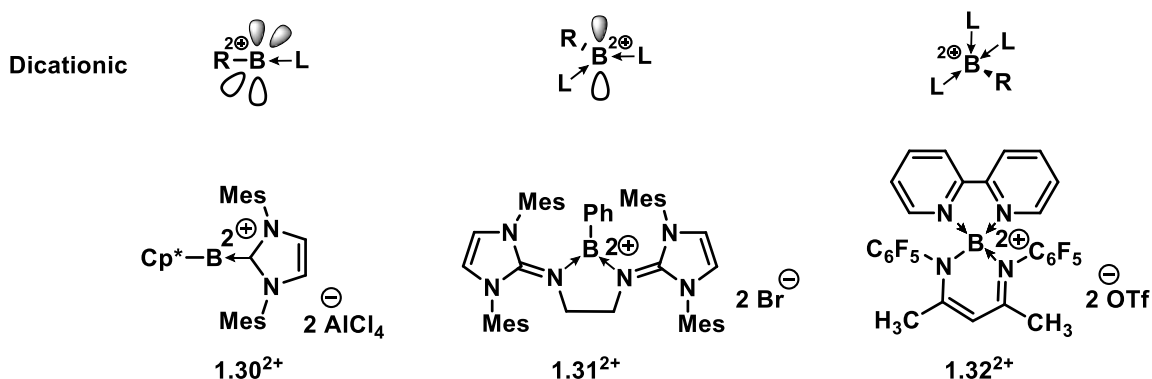
Figure 1.11. Hypothetical representations of dicationic boron and examples. R denotes an anionic donor ligand, while L represents a two-electron neutral donor.

The increasing positive charge is expected to further increase the Lewis acidity of the boron center. However, their increased instability does not allow many applications, therefore studies of boron dications beyond basic characterization (NMR, X-ray crystallography) are limited.

1.3.2 Stabilization of Cationic Boron

Low valent boron cations often suffer from immense instability, but several measures can be taken to help increase stability and prevent nucleophilic attack. Strong donor ligands are frequently necessary, with *N*-heterocyclic carbenes (NHC) being the most employed. NHCs are neutral two electron sigma donors, where a sp^2 hybridized carbon is the donor atom.[78] The Stephan group isolated a borenium cation (**1.33⁺**), where the NHC aryl substituents force planarity and allow for adduct formation with various large and bulky Lewis bases (e.g. PPh_3, Et_3PO, DABCO) (**1.34⁺**) (Scheme 1.12). This work provided a strategy for further extending the π-system in planar borenium complexes.[79]
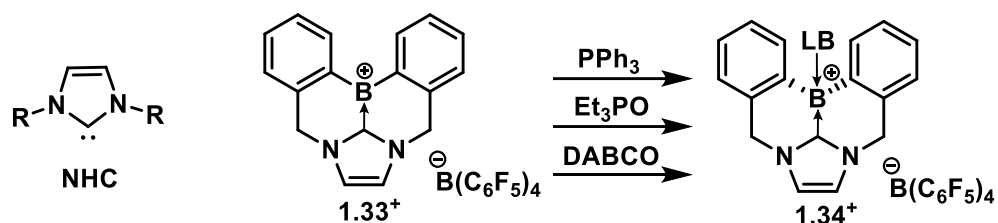
Scheme 1.12. Representation of a NHC supporting a borenium cation **1.33⁺**.

Large and bulky aromatic substituents are typically employed to sterically shield the boron center from nucleophilic attack of small molecules (e.g. H_2O). The Jäkle group recently isolated a borenium complex with NHC stabilization (**1.35⁺**), containing bulky *t*-butyl groups, which allowed for late-stage functionalization to form a dicationic dimer (**1.36²⁺**) (Scheme 1.13).[60] The stability imparted by the sterically demanding NHC ligand substituents allowed for these borenium cations to be handled in air. Further, these cations exhibited unique absorption and emissive properties, as well as relatively high (−1.36 V) reversible reduction potentials probed by cyclic voltammetry. These solution-based measurements are not typically carried out for borenium cations due to solution instability, thus the steric protection provided by the ligands is crucial for design. The capability of late-stage lithiation and functionalization allows for future exploration of larger and more diverse borenium cationic complexes with extended π-conjugation.
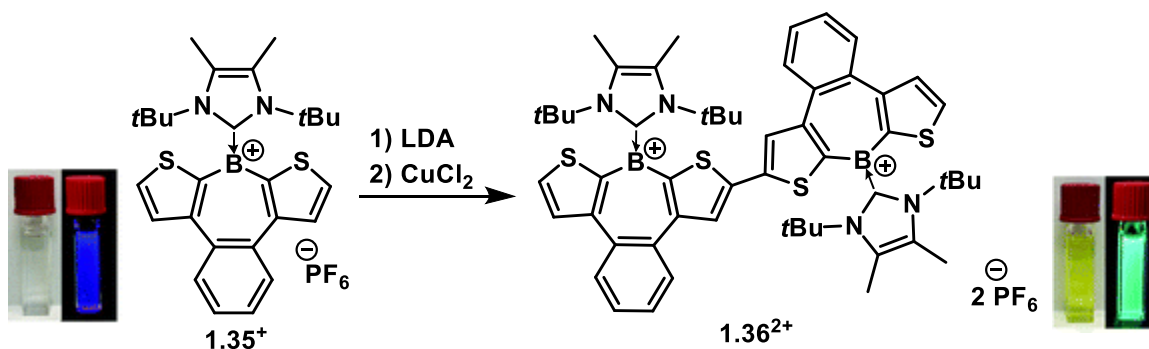
Scheme 1.13. Late-stage functionalization of **1.35⁺** form dimer **1.36²⁺**. Image insets reproduced from Ref. 60 with permission.

The electrophilicity of low valent cationic boron often renders classical counterions (e.g. halides) ineffective due to their propensity to coordinate to boron. Thus, the utilization of

non/weakly-coordinating anions are needed for stabilization. Anions such as tetrakis(pentafluorophenyl)borate ($[B(C_6F_5)_4]^-$) ($\mathbf{1.37^+}$)[80], carboranes ($[CH_6B_{11}Br_6]^-$) ($\mathbf{1.38^+}$)[81] and occasionally triflate (OTf$^-$) ($\mathbf{1.39^+}$)[82] are encountered.
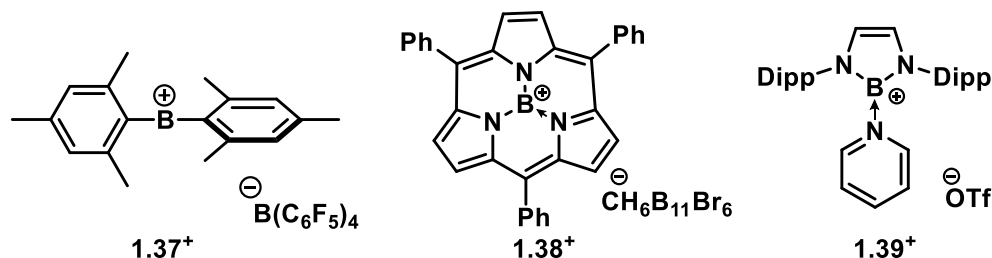
In addition to these common stabilizing features, cationic boron is often contained within a heterocyclic framework. B-C cationic frameworks, such as boroles, have only recently been reported by the Sindlinger group ($\mathbf{1.40^+}$).[83] They isolated the first C_4B cationic borole, without additional aromatic stabilization (*e.g.* $\mathbf{1.22^+}$ isolated by the Gilliard group). More often, B-N heterocyclic frameworks are observed, as these systems are isoelectronic to C-C and are implicated as potential hydrogen storage devices.[84-86] β-diketiminate ligands are often for stabilization of metal and main group elements.[87-89] The Cowley group reported the first ever β-diketiminate supported boron cation ($\mathbf{1.41^+}$) with a corroborating X-ray molecular structure, revealing a naked cation, with no close anion-cation contacts.[90] One of the most widely known and used B-N heterocycles is the BODIPY dye. These molecules are targeted for their impressive fluorescent properties, occasionally with fluorescence quantum yields near 1.0.[91] The parent dipyrrinate ligand is structurally related to the β-diketiminate ligand, and has also been used to support cationic boron. The Piers group isolated two borenium cationic complexes, with either a fluoride ($\mathbf{R}$ = F) or hydride substituent ($\mathbf{R}$ = H) ($\mathbf{1.42^+}$).[92] The researchers reported that both cations had excellent Lewis acidity (Childs' values 0.72 and 0.78 respectively), but could not catalyze several reactions. Furthermore, it was stated that these compounds exhibited interesting photophysical properties, but corresponding characterization was not reported.

1.40⁺   1.41⁺   1.42⁺
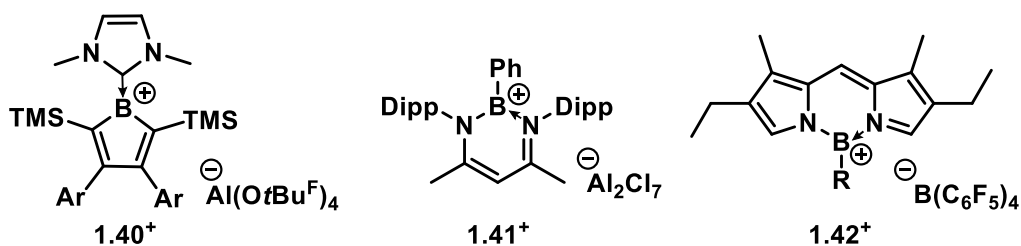
1.4 Formazans & Formazanate Ligands

Formazans (**1.43**) are nitrogen rich analogues of β-diketimines (**1.44**), and are of the general form R^1-N(H)-N=C(R^3)-N=N-R^5.[93] The R^1 and R^5 substituents are typically aromatic, including the potential appendage of electron donating groups (*e.g., p*-anisole) or electron withdrawing groups (*e.g., p*-trifluoromethylbenzene).[94] The R^3 substituent is more diverse, and is commonly an aromatic, cyano or nitro group, but can also be small aliphatic substituents. Based on the R^3 group, formazans can exist in three isomeric forms; closed, open or linear. Larger and non-linear substituents (*e.g.,* phenyl or nitro) will favour the closed form, while smaller or linear substituents (*e.g.,* cyano) may favour the open or linear form.[95] All compounds discussed in subsequent chapters contain a phenyl group at the R^3 position, therefore the remainder of this section will focus on triaryl (R^3 = Ph) formazans and formazanate ligands.

1.43   1.44

closed   *open*   *linear*
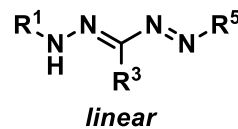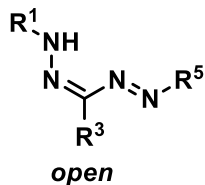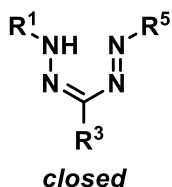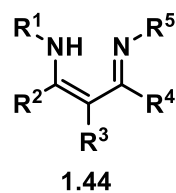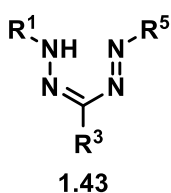
There are two main synthetic methods commonly used to access triaryl formazans. The first is to condense an aryl hydrazine with an aryl aldehyde in MeOH or EtOH, to make an

aryl hydrazone. This hydrazone can be isolated and purified, or the reaction can proceed *in-situ*. The aryl hydrazone is treated with an aryl diazonium salt under alkaline conditions to complete the reaction and produce a formazan (Scheme 1.14). This synthetic method is also effective for synthesizing asymmetric formazans ($R^1 \neq R^5$).
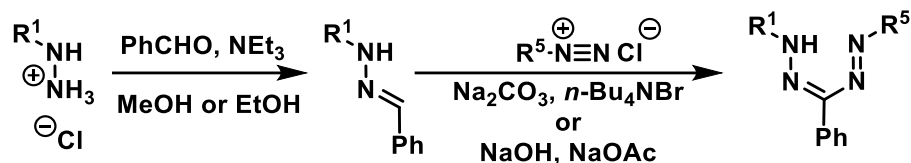
Scheme 1.14. Formazan synthesis beginning with an aryl hydrazine.

The second method couples two equivalents of an aryl diazonium salt with an active methylene species (*e.g.,* phenylpyruivc acid) under alkaline conditions (Scheme 1.16). This method is best suited for the synthesis of symmetric formazans ($R^1 = R^5$).
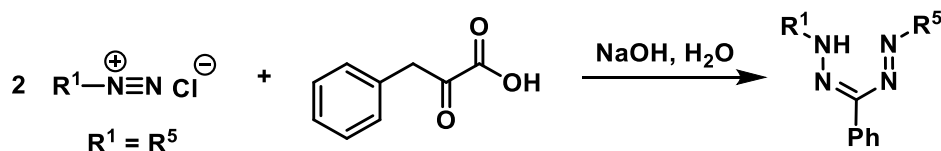
Scheme 1.15. Formazan synthesis via active methylene species.

Formazan dyes are characteristically intense in colour and have found use in the textile industry (dyeing textile fibres)[96] and chemical biology for their use in cell viability,[97] proliferation[98] and cytotoxicity[99] assays. The MTT viability assay requires the dissolution of a weakly coloured tetrazolium salt (**1.45**) with cells of interest. If the cells are living, their oxidoreductase enzymes will reduce the tetrazolium salt to a deeply coloured formazan (**1.46**) (Scheme 1.16).[100] The intensity of the solution colour is a qualitative method to observe viability, and measuring the intensity of the absorption can give a quantitative measure of viability.
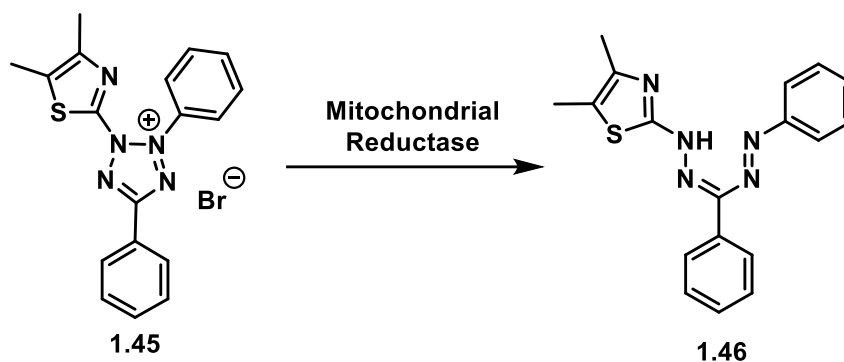
Scheme 1.16. Assay for assessment of cell viability.

Formazans are often deprotonated to form anionic formazanates (**1.47**⁻), which act as monoanionic chelating ligands capable of coordinating to various main group or transition metal centers. The Otten group examined the redox character of bis(formazanate) complexes chelated to zinc (**1.48**). The researchers were able to successfully isolate both the radical anion and dianionic complexes.[101] The Teets group has prepared several metal formazanate complexes (e.g. **1.49**), which features a platinum formazanate complex, with unique electrochemical and optical properties.[102] The Gilroy group has reported hypervalent group 14 (Si, Ge and Sn) formazanate complexes (**1.50**) that acted as a framework for isolation of stable radical species, based on the square pyramidal geometry adopted by the group 14 atoms.

1.47⁻   1.48   1.49   1.50 E = Si, Ge or Sn
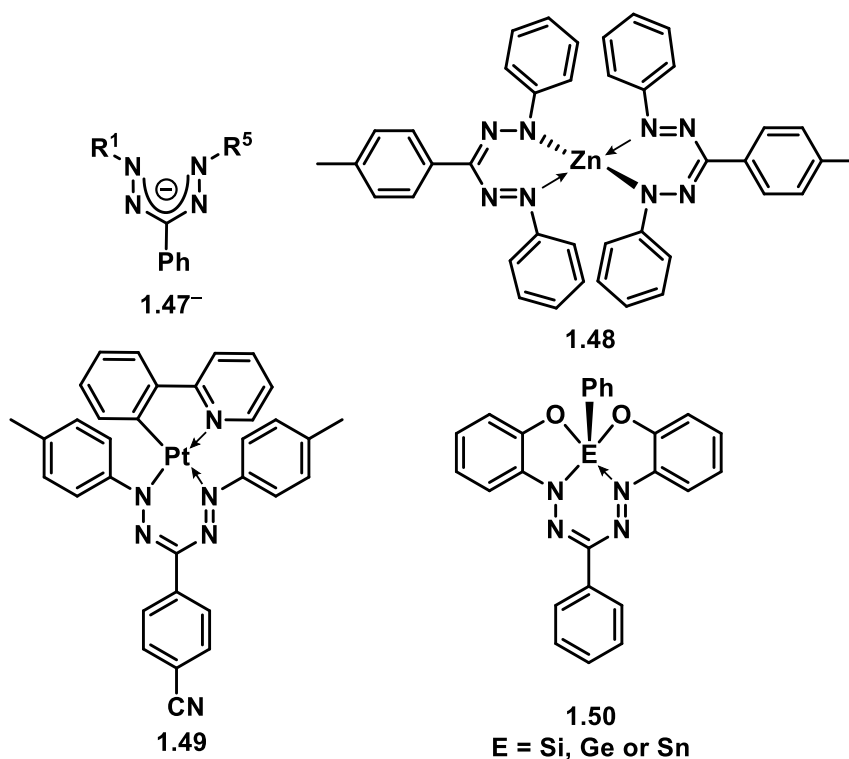
The Gilroy group has primarily developed main-group adducts of formazanate ligands, specifically the coordination of the $[BF_2]^+$ fragment, to isolate boron difluoride (BF_2) formazanate dyes. These complexes are synthesized in one simple, straightforward step and is typically high yielding. The parent formazan is dissolved in a non-coordinating solvent (*e.g.*, toluene) and treated with an excess of triethylamine and boron trifluoride diethyl etherate in order to afford the BF_2 formazanate (Scheme 1.17).
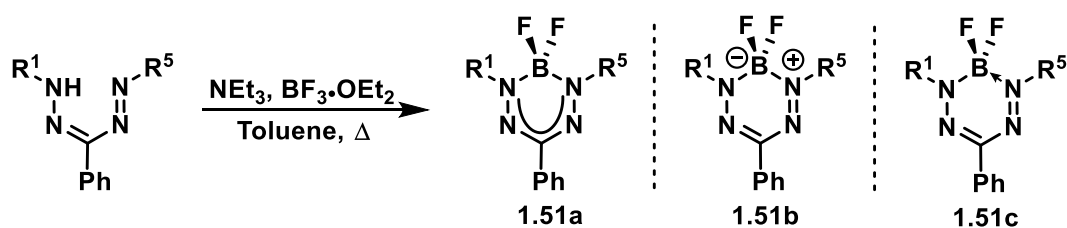
Scheme 1.17. Synthesis of a BF_2 formazanate and possible representations.

There are many possible representations of a BF_2 formazanate, and three are showcased in Scheme 1.17. **1.51a** denotes a delocalized charge over the backbone of the formazanate, which has been evidenced via X-ray crystallography, where the C-N and N-N bond lengths

fall between the standard lengths for single and double bonds. This depiction denotes a chelating, bidentate anionic ligand. **1.51b** represents the complex with a formal positive charge on the nitrogen and a formal negative charge on boron. **1.51c** shows a dative bond between a nitrogen of the formazanate and boron, which is the preferred convention in the context of cationic boron complexes in BN heterocycles. Therefore, **1.51c** will be the representation used herein.

BF$_2$ formazanates are targeted due to their stable architecture and attractive/tunable redox and electronic properties. Arguably one of the most attractive features of formazanate ligands is their reduction and oxidation chemistry, mainly as a result of their accessible frontier molecular orbitals.[103-105] The normally high-lying HOMO and low-lying LUMO are generally both of π-symmetry, and substitution and derivatization of the formazanate ligands allows for tuning of the energy levels of these molecular orbitals.[94, 106] Figure 1.12 shows a representative triaryl BF$_2$ formazanate (**1.52**) and the calculated frontier molecular orbitals using time-dependent density functional theory (TDDFT).[107] The HOMO is delocalized over the formazanate backbone, *N*-aryl substituents and phenyl substituent at the 3 position.[108] However, the LUMO is highly delocalized over the formazanate backbone and *N*-aryl substituents, but not the phenyl (R^3) substituent. In most cases, the boron bound substituent does not contribute to the frontier molecular orbitals.[109] The delocalization leads to molecules that are relatively simple to reduce, and attractive optical properties due to HOMO-LUMO energy gaps typically within the visible or near-IR range.[110, 111]
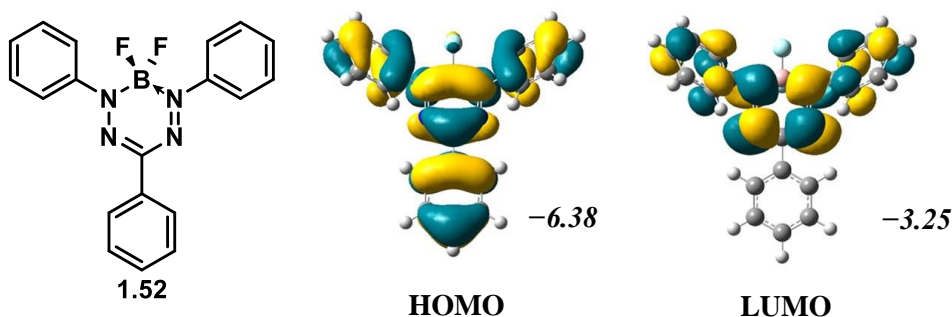
Figure 1.12. HOMO and LUMO of **1.52** using M06/6-311+G* SCRF=PCM method. Orbital energies in eV.[108] Image reproduced from Ref. 108 with permission.

Many efforts have been devoted towards narrowing the HOMO-LUMO gap to design compounds capable of absorbing and emitting lower energy light. The effect of extending π-conjugation on the spectroscopic and electronic properties were examined, first by installing a naphthyl group at R^1 (**1.53**) and then at both R^1 and R^5 (**1.54**) of the formazanate.[108] Increasing the π-conjugation at these positions expectedly red-shifts the absorption maxima, increases the fluorescence quantum yields (Φ_F) and raises the reduction potentials (Table 2).

1.52   **1.53**   **1.54**
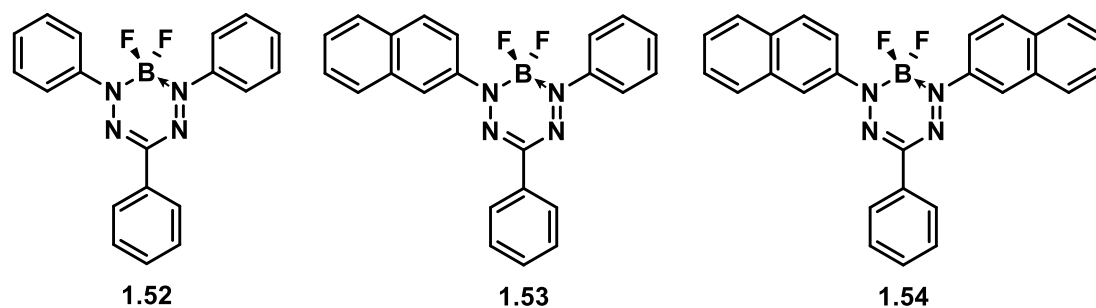
Table 1.2. Spectroscopic and electrochemical data for extended π-conjugation formazanates.

Compound	λ_{max} (nm)	λ_{em} (nm)	Φ_F	E_{red1} (V)
1.52	517	626	<0.01	−0.82
1.53	535	659	0.02	−0.80
1.54	556	681	0.05	−0.78

A commonality encountered with nearly all triaryl BF_2 formazanates is the weak or lack of fluorescence, as evidenced by the consistently low fluorescence quantum yields (often <0.05). Significantly higher quantum yields are often observed with $R^3 = CN$ compounds, with values reaching as high as 0.77. **1.55** exhibited strong red fluorescence ($\lambda_{em} = 656$ nm, $\varepsilon = 42,700$ M^{-1} cm^{-1}) and combined with its simple synthesis, allowed it to be an excellent candidate for fluorescent cell imaging (Figure 1.13).[112]
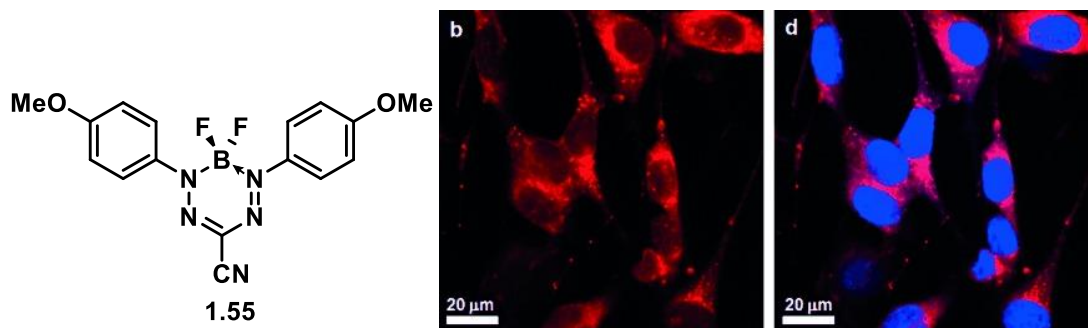
Figure 1.13. Confocal fluorescence of mouse fibroblast cells stained with **1.55**. Image reproduced from Ref. 112 with permission.

Upon relaxation to the ground state, there is likely a vibrational non-radiative decay pathway associated with the R^3 = phenyl substituent.[94, 108] This has been probed by placing a pyridyl moiety in place of the typical Ph substituent (**1.56**). Successful protonation of this substituent (**1.57$^+$**), at progressively lower pH, led to a drastic increase in the quantum yield (Scheme 1.18). The protonation resulted in *intramolecular* hydrogen bonding with a nitrogen of the formazanate and *intermolecular* hydrogen bonding with nearby formazanate molecules and the counterion, which likely restricted vibrational and rotational non-radiative relaxation pathways, boosting the quantum yield, providing support for the original theory.[113]
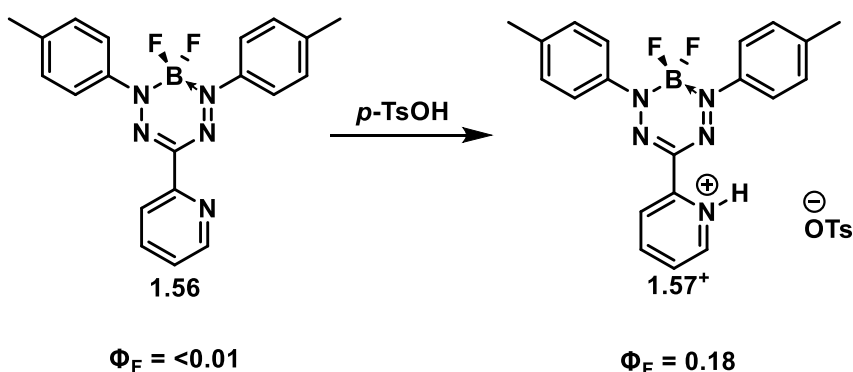
Scheme 1.18. Protonation of **1.56** to increase Φ_F.

To better understand and illustrate the electronic pathway for non-radiative decay associated with triaryl BF$_2$ formazanates, the Perrin-Jablonski diagram is an excellent aid for representation (Figure 1.14). Upon absorption of light (~10^{-15} s), a molecule transitions

typically from its lowest vibrational level of its ground state (S_0) to an excited state (S_n, n = 1, 2, 3…). Once in the excited state, there are several fates of the molecule in order to release energy and return to the ground state. All relaxation pathways are in competition with one another to dissipate the energy. Vibrational relaxation is quick ($10^{-12} - 10^{-10}$ s), and will allow the molecule to relax to the lowest vibrational level of S_2 (if excitation was S_0–S_2). At this point, internal conversion (IC) is likely to occur ($10^{-11} - 10^{-9}$ s), where there is an isoelectronic transition to an upper vibrational level of S_1 before continued vibrational relaxation to the lowest vibrational state of S_1. At this level, there are several possible final fates of the excited state. Fluorescence can occur ($10^{-10} - 10^{-7}$ s), where light is emitted and observable to the naked eye if emission is in the visible range. There is no change in spin multiplicity in this radiative process. Intersystem crossing (ISC) ($10^{-10} - 10^{-8}$ s) can occur, a spin forbidden process where the spin multiplicity flips from singlet to triplet, before decaying to the ground state. ISC can result in a radiative decay called phosphorescence ($10^{-6} - 10$ s). Finally, IC to an upper vibrational electronic state of S_0 is possible, which allows for non-radiative decay to the ground state. This final IC pathway is likely the dominant relaxation pathway for the excited states of triarylformazanates.
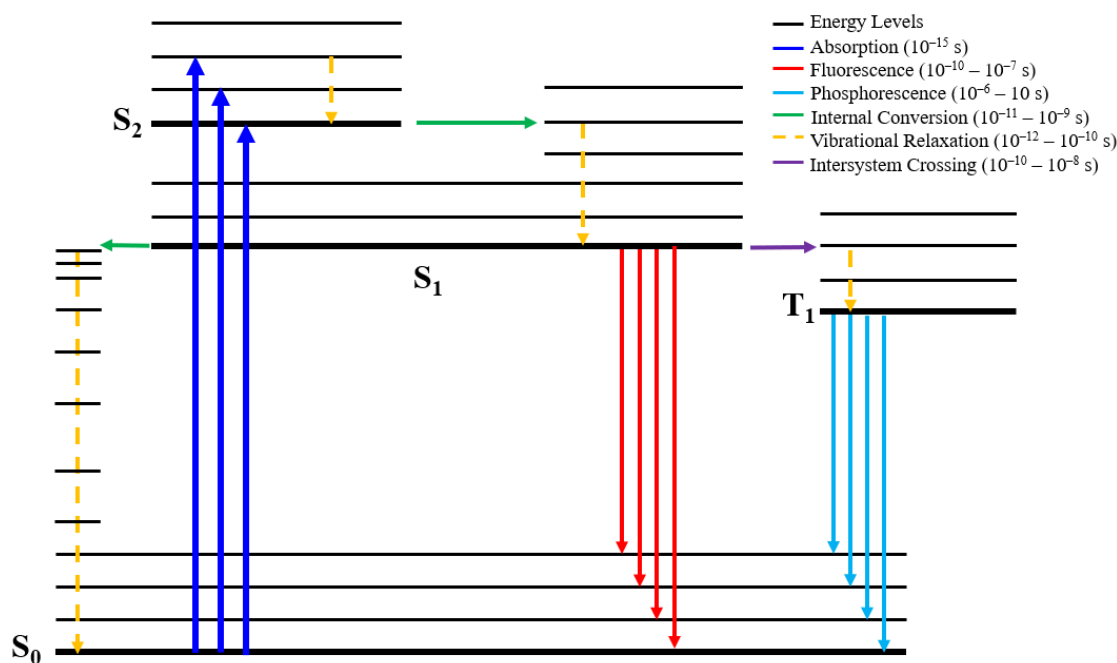
Figure 1.14. Perrin-Jablonski diagram representing the various electronic excitation and relaxation pathways.

The presence of this vibrational non-radiative decay pathway is a barrier for using triarylformazanates for applications that require luminescence. In order to address this problem, the Gilroy group has investigated the "turn-on" of photoluminescence upon introducing a B=O (oxoborane) to the formazanate system.[114] This was accomplished by treating an essentially non-emissive (Φ_F <0.01) BF_2 formazanate (**1.58**) with an excess of boron trichloride (BCl_3) to make an air and moisture stable BCl_2 formazanate (Φ_F <0.01) (**1.59**) (Scheme 1.19). A B-Cl bond is a more attractive choice for boron functionalization due its weak and labile nature, and is used frequently for developing boron species for catalytic processes, such as boronic acids for Suzuki coupling.[82, 115] The oxoborane formazanate was obtained after treatment with $AlCl_3/H_2O$ (**1.60**) (Φ_F = 0.36). **1.60** was strongly emissive despite its precursors lack of emission intensity.

Φ_F <0.01
ν_{ST} = 3610 cm^{-1}

Φ_F <0.01
ν_{ST} = 4757 cm^{-1}

Φ_F = 0.36
ν_{ST} = 1342 cm^{-1}
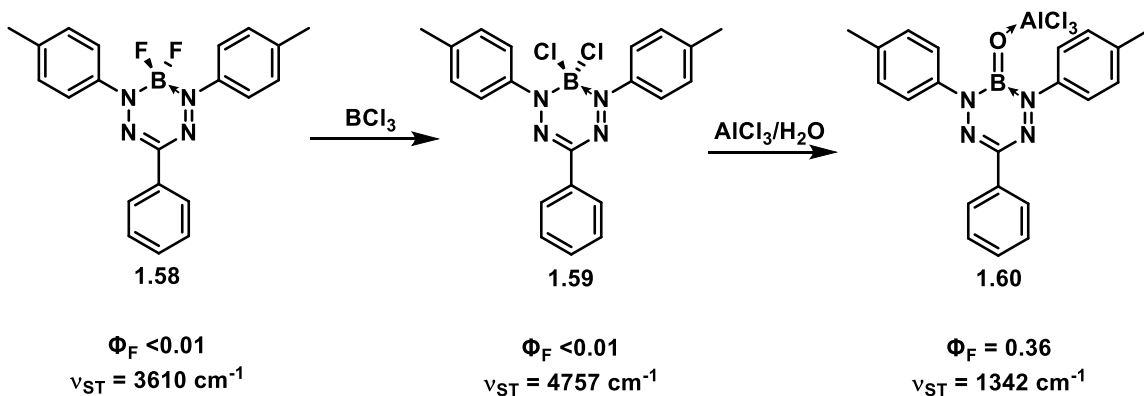
Scheme 1.19. Synthesis of oxoborane **1.60**.

In order to understand the *ca.* 36-fold enhancement in PL intensity, the optimized ground (S_0) and excited state (S_1) geometries were determined (Figure 1.15). There is a significant change in geometry between S_0 and S_1 for BF_2 (**1.58**) and BCl_2 (**1.59**) formazanates, likely the cause of the weak fluorescence and large Stokes shifts. There is a large structural reorganization that must take place in order to return to the ground state, likely promoting a non-radiative decay pathway. However, for oxoborane **1.60**, there is minimal change in geometry upon excitation, therefore upon relaxation, a fluorescent decay pathway with a smaller Stokes shift is favoured.

Ground States (S₀)   **Excited States (S₁)**
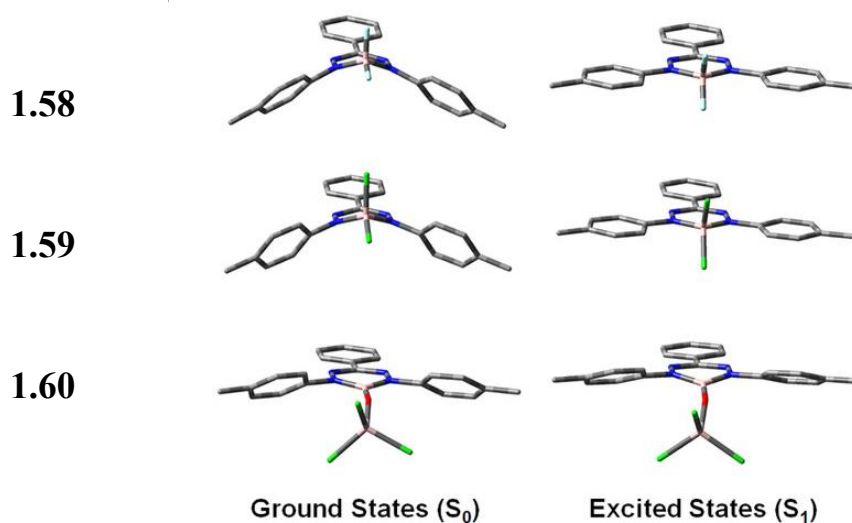
Figure 1.15. Ground and excited state geometries of **1.58**, **1.59** and **1.60**.[114] Image reproduced from Ref. 114 with permission.

This work contributes to the understanding of enhancing fluorescence in triarylformazanate complexes and opens possibilities of further functionalization at boron using B-Cl bonds.

1.5 Scope of Thesis

This thesis reports the first examples of cationic boron formazanate complexes and thorough, systematic characterization of such compounds. Their unique properties are highlighted for potential use in the design of optoelectronic materials and applications.

Chapter 2 focuses on the synthesis and characterization of several three- and four-coordinate cationic and dicationic boron formazanate dyes. A systematic evaluation is performed to understand the effect of changing the boron coordination number (*i.e.,* three or four) and charge (*i.e.,* +1 or +2) on the electronic structure.

Chapter 3 highlights a set of highly Lewis acidic borenium formazanates with novel optical properties, including low-energy absorption and fluorescence. Unique electrochemical trends are discussed, and properties are rationalized with TDDFT calculations.

Chapter 4 summarizes the key findings and conclusions of each chapter and provides future possibilities of synthetic work to be done in order to further advance our understanding of cationic boron formazanate complexes.

1.6 References

1. Baumgartner, T.; Jäkle, F., *Main Group Strategies Towards Functional Hybrid Materials*. Wiley, Chichester: 2018.

2. Shoji, Y.; Tanaka, N.; Mikami, K.; Uchiyama, M.; Fukushima, T. *Nat. Chem.* **2014**, *6*, 498–503.

3. Mellerup, S. K.; Wang, S. *Trends Chem.* **2019**, *1*, 77–89.

4. Ji, L.; Griesbeck, S.; Marder, T. B. *Chem. Sci.* **2017**, *8*, 846–863.

5. Matsumi, N.; Chujo, Y. *Polym. J.* **2008**, *40*, 77–89.

6. Matsumi, N.; Naka, K.; Chujo, Y. *J. Am. Chem. Soc.* **1998**, *120*, 5112–5113.

7. Jäkle, F. *Chem. Rev.* **2010**, *110*, 3985–4022.

8. Yin, X.; Liu, J.; Jäkle, F. *Chem. Eur. J.* **2021**, *27*, 2973–2986.

9. Yamaguchi, S.; Wakamiya, A. *Pure Appl. Chem.* **2006**, *78*, 1413–1424.

10. Yamaguchi, S.; Akiyama, S.; Tamao, K. *J. Am. Chem. Soc.* **2000**, *122*, 6335–6336.

11. Kitamura, N.; Sakuda, E. *J. Phys. Chem. A* **2005**, *109*, 7429–7434.

12. Kitamura, N.; Sakuda, E.; Yoshizawa, T.; Iimori, T.; Ohta, N. *J. Phys. Chem. A* **2005**, *109*, 7435–7441.

13. Rao, B.; Kinjo, R. *Chem. Asian J.* **2018**, *13*, 1279–1292.

14. Ma, Y.; Lou, S.-J.; Hou, Z. *Chem. Soc. Rev.* **2021**, *50*, 1945–1967.

15. Welch, G. C.; Juan, R. R. S.; Masuda, J. D.; Stephan, D. W. *Science* **2006**, *314*, 1124–1126.

16. Stephan, D. W. *Science* **2016**, *354*, aaf7229.

17. McCahill, J. S. J.; Welch, G. C.; Stephan, D. W. *Angew. Chem. Int. Ed.* **2007**, *46*, 4968–4971.

18. Stephan, D. W.; Erker, G. *Angew. Chem. Int. Ed.* **2015**, *54*, 6400–6441.

19. Stephan, D. W. *Dalton Trans.* **2009**, 3129–3136.

20. Houghton, A. Y.; Hurmalainen, J.; Mansikkamäki, A.; Piers, W. E.; Tuononen, H. M. *Nat. Chem.* **2014**, *6*, 983–988.

21. Miller, A. J. M.; Labinger, J. A.; Bercaw, J. E. *J. Am. Chem. Soc.* **2010**, *132*, 3301–3303.

22. Zhao, X.; Stephan, D. W. *Chem. Commun.* **2011**, *47*, 1833–1835.

23. Otten, E.; Neu, R. C.; Stephan, D. W. *J. Am. Chem. Soc.* **2009**, *131*, 9918–9919.

24. Mellerup, S. K.; Wang, S. *Chem. Soc. Rev.* **2019**, *48*, 3537–3549.

25. Pandey, U. P.; Thilagar, P. *Adv. Opt. Mater.* **2020**, *8*, 1902145.

26. Shimogawa, H.; Yoshikawa, O.; Aramaki, Y.; Murata, M.; Wakamiya, A.; Murata, Y. *Chem. Eur. J.* **2017**, *23*, 3784–3791.

27. Jäkle, F. *Chem. Rev.* **2010**, *110*, 3985-4022.

28. Jäkle, F. *Coord. Chem. Rev.* **2006**, *250*, 1107–1121.

29. Yin, X.; Guo, F.; Lalancette, R. A.; Jäkle, F. *Macromolecules* **2016**, *49*, 537–546.

30. Adachi, Y.; Ooyama, Y.; Ren, Y.; Yin, X.; Jäkle, F.; Ohshita, J. *Polym. Chem.* **2018**, *9*, 291–299.

31. Chen, H.-W.; Lee, J.-H.; Lin, B.-Y.; Chen, S.; Wu, S.-T. *Light Sci. Appl.* **2018**, *7*, 17168–17168.

32. Zou, S.-J.; Shen, Y.; Xie, F.-M.; Chen, J.-D.; Li, Y.-Q.; Tang, J.-X. *Mater. Chem. Front.* **2020**, *4*, 788–820.

33. Turkoglu, G.; Cinar, M. E.; Ozturk, T. *Molecules* **2017**, *22*, 1522.

34. Lee, H.; Karthik, D.; Lampande, R.; Ryu, J. H.; Kwon, J. H. *Front. Chem.* **2020**, *8*.

35. Jia, W. L.; Feng, X. D.; Bai, D. R.; Lu, Z. H.; Wang, S.; Vamvounis, G. *Chem. Mater.* **2005**, *17*, 164–170.

36. Jia, W.-L.; Bai, D.-R.; McCormick, T.; Liu, Q.-D.; Motala, M.; Wang, R.-Y.; Seward, C.; Tao, Y.; Wang, S. *Chem. Eur. J.* **2004**, *10*, 994–1006.

37. Morrison, G. What is OLED and what can it do for your TV? https://www.cnet.com/news/what-is-oled-and-what-can-it-do-for-your-tv/ (last accessed April 21, 2021).

38. Gillespie, R. J.; Robinson, E. A. *J. Comput. Chem.* **2007**, *28*, 87–97.

39. Mayer, U.; Gutmann, V.; Gerger, W. *Monatsh. Chem.* **1975**, *106*, 1235–1257.

40. Gutmann, V. *Coord. Chem. Rev.* **1976**, *18*, 225–255.

41. Sivaev, I. B.; Bregadze, V. I. *Coord. Chem. Rev.* **2014**, *270-271*, 75–88.

42. Childs, R. F.; Mulholland, D. L.; Nixon, A. *Can. J. Chem.* **1982**, *60*, 801–808.

43. Mayer, R. J.; Hampel, N.; Ofial, A. R. *Chem. Eur. J.* **2021**, *27*, 4070–4080.

44. Bentley, J. N.; Elgadi, S. A.; Gaffen, J. R.; Demay-Drouhard, P.; Baumgartner, T.; Caputo, C. B. *Organometallics* **2020**, *39*, 3645–3655.

45. Gaffen, J. R.; Bentley, J. N.; Torres, L. C.; Chu, C.; Baumgartner, T.; Caputo, C. B. *Chem.* **2019**, *5*, 1567–1583.

46. Lawson, J. R.; Melen, R. L., Recent developments and applications of Lewis acidic boron reagents. In *Organometallic Chemistry: Volume 41*, The Royal Society of Chemistry: 2017; Vol. 41, p 1–27.

47. Massey, A. G.; Park, A. J. *J. Org. Chem.* **1964**, *2*, 245–250.

48. Lawson, J. R.; Melen, R. L. *Inorg. Chem.* **2017**, *56*, 8627–8643.

49. Chen, E. Y.-X.; Marks, T. J. *Chem. Rev.* **2000**, *100*, 1391–1434.

50. Chen, Y.-X.; Metz, M. V.; Li, L.; Stern, C. L.; Marks, T. J. *J. Am. Chem. Soc.* **1998**, *120*, 6287–6305.

51. Li, L.; Marks, T. J. *Organometallics* **1998**, *17*, 3996–4003.

52. Vanka, K.; Chan, M. S. W.; Pye, C. C.; Ziegler, T. *Organometallics* **2000**, *19*, 1841–1849.

53. Braunschweig, H.; Kupfer, T. *Chem. Commun.* **2011**, *47*, 10903–10914.

54. Braunschweig, H.; Kupfer, T. *Chem. Commun.* **2008**, 4487–4489.

55. Braunschweig, H.; Damme, A.; Gamon, D.; Kelch, H.; Krummenacher, I.; Kupfer, T.; Radacki, K. *Chem. Eur. J.* **2012**, *18*, 8430–8436.

56. Braunschweig, H.; Fernández, I.; Frenking, G.; Kupfer, T. *Angew. Chem. Int. Ed.* **2008**, *47*, 1951–1954.

57. Bertermann, R.; Braunschweig, H.; Dewhurst, R. D.; Hörl, C.; Kramer, T.; Krummenacher, I. *Angew. Chem. Int. Ed.* **2014**, *53*, 5453–5457.

58. Braunschweig, H.; Damme, A.; Jimenez-Halla, J. O. C.; Hörl, C.; Krummenacher, I.; Kupfer, T.; Mailänder, L.; Radacki, K. *J. Am. Chem. Soc.* **2012**, *134*, 20169–20177.

59. Zhang, Z.; Edkins, R. M.; Haehnel, M.; Wehner, M.; Eichhorn, A.; Mailänder, L.; Meier, M.; Brand, J.; Brede, F.; Müller-Buschbaum, K.; Braunschweig, H.; Marder, T. B. *Chem. Sci.* **2015**, *6*, 5922–5927.

60. Adachi, Y.; Arai, F.; Jäkle, F. *Chem. Commun.* **2020**, *56*, 5119–5122.

61. Sato, K.; Tan, T. T. Y.; Schäfers, F.; Hahn, F. E.; Stephan, D. W. *Dalton Trans.* **2017**, *46*, 16404–16407.

62. Piers, W. E.; Bourke, S. C.; Conroy, K. D. *Angew. Chem. Int. Ed.* **2005**, *44*, 5016–5036.

63. De Vries, T. S.; Prokofjevs, A.; Vedejs, E. *Chem. Rev.* **2012**, *112*, 4246–4282.

64. Scherpf, T.; Feichtner, K.-S.; Gessner, V. H. *Angew. Chem. Int. Ed.* **2017**, *56*, 3275–3279.

65. Cheng, J.; Handoo, K. L.; Parker, V. D. *J. Am. Chem. Soc.* **1993**, *115*, 2655–2660.

66. Tseng, H.-C.; Shen, C.-T.; Matsumoto, K.; Shih, D.-N.; Liu, Y.-H.; Peng, S.-M.; Yamaguchi, S.; Lin, Y.-F.; Chiu, C.-W. *Organometallics* **2019**, *38*, 4516-4521.

67. Eisenberger, P.; Crudden, C. M. *Dalton Trans.* **2017**, *46*, 4874–4887.

68. Devillard, M.; Brousses, R.; Miqueu, K.; Bouhadir, G.; Bourissou, D. *Angew. Chem. Int. Ed.* **2015**, *54*, 5722-5726.

69. Yang, W.; Krantz, K. E.; Freeman, L. A.; Dickie, D. A.; Molino, A.; Kaur, A.; Wilson, D. J. D.; Gilliard Jr., R. J. *Chem. Eur. J.* **2019**, *25*, 12512–12516.

70. Farrell, J. M.; Hatnean, J. A.; Stephan, D. W. *J. Am. Chem. Soc.* **2012**, *134*, 15728–15731.

71. Wood, T. K.; Piers, W. E.; Keay, B. A.; Parvez, M. *Chem. Commun.* **2009**, 5147–5149.

72. Wade, C. R.; Broomsgrove, A. E. J.; Aldridge, S.; Gabbaï, F. P. *Chem. Rev.* **2010**, *110*, 3958–3984.

73. Hudnall, T. W.; Gabbaï, F. P. *Chem. Commun.* **2008**, 4596–4597.

74. Lin, Y.-F.; Chiu, C.-W. *Chem. Lett.* **2017**, *46*, 913–922.

75. Shen, C.-T.; Liu, Y.-H.; Peng, S.-M.; Chiu, C.-W. *Angew. Chem. Int. Ed.* **2013**, *52*, 13293-13297.

76. Franz, D.; Szilvási, T.; Pöthig, A.; Deiser, F.; Inoue, S. *Chem. Eur. J.* **2018**, *24*, 4283–4288.

77. Vidovic, D.; Findlater, M.; Cowley, A. H. *J. Am. Chem. Soc* **2007**, *129*, 8436-8437.

78. Hopkinson, M. N.; Richter, C.; Schedler, M.; Glorius, F. *Nature* **2014**, *510*, 485–496.

79. Farrell, J. M.; Stephan, D. W. *Angew. Chem. Int. Ed.* **2015**, *54*, 5214–5217.

80. Tanaka, N.; Shoji, Y.; Hashizume, D.; Sugimoto, M.; Fukushima, T. *Angew. Chem. Int. Ed.* **2017**, *56*, 5312–5316.

81. Tsurumaki, E.; Hayashi, S.-y.; Tham, F. S.; Reed, C. A.; Osuka, A. *J. Am. Chem. Soc.* **2011**, *133*, 11956–11959.

82. Loh, Y. K.; Porteous, K.; Fuentes, M. Á.; Do, D. C. H.; Hicks, J.; Aldridge, S. *J. Am. Chem. Soc.* **2019**, *141*, 8073–8077.

83. Heitkemper, T.; Sindlinger, C. P. *Chem. Eur. J.* **2020**, *26*, 11684–11689.

84. Bosdet, M. J. D.; Piers, W. E. *Can. J. Chem.* **2009**, *87*, 8–29.

85. Bélanger-Chabot, G.; Braunschweig, H.; Roy, D. K. *Eur. J. Chem* **2017**, *2017*, 4353–4368.

86. McConnell, C. R.; Liu, S.-Y. *Chem. Soc. Rev.* **2019**, *48*, 3436–3453.

87. Bourget-Merle, L.; Lappert, M. F.; Severn, J. R. *Chem. Rev.* **2002**, *102*, 3031–3066.

88. Qian, B.; Baek, S. W.; Smith Iii, M. R. *Polyhedron* **1999**, *18*, 2405–2414.

89. Cui, C.; Roesky, H. W.; Schmidt, H.-G.; Noltemeyer, M.; Hao, H.; Cimpoesu, F. *Angew. Chem. Int. Ed.* **2000**, *39*, 4274–4276.

90. Cowley, A. H.; Lu, Z.; Jones, J. N.; Moore, J. A. *J. Org. Chem.* **2004**, *689*, 2562–2564.

91. Loudet, A.; Burgess, K. *Chem. Rev.* **2007**, *107*, 4891–4932.

92. Bonnier, C.; Piers, W. E.; Parvez, M.; Sorensen, T. S. *Chem. Commun.* **2008**, 4593–4595.

93. Gilroy, J. B.; Ferguson, M. J.; McDonald, R.; Patrick, B. O.; Hicks, R. G. *Chem. Commun.* **2007**, 126–128.

94. Barbon, S. M.; Price, J. T.; Reinkeluers, P. A.; Gilroy, J. B. *Inorg. Chem.* **2014**, *53*, 10585–10593.

95. Gilroy, J. B.; Otieno, P. O.; Ferguson, M. J.; McDonald, R.; Hicks, R. G. *Inorg. Chem.* **2008**, *47*, 1279–1286.

96. Gök, Y. *Dyes Pigm.* **1989**, *11*, 101–107.

97. Hansen, M. B.; Nielsen, S. E.; Berg, K. *J. Immunol. Methods* **1989**, *119*, 203–210.

98. Denizot, F.; Lang, R. *J. Immunol. Methods* **1986**, *89*, 271–277.

99. Green, L. M.; Reade, J. L.; Ware, C. F. *J. Immunol. Methods* **1984**, *70*, 257–268.

100. Mosmann, T. *J. Immunol. Methods* **1983**, *65*, 55–63.

101. Chang, M.-C.; Dann, T.; Day, D. P.; Lutz, M.; Wildgoose, G. G.; Otten, E. *Angew. Chem. Int. Ed.* **2014**, *53*, 4118-4122.

102. Kabir, E.; Patel, D.; Clark, K.; Teets, T. S. *Inorg. Chem.* **2018**, *57*, 10906–10917.

103. Chang, M.-C.; Otten, E. *Chem. Commun.* **2014**, *50*, 7431–7433.

104. Chang, M.-C.; Chantzis, A.; Jacquemin, D.; Otten, E. *Dalton Trans.* **2016**, *45*, 9477–9484.

105. Chang, M.-C.; Roewen, P.; Travieso-Puente, R.; Lutz, M.; Otten, E. *Inorg. Chem.* **2015**, *54*, 379–388.

106. Barbon, S. M.; Reinkeluers, P. A.; Price, J. T.; Staroverov, V. N.; Gilroy, J. B. *Chem. Eur. J.* **2014**, *20*, 11340–11344.

107. Frisch, M. J.; Trucks, G. W.; Schlegel, H. B.; Scuseria, G. E.; Robb, M. A.; Cheeseman, J. R.; Scalmani, G.; Barone, V.; Petersson, G. A.; Nakatsuji, H.; Li, X.; Caricato, M.; Marenich, A. V.; Bloino, J.; Janesko, B. G.; Gomperts, R.; Mennucci, B.; Hratchian, H. P.; Ortiz, J. V.; Izmaylov, A. F.; Sonnenberg, J. L.; Williams; Ding, F.; Lipparini, F.; Egidi, F.; Goings, J.; Peng, B.; Petrone, A.; Henderson, T.; Ranasinghe, D.; Zakrzewski, V. G.; Gao, J.; Rega, N.; Zheng, G.; Liang, W.; Hada, M.; Ehara, M.; Toyota, K.; Fukuda, R.; Hasegawa, J.; Ishida, M.; Nakajima, T.; Honda, Y.; Kitao, O.; Nakai, H.; Vreven, T.; Throssell, K.; Montgomery Jr., J. A.; Peralta, J. E.; Ogliaro, F.; Bearpark, M. J.; Heyd, J. J.; Brothers, E. N.; Kudin, K. N.; Staroverov, V. N.; Keith, T. A.; Kobayashi, R.; Normand, J.; Raghavachari, K.; Rendell, A. P.; Burant, J. C.; Iyengar, S. S.; Tomasi, J.; Cossi, M.; Millam, J. M.; Klene, M.; Adamo, C.; Cammi, R.; Ochterski, J. W.; Martin, R. L.; Morokuma, K.; Farkas, O.; Foresman, J. B.; Fox, D. J. *Gaussian 09, Revision, B.01*, Wallingford, CT, 2009.

108. Barbon, S. M.; Staroverov, V. N.; Gilroy, J. B. *J. Org. Chem.* **2015**, *80*, 5226-5235.

109. Van Belois, A.; Maar, R. R.; Workentin, M. S.; Gilroy, J. B. *Inorg. Chem.* **2019**, *58*, 834–843.

110. Buguis, F. L.; Maar, R. R.; Staroverov, V. N.; Gilroy, J. B. *Chem. Eur. J.* **2021**, *27*, 2854–2860.

111. Maar, R. R.; Zhang, R.; Stephens, D. G.; Ding, Z.; Gilroy, J. B. *Angew. Chem. Int. Ed.* **2019**, *58*, 1052-1056.

112. Maar, R. R.; Barbon, S. M.; Sharma, N.; Groom, H.; Luyt, L. G.; Gilroy, J. B. *Chem. Eur. J.* **2015**, *21*, 15589–15599.

113. Barbon, S. M.; Buddingh, J. V.; Maar, R. R.; Gilroy, J. B. *Inorg. Chem.* **2017**, *56*, 12003–12011.

114. Maar, R. R.; Hoffman, N. A.; Staroverov, V. N.; Gilroy, J. B. *Chem. Eur. J.* **2019**, *25*, 11015–11019.

115. Segawa, Y.; Suzuki, Y.; Yamashita, M.; Nozaki, K. *J. Am. Chem. Soc.* **2008**, *130*, 16069–16079.

Chapter 2

2   Electronic Structure Modulation in Cationic Boron Formazanate Complexes

Adapted from:

1. Maar, R.R.[‡]; Katzman, B.D.[‡]; Boyle, P.N.; Staroverov, V.N.; Gilroy, J.B. *Angew. Chem. Int. Ed.* **2021**, 60, 5152–5156. (‡ = Shared first authorship)

2.1   Introduction

Main-group elements that form stable complexes with unusual structure, bonding and reactivity have paved the way for several applications including catalysis, small molecule activation and development of functional materials.[1-5] Strategies for material design have brought the necessity of incorporating main-group elements into π-conjugated frameworks for the development of novel optoelectronic materials.[6] The inherent electron deficiency of boron has made it an attractive candidate for combination with organic fragments to modulate frontier molecular orbital energies for organic electronics applications.[7-9] Tuning the optoelectronic properties of these complexes requires the enhancement of the boron Lewis acidity. There are several strategies used, including installing anti-aromatic scaffolds surrounding boron[10-13] or using electron withdrawing substituents.[14] A relatively unexplored strategy is varying the charge and coordination number of boron atoms, [15, 16] and isolating two-[17-20], three-[21-28] and four-coordinate[29-35] cations and dications such as **2.1+–2.6²⁺**.[15, 36-40]
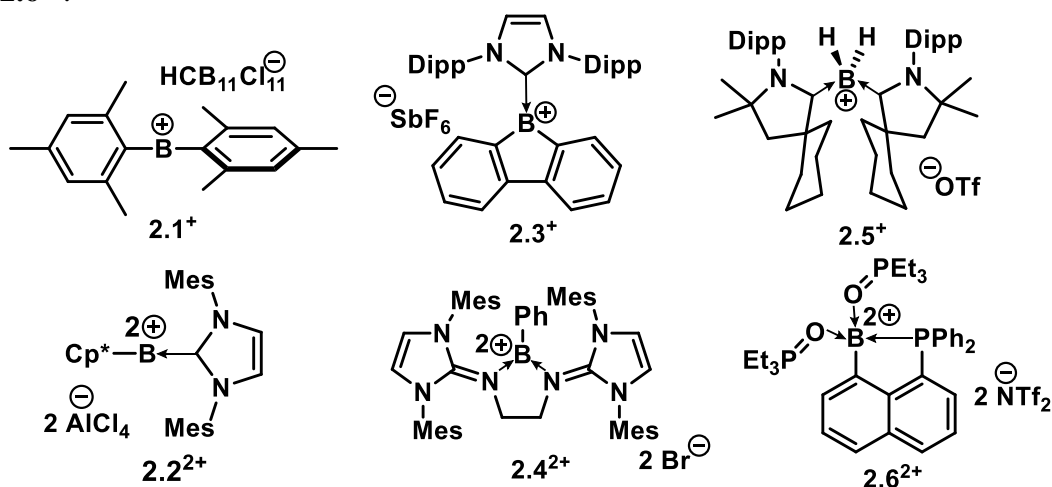
Using cationic boron species is well established in the realm of catalysis,[41] and fundamental research on structure and bonding of cationic boron compounds is well developped,[42] but work in the direction of complexes designed for optoelectronic materials is unexplored. An excellent platform for the expansion of main-group chemistry is the use of formazanate ligands.[43-50] Boron difluoride (BF_2) formazanate dyes exhibit exceptional tunability through substituent modification,[51-54] and find various applications as cell imaging agents,[55] electrochemiluminecsent emitters,[56, 57] and precursors to a wide variety of BN heterocycles with unique structure and properties.[58-60]

Herein, the effect of boron charge variation (0, +1 or +2) and coordination number (three or four) on the electronic structure and properties is examined for boron formazanate complexes **2.9−2.15**. This systematic demonstration is the first study for BN heterocycles and the principles can be extended to other main group elements and similar ligand families (*e.g.,* dipyrrin, *aza*-dipyrrin and β-diketiminates).

2.2   Results

2.2.1   Synthesis

1,5-(*p*-tolyl)-3-phenylformazan (**2.7**) was prepared using an established procedure[61] and was used as the parent formazan for all reactions in this work. BPhF formazanate **2.8** was prepared utilizing a slightly modified method from the traditional BF_2 synthesis. The parent formazan was refluxed in a combination of CH_2Cl_2/CH_3CN, in the presence of N(iPr)$_2$Et, followed by the addition of excess $KBPhF_3$ and TMSCl for 36 h (Scheme 2.1). The reaction resulted in a colour change from red to purple and the crude product was purified using column chromatography to afford **2.8** in 75% yield. This transformation was confirmed by the absence of the characteristic 1,5-(*p*-tolyl)-3-phenylformazan N-H resonance in the ^{1}H NMR spectrum (δ = 15.51) and the appearance of a signal in the ^{19}F{^{1}H} (δ = −164.6) and ^{11}B{^{1}H} (δ = 2.9) NMR spectra. A halide exchange was performed using one equiv. BCl_3 to quantitatively convert **2.8** to BPhCl formazanate **2.9** as an air and moisture sensitive solid. The exchange was confirmed with the disappearance of the ^{19}F{^{1}H} resonance and shifting of the ^{11}B{^{1}H} NMR signal to 2.4 ppm.
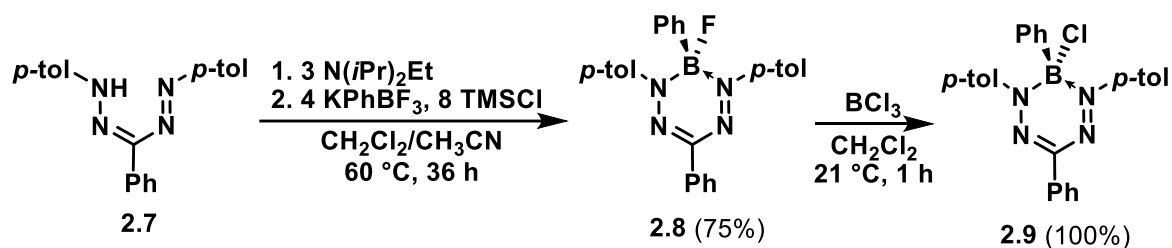
Scheme 2.1. Synthesis of BPhF **2.8** and BPhCl **2.9** formazanates.

Complex **2.9** was treated with an equimolar amount of AlCl$_3$ to form three-coordinate (borenium) cation **2.10$^+$** as an air and moisture sensitive dark purple solid in 98% yield (Scheme 2.2). A broad signal, indicative of three-coordinate boron, appeared in the ^{11}B{^{1}H} NMR spectrum (δ = 35.5) and a sharp singlet at 103.6 ppm appeared in the ^{27}Al{^{1}H} NMR spectrum, representing the [AlCl$_4$]$^-$ counterion. Attempts to form a four-coordinate adduct upon the reaction between **2.10$^+$** and 4-dimethylaminopyridine (DMAP) were thwarted by the regeneration of BPhCl formazanate **2.9** and a DMAP·AlCl$_3$ adduct. Alternatively, **2.9** was treated first with silver trifluoromethanesulfonate (AgOTf) followed by DMAP to afford DMAP-supported boronium cation **2.11$^+$** as a dark red sold in 92% yield. Boronium cation **2.11$^+$** exhibited a broad singlet in the ^{11}B{^{1}H} NMR spectrum (δ = 2.9 ppm) and a sharp singlet in the ^{19}F{^{1}H} NMR spectrum (δ = –77.5) representing OTf$^-$.
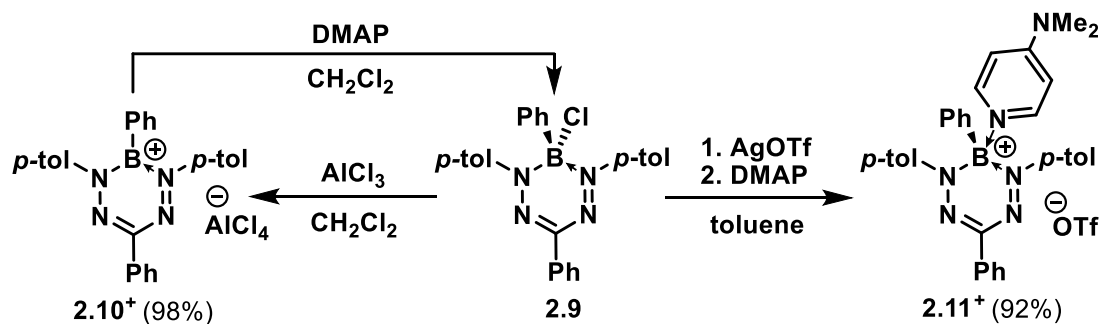
Scheme 2.2. Synthesis of borenium cation **2.10$^+$** and boronium cation **2.11$^+$**.

BCl$_2$ formazanate **2.12**, prepared via addition of excess BCl$_3$ to a BF$_2$ formazanate,[60] is also a useful precursor to form cationic adducts. To make oxygen-bound cationic boron formazanates, **2.12** was first treated with lithium dibenzoylmethanate (Scheme 2.3) to afford boronium cation **2.13$^+$** as a microcrystalline red solid in 94% yield with a ^{11}B{^{1}H}

NMR chemical shift at 1.8 ppm. In addition, **2.12** was treated with two equiv. of AgOTf, generating a B(OTf)$_2$ formazanate *in situ*, followed by the addition of bis(diphenylphosphinomethane) oxide (dppmo) to afford complex **2.14²⁺**, a boron dication, as an extremely moisture/air sensitive orange solid in 88% yield. Dication **2.14²⁺** displayed a characteristically broad $^{11}B\{^1H\}$ NMR signal ($\delta = 0.0$) and a singlet in the $^{31}P\{^1H\}$ NMR spectrum ($\delta = 54.9$). The chelating dppmo donor ligand was crucial for stabilization of **2.14²⁺**. Neutral B(OCH$_3$)$_2$ formazanate **2.15** was prepared upon addition of excess methanol to **2.15,** according to a literature procedure.[60] Compound **2.15** was added to this set of compounds to serve as a *neutral* oxygen-bound formazanate complex.
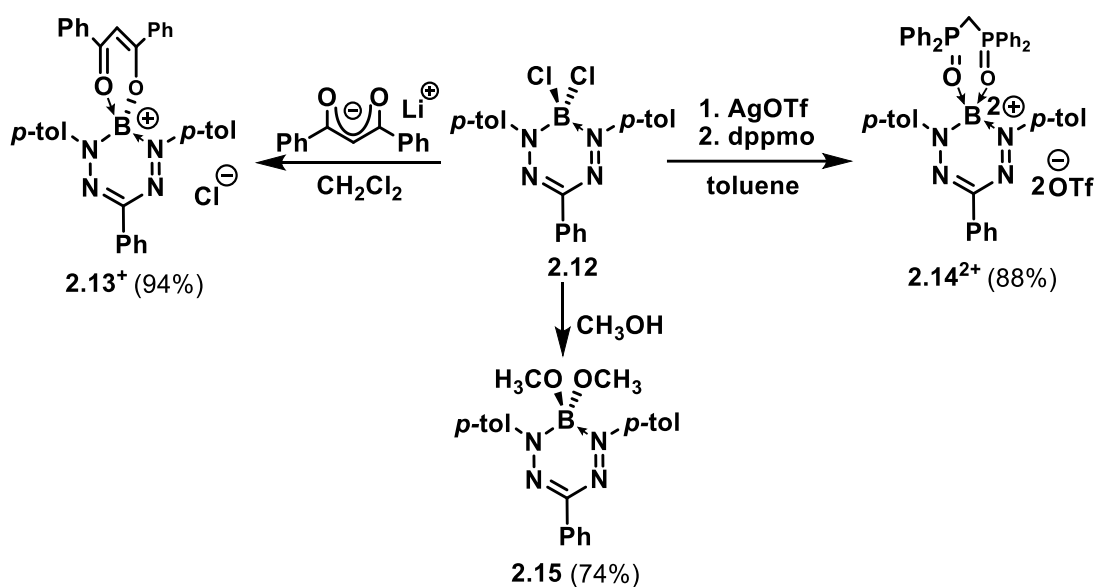
Scheme 2.3. Synthesis of four coordinate oxygen-bound boron formazanates derived from a BCl$_2$ formazanate **2.12** precursor.

2.2.2   X-ray Crystallography

Single crystals were obtained for compounds **2.9**, **2.10⁺**, **2.13⁺** and **2.14²⁺** and were analyzed using X-ray diffraction to elucidate their solid-state structures (Figure 2.1). Crystals were grown by layering a CH$_2$Cl$_2$ (**2.10⁺**) or CDCl$_3$ (**2.9**) solution with *n*-pentane, a CH$_2$Cl$_2$ solution (**2.14²⁺**) with 1:1 toluene:hexanes or a CDCl$_3$ solution (**2.13⁺**) with hexanes. Repeated attempts, using various solvent combinations and techniques, were made to produce single crystals of **2.11⁺**, but none suitable for analysis were obtained.
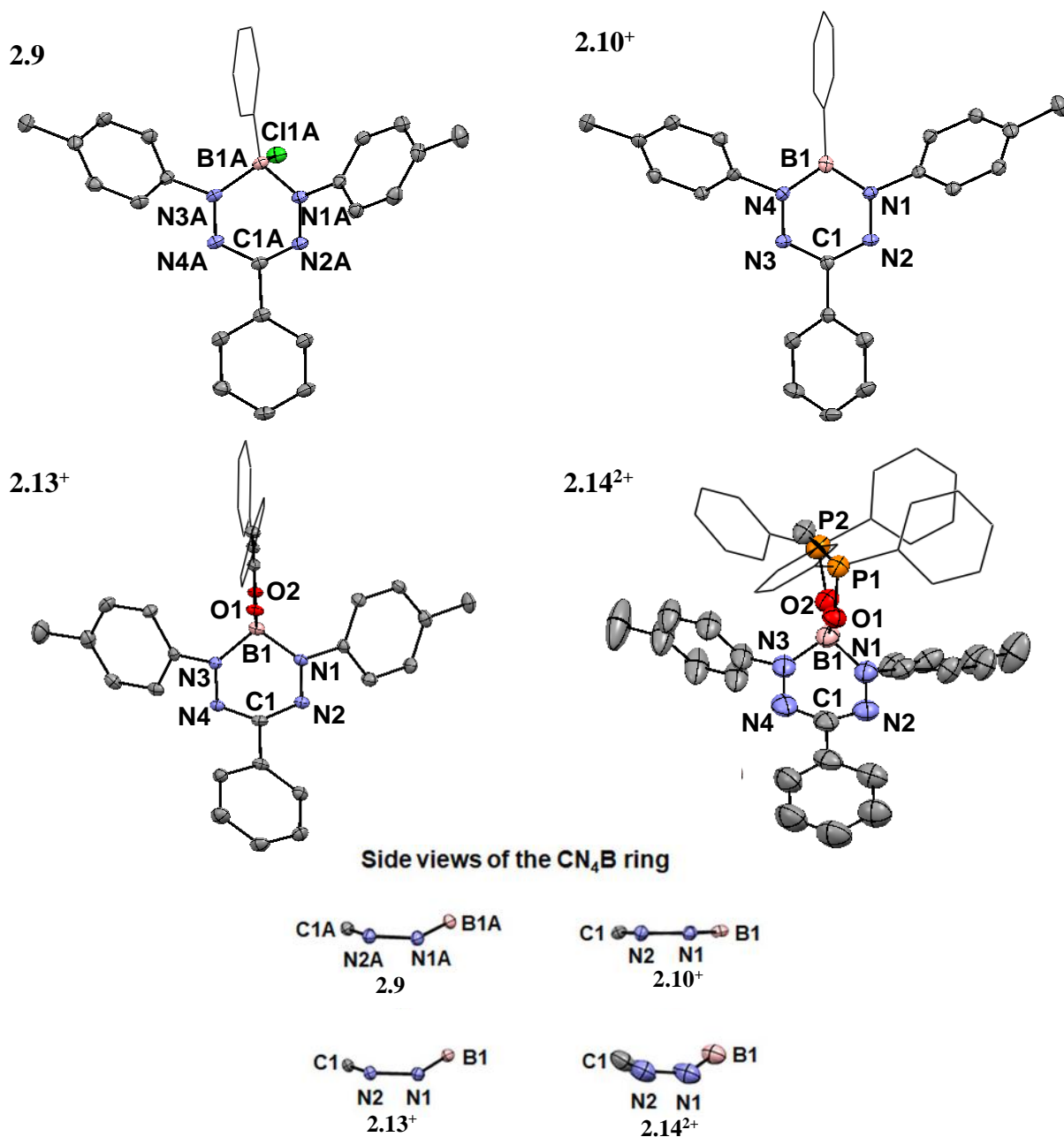
Figure 2.1. Solid-state structures of compounds **2.9**, **2.10⁺**, **2.13⁺**, and **2.14²⁺**. Anisotropic displacement ellipsoids are shown at the 50% probability level. Hydrogen atoms and counterions are omitted and selected phenyl groups are shown as wireframe for clarity. Side views of N1-N2-C1-N3-N4-B1 (CN₄B) formazanate core are shown.

All C-N and N-N bond lengths on the formazanate backbone for compounds **2.9**, **2.10⁺**, **2.13⁺** and **2.14²⁺** were between 1.334(7) to 1.356(7) Å and 1.307(2) to 1.325(6) Å, respectively. These bond lengths fall between those expected of single and double bond lengths of the atoms involved,[36] thus indicating a degree of delocalization across the formazanate backbone, consistent with previously reported BF₂ formazanate complexes.

The analysis reveals that nitrogen atoms of the formazanate backbone (N_4: N1, N2, N3, N4) are planar, and there is a varying degree of displacement of the boron atom from this plane. Of the four compounds examined, **2.9**, **2.13$^+$** and **2.14^{2+}** have a sp^3 hybridized boron center, whilst borenium cation **2.10$^+$** is sp^2 hybridized. The sp^3 boron atom in **2.9**, **2.13$^+$** and **2.14^{2+}** is displaced from the formazanate backbone by 0.380(3)–0.619(7) Å, but the sp^2 boron atom (**2.10$^+$**) is minimally displaced by 0.041(4) Å from the same plane. Upon closer examination of the B1-N1 bond lengths, **2.10$^+$** contains a significantly shorter length (1.451(4) Å) then **2.9**, **2.13$^+$** and **2.14^{2+}**, which have lengths ranging from 1.523(6) − 1.557(2) Å. The shorter bond length suggests that the B-N bond order is greater than 1 in **2.10$^+$**. As the boron is sp^2 hybridized, and minimally displaced from the N_4 plane, it is likely participating in π-electron delocalization via resonance, because of boron's empty p orbital.

Another parameter measured is the angle between the N_4 plane and the *N*-aryl substituents of the formazanate backbone, known as the dihedral angle. This value ranges from 48.59(7) to 83.77(10)° in **2.9**, **2.10$^+$**, **2.13$^+$** and **2.14^{2+}**. All bond lengths and angles are summarized in Table 2.1.

Table 2.1. Selected bond lengths (Å), bond angles (°) and structural metrics extracted from the solid-state structures of boron formazanates **2.9**, **2.10$^+$**, **2.13$^+$** and **2.14^{2+}**.

	2.9^a		**2.10$^+$**	**2.13$^+$**	**2.14^{2+}**
	Conformer A	Conformer B			
N1-N2	1.313(2)	1.307(2)	1.321(3)	1.310(6)	1.311(5)
N3-N4	1.307(2)	1.311(2)	1.323(3)	1.325(6)	1.318(6)
N2-C1	1.341(2)	1.346(2)	1.343(3)	1.356(7)	1.353(6)
N4-C1	1.343(2)	1.338(2)	1.341(3)	1.334(7)	1.339(6)
B1-N1	1.556(2)	1.557(2)	1.457(4)	1.544(8)	1.523(6)
B1-N3	1.555(2)	1.560(2)	1.444(4)	1.542(7)	1.520(7)
B1-O1	–	–	–	1.475(7)	1.492(6)
B1-O2	–	–	–	1.439(7)	1.445(6)
Dihedral angles^b	59.60(6), 48.59(7)	49.88(7), 54.56(6)	45.13(10), 53.12(8)	50.16(21), 53.88(20)	52.13(21), 83.77(19)
Boron displacement^c	0.499(3)	0.380(3)	0.041(4)	0.536(8)	0.619(7)

^{a}The asymmetric unit of complex **2.9** contained two unique conformers. ^{b}Defined as the angle between the *N*-aryl substituents and the N_4 (N1-N2-N3-N4) plane of the formazanate ligand backbone. ^{c}Defined as the distance between B1 and the N_4 (N1-N2-N3-N4) plane of the formazanate ligand backbone.

2.2.3   UV-Visible Absorption Spectroscopy

To probe the electronic properties of neutral and cationic boron formazanate complexes, and as a means of observing the influence of structural variation of such complexes, all compounds were characterized using UV-vis spectroscopy. Commonly, absorption spectra cannot be reliably obtained for cationic boron complexes due to their instability in dilute solution due to trace impurities in the solvent. Therefore, the solvents used for characterization of the cations were stirred over and distilled from CaH_2 and $AlCl_3$ at least twice prior to their use. The UV-vis spectra were collected in two sets. **2.9**, **2.10**$^+$ and **2.11**$^+$ were collected in toluene (Figure 2.2), while **2.13**$^+$, **2.14**$^{2+}$ and **2.15** were collected in CH_2Cl_2 (Figure 2.3). All experimental and theoretical spectral data are summarized in Table 2.2 in Section 2.2.4.

The UV-visible absorption spectra of compounds **2.9**, **2.10**$^+$ and **2.11**$^+$ (Figure 2.2) contain neutral four coordinate BPhCl formazanate, three-coordinate cationic BPh$^+$ formazanate and four-coordinate cationic BPhDMAP$^+$ formazanate, respectively. This allows for direct spectroscopic comparison of the effect of electronic structure on the properties, accounting for both coordination number (three or four) and charge (0 or +1). All compounds exhibit broad absorptions in the visible region, with molar extinction coefficients (ε) ranging from 6,300–12,100 M^{-1} cm^{-1}. **2.9** exhibits a wavelength of max absorption (λ_{max}) at 521 nm, which is consistent with numerous reported neutral four-coordinate boron formazanate adducts. In comparison, four-coordinate **2.11**$^+$ shows a slight hypsochromic ('blue') shift ($\lambda_{max} = 510$ nm), and a reduction in ε from 12,100 to 8,300 M^{-1} cm^{-1}. Examination of three coordinate cation **2.10**$^+$ instead reveals a large bathochromic ('red') shift ($\lambda_{max} = 597$ nm) compared to both complexes **2.9** and **2.11**$^+$, and a further reduction in absorption intensity to 6,300 M^{-1} cm^{-1}. The vast observed differences between these complexes strongly suggest that the exact coordination number and charge at boron significantly alter the electronic structure.
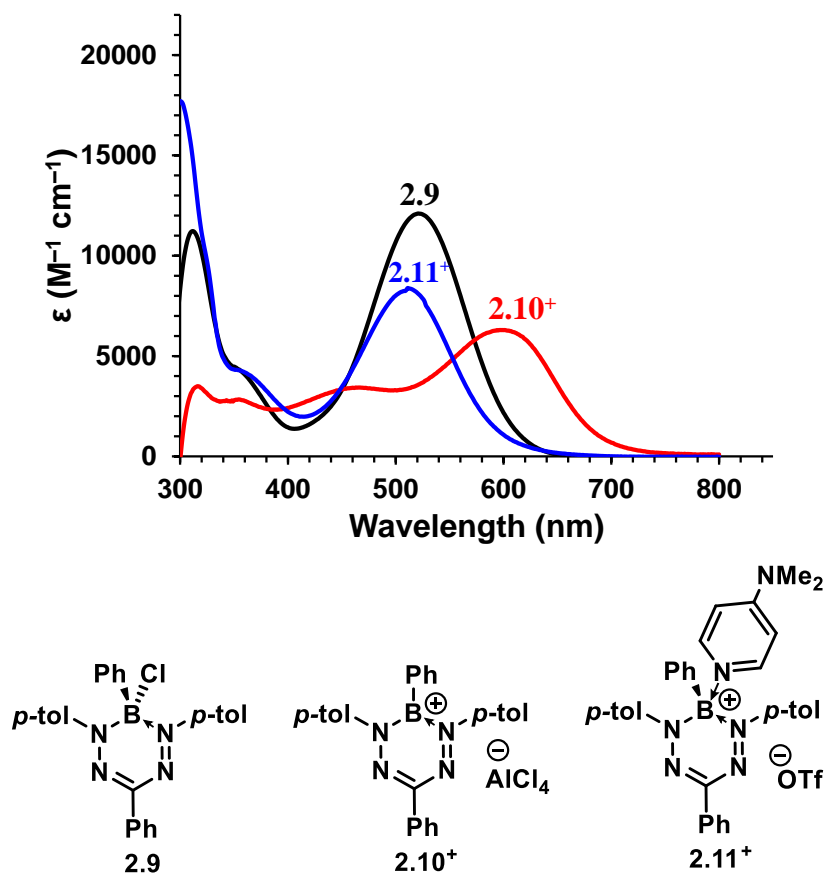
Figure 2.2. UV-vis absorption spectra of 10^{-6} M dry and degassed toluene solutions of complexes **2.9**, **2.10⁺** and **2.11⁺**.

In the CH_2Cl_2 set (Figure 2.3), four coordinate adducts **2.13⁺**, **2.14²⁺** and **2.15** were compared to evaluate the effect of increased positive charge of boron on electronic structure. **2.15** was selected to serve as a neutral oxygen-bound neutral boron formazanate complex. Complexes **2.15**, **2.13⁺** and **2.14²⁺** featured low energy absorption maxima at 549 nm (ε = 18,000 M^{-1} cm^{-1}), 540 nm (ε = 5,900 M^{-1} cm^{-1}), and 505 nm (ε = 9,400 M^{-1} cm^{-1}) respectively. Upon an increase of positive charge (neutral → cationic → dicationic), there is a blue shift in the absorption maxima. There is also a drastic decrease in the ε values while transitioning from a neutral to cationic boron center.
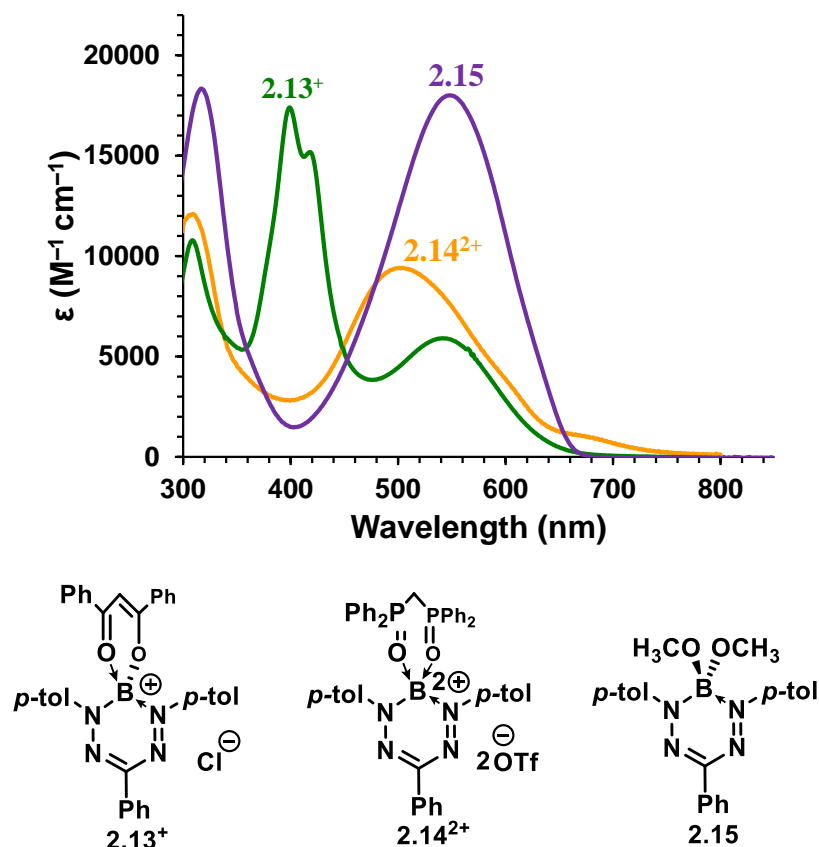
Figure 2.3. UV-vis absorption spectra of 10^{-6} M dry and degassed CH_2Cl_2 solutions of oxygen-bound boron complexes **2.13⁺**, **2.14²⁺** and **2.15**.

2.2.4   Computational Studies

To provide insight on the UV-visible spectroscopic trends, we investigated complexes **2.9**–**2.11⁺** and **2.13⁺**–**2.15** using Density Functional Theory (DFT). The computational methodology used is outlined in Section 2.4.4. The theoretical low-energy absorptions and oscillator strengths can be found in Table 2.2. In all cases, time-dependent DFT (TDDFT) calculations revealed that the dominant orbital pair resulting in the low-energy absorption bands in the UV-vis spectra (Figures 2.3 and 2.4) involved the HOMO and LUMO. The frontier molecular orbital energies decrease with increasing cationic charge within each series of compounds (**2.9**–**2.11⁺** and **2.13⁺**–**2.15**). Furthermore, all the low energy excitations are generally of π→π* type.

Table 2.2. Experimental and calculated spectroscopic properties of complexes **2.9**, **2.10⁺** and **2.11⁺** and **2.13⁺**, **2.14²⁺** and **2.15** recorded in toluene or CH_2Cl_2 solutions. The absorption band maxima were calculated by linear-response TDDFT using the PBE1PBE/DGDZVP2 method and the CPCM model of implicit solvation.

Complex	Solvent	Experiment		Theory		
		λ_{max} (nm)	ε (M^{-1} cm^{-1})	λ_{max} (nm)	Intensity	Transition
2.9	toluene	521	12,100	507	0.417	HOMO→LUMO
2.10⁺	toluene	597	6,300	637[a]	0.259	HOMO→LUMO
2.11⁺	toluene	510	8,300	502	0.401	HOMO→LUMO
2.13⁺	CH_2Cl_2	540	5,900	569[a]	0.134	HOMO→LUMO
2.14²⁺	CH_2Cl_2	505	9,400	514	0.308	HOMO→LUMO
2.15	CH_2Cl_2	549	18,000	546	0.500	HOMO→LUMO

[a]These theoretical values are overestimated relative to the experiment because PBE1PBE is unable to accurately describe geometries and/or energies of excited states with at least partial charge-transfer character.

The calculated HOMOs and LUMOs of **2.9**, **2.10⁺** and **2.11⁺** and orbital energy values (in eV) can be found in Figure 2.4. Four-coordinate complexes **2.9** and **2.11⁺** have strikingly similar HOMO and LUMO compositions. The HOMOs span the N_4 plane, *N*-aryl substituents, and the phenyl (R^3) substituent. The LUMO only spans the N_4 plane and *N*-aryl substituents for both complexes. The orbital studies suggest that the modest high energy shift ($\Delta\lambda_{max} = -11$ nm) observed in the absorption spectra exhibited by **2.11⁺** relative to **2.9** may be attributed to the positive charge on boron in **2.11⁺**. Compound **2.10⁺** also has a positive charge on boron, but a large shift ($\Delta\lambda_{max} = +76$ nm) in comparison to **2.9**. This can be reasonably attributed to the planar CN_4B formazanate ring, allowing the HOMO to extend into the boron-bound phenyl substituent. The HOMO-LUMO energy gap for **2.10⁺** is narrowed to 2.64 eV, compared to 3.04 eV and 3.05 eV for **2.9** and **2.11⁺** respectively, because of the extended π-conjugation. The LUMO energy (-5.45 eV) of three-coordinate **2.10⁺** is decreased when compared to **2.9** (-3.16 eV) and **2.11⁺** (-4.29 eV), which is expected in borenium cations.
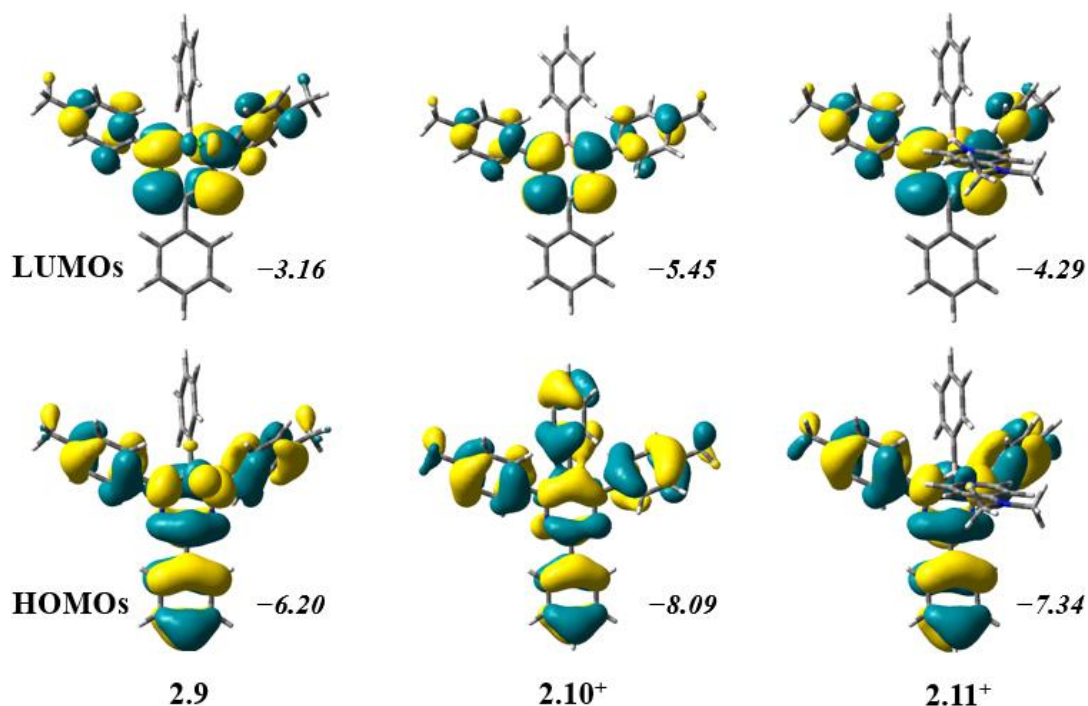
Figure 2.4. Frontier molecular orbitals of **2.9, 2.10⁺** and **2.11⁺** and their energies (in eV) for toluene solvated complexes using the PBE1PBE/DGDZVP2 SCRF = CPCM method.

The calculated HOMOs and LUMOs of **2.13⁺**, **2.14²⁺** and **2.15** and orbital energy values (in eV) can be found in Figure 2.5. The non-planarity of the formazanate CN_4B ring results in qualitatively similar HOMOs for all three complexes. As a result, the low energy absorption maxima are directly correlated with the charges at boron. This is to say $\lambda_{max}(\mathbf{2.15}) > \lambda_{max}(\mathbf{2.13^+}) > \lambda_{max}(\mathbf{2.14^{2+}})$. Finally, there is a gradual reduction in HOMO and LUMO energies upon increasing cationic charge ($\mathbf{2.15} \rightarrow \mathbf{2.13^+} \rightarrow \mathbf{2.14^{2+}}$).
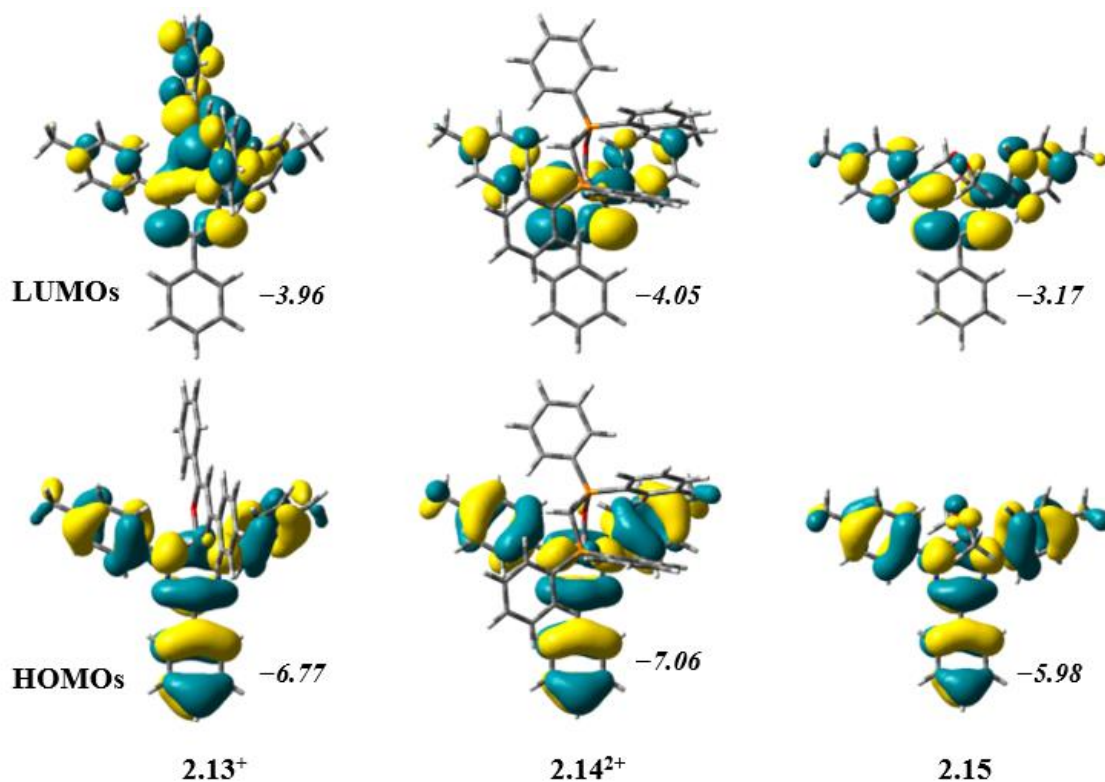
Figure 2.5. Frontier molecular orbitals of **2.13$^+$**, **2.14^{2+}** and **2.15** and their energies (in eV) for toluene solvated complexes using the PBE1PBE/DGDZVP2 SCRF = CPCM method.

Upon closer examination of the HOMO and LUMO of **2.10$^+$** and **2.13$^+$**, it appears there is a degree of charge transfer character between the boron formazanate and boron-bound substituents (Ph for **2.10$^+$** and dibenzoylmethanate for **2.13$^+$**). This analysis is supported by the overestimation of the calculated λ_{max} values (Table 2.2) for these complexes relative to the experimental values. The PBE1PBE functional is known to underestimate the energies of charge transfer excitations, rationalizing this observation.[62-64] A second charge transfer band with vibronic structure is also observed for **2.13$^+$** (λ_{max} = 400 nm, HOMO → LUMO+1).

2.3 Conclusions

In conclusion, a new series of cationic boron formazanates were synthesized and the impact of structural variation (*i.e.,* charge and coordination number) on electronic structure was investigated. TDDFT studies were used to rationalize low energy absorption trends found

in the optical spectra. An increase in cationic charge in four coordinate boron compounds (*i.e.* **2.15** to **2.13**[+] to **2.14**[2+] or **2.9** to **2.11**[+]) consistently resulted in a blue shift in the absorption spectra. Upon introduction of a planar, three coordinate borenium cation **2.10**[+], the absorption maxima red-shifted drastically due to the extended π-electron conjugation in the HOMO. Finally, the importance of the boron-bound substituent was evidenced, as the substituents in **2.10**[+] and **2.13**[+] dramatically altered the electronic structure, resulting in the lowest energy transition having charge transfer character. This work establishes methods for the design of optoelectronic molecular materials including cationic (or dicationic) boron fragments that can be applied to π-conjugated heterocycles containing main group elements.

2.4   Experimental Section

2.4.1   General Considerations

Reactions and manipulations were carried out under an N_2 atmosphere using standard glove box or Schlenk techniques unless otherwise stated. Reagents were purchased from Sigma-Aldrich or Alfa Aesar and used as received unless otherwise noted. The synthesis of 1,5-(*p*-tolyl)-3-phenylformazan[61] (**2.7**) and boron complexes **2.8** and **2.15** have been reported previously.[60] Potassium trifluorophenyl borate (KBPhF$_3$)[65] and bis(diphenylphosphinomethane) oxide[66] were prepared according to a literature procedures. *N*,*N*-diisopropylethylamine (N(*i*Pr)$_2$Et) and trimethylsilyl chloride (TMSCl) were dried over and distilled from CaH$_2$ and stored over 4 Å molecular sieves. Solvents were purchased from Caledon Laboratories, dried using an Innovative Technologies Inc. solvent purification system, collected under vacuum, and stored under an N_2 atmosphere over 4 Å molecular sieves. NMR spectra were recorded on a 400 MHz (^{1}H: 399.8 MHz; ^{11}B{^{1}H}: 128.3 MHz; ^{19}F{^{1}H}: 376.1 MHz; ^{13}C{^{1}H}: 100.5 MHz) or 600 MHz (^{1}H: 599.2 MHz; ^{13}C{^{1}H}: 150.7 MHz, ^{27}Al: 156.1 MHz) Varian INOVA spectrometer at 25 °C. ^{1}H NMR spectra were referenced to residual CHCl$_3$ (δ = 7.26) and ^{13}C{^{1}H} NMR spectra were referenced to CDCl$_3$ (δ = 77.0). ^{11}B{^{1}H} spectra were referenced to BF$_3$•OEt$_2$ (δ = 0) and ^{27}Al{^{1}H} spectra were referenced relative to Al(NO$_3$)$_3$ (δ = 0). Mass-spectrometry data were recorded in positive-ion mode using a high-resolution Thermo Scientific DFS

(Double Focusing Sector) mass spectrometer using electron impact ionization or using a Bruker microTOF II electrospray ionization spectrometer. FT-IR spectra were recorded on a PerkinElmer Spectrum Two instrument using an attenuated total reflectance accessory. UV-vis absorption spectra were recorded on a Cary 5000 UV-Vis-NIR spectrophotometer. Molar extinction coefficients were determined from the slope of a plot of absorbance against concentration using four solutions with known concentrations ranging between 8 and 73 μM.

Elemental Analysis

Data were recorded using an Elementar Vario Isotope Cube at Western University (for **2.8**) or a Elementar Vario EL Cube (for **2.9** and **2.10$^+$**) at York University. For the latter, samples were prepared in an MBraun Glovebox and sulfur levels were either below the detection limit (<0.2%) or not detected.

Proof of Purity and Identity

Novel compounds were characterized by multinuclear NMR, UV-vis and IR spectroscopy, and high-resolution mass spectrometry performed immediately upon isolation. The identity of compounds **2.9**, **2.10$^+$**, **2.13$^+$**, and **2.14^{2+}** has been further corroborated by the determination of solid-state structures. Compounds **2.8**, **2.9**, and **2.10$^+$** afforded satisfactory elemental analyses. However, as is often encountered for cationic boron compounds, thermal degradation of compounds **2.11$^+$**, **2.13$^+$**, and **2.14^{2+}** over the time period required to isolate, grind, dry, and transport these compounds for analyses thwarted multiple attempts to obtain satisfactory elemental analyses.

2.4.2   X-ray Crystallography Methods

The samples **2.9**, **2.10$^+$**, **2.13$^+$** and **2.14^{2+}** were mounted on MiTeGen polyimide micromounts with a small amount of Paratone *N* oil. X-ray diffraction measurements were made on a Bruker Kappa Axis Apex2 diffractometer at a temperature of 110 K. The data collection strategy involved a number of ω and φ scans, which collected data up to 66.172° (2θ, **2.9**), 50.46° (2θ, **2.10$^+$**), 53.488° (2θ, **2.13$^+$**), and 44.544° (2θ, **2.14^{2+}**). The frame integration was performed using SAINT.[67] The resulting raw data was scaled and absorption corrected using a multi-scan averaging of symmetry equivalent data using

SADABS[68] (**2.9**, **2.10**$^+$, **2.14**$^{2+}$) or TWINABS[69] (**2.13**$^+$). The structures were solved by using a dual space methodology using the SHELXT[70] program. All non-hydrogen atoms were obtained from the initial solution for **2.9**, **2.10**$^+$ and **2.13**$^+$. For **2.14**$^{2+}$, most non-hydrogen atoms were obtained from the initial solution. Except for atoms in the disordered phenyl ring, the remaining atomic positions were recovered from difference Fourier maps.

Analysis of Twinning:

For **2.13**$^+$: Initial indexing indicated that the sample crystal **2.13**$^+$ was non-merohedrally twinned.

The twin law for the first component of **2.13**$^+$ was determined to be:

$$\begin{matrix} -1.00003 & -0.00015 & 0.00002 \\ 0.00029 & -0.99989 & 0.00015 \\ 0.93734 & 0.97031 & 0.99992 \end{matrix}$$

which represents a $-179.98°$ rotation about the [001] in reciprocal space (approximately the [112] in direct space). The twin fraction for the minor component of **25**$^+$ refined to a value of 0.3347(12).

Treatment of Disorders:

For **2.9**: The electron density difference map of **21** showed regions that could not be modeled accurately. As a consequence, the electron density associated with these regions was masked out of the refinement using the SQUEEZE algorithm as implemented in PLATON.[71]

For **2.13**$^+$: One of the $CDCl_3$ molecules of solvation exhibited a minor disorder in one of the chlorine atom positions. The occupancy of the primary atomic position converged to a value of 0.902(7).

For **2.14**$^{2+}$: The structure analysis was hampered by a number of factors: 1) Resolution of the data were limited. There was no observable data above 0.94 Å, 2) disorder of one of the phosphorus bound phenyl groups, 3) disorder of one of the triflate ions, 4) regions of disordered solvents. Despite repeated calculation and careful examination of the difference

Fourier maps, peaks for the some of the disordered phenyl carbons could not be recovered. Therefore, the reasonable positions which were found, two 50% occupied hexagonal groups of carbon with carbon–carbon distances of 1.39 Å were introduced into the model. In order to keep the rings properly oriented additional restraints on the P1 to *ortho* carbon distances were also introduced. In addition to similarity and rigid bond restraints, the anisotropic displacement parameters (ADPs) were constrained to be equal for the following pairs of atoms: C30/C34; C31/C33; C30'/C34'; and C31'/C33'. The model was then refined for several cycles using SHELXL's conjugate-gradient algorithm. After that series of refinements were converged, the subsequent refinement cycles were performed using full matrix least-squares. The normalized occupancy for the primary conformer converged to a value of 0.508(7). Treatment of the disordered triflate anion was more straightforward. The anion was disordered over two sites, with co-incident positions for O3/O3'; O4/O4'; F1/F1'; and F2/F2'. The split atom positions for S1/S1', C47/C47', and F3/F3' were obtained from difference Fourier maps. The distances for the minor component were restrained to match the values for the major component. The normalized occupancy of the major component converged to a value of 0.763(5). As noted above, the structure also contained regions of highly disordered solvent molecules (presumably a mixture of CH_2Cl_2 hexanes, and toluene) for which a chemically sensible model could not be derived. As a consequence, the electron density associated with this moiety was masked out of the refinement using the SQUEEZE algorithm as implemented in PLATON.[71]

For all compounds, hydrogen atoms were introduced at idealized positions and allowed to ride on the parent atom. The structural models were fit to the data using full matrix least-squares based on F^2. The calculated structure factors included corrections for anomalous dispersion from the usual tabulation. The structures were refined using the SHELXL-2014 program from the SHELX suite of crystallographic software.[72] The Mercury v3.10.3 software package was used to generate graphical representations of the solid-state structures. See Table 2.3 for additional crystallographic data.

Table 2.3. X-ray diffraction data collection and refinement details for complexes **2.9**, **2.10$^+$**, **2.13$^+$**and **2.14^{2+}**.

	2.9	2.10$^+$	2.13$^+$•5CDCl$_3$	2.14^{2+}
Formula	C$_{27}$H$_{24}$BClN$_4$	C$_{27}$H$_{24}$AlBCl$_4$N$_4$	C$_{41}$H$_{30}$BCl$_{16}$D$_5$N$_4$O$_2$	C$_{48}$H$_{41}$BF$_6$N$_4$O$_8$P$_2$S$_2$
FW (g mol^{-1})	450.76	584.09	1198.77	1052.72
Crystal Habit	Purple Block	Purple Plate	Red Plate	Orange Plate
Crystal System	Triclinic	Orthorhombic	Triclinic	Monoclinic
Space Group	$P\bar{1}$	$Pbca$	$P\bar{1}$	$P2_1/c$
T (K)	110	110	110	110
λ (Å)	0.71073	0.71073	0.71073	0.71073
a (Å)	9.663(3)	20.074(8)	12.0720(14)	15.272(6)
b (Å)	15.369(4)	12.341(3)	14.240(2)	22.419(8)
c (Å)	17.550(4)	22.626(9)	17.401(2)	16.793(7)
α (°)	86.523(12)	90	109.162(8)	90
β (°)	89.830(14)	90	103.963(7)	101.070(16)
γ (°)	81.925(15)	90	102.197(10)	90
V (Å^3)	2575.7(12)	5605(4)	2600.7(6)	5643(4)
Z	4	8	2	4
ρ (g cm^{-3})	1.162	1.384	1.531	1.239
μ (cm^{-1})	0.169	0.478	0.884	0.221
R$_1$,^{a} ωR$_2$^{b}[I > 2σ]	0.0500,	0.0393, 0.0837	0.0777, 0.2096	0.0637,0.1594
R$_1$, ωR$_2$ (all data)	0.0864,	0.0668, 0.0959	0.1029, 0.2251	0.0860, 0.1732
GOF^c	1.039	1.019	1.068	1.035

Where:

^{a}R$_1$ = $\Sigma(|F_o|-|F_c|)/\Sigma F_o$

$^b\omega$R$_2$ = $[\Sigma(\omega(F_o{}^2-F_c{}^2)^2)/\Sigma(\omega F_o{}^4)]^{1/2}$

^{c}GOF = $[\Sigma(\omega(F_o{}^2-F_c{}^2)^2)/(\text{No. of reflns.}-\text{No. of params.})]^{1/2}$

2.4.3 Computational Methodology

All electronic structure calculations were carried out with the Gaussian program[73] using the PBE1PBE functional, DGDZVP2 basis set, and the CPCM method of implicit solvation. Geometry optmizations, molecular orbital calculations, and TDDFT simulations of UV-vis spectra were all performed at the same level of theory: PBE1PBE/DGDZVP2 SCRF=CPCM. All optimized structures were confirmed by vibrational analysis to be global minima. The optimized geometries can be found in the appendix (A2). The TDDFT calculations were performed using non-equilibrium solvation (which is the default for singlepoint TDDFT runs). The UV-vis absorption spectra of **2.9**–**2.11$^+$** and **2.13$^+$**–**2.15** were simulated using the GaussView program with the half-width at half-maximum (HWHM) set to 0.25 eV.

2.4.4　Synthetic Procedures

NMR spectra can be found in the appendix (Fig A2.1 – Fig A2.24).

BPhF formazanate 2.8

1,5-(*p*-tolyl)-3-phenylformazan (1.02 g, 3.11 mmol) was dissolved in
dry CH_2Cl_2 (60 mL) in a 250 mL Schlenk flask. N(*i*Pr)$_2$Et (1.22 g,
1.65 mL, 9.44 mmol) was added slowly and the solution was stirred
at 21 °C for 20 min. In a separate 100 mL Schlenk flask, KBPhF$_3$
(2.30 g, 12.5 mmol) was combined with dry CH_3CN (25 mL) and
stirred for 5 min at 21 °C. TMSCl (2.74 g, 3.29 mL, 25.2 mmol) was added which resulted
in the formation of a milky white suspension. This suspension was stirred for 15 min,
before being transferred *via* syringe to the flask containing 1,5-(*p*-tolyl)-3-phenylformazan
and DIPEA resulting in a colour change from red to purple. The resulting solution was
stirred for 36 h at 60 °C. After cooling to 21 °C, deionized H_2O (10 mL) was added. In air,
the resulting mixture was transferred to a separatory funnel and the organic layer was
washed with H_2O (2 × 50 mL) and brine (1 × 50 mL), and subsequently dried over MgSO$_4$,
gravity filtered, and concentrated *in vacuo*. The crude mixture was purified by column
chromatography (neutral alumina, 25 mL) using toluene as the eluent (R$_f$ = 0.90). The dark
purple fraction containing **7** and 1,5-(*p*-tolyl)-3-phenylformazan was concentrated *in
vacuo*. The solid was further purified using column chromatography (silica, 200 mL) using
2:1 v/v hexanes/toluene as the eluent (R$_f$ = 0.35). The dark purple fraction containing pure
2.8 was concentrated *in vacuo* to afford a dark purple solid (green reflex). Yield = 1.01 g,
75%. M.p.: 147–149 °C. ^{1}H NMR (599.2 MHz, CDCl$_3$): δ 8.13 (d, $^3J_{HH}$ = 8.5 Hz, 2H, aryl
C*H*), 7.73 (d, $^3J_{HH}$ = 8.2 Hz, 4H, aryl C*H*), 7.50–7.48 (m, 2H, aryl C*H*), 7.46–7.42 (m, 3H,
aryl C*H*), 7.23–7.22 (m, 3H, aryl C*H*), 7.20 (d, $^3J_{HH}$ = 8.5 Hz, 4H, aryl C*H*), 2.39 (s, 6H,
C*H*$_3$). ^{11}B{^{1}H} NMR (128.3 MHz, CDCl$_3$): δ 2.9 (s). ^{13}C{^{1}H} NMR (150.7 MHz, CDCl$_3$):
δ 149.9, 142.9, 139.3, 134.1, 132.2, 129.2, 128.8, 128.6, 127.8, 127.5, 125.1, 124.23,
124.21, 21.2. ^{19}F{^{1}H} NMR (376.1 MHz, CDCl$_3$): δ −164.6 (s). FT-IR (ATR): 3036 (w),
3011 (w), 2923 (w), 2862 (w), 1761 (m), 1605 (m), 1505 (m), 1433 (m), 1349 (m), 1285
(s), 1263 (s), 1176 (s), 1117 (m), 1022 (m), 955 (s), 896 (m), 817 (s), 799 (m), 764 (m),
695 (m), 641 (w), 598 (w) cm^{-1}. UV-vis (toluene): λ$_{max}$ 528 nm (ε = 13,000 M^{-1} cm^{-1}), 317
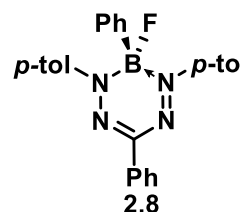
nm (ε = 18,300 M^{-1} cm^{-1}). Mass Spec. (EI, +ve mode): exact mass calculated for [C$_{27}$H$_{24}$BFN$_4$]$^+$, [M]$^+$: 434.2078; exact mass found: 434.2075; difference: –0.7 ppm. Anal. Calcd. (%) for C$_{27}$H$_{24}$BFN$_4$: C, 74.67; H, 5.57; N, 12.90. Found: C, 74.69; H, 5.31; N, 12.77.

BPhCl formazanate 2.9

BPhF formazanate **2.8** (0.11 g, 0.25 mmol) was dissolved in dry CH$_2$Cl$_2$ (10 mL) in a 50 mL flask. BCl$_3$ (1 M in heptane, 0.30 mL, 0.30 mmol) was added slowly and the colour of the solution changed from dark purple to magenta. This solution was stirred for 1 h at 21 °C before being concentrated *in vacuo* and the resulting dark purple solid (complex **2.9**) collected. Yield = 0.11 g, 100%. M.p.: 189–191 °C. ^{1}H NMR (399.8 MHz, CDCl$_3$): δ 8.19–8.16 (m, 2H, aryl C*H*), 7.51–7.42 (m, 3H, aryl C*H*), 7.39–7.37 (m, 2H, aryl C*H*), 7.31 (d, $^3J_{HH}$ = 8.4 Hz, 4H, aryl C*H*), 7.05–7.02 (m, 3H, aryl C*H*), 6.96 (d, $^3J_{HH}$ = 8.2 Hz, 4H, aryl C*H*), 2.26 (s, 6H, C*H*$_3$). ^{11}B{^{1}H} NMR (128.3 MHz, CDCl$_3$): δ 2.4 (s). ^{13}C{^{1}H} NMR (100.5 MHz, CDCl$_3$): δ 151.2, 143.4, 139.2, 134.6, 133.8, 132.0, 129.1, 128.7, 128.6, 127.2, 127.1, 125.3, 125.0, 21.2. FT-IR (ATR): 3227 (w), 3037 (w), 2920 (w), 1900 (w), 1604 (m), 1505 (m), 1434 (m), 1350 (m), 1286 (s), 1261 (s), 1210 (s), 1174 (s), 1117 (m), 1022 (m), 969 (s), 910 (s), 815 (s), 802 (s), 800 (m), 732 (s), 694 (m), 655 (s), 569 (m) cm^{-1}. UV-vis (toluene): λ_{max} 521 nm (ε = 12,100 M^{-1} cm^{-1}), 350 nm (ε = 4,700 M^{-1} cm^{-1}), 310 nm (ε = 12,500 M^{-1} cm^{-1}). Mass Spec. (EI, +ve mode): exact mass calculated for [C$_{27}$H$_{24}$BClN$_4$]$^+$, [M]$^+$: 450.1783; exact mass found: 450.1773; difference: –2.2 ppm. Anal. Calcd. (%) for C$_{27}$H$_{24}$BClN$_4$: C, 71.94; H, 5.37; N, 12.43. Found: C, 71.65; H, 5.57; N, 11.97.
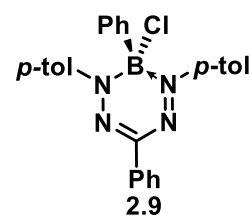
Borenium cation 2.10$^+$

BPhF formazanate **7** (0.192 g, 0.44 mmol) was dissolved in dry CH$_2$Cl$_2$ (10 mL) in a 50 mL flask. BCl$_3$ (1 M in heptane, 0.50 mL, 0.50 mmol) was added slowly and the colour of the solution changed from dark purple to magenta. This solution was stirred for 2 h before being concentrated *in vacuo*. The resulting purple residue was re-dissolved in dry CH$_2$Cl$_2$ (10 mL) and AlCl$_3$ (0.057 g, 0.43 mmol) was added. The solution
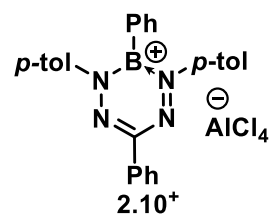
instantly turned dark purple and was stirred at 21 °C for 12 h before the solvent was removed *in vacuo* leaving a dark-purple solid. The solid was suspended in dry *n*-pentane (10 mL) and stirred for 15 min before it was collected *via* vacuum filtration. The solid was washed with additional dry *n*-pentane (10 mL) and dried *in vacuo* to afford complex **2.10⁺** as a dark-purple microcrystalline solid. Yield = 0.245 g, 98%. M.p.: 203–205 °C. ^{1}H NMR (399.8 MHz, CDCl$_3$): δ 8.28 (d, $^3J_{HH}$ = 7.1 Hz, 2H, aryl C*H*), 7.61–7.56 (m, 3H, aryl C*H*), 7.42 (d, $^3J_{HH}$ = 8.0 Hz, 4H, aryl C*H*), 7.36 (d, $^3J_{HH}$ = 7.5 Hz, 3H, aryl C*H*), 7.24–7.20 (m, 2H, aryl C*H*), 7.17 (d, $^3J_{HH}$ = 8.1 Hz, 4H, aryl C*H*), 2.39 (s, 6H, C*H*$_3$). ^{11}B{^{1}H} NMR (128.3 MHz, CDCl$_3$): δ 35.5 (s). We were unable to obtain a ^{13}C{^{1}H} NMR spectrum for borenium cation **9⁺** due to its poor solubility and long-term solution stability. ^{27}Al{^{1}H} NMR (156.1 MHz, CDCl$_3$): δ 103.6 (s). FT-IR (ATR): 3056 (w), 2917 (w), 1600 (m), 1357 (m), 1287 (m), 1146 (s), 1026 (s), 1000 (s), 816 (s), 777 (s), 695 (s), 500 (s) cm^{-1}. UV-vis (toluene): λ$_{max}$ 597 nm (ε = 6,300 M^{-1} cm^{-1}), 463 nm (ε = 3,400 M^{-1} cm^{-1}), 355 nm (ε = 2,800 M^{-1} cm^{-1}), 318 nm (ε = 3,500 M^{-1} cm^{-1}). Mass Spec. (ESI, +ve mode): exact mass calculated for [C$_{27}$H$_{24}$BN$_4$]$^+$, [M]$^+$: 415.2094; exact mass found: 415.2096; difference: +0.5 ppm. Anal. Calcd. (%) for C$_{27}$H$_{24}$AlBCl$_4$N$_4$: C, 55.52; H, 4.14; N, 9.59. Found: C, 55.63; H, 4.12; N, 9.31.

Boronium cation 2.11⁺

AgOTf (0.060 g, 0.23 mmol) was suspended in dry toluene (1 mL) in a 30 mL vial and stirred for 10 min. BPhCl formazanate **8** (0.105 g, 0.233 mmol) was dissolved in dry toluene (5 mL) and added dropwise to the AgOTf solution. The magenta solution was stirred at 21 °C for 2 h before it was filtered through Celite and collected in a 100 mL round-bottom flask. In a separate vial, 4-dimethylaminopyridine (0.029 g, 0.24 mmol) was dissolved in dry toluene (2 mL) and added dropwise to the round-bottom flask. The reaction mixture was heated to 60 °C and stirred for 4 h, during which time the colour changed from magenta to red. The solution was concentrated *in vacuo* and stirred in dry *n*-pentane (15 mL) for 30 min. The resulting suspension was vacuum filtered and complex **2.11⁺** was collected as a dark-red microcrystalline powder. Yield = 0.147 g, 92%. M.p.: 222–224 °C. ^{1}H NMR (599.1 MHz, CDCl$_3$) δ 7.98–7.96 (m, 2H, aryl C*H*), 7.79 (d, $^3J_{HH}$ = 7.6 Hz, 2H, aryl C*H*), 7.46–7.45 (m,
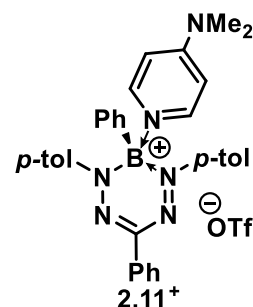
3H, aryl C*H*), 7.29 (t, $^3J_{HH}$ = 7.2 Hz, 1H, aryl C*H*), 7.15 (t, $^3J_{HH}$ = 7.6 Hz, 2H, aryl C*H*), 7.08 (s, 8H, aryl C*H*), 6.82 (d, $^3J_{HH}$ = 7.7 Hz, 2H, aryl C*H*), 6.62 (d, $^3J_{HH}$ = 7.1 Hz, 2H, aryl C*H*), 3.21 (s, 6H, C*H₃*), 2.34 (s, 6H, C*H₃*). ^{11}B{^{1}H} NMR (128.3 MHz, CDCl₃): δ 1.9 (s). ^{13}C{^{1}H} NMR (100.5 MHz, CDCl₃) δ 156.9, 153.9, 142.4, 142.3, 141.9, 134.4, 132.1, 130.3, 129.5, 128.9, 128.7, 127.7, 125.9, 125.8, 108.2, 107.1, 40.2, 21.4. ^{19}F{^{1}H} NMR (376.1 MHz, CDCl₃): δ –77.5 (s). FT-IR (ATR): 3081 (w), 2925 (w), 1771 (m), 1640 (s), 1603 (m), 1568 (s), 1435 (m), 1343 (m), 1279 (s), 1256 (s), 1222 (s), 1204 (s), 1154 (s), 1027 (s), 962 (m), 876 (m), 815 (s), 740 (s), 695 (s), 634 (s), 511 (s) cm^{-1}. UV-vis (toluene): λ_{max} 510 nm (ε = 8,300 M^{-1} cm^{-1}), 357 nm (ε = 4,300 M^{-1} cm^{-1}), 302 nm (ε = 17,600 M^{-1} cm^{-1}). Mass Spec. (ESI, +ve mode): exact mass calculated for [C₃₄H₃₄BN₆]$^+$, [M]$^+$: 537.2938; exact mass found: 537.2958; difference: +3.7 ppm.

Lithium dibenzoylmethanate

Dibenzoylmethane (1.00 g, 4.46 mmol) was dissolved in dry toluene (40 mL) and stirred for 10 min. 2.5 M *n*-BuLi in hexanes (1.96 mL, 4.90 mmol) was added dropwise over 30 min and an off-white precipitate formed in solution. The suspension was stirred for an additional 2 h before it was vacuum filtered, washed with dry hexanes (30 mL) and dried to afford lithium dibenzoylmethanate as a pale yellow solid. The resulting product was used without further purification or characterization. Yield = 0.922 g, 90%. ^{1}H NMR (599.1 MHz, THF-d_8) δ 7.98–7.96 (m, 4H, aryl C*H*), 7.33–7.31 (m, 6H, aryl C*H*), 6.60 (s, 1H, C*H*). ^{13}C{^{1}H} NMR (101 MHz, THF-d_8) δ 184.6, 144.1, 130.1, 128.4, 127.9, 92.2.

Boronium cation 2.13$^+$

Lithium dibenzoylmethanate (0.073 g, 0.317 mmol) was suspended in dry CH₂Cl₂ (2 mL) and stirred for 20 min. In a separate vial, BCl₂ formazanate **11** (0.125 g, 0.306 mmol) was dissolved in dry CH₂Cl₂ (4 mL) and added dropwise to the suspension. The reaction was stirred for 16 h and then filtered through Celite. The red solution was concentrated *in vacuo* and then re-dissolved in dry CH₂Cl₂ (2 mL) and carefully layered with dry *n*-pentane (10 mL). The vial was placed in a freezer at –20 °C for 16 h before it was filtered and dried to afford complex **2.13$^+$** as a shiny red
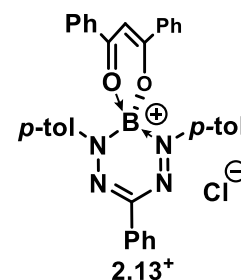
microcrystalline powder. Yield = 0.171 g, 94%. M.p.: 208–210 °C. ^{1}H NMR (399.8 MHz, CDCl$_3$) δ 9.61 (s, 1H, C*H*), 8.85 (d, $^3J_{HH}$ = 7.9 Hz, 4H, aryl C*H*), 8.21 (d, $^3J_{HH}$ = 7.5 Hz, 2H, aryl C*H*), 7.72 (t, $^3J_{HH}$ = 7.3 Hz, 2H, aryl C*H*), 7.60–7.56 (m, 7H, aryl C*H*), 7.33 (d, $^3J_{HH}$ = 8.5 Hz, 4H, aryl C*H*), 7.19 (d, $^3J_{HH}$ = 8.6 Hz, 4H, aryl C*H*), 2.35 (s, 6H, C*H$_3$*). ^{11}B{^{1}H} NMR (128.3 MHz, CDCl$_3$) δ 1.8 (s). ^{13}C{^{1}H} NMR (100.5 MHz, CDCl$_3$) δ 181.9, 142.1, 140.5, 137.9, 132.6, 132.4, 130.6, 130.5, 130.1, 129.82, 129.80, 129.3, 125.9, 123.8, 99.6, 21.5. FT-IR (ATR): 3061 (w), 3028 (w), 2920 (w), 1595 (m), 1534 (s), 1512 (s), 1484 (s), 1384 (m), 1349 (m), 1284 (m), 1260 (m), 1126 (s), 1026 (s), 996 (s), 909 (m), 718 (s), 695 (s), 579 (s), 510 (m) cm^{-1}. UV-vis (CH$_2$Cl$_2$): λ$_{max}$ 540 nm (ε = 5,900 M^{-1} cm^{-1}), 418 nm (ε = 15,200 M^{-1} cm^{-1}), 399 nm (ε = 17,400 M^{-1} cm^{-1}), 309 nm (ε = 10,800 M^{-1} cm^{-1}). Mass Spec. (ESI, +ve mode): exact mass calculated for [C$_{36}$H$_{30}$BN$_4$O$_2$]$^+$, [M]$^+$: 561.2462; exact mass found: 561.2470; difference: +1.4 ppm.

Boron dication 2.14^{2+}

AgOTf (0.122 g, 0.475 mmol) was suspended in dry toluene (2 mL) in a 30 mL vial and stirred for 10 min. BCl$_2$ formazanate **11** (0.095 g, 0.23 mmol) was dissolved in dry toluene (5 mL) and added dropwise to the AgOTf solution. The solution turned dark blue and was stirred at 21 °C for 2 h before it was filtered through Celite into 100 mL round-bottom flask containing bis(diphenylphosphino)methane dioxide (0.096 g, 0.23 mmol) suspended in dry toluene (2 mL). The reaction was stirred for 12 h, during which time an orange precipitate formed. Dry *n*-pentane (20 mL) was added and the solution was stirred for an additional 30 min before the reaction mixture was vacuum filtered to afford complex **2.14^{2+}** as an orange powder. Yield = 0.213 g, 88%. M.p.: 210–212 °C. ^{1}H NMR (599.1 MHz, CDCl$_3$) δ 8.09 (d, *J* = 9.7 Hz, 2H, aryl C*H*), 7.68 (t, $^3J_{HH}$ = 7.5 Hz, 5H, aryl C*H*), 7.60–7.56 (m, 11H, aryl C*H*), 7.47–7.44 (m, 11H, aryl C*H*), 7.21 (d, $^3J_{HH}$ = 8.0 Hz, 4H, aryl C*H*), 5.01 (t, $^2J_{HP}$ = 13.0 Hz, 2H, PC*H$_2$*P), 2.36 (s, 6H, C*H$_3$*). ^{11}B{^{1}H} NMR (128.3 MHz, CDCl$_3$): δ 0.0 (s). ^{13}C{^{1}H} NMR (101 MHz, CDCl$_3$) δ 152.3, 142.1, 138.7, 136.6, 131.3–131.2 (m), 130.81, 130.6–130.4 (m), 129.4, 126.1, 125.2, 122.4, 120.0 (d, *J* = 113 Hz), 119.3, 21.3. ^{19}F{^{1}H} NMR (376.1 MHz, CDCl$_3$) δ –78.2 (s). ^{31}P{^{1}H} NMR (161.8 MHz, CDCl$_3$) δ 54.9 (s). FT-IR (ATR): 3056 (w), 2923 (w), 1589 (w), 1505 (w), 1439 (m), 1354 (w), 1272 (s), 1253
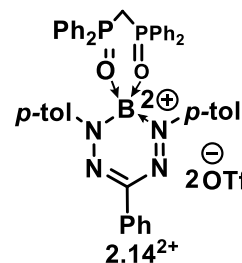
(s), 1155 (s), 1120 (s), 1026 (s), 996 (s), 870 (m), 799 (m), 635 (s), 515 (s) cm^{-1}. UV-vis (CH$_2$Cl$_2$): λ_{max} 505 nm (ε = 9,400 M^{-1} cm^{-1}), 309 nm (ε = 12,100 M^{-1} cm^{-1}), 275 nm (ε = 13,300 M^{-1} cm^{-1}), 268 nm (ε = 15,100 M^{-1} cm^{-1}), 262 nm (ε = 14,900 M^{-1} cm^{-1}). Mass Spec. (ESI, +ve mode): exact mass calculated for [C$_{46}$H$_{40}$BN$_4$O$_2$P$_2$]$^+$, [M−H]$^+$: 753.2719; exact mass found: 753.2746; difference: +3.6 ppm.

2.5 References

1. Melen, R. L. *Science* **2019**, *363*, 479–484.

2. Lam, J.; Szkop, K. M.; Mosaferi, E.; Stephan, D. W. *Chem. Soc. Rev.* **2019**, *48*, 3592–3612.

3. Chu, T.; Nikonov, G. I. *Chem. Rev.* **2018**, *118*, 3608–3680.

4. Welch, G. C.; Juan, R. R. S.; Masuda, J. D.; Stephan, D. W. *Science* **2006**, *314*, 1124–1126.

5. Baumgartner, T.; Jäkle, F., *Main Group Strategies towards Functional Hybrid Materials*. Wiley, Chichester: 2018.

6. Hirai, M.; Tanaka, N.; Sakai, M.; Yamaguchi, S. *Chem. Rev.* **2019**, *119*, 8291–8331.

7. Jäkle, F. *Chem. Rev.* **2010**, *110*, 3985–4022.

8. Ji, L.; Griesbeck, S.; Marder, T. B. *Chem. Sci.* **2017**, *8*, 846–863.

9. Mellerup, S. K.; Wang, S. *Trends Chem.* **2019**, *1*, 77–89.

10. Braunschweig, H.; Kupfer, T. *Chem. Commun.* **2011**, *47*, 10903–10914.

11. Houghton, A. Y.; Hurmalainen, J.; Mansikkamäki, A.; Piers, W. E.; Tuononen, H. M. *Nat. Chem.* **2014**, *6*, 983–988.

12. Zhang, Z.; Edkins, R. M.; Haehnel, M.; Wehner, M.; Eichhorn, A.; Mailänder, L.; Meier, M.; Brand, J.; Brede, F.; Müller-Buschbaum, K.; Braunschweig, H.; Marder, T. B. *Chem. Sci.* **2015**, *6*, 5922–5927.

13. Barnard, J. H.; Yruegas, S.; Huang, K.; Martin, C. D. *Chem. Commun.* **2016**, *52*, 9985–9991.

14. Sivaev, I. B.; Bregadze, V. I. *Coord. Chem. Rev.* **2014**, *270-271*, 75–88.

15. Yang, W.; Krantz, K. E.; Freeman, L. A.; Dickie, D. A.; Molino, A.; Kaur, A.; Wilson, D. J. D.; Gilliard Jr., R. J. *Chem. Eur. J.* **2019**, *25*, 12512–12516.

16. Adachi, Y.; Arai, F.; Jäkle, F. *Chem. Commun.* **2020**, *56*, 5119–5122.

17. Scherpf, T.; Feichtner, K.-S.; Gessner, V. H. *Angew. Chem. Int. Ed.* **2017**, *56*, 3275–3279.

18. Tanaka, N.; Shoji, Y.; Hashizume, D.; Sugimoto, M.; Fukushima, T. *Angew. Chem. Int. Ed.* **2017**, *56*, 5312–5316.

19. Tseng, H.-C.; Shen, C.-T.; Matsumoto, K.; Shih, D.-N.; Liu, Y.-H.; Peng, S.-M.; Yamaguchi, S.; Lin, Y.-F.; Chiu, C.-W. *Organometallics* **2019**, *38*, 4516–4521.

20. Lee, W.-H.; Lin, Y.-F.; Lee, G.-H.; Peng, S.-M.; Chiu, C.-W. *Dalton Trans.* **2016**, *45*, 5937–5940.

21. Bonnier, C.; Piers, W. E.; Parvez, M.; Sorensen, T. S. *Chem. Commun.* **2008**, 4593–4595.

22. Tsurumaki, E.; Hayashi, S.-y.; Tham, F. S.; Reed, C. A.; Osuka, A. *J. Am. Chem. Soc.* **2011**, *133*, 11956–11959.

23. Franz, D.; Irran, E.; Inoue, S. *Angew. Chem. Int. Ed.* **2014**, *53*, 14264–14268.

24. Devillard, M.; Brousses, R.; Miqueu, K.; Bouhadir, G.; Bourissou, D. *Angew. Chem. Int. Ed.* **2015**, *54*, 5722-5726.

25. Farrell, J. M.; Stephan, D. W. *Angew. Chem. Int. Ed.* **2015**, *54*, 5214–5217.

26. Loh, Y. K.; Porteous, K.; Fuentes, M. Á.; Do, D. C. H.; Hicks, J.; Aldridge, S. *J. Am. Chem. Soc.* **2019**, *141*, 8073–8077.

27. Janes, T.; Diskin-Posner, Y.; Milstein, D. *Angew. Chem. Int. Ed.* **2020**, *59*, 4932–4936.

28. Chen, W.-C.; Lee, C.-Y.; Lin, B.-C.; Hsu, Y.-C.; Shen, J.-S.; Hsu, C.-P.; Yap, G. P. A.; Ong, T.-G. *J. Am. Chem. Soc.* **2014**, *136*, 914–917.

29. Hudnall, T. W.; Gabbaï, F. P. *Chem. Commun.* **2008**, 4596-4597.

30. Prokofjevs, A.; Kampf, J. W.; Solovyev, A.; Curran, D. P.; Vedejs, E. *J. Am. Chem. Soc.* **2013**, *135*, 15686–15689.

31. Kong, L.; Lu, W.; Li, Y.; Ganguly, R.; Kinjo, R. *J. Am. Chem. Soc.* **2016**, *138*, 8623–8629.

32. Lu, W.; Li, Y.; Ganguly, R.; Kinjo, R. *Angew. Chem. Int. Ed.* **2017**, *56*, 9829–9832.

33. Rixin Wang, S.; Arrowsmith, M.; Braunschweig, H.; Dewhurst, R. D.; Paprocki, V.; Winner, L. *Chem. Commun.* **2017**, *53*, 11945–11947.

34. Geier, S. J.; Vogels, C. M.; Mellonie, N. R.; Daley, E. N.; Decken, A.; Doherty, S.; Westcott, S. A. *Chem. Eur. J.* **2017**, *23*, 14485–14499.

35. Hagspiel, S.; Arrowsmith, M.; Fantuzzi, F.; Hermann, A.; Paprocki, V.; Drescher, R.; Krummenacher, I.; Braunschweig, H. *Chem. Sci.* **2020**, *11*, 551–555.

36. Kinjo, R.; Donnadieu, B.; Celik, M. A.; Frenking, G.; Bertrand, G. *Science* **2011**, *333*, 610–613.

37. Shen, C.-T.; Liu, Y.-H.; Peng, S.-M.; Chiu, C.-W. *Angew. Chem. Int. Ed.* **2013**, *52*, 13293–13297.

38. Shoji, Y.; Tanaka, N.; Mikami, K.; Uchiyama, M.; Fukushima, T. *Nat. Chem.* **2014**, *6*, 498–503.

39. Devillard, M.; Mallet-Ladeira, S.; Bouhadir, G.; Bourissou, D. *Chem. Commun.* **2016**, *52*, 8877–8880.

40. Franz, D.; Szilvási, T.; Pöthig, A.; Deiser, F.; Inoue, S. *Chem. Eur. J.* **2018**, *24*, 4283–4288.

41. Eisenberger, P.; Crudden, C. M. *Dalton Trans.* **2017**, *46*, 4874–4887.

42. Piers, W. E.; Bourke, S. C.; Conroy, K. D. *Angew. Chem. Int. Ed.* **2005**, *44*, 5016–5036.

43. Gilroy, J. B.; Otten, E. *Chem. Soc. Rev.* **2020**, *49*, 85–113.

44. Chang, M.-C.; Dann, T.; Day, D. P.; Lutz, M.; Wildgoose, G. G.; Otten, E. *Angew. Chem. Int. Ed.* **2014**, *53*, 4118–4122.

45. Chang, M.-C.; Otten, E. *Chem. Commun.* **2014**, *50*, 7431–7433.

46. Travieso-Puente, R.; Broekman, J. O. P.; Chang, M.-C.; Demeshko, S.; Meyer, F.; Otten, E. *J. Am. Chem. Soc.* **2016**, *138*, 5503–5506.

47. Kabir, E.; Wu, C.-H.; Wu, J. I.-C.; Teets, T. S. *Inorg. Chem.* **2016**, *55*, 956–963.

48. Broere, D. L. J.; Mercado, B. Q.; Holland, P. L. *Angew. Chem. Int. Ed.* **2018**, *57*, 6507–6511.

49. Maar, R. R.; Catingan, S. D.; Staroverov, V. N.; Gilroy, J. B. *Angew. Chem. Int. Ed.* **2018**, *57*, 9870–9874.

50. Maar, R. R.; Rabiee Kenaree, A.; Zhang, R.; Tao, Y.; Katzman, B. D.; Staroverov, V. N.; Ding, Z.; Gilroy, J. B. *Inorg. Chem.* **2017**, *56*, 12436–12447.

51. Barbon, S. M.; Price, J. T.; Reinkeluers, P. A.; Gilroy, J. B. *Inorg. Chem.* **2014**, *53*, 10585–10593.

52. Barbon, S. M.; Staroverov, V. N.; Gilroy, J. B. *J. Org. Chem.* **2015**, *80*, 5226–5235.

53. Dhindsa, J. S.; Maar, R. R.; Barbon, S. M.; Olivia Avilés, M.; Powell, Z. K.; Lagugné-Labarthet, F.; Gilroy, J. B. *Chem. Commun.* **2018**, *54*, 6899–6902.

54. Maar, R. R.; Zhang, R.; Stephens, D. G.; Ding, Z.; Gilroy, J. B. *Angew. Chem. Int. Ed.* **2019**, *58*, 1052–1056.

55. Maar, R. R.; Barbon, S. M.; Sharma, N.; Groom, H.; Luyt, L. G.; Gilroy, J. B. *Chem. Eur. J.* **2015**, *21*, 15589–15599.

56. Hesari, M.; Barbon, S. M.; Mendes, R. B.; Staroverov, V. N.; Ding, Z.; Gilroy, J. B. *J. Phys. Chem. C* **2018**, *122*, 1258–1266.

57. Hesari, M.; Barbon, S. M.; Staroverov, V. N.; Ding, Z.; Gilroy, J. B. *Chem. Commun.* **2015**, *51*, 3766–3769.

58. Chang, M.-C.; Otten, E. *Inorg. Chem.* **2015**, *54*, 8656–8664.

59. Barbon, S. M.; Staroverov, V. N.; Gilroy, J. B. *Angew. Chem. Int. Ed.* **2017**, *56*, 8173–8177.

60. Maar, R. R.; Hoffman, N. A.; Staroverov, V. N.; Gilroy, J. B. *Chem. Eur. J.* **2019**, *25*, 11015–11019.

61. Gilroy, J. B.; Ferguson, M. J.; McDonald, R.; Patrick, B. O.; Hicks, R. G. *Chem. Commun.* **2007**, 126–128.

62. Kümmel, S. *Adv. Energy Mater.* **2017**, *7*, 1700440.

63. Yanai, T.; Tew, D. P.; Handy, N. C. *Chem. Phys. Lett.* **2004**, *393*, 51–57.

64. Tawada, Y.; Tsuneda, T.; Yanagisawa, S.; Yanai, T.; Hirao, K. *J. Chem. Phys.* **2004**, *120*, 8425–8433.

65. Vedejs, E.; Chapman, R. W.; Fields, S. C.; Lin, S.; Schrimpf, M. R. *J. Org. Chem.* **1995**, *60*, 3020–3027.

66. Kannan, S.; Rajalakshmi, N.; Chetty, K. V.; Venugopal, V.; Drew, M. G. B. *Polyhedron* **2004**, *23*, 1527–1533.

67. Bruker-AXS, SAINT version 2013.8, **2013**, Bruker-AXS, Madison, WI 53711, USA.

68. Bruker-AXS, SADABS version 2012.1, **2012**, Bruker-AXS, Madison, WI 53711, USA.

69.   Bruker-AXS, TWINABS version 2012.1, **2012**, Bruker-AXS, Madison, WI 53711, USA.

70.   Sheldrick, G. M. *Acta Cryst.* **2015**, *A71*, 3–8.

71.   Spek, A. L. *Acta Cryst.* **2015**, *C71*, 9–18.

72.   Sheldrick, G. M. *Acta Cryst.* **2015**, *C71*, 3–8.

73.   Frisch, M. J.; Trucks, G. W.; Schlegel, H. B.; Scuseria, G. E.; Robb, M. A.; Cheeseman, J. R.; Scalmani, G.; Barone, V.; Petersson, G. A.; Nakatsuji, H.; Li, X.; Caricato, M.; Marenich, A. V.; Bloino, J.; Janesko, B. G.; Gomperts, R.; Mennucci, B.; Hratchian, H. P.; Ortiz, J. V.; Izmaylov, A. F.; Sonnenberg, J. L.; Williams; Ding, F.; Lipparini, F.; Egidi, F.; Goings, J.; Peng, B.; Petrone, A.; Henderson, T.; Ranasinghe, D.; Zakrzewski, V. G.; Gao, J.; Rega, N.; Zheng, G.; Liang, W.; Hada, M.; Ehara, M.; Toyota, K.; Fukuda, R.; Hasegawa, J.; Ishida, M.; Nakajima, T.; Honda, Y.; Kitao, O.; Nakai, H.; Vreven, T.; Throssell, K.; Montgomery Jr., J. A.; Peralta, J. E.; Ogliaro, F.; Bearpark, M. J.; Heyd, J. J.; Brothers, E. N.; Kudin, K. N.; Staroverov, V. N.; Keith, T. A.; Kobayashi, R.; Normand, J.; Raghavachari, K.; Rendell, A. P.; Burant, J. C.; Iyengar, S. S.; Tomasi, J.; Cossi, M.; Millam, J. M.; Klene, M.; Adamo, C.; Cammi, R.; Ochterski, J. W.; Martin, R. L.; Morokuma, K.; Farkas, O.; Foresman, J. B.; Fox, D. J. *Gaussian Development Version, Revision I.13*, Wallingford, CT, 2016.

Chapter 3

3 A Highly Lewis Acidic, Redox-Active and Fluorescent Borenium Formazanate Dye

3.1 Introduction

The production and utility of functional boron-containing complexes is a rapidly evolving area of research in main-group chemistry.[1] Emissive boron complexes find frequent use in the development of organic light emitting diodes (OLEDs),[2-4] cell imaging agents,[5-7] and stimuli-responsive materials.[8-11] Three-coordinate boron is often sought after for material design, due to the presence of an unoccupied p orbital, which results in a more electron deficient and Lewis acidic boron atom.[12, 13] Low-valent boron often finds use in catalytic reactions,[14-16] especially in the development of Frustrated Lewis Pairs, [17-19] and anion sensing technologies.[20, 21]

Several measures can be taken to enhance the electron deficiency of boron to increase Lewis acidity. An evolving strategy is to employ a three-coordinate, cationic boron atom (borenium cation),[22, 23] which has been proven to augment Lewis acidity.[22, 24] Often, when cationic boron is combined with organic π-conjugated fragments, the energy of the lowest unoccupied molecular orbital (LUMO) is reduced, usually as a result of the p-π* interactions.[25-27] This interaction narrows the band gap, allowing for a wider reach of applications. Despite the rich potential use of cationic boron in material design, the air, moisture and solution sensitivity prevent many applications and create challenges for optical and electrochemical characterization.[25, 28, 29] Efforts to achieve sufficient stabilization is an issue currently being addressed by researchers. There are no reports of borenium cations utilized for anion sensing, but the Gabbaï group has utilized a four-coordinate (boronium) cation as a means for fluoride detection (**3.1$^+$**).[30] The 4-dimethylaminopyridine (DMAP) ligand acts as a mask and is easily displaced upon addition of fluoride, resulting in a drastic increase in fluorescence intensity. Fluorescent three-coordinate (borenium) cations have been reported, demonstrating solid state (**3.2$^+$**)[31] and solution (**3.3$^+$** and **3.4^{2+}**)[26, 32] based emission. Cyclic voltammetry is a tool used to investigate the electrochemical properties of complexes, and specifically can be used to

evaluate reduction in LUMO energies in cationic boron complexes. The Jäkle group reported a dimeric boron dicationic complex, with a reduction potential of -1.36 V versus the ferrocene/ferrocenium (Fc/Fc$^+$) redox couple (**3.4^{2+}**).[32] The Gabbaï group reported **3.5$^+$**, with a reduction potential of -1.81 V, a value that is significantly more positive than related neutral boranes. [33]
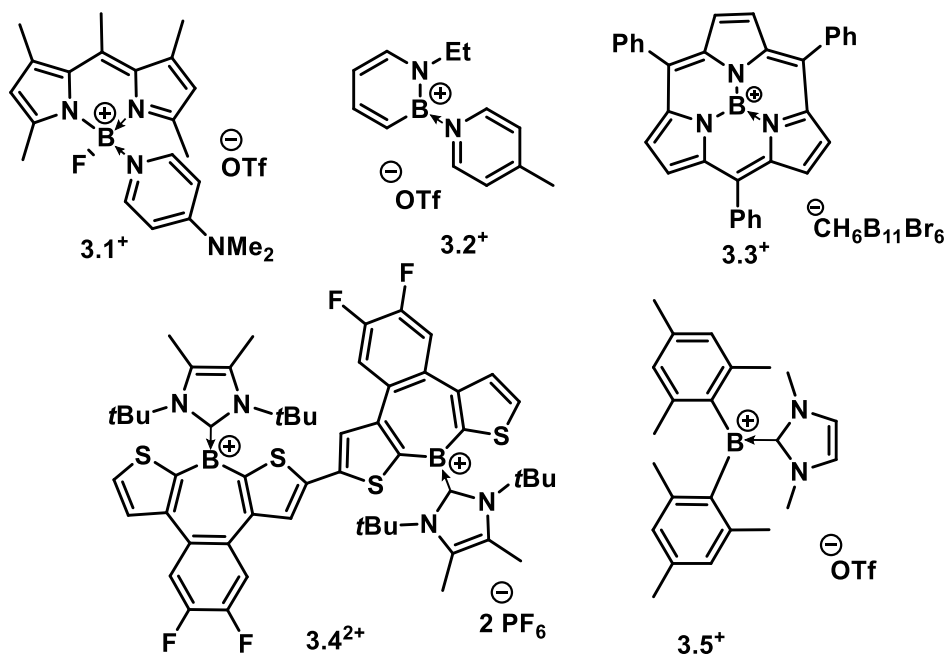
Expanded π-conjugation can allow for narrower HOMO-LUMO band gaps and increased reduction potentials. This result is often achieved by employing π-conjugated chelating heterocyclic ligands to support boron. N_2O^{2-} type chelating ligands are often used to stabilize four-coordinate boron atoms in dypyrinnate frameworks, with several examples of absorption and emission bands in the red to near-IR region of the electromagnetic spectrum.[34-37] These chelating ligands yield a relatively planar, chelate restrained complex with reduced dihedral angles, suitable for extension of π-conjugation and leading to increased quantum yields, with larger stokes shifts than a classical boron difluoride dipyrromethenes (BODIPYs).[35, 38]

Formazanate ligands are nitrogen rich analogues of β-diketiminates, and are typically complexed with either metal[39-41] or main group atoms.[42-44] Boron difluoride (BF$_2$) formazanate complexes are often targeted as a result of their tunable optical and redox

properties.[45-52] Recently, there have been advances in the production of unique boron formazanate complexes with atypical boron coordination environments. The Otten (**3.6**)[53] and Gilroy (**3.7**)[54] groups have both reported unusual boron heterocycles, with interesting optical and redox properties. Boron formazanate complexes with non-fluoride substituents have been produced, for example B(Ph)$_2$ formazanate complex (**3.8**) was used as a precursor for the isolation of stable radical dianionic and trianionic formazanate complexes.[55] Oxoborane (B=O) formazanate **3.9** exhibited a drastic enhancement of formazanate based fluorescence, which is often not observed for triarylformazanate complexes.[56] Finally, the first report of cationic boron formazanate complexes (*e.g.,* borenium cation **3.10**$^+$) were recently reported, along with an evaluation of the effect of coordination number and charge on the electronic structure.[25]
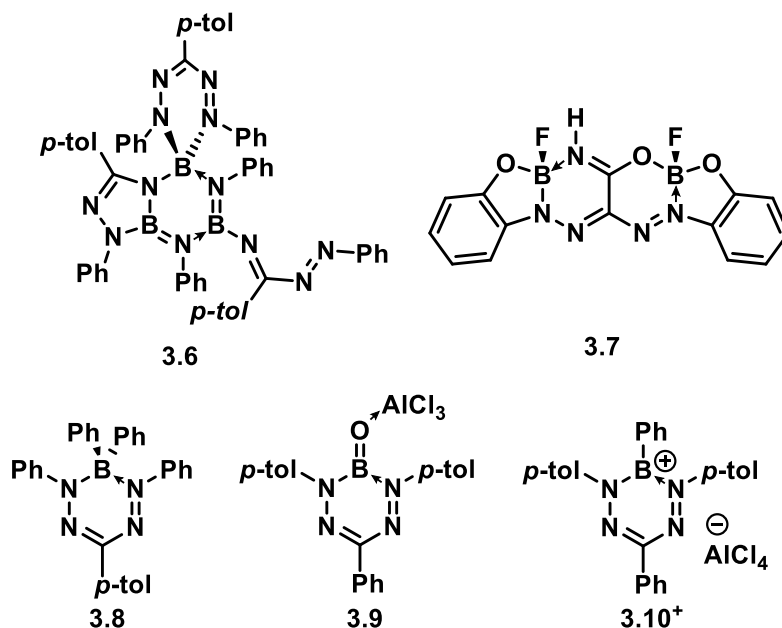
Herein, we report the synthesis of unique N$_2$O^{2-} chelating BF formazanate complexes, which are used as precursors to stable, sterically unencumbered borenium cations. These complexes possess high Lewis acidity, interesting redox chemistry and low-energy absorption/emission properties.

3.2 Results

3.2.1 Synthesis

The precursor formazans were synthesized by adapting a stepwise protocol commonly used to produce asymmetric formazans (Scheme 3.1). *p*-Tolylphenylhydrazine hydrochloride was treated with NEt$_3$ and benzaldehyde to form an aryl hydrazone, which was treated with base *in-situ*, and coupled with hydroxyl containing diazonium salts (n = 0 or n = 1) to afford formazans, after purification by column chromatography, **3.11a** and **3.11b** in 60% and 43% yield, respectively.
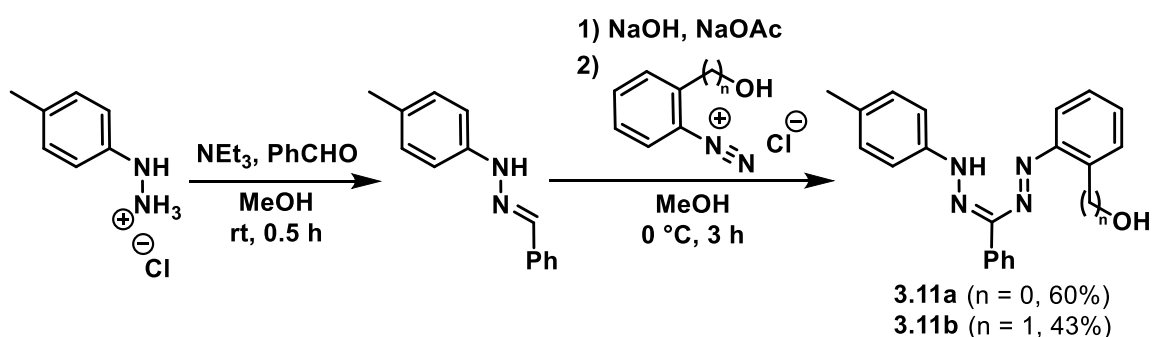
Scheme 3.1. Synthesis of Formazans **3.11a** and **3.11b**.

Formazans **3.11a** and **3.11b** were treated with an excess of NEt$_3$ and BF$_3$·OEt$_2$ (Scheme 3.2), leading to gradual colour changes from magenta to purple (**3.11a**) and red to magenta (**3.11b**). Following purification by column chromatography, BF formazanate complexes **3.12a** (68%) and **3.12b** (61%) were isolated as dark purple microcrystalline solids. These transformations were confirmed by the absence of the characteristic -N-H signal in the ^{1}H NMR spectra, the presence of a doublet in the ^{11}B{^{1}H} NMR spectrum and quartet in the ^{19}F{^{1}H} NMR spectrum. Compound **3.12a** forms a five-member boron-containing heterocyclic ring, while **3.12b** forms a six-member heterocyclic ring.
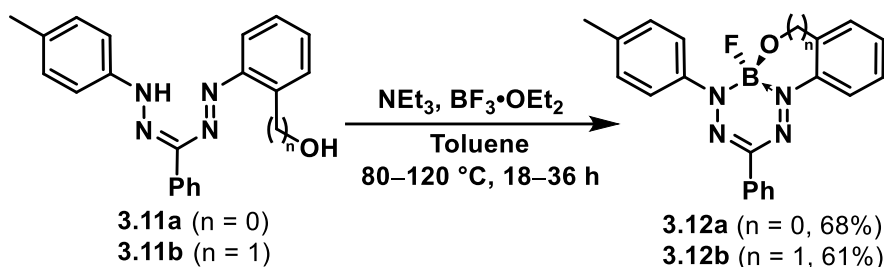
Scheme 3.2. Synthesis of BF formazanate complexes **3.12a** and **3.12b**.

BF Formazanates **3.12a** and **3.12b** were treated with one equiv. of $[Et_3Si(C_7H_8)][B(C_6F_5)_4]$ ("triethylsilylium cation")[57] (Scheme 3.3), a potent Lewis acid often used for halide abstraction. The toluene (C_7H_8) adduct of the triethylsilium cation is utilized as the free cation is challenging to isolate and has a tendency to decompose upon dissolution in aromatic solvents.[57] This reagent will abstract the fluoride ion, but also introduce a non/weakly coordinating anion, tetrakis(pentafluorophenyl)borate ($[B(C_6F_5)_4]^-$). Upon addition of the triethylsilylium cation to solutions of BF formazanates **3.12a** and **3.12b**, the colours instantly changed from purple to blue and magenta to teal, respectively. The reaction byproduct, triethylsilylfluoride (Et_3SiF), is easily removed by concentrating the solution *in vacuo*, followed by washing with *n*-pentane. Three-coordinate borenium formazanate complexes were isolated as microcrystalline blue and teal solids in 80% (**3.13a$^+$**) or 87% (**3.13b$^+$**) yield. Borenium cations **3.13a$^+$** and **3.13b$^+$** contained a diagnostic broad resonance in the $^{11}B\{^1H\}$ NMR spectra at 20.1 and 21.2 ppm respectively. The $^{19}F\{^1H\}$ NMR spectra revealed an absence of the B-F quartet resonance upon halide abstraction, and the presence of three signals from the $[B(C_6F_5)_4]^-$ counterion.
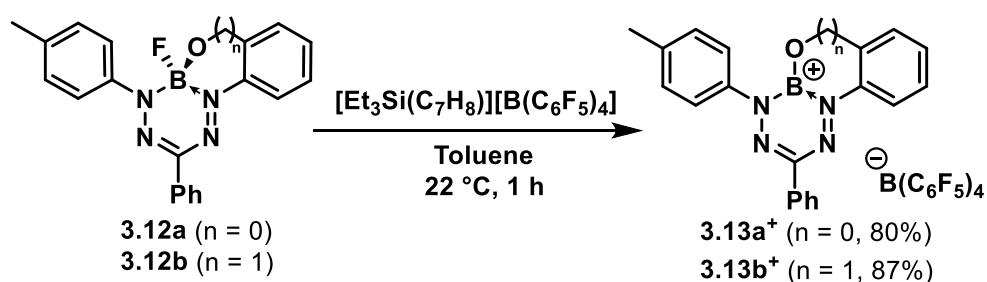
Scheme 3.3. Synthesis of borenium cations **3.13a$^+$** and **3.13b$^+$**.

In previous work, cationic boron formazanate complexes were generated from BCl formazanate complexes.[25] Using the triethylsilylium cation bypasses the necessity of installing B-Cl bonds, as the formation of the strong Si-F bond in the byproduct (Et₃SiF) provides a thermodynamic driving force for this reaction.[58] Often, bulky ligands are required in order to sufficiently stabilize and isolate low-coordinate boron cations.[59-62] Our borenium formazanate complexes are sterically unencumbered, which is likely a consequence of the stability gained from the nitrogen-rich formazanate ligand.

Extensive solvent purification (outlined in Section 3.4.1) was carried out to allow for solution-based characterization of borenium cations **3.13a⁺** and **3.13b⁺**. While **3.13a⁺** was stable in the solid state (satisfactory elemental analysis obtained) and at NMR concentration levels, further dilution repeatedly resulted in its decomposition. Thus, for complex **3.13a⁺**, we could not obtain reproducible solution-based characterization (*i.e.,* cyclic voltammetry, UV-vis, and fluorescence spectroscopy).

3.2.2   Gutmann-Beckett Lewis Acidity

Borenium cations **3.13a⁺** and **3.13b⁺** were subjected to the Gutmann-Beckett experimental NMR method to quantitatively evaluate their Lewis acidity.[63, 64] **3.13a⁺** and **3.13b⁺** were combined with one equiv. of Et₃PO and $^{31}P\{^{1}H\}$ NMR spectra were obtained in CD_2Cl_2 (Figure 3.1). This resulted in chemical shifts of 87.3 ppm for **3.13a⁺** and 86.7 ppm for **3.13b⁺**, resulting in acceptor number (AN = 2.21× (δ_{sample} − 41)) values of 102 and 101 respectively.
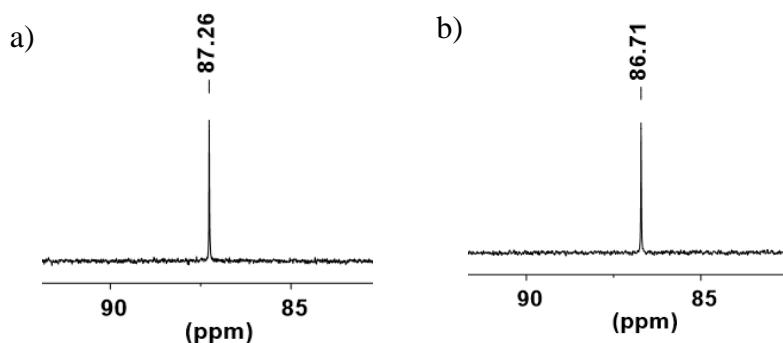
Figure 3.1. $^{31}P\{^{1}H\}$ NMR spectra of a) borenium cation **3.13a⁺** and b) borenium cation **3.13b⁺** after combination with one equiv. of Et₃PO in CD_2Cl_2.

These AN values indicate very high Lewis acidity beyond what is observed for widely used boron Lewis acids (*e.g.* $B(C_6F_5)_3$ AN = 78, BCl_3 AN = 97).[12] Cationic boron Lewis acids with large AN values are often implicated for use in catalytic reactions,[65] such as hydrosilylation of ketones (AN = 105).[66] These cationic boron Lewis acids may also find use in anion sensory applications, as the electron deficient boron centre is susceptible to nucleophilic attack.[21, 30, 67] We have selected **3.13b⁺** as a potential fluoride anion sensor, and tested its fluoride ion affinity by combining **3.13b⁺** with one equiv. of [*n*BuN][SiF$_2$Ph$_3$], an anhydrous fluoride source (Scheme 3.4). Preliminary results show complete conversion to a BF formazanate (complex **3.12b**), demonstrating successful fluorination. Further photophysical studies are underway to verify the utility as an optical anion sensor.
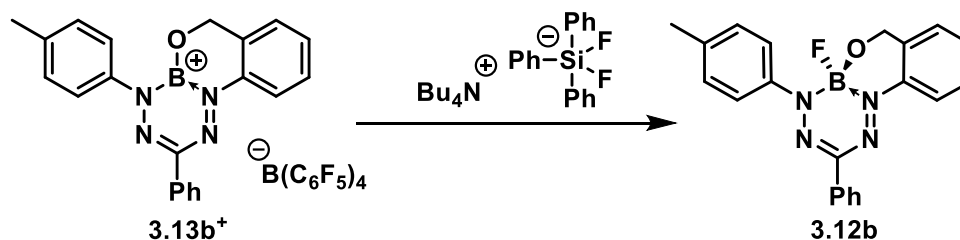
Scheme 3.4. Fluorination of borenium cation **3.13b⁺**.

3.2.3 X-ray Crystallography

Single crystals of **3.12a**, **3.12b**, **3.13a⁺** and **3.13b⁺** were obtained and analyzed using X-ray diffraction. Suitable crystals were grown by layering THF solutions with *n*-pentane and cooling at –20 °C (**3.12a** and **3.12b**), layering a CH_2Cl_2 solution with hexanes at 21 °C (**3.13a⁺**) or from a saturated toluene solution cooled at –20 °C (**3.13b⁺**). Solid-state molecular structures can be found in Figure 3.2 and selected bond lengths and angles in Table 3.1.
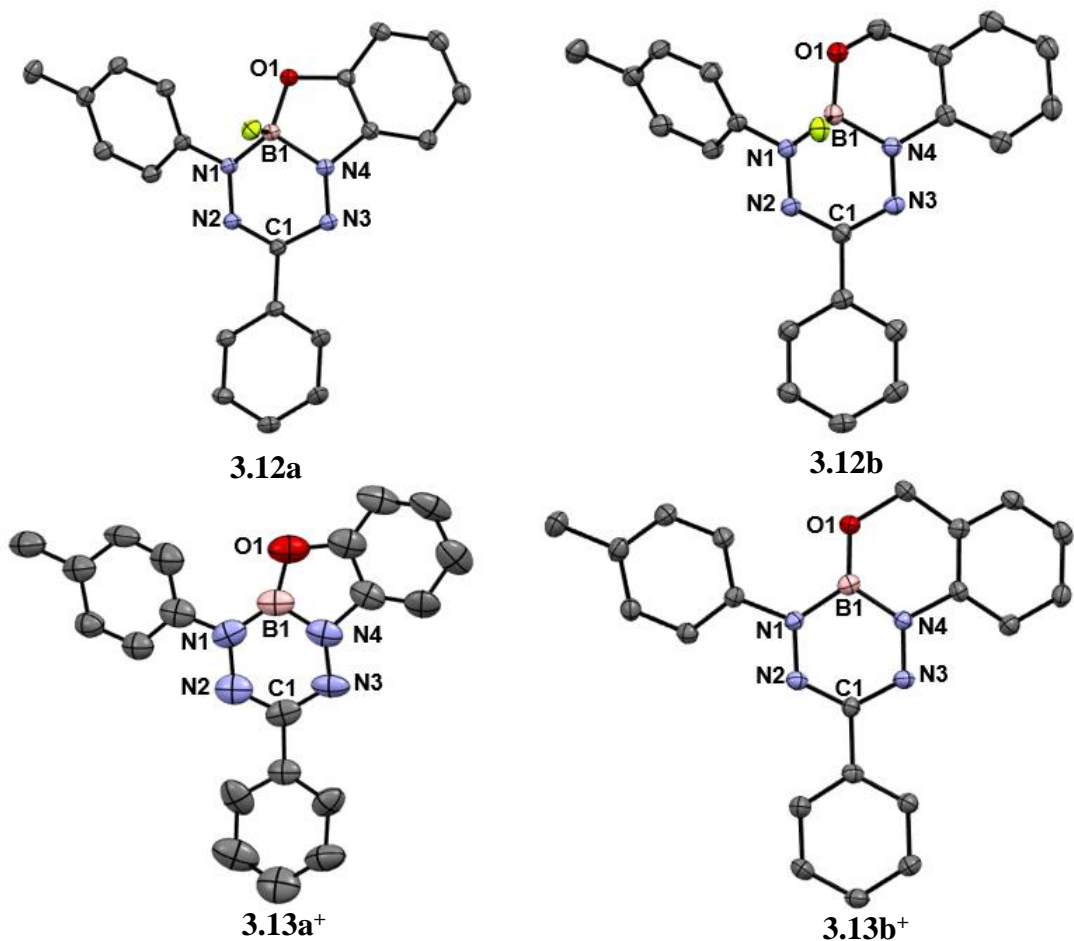
Figure 3.2. Solid-state structures of BF formazanates (**3.12a** and **3.12b**), and borenium cations (**3.13a⁺** and **3.13b⁺**). Anisotropic displacement ellipsoids are shown at the 50% probability level. Hydrogen atoms and counteranions are omitted for clarity.

The N-N and N-C bond lengths of the formazanate backbone in all four complexes ranged from 1.3018(12)−1.370(8) Å and 1.339(2)−1.365(9) Å, respectively. These values lie between the typical values for single and double bond lengths of the respective atoms, thus indicating a degree of electron delocalization. Complexes **3.12a** and **3.12b** contain B1-O1 [1.4584(14) Å or 1.4043(17) Å] and B1-N1 [1.5358(15) Å or 1.5827(17) Å] bond lengths indicative of single bond character. However, cationic complexes **3.13a⁺** and **3.13b⁺** have significantly shorter B1-O1 [1.375(8) Å or 1.333(3) Å] and B1-N1 [1.395(9) Å or 1.460(3) Å] bond lengths, suggesting a potential bond order greater than one. The B1-O1 bond lengths for five-member rings complexes **3.12a** and **3.13a⁺** are elongated compared to their six-member ring counterparts, due to enhanced ring strain.

BF formazanates **3.12a** and **3.12b** feature sp^3 hybridized boron centres with distorted tetrahedral geometry. As such, the boron atom is displaced from the plane defined by the four nitrogen atoms (N_4) by values of 0.4869(16) Å (**3.12a**) and 0.6190(19) Å (**3.12b**) (Figure 3.3). This also results in the fluorine atom protruding from the plane, rendering it accessible for abstraction. Three-coordinate complexes **3.13a⁺** and **3.13b⁺** contain boron atoms with trigonal planar geometry. In these complexes, boron is only minimally displaced from the N_4 plane by values of 0.044(12) Å and 0.056(3) Å for complexes **3.13a⁺** and **3.13b⁺**, respectively (Figure 3.3). The dihedral angles (angles between planes defined by the *N*-aryl substituents and N_4 formazanate backbone) for BF formazanates **3.12a** and **3.12b** range from 20.58(6) to 42.29(5)°, resembling typical four-coordinate boron formazanate complexes. Borenium cations **3.13a⁺** and **3.13b⁺** have markedly decreased values ranging from 6.1(8) to 25.75(11)°. These metrics result in highly planar three-coordinate borenium cation complexes.
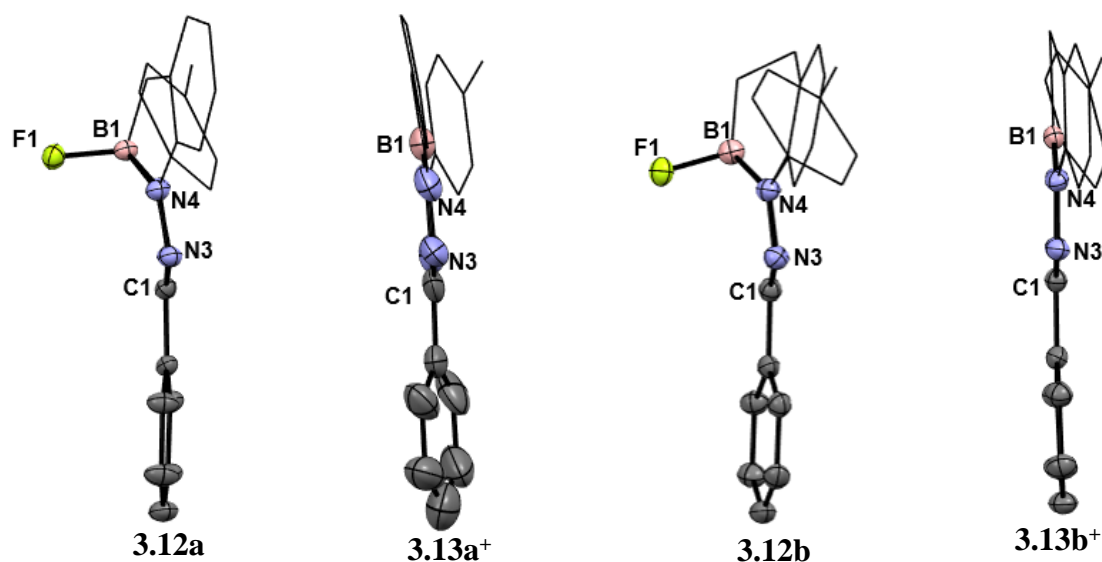
Figure 3.3. Side views of formazanate complexes **3.12a**, **3.12b**, **3.13a⁺** and **3.13b⁺**. Anisotropic displacement ellipsoids are shown at the 50% probability level. For clarity, hydrogen atoms and counteranions are omitted and *N*-aryl substituents are shown as wireframes.

The empty p orbital at boron, planarity and increased bond order of the B1-N1 bond lengths suggest that borenium cations **3.13a⁺** and **3.13b⁺** have some degree of aromaticity in the central N1-N2-C1-N3-N4-B1 (CN_4B) formazanate heterocyclic ring.

**Table 3.1.** Selected bond lengths (Å), bond angles (°) and structural metrics extracted from the solid-state structures of BF formazanates (**3.12a** and **3.12b)** and borenium cations (**3.13a⁺** and **3.13b⁺**).

	3.12a	3.12b	3.13a⁺	3.13b⁺
N1-N2	1.3213(12)	1.3115(14)	1.370(8)	1.334(2)
N3-N4	1.3018(12)	1.3123(14)	1.303(7)	1.319(2)
N2-C1	1.3406(13)	1.3499(16)	1.365(9)	1.339(2)
N3-C1	1.3584(14)	1.3372(16)	1.351(9)	1.339(2)
B1-N1	1.5358(15)	1.5827(17)	1.395(9)	1.460(3)
B1-N4	1.5443(14)	1.5525(17)	1.420(10)	1.451(3)
B1-O1	1.4584(14)	1.4043(17)	1.375(8)	1.333(3)
N1-B1-N4	102.16(8)	99.48(10)	114.3(7)	113.09(17)
N1-B1-O1	118.29(9)	117.48(11)	138.0(8)	124.44(18)
N4-B1-O1	102.21(8)	112.70(11)	107.7(6)	122.41(19)
Dihedral angles*a*	22.79(4),	20.58(6),	6.1 (8),	11.03(13),
	27.10(4)	42.29(5)	18.1(8)	25.75(11)
Boron displacement*b*	0.4869(16)	0.6190(19)	0.044(12)	0.056(3)

*a*Defined as the angle between the *N*-aryl substituents and the N_4 (N1-N2-N3-N4) plane of the formazanate ligand backbone. *b*Defined as the distance between B1 and the N_4 (N1-N2-N3-N4) plane of the formazanate ligand backbone.

3.2.4   Computational Studies of Frontier Molecular Orbitals

To gain an understanding of the electronic structure differences of complexes **3.12a**, **3.12b** and **3.13b⁺**, we used Density Functional Theory (DFT), calculated with the Gaussian program,[68] using the TPSSh/def2-TZVP SCRF=PCM method for CH_2Cl_2 solvated complexes. The frontier molecular orbitals (HOMO and LUMO) and corresponding energies were estimated using this method. (Figure 3.4). **3.13a⁺** is excluded from this analysis, as we do not report its solution-based characterization.

Comparison of the frontier molecular orbitals for neutral BF formazanates **3.12a** and **3.12b** reveal many similarities. The HOMOs are both delocalized over the entire complex, and the LUMOs are delocalized on the N_4 formazanate backbone and *N*-aryl substituents, with a nodal plane bisecting the centre of each compound. These results are consistent with typical four-coordinate boron formazanate complexes.[49, 50, 69]

The calculated molecular orbitals for borenium cation **3.13b⁺** exhibit many similarities compared to the neutral complexes. The HOMO is highly delocalized throughout the entire complex, including the CN_4B central heterocyclic ring providing evidence that there is

some degree of aromaticity in this ring. This is supported by the planarity and decreased B-N bond order observed in the solid-state structure. The LUMO is similar to the neutral complexes, including a central nodal plane. The HOMO and LUMO energies have both decreased compared to the neutral BF formazanates, as a result of the electron deficient three-coordinate cationic boron atom.
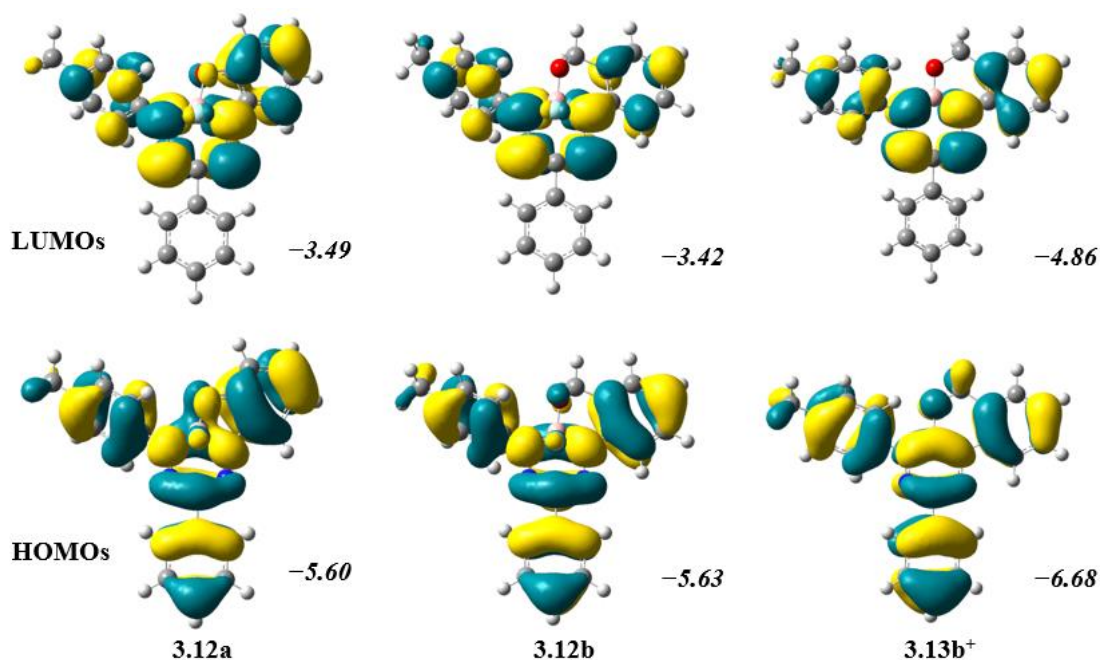
Figure 3.4. Frontier molecular orbitals and their energies (in eV) for CH_2Cl_2 solvated complexes **3.12a**, **3.12b** and **3.13b$^+$** calculated using TPSSh/def2-TZVP SCRF=PCM.

3.2.5 Cyclic Voltammetry

The electrochemical properties of **3.12a**, **3.12b** and **3.13b$^+$** were probed using cyclic voltammetry (CV). Cyclic voltammograms of all complexes collected in CH_2Cl_2 are shown in Figure 3.5 and the data are summarized in Table 3.2. The neutral BF formazanates **3.12a** and **3.12b** can be reversibly reduced electrochemically to their corresponding radical anion [**BFL**→**BFL$^{\bullet-}$**, L = formazanate ligand; $E_{red1} = -1.09$ V (**3.12a**) and $E_{red1} = -1.12$ V (**3.12b**)] and then irreversibly reduced to a dianion at more negative potential [**BFL$^{\bullet-}$**→**BFL^{2-}**; $E_{red2} = -2.05$ V (**3.12a**) and $E_{red2} = -2.12$ (**3.12b**)] relative to the ferrocene/ferrocenium (Fc/Fc$^+$) redox couple. Both neutral compounds also exhibit a

reversible oxidation [$\mathbf{BFL} \rightarrow \mathbf{BFL^{\bullet+}}$; E_{ox1} = 0.90 V (**3.12a**) and E_{ox1} = 0.89 V (**3.12b**)] to a radical cation when scanning to positive potential. The CV of borenium cation **3.13b⁺** is markedly different from the neutral complexes. The proximity in electrochemical potentials to the Fc/Fc⁺ redox couple caused **3.13b⁺** to react with ferrocene, thus 1,1'-dibromoferrocene was used as the internal standard (Section 3.4.1). The first reduction to a neutral radical occurred at E_{red1} = −0.30 V (**BFL⁺→BFL•**), with a second reduction to an anion at E_{red2} = −1.67V (**BFL•→BFL⁻**). Upon comparison of the CVs of BF formazanate **3.12b** and borenium cation **3.13b⁺**, there is a drastic increase in first reduction potential (ΔE_{red1} = +0.82 V).
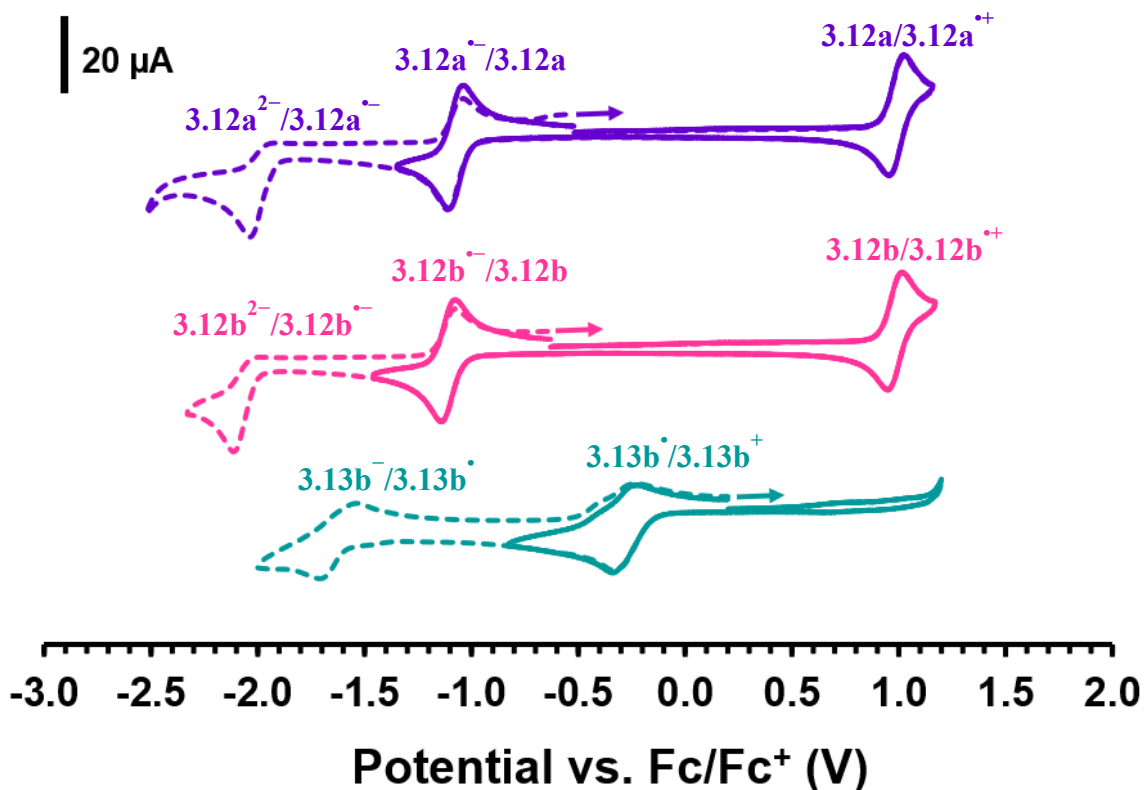

Figure 3.5. Cyclic voltammograms of *ca.* 1 mM CH_2Cl_2 solutions (containing 0.1 M [nBu₄N][B(C₆F₅)₄] as supporting electrolyte) of BF formazanates **3.12a** (purple) and **3.12b** (pink), and borenium cation **3.13b⁺** (teal) recorded at a scan rate 250 mVs⁻¹. The dashed lines represent a wide scan and solid line represent a narrower scan. The arrow denotes scan direction.

Table 3.2. Cyclic voltammetry data for BF formazanates **3.12a** and **3.12b,** and borenium cation **3.13b$^+$** in CH_2Cl_2 reported relative to the ferrocene/ferrocenium redox couple.

	E_{red2} (V)	E_{red1} (V)	E_{ox1} (V)
3.12a	-2.05^a	-1.09	0.99
3.12b	-2.12^a	-1.12	0.97
3.13b$^+$	-1.67^a	-0.30	$-$

^{a}Irreversible process, potential at maximum cathodic potential reported.

Comparison of E_{red1} values for neutral BF formazanate **3.12b** and borenium cation **3.13b$^+$** suggest the LUMO energy has been substantially lowered upon introduction of a three-coordinate cationic boron atom. To gain a better quantitative assessment, the frontier molecular orbital energies can be experimentally estimated using the onset of the redox event ($E_{Orbital}^{CV} = -4.8 - E_{onset}$) (Table 3.3).[70, 71] The computed LUMO energies (from CV) were $E_{LUMO}^{CV} = -3.77$ eV (**3.12b**) and $E_{LUMO}^{CV} = -4.70$ eV (**3.13b$^+$**), revealing a difference of 0.93 eV. This provides evidence that the introduction of a cationic, three-coordinate boron centre substantially lowers the energy level of the LUMO, allowing for a more facile reduction, rendering it strongly electron accepting.

HOMO energies can be calculated in a similar manner along with the LUMO energies to estimate the experimental band gaps (E_g^{CV}), representing the difference between the HOMO and LUMO energy levels (Table 3.3). Using the same methodology, the calculated values are $E_{HOMO}^{CV} = -6.00$ eV (**3.12a**) and $E_{HOMO}^{CV} = -5.99$ eV (**3.12b**). Together with the E_{LUMO}^{CV} values, the E_g^{CV} can be calculated [$E_g^{CV} = 1.89$ eV (**3.12a**) and $E_g^{CV} = 1.92$ (**3.12b**)]. The experimental data suggests that BF formazanate **3.12a** has a slightly narrowed HOMO-LUMO energy gap [$\Delta E_g^{CV} = -0.03$ eV], approximately matching the computationally calculated band gap difference [$\Delta E_g^{DFT} = -0.10$ eV)] There was no oxidation event observed within the solvent window for **3.13b$^+$**, thus a E_{HOMO}^{CV} and corresponding E_g^{CV} could not be calculated. However, the value was estimated computationally as $E_g^{DFT} = 1.82$ eV, which is significantly lower than the E_g^{DFT} values for neutral BF formazanates **3.12a** and **3.12b**.

Table 3.3. Experimental and theoretical frontier molecular orbital energies and band gaps.

	Experimental					Theory[d]		
	E_{onset}^{red}	E_{LUMO}^{CV}	E_{onset}^{ox}	E_{HOMO}^{CV}	E_g^{CV}	E_{LUMO}^{DFT}	E_{HOMO}^{DFT}	E_g^{DFT}
	(V)	$(eV)^a$	(V)	$(eV)^b$	$(eV)^c$	(eV)	(eV)	$(eV)^c$
3.12a	–0.99	–3.81	0.90	–5.70	1.89	–3.49	–5.60	2.11
3.12b	–1.03	–3.77	0.89	–5.69	1.92	–3.42	–5.63	2.21
3.13b$^+$	–0.10	–4.70	–	N/A	N/A	–4.86	–6.68	1.82

^{a}$E_{LUMO}^{CV} = -4.8 - E_{onset}^{red}$. ^{b}$E_{HOMO}^{CV} = -4.8 - E_{onset}^{ox}$. ^{c}$E_g = |E_{LUMO} - E_{HOMO}|$. ^{d}Estimated using TDDFT (TPSSh/def2–TZVP SCRF=PCM) for CH_2Cl_2 solvated complexes.

3.2.6   UV-Visible Absorption & Emission Spectroscopy

The UV-vis absorption spectra of **3.12a**, **3.12b** and **3.13b$^+$** were measured in CH_2Cl_2 (Figure 3.6) and all data is summarized in Table 3.4. TDDFT results reveal that the dominant orbital pair involved in all low-energy absorptions for **3.12a**, **3.12b** and **3.13b$^+$** is the HOMO and LUMO. Furthermore, all low energy excitations are of $\pi \rightarrow \pi^*$ type.

Four-coordinate neutral BF formazanates **3.12a** and **3.12b** were strongly absorbing (19,900−20,200 $M^{-1}cm^{-1}$) in the visible region of the electromagnetic spectrum and had broad absorption profiles with low-energy maxima at 530 (**3.12b**) and 559 (**3.12a**) nm. The absorption maximum (λ_{max}) for **3.12a** is of lower energy, because of the electron-donating oxygen substituent directly appended to the *N*-aryl substituent. This increases the π-conjugation and will consequently narrow the HOMO-LUMO gap. To better illustrate this effect, optical band gaps (E_g^{opt}) were estimated using the onset of absorption ($E_g^{opt} = 1240/\lambda_{abs}^{onset}$) as $E_g^{opt} = 1.95$ eV (**3.12a**) and $E_g^{opt} = 1.99$ eV (**3.12b**). The E_g^{opt} values support a reduction in the HOMO-LUMO gap for compound **3.12a** compared to compound **3.12b** by 0.04 eV. Upon comparison with the CV band gap [$\Delta E_g^{CV} = -0.03$ eV, Section 3.2.5], there is a close match in the experimentally obtained values.

The UV-vis spectrum of borenium cation **3.13b$^+$** differs greatly from the neutral complexes. There is a large reduction in the molar extinction coefficient, down to a value of 8,000 M^{-1} cm^{-1}. Upon comparison with the neutral precursor (**3.12b**), the low energy

maximum of borenium cation **3.13b$^+$** is red-shifted to 650 nm ($\Delta\lambda_{max}$ = +120 nm). There is a second maximum at 605 nm (ε = 7,100 M^{-1}cm^{-1}), which likely arises due to vibronic fine structure. The optical band gap for borenium cation **3.13$^+$** is $E_g{}^{opt}$ = 1.80 eV, representing a 0.15 eV reduction upon comparison with BF formazanate **3.12b**. Although $E_g{}^{CV}$ could not be determined (Section 3.2.5), the $E_g{}^{opt}$ is in close agreement with the theoretical value [$E_g{}^{DFT}$ = 1.82 eV]. This large shift and different UV-vis profile compared to BF formazanate **3.12b** is indicative of a significant alteration of the electronic structure upon transformation from a neutral four-coordinate to a cationic three-coordinate boron atom supported by a common N$_2$O^{2-} formazanate ligand.
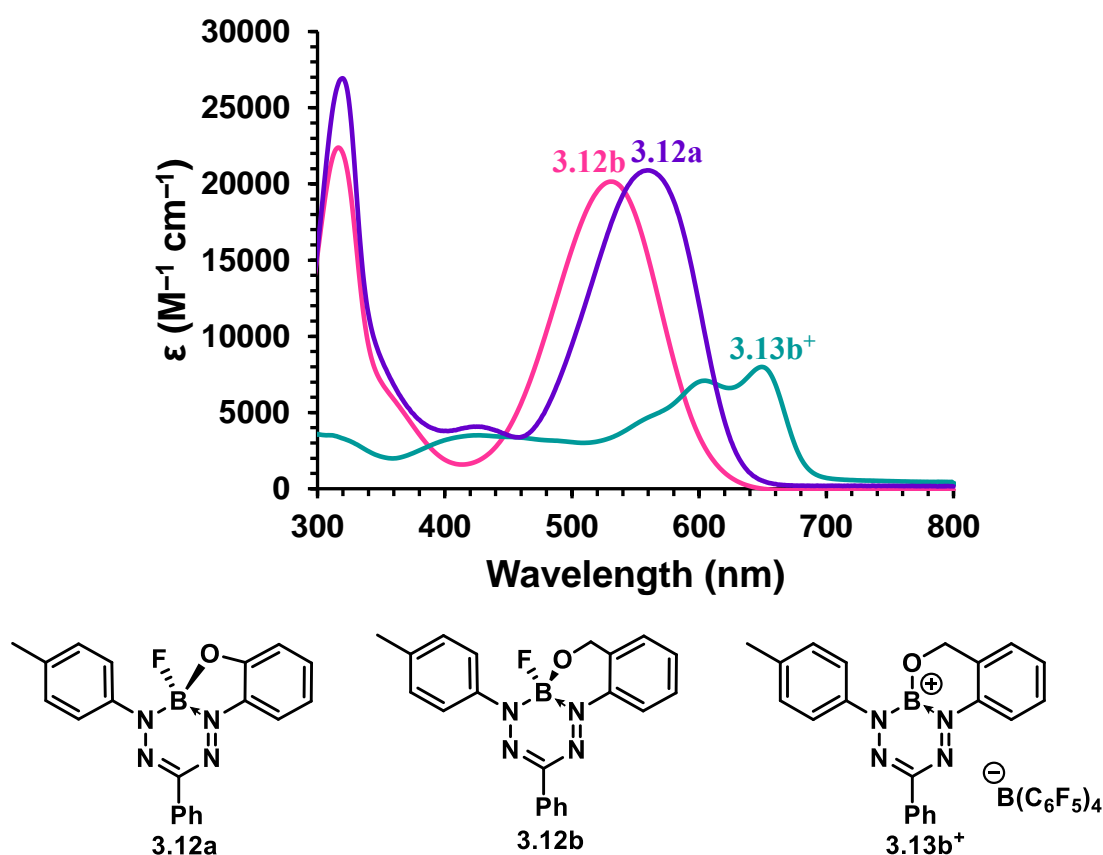
Figure 3.6. UV-vis spectra of BF formazanates **3.12a**, **3.12b**, and borenium cation **3.13b$^+$** recorded for 10^{-5} M CH$_2$Cl$_2$ solutions.

All complexes were excited at their low-energy λ_{max} to probe for fluorescence. Complexes **3.12a** and **3.12b** were non-emissive in solution upon excitation. This may be due to the presence of a vibrational/rotational non-radiative decay pathway associated with the phenyl substituent, often encountered with other triarylformazanates complexes.[42, 49, 50] However,

it should be noted that it is uncommon for triarylformazanate complexes to be completely non-emissive. Interestingly, borenium cation **3.13b$^+$** was highly fluorescent ($\lambda_{em} = 672$ nm) in CH$_2$Cl$_2$ (Figure 3.7), with a fluorescence quantum yield (Φ_F) of 0.38. The narrow Stokes shift ($\upsilon_{ST} = 504$ cm^{-1} or 22 nm) is indicative of minimal structural reorganization upon relaxation to the ground state, likely also providing rationale for the emission observed. This effect has been observed in an oxoborane containing triarylformazanate, which also exhibited strong fluorescence.[56]
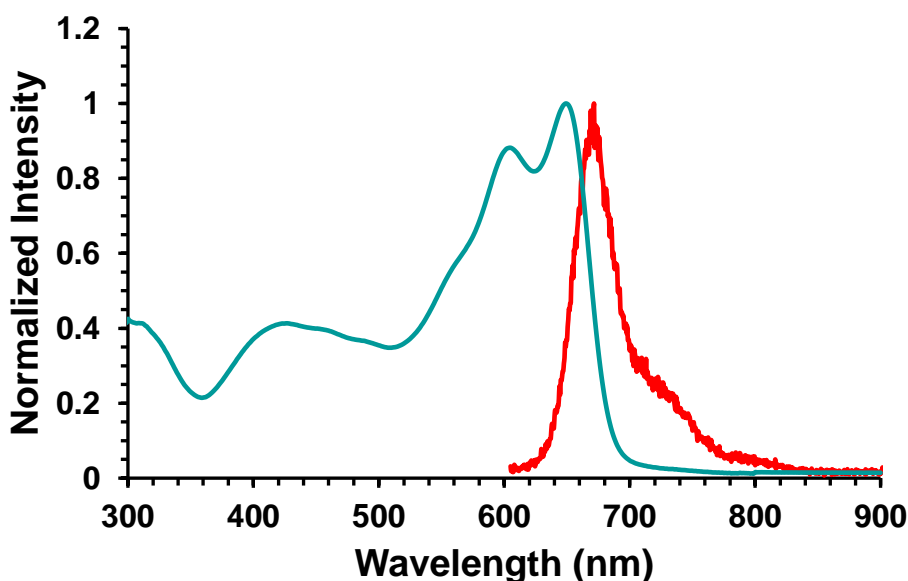

Figure 3.7. Normalized absorption (teal) and fluorescence (red) spectra recorded for 10^{-5} M CH$_2$Cl$_2$ solutions of borenium cation **3.13b$^+$**.

Table 3.4. Experimental and simulated spectroscopic properties of complexes **3.12a**, **3.12b** and **3.13b$^+$** in CH$_2$Cl$_2$ solution.

	Experimental									Theory^c	
	λ_{max}	ε	E_g^{opt}	E_g^{CV}	λ_{em}	Φ_F	υ_{ST}	υ_{ST}		λ_{max}	E_g^{DFT}
	(nm)	(M^{-1} cm^{-1})	(eV)^a	(eV)	(nm)	(%)^b	(nm)	(cm^{-1})		(nm)	(eV)
3.12a	559	19 900	1.95	1.89	−	−	−	−		556	2.11
3.12b	530	20 200	1.99	1.92	−	−	−	−		527	2.21
3.13b$^+$	650	8 000	1.80	N/A	672	38	22	504		663	1.82

^{a}E$_g^{opt}$ = 1240/ λ_{abs}^{onset}. ^{b}Absolute quantum yields were measured using the integrated sphere method. ^{c}Estimated using TDDFT (TPSSh/def2–TZVP SCRF=PCM) for CH$_2$Cl$_2$ solvated complexes.

3.3   Conclusions

In conclusion, a new set of BF formazanates (**3.12a** and **3.12b**) and borenium cations (**3.13a$^+$** and **3.13b$^+$**) supported by a tridentate N_2O^{2-} ligand were synthesized and the optical and electrochemical properties were examined. Both borenium cations were highly Lewis acidic, with AN values >100. Upon comparison of the cyclic voltammograms of neutral BF formazanate **3.12b** and borenium formazanate **3.13b$^+$**, it became clear that complex **3.13b$^+$** was significantly easier to reduce (ΔE_{red1} = –0.82 V). Experimentally, we verified that the LUMO energy of **3.13b$^+$** was substantially lower than that of **3.12b** (ΔE_{LUMO}^{CV} = –0.93 eV), suggesting an enhancement in the electron deficiency. Neutral BF formazanates **3.12a** and **3.12b** were strongly absorbing (ε = 19,900–20,200 M^{-1} cm^{-1}) and exhibit low-energy absorption maxima at 559 nm and 530 nm, respectively. Borenium cation **3.13b$^+$** had a weakly absorbing (ε = 8,000 M^{-1} cm^{-1}) low energy band at 650 nm, which was drastically red-shifted from its neutral counterpart **3.12b** ($\Delta\lambda_{max}$ = +120 nm). BF formazanates were none-emissive in solution, however borenium cation **3.13b$^+$** was strongly emissive (Φ_F = 0.38), likely because of the planarity induced upon fluoride abstraction. Preliminary studies indicate that the borenium cation (**3.13b$^+$**) could be used for fluoride sensing, and act as an emission "turn-off" sensor upon binding fluoride. This work provides the basis and methodology required to design optoelectronic materials with cationic boron, that contain significantly reduced HOMO and LUMO energies and high Lewis acidity.

3.4   Experimental Section

3.4.1   General Considerations

Reactions and manipulations were carried out under an N_2 atmosphere using standard glove box or Schlenk techniques unless otherwise stated. Reagents were purchased from Sigma-Aldrich, Alfa Aesar or Oakwood Chemicals and used as received unless otherwise noted. [Et$_3$Si(C$_7$H$_8$)][B(C$_6$F$_5$)$_4$] was prepared according to a published procedure[57] and used immediately. Solvents were purchased from Caledon Laboratories, dried using an Innovative Technologies Inc. solvent purification system, collected under vacuum, and

stored under an N$_2$ atmosphere over 4 Å molecular sieves. Toluene used for the synthesis of **3.13a**$^+$ and **3.13b**$^+$ was further stirred over and distilled from CaH$_2$ and stored over 4 Å molecular sieves before use. CH$_2$Cl$_2$ used for cyclic voltammetry, UV-vis absorption, and emission studies of **3.13b**$^+$ was passed through a silica (oven dried at 180 °C for 72 h) packed column, stirred over and distilled from CaH$_2$, followed by stirring and distillation from AlCl$_3$ twice before being stored over 4 Å molecular sieves for 48 h before use. NMR spectra were recorded at 25 °C on a 400 MHz (^{1}H: 399.8 MHz; ^{11}B{^{1}H}: 128.3 MHz; ^{13}C{^{1}H}: 100.5 MHz; ^{19}F{^{1}H}: 376.1 MHz) Varian INOVA spectrometer at 25 °C. ^{1}H NMR spectra were referenced to residual CHCl$_3$ (δ = 7.26) or CHDCl$_2$ (δ = 5.32) or DMSO-d$_5$ (δ = 2.50), ^{11}B{^{1}H} spectra were referenced to BF$_3$•OEt$_2$ (δ = 0), ^{13}C{^{1}H} NMR spectra were referenced to CDCl$_3$ (δ = 77.2) or CD$_2$Cl$_2$ (δ = 54.0) or DMSO-d$_6$ (δ = 39.5) and ^{19}F{^{1}H} NMR spectra were referenced to CFCl$_3$ (δ = 0). Mass-spectrometry data were recorded in positive or negative ion mode using a Bruker microTOF II electrospray ionization spectrometer. FT-IR spectra were recorded on a PerkinElmer Spectrum Two instrument using an attenuated total reflectance accessory. UV-vis absorption spectra were recorded on a Cary 5000 UV-Vis-NIR spectrophotometer. Molar extinction coefficients were determined from the slope of a plot of absorbance against concentration using four solutions with various known concentrations. Emission spectra were obtained using a Photon Technology International (PTI) QM-4 SE spectrofluorometer. Excitation wavelengths were chosen based on λ_{max} from the respective UV/Vis absorption spectrum of each compound in the same solvent. Absolute emission quantum yields were measured using a Hamamatsu C11347-11 Quantaurus Absolute PL Quantum Yield Spectrometer.

Elemental Analysis

Data were recorded at York University using an Elementar Vario EL Cube (VarioElcube Software v4.0.13) instrument operated at 1150 °C under Ar in CHNS mode. Samples were prepared in an MBraun Glovebox and sulfur levels were either below the detection limit (<0.2%) or not detected.

Cyclic Voltammetry

Cyclic voltammetry experiments were performed in an Ar filled glovebox, using a Bioanalytical Systems Inc. (BASi) Epsilon potentiostat and analyzed using BASi Epsilon software. Typical electrochemical cells consisted of a three-electrode setup including a silver *pseudo*-reference electrode, glassy carbon working electrode, and platinum counter electrode. Experiments were run at a scan rate of 250 mV s^{-1} in CH_2Cl_2 solutions of the analyte (~1 mM) and supporting electrolyte (0.1 M [nBu$_4$N][B(C$_6$F$_5$)$_4$]). Cyclic voltammograms were referenced relative to the ferrocene/ferrocenium (Fc/Fc$^+$) redox couples (~1 mM internal standard) and corrected for internal cell resistance using the BASi Epsilon software. Compound **3.13b$^+$** reacts with ferrocene. To circumvent this issue, 1,1'-dibromoferrocene was added as an internal reference for **3.13b$^+$**. A scan of a 1:1 solution of ferrocene:1,1'-dibromoferrocene under identical conditions was then collected to determine an oxidation potential 1,1'-dibromoferrocene relative to Fc/Fc$^+$. This value was then used to reference the voltammogram of **3.13b$^+$** to the Fc/Fc$^+$ redox couple.

3.4.2   X-ray Diffraction Methods

Data Collection and Processing:

Single crystals suitable for X-ray diffraction studies were grown by layering a THF solution with *n*-pentane and cooling at –20 °C (**3.12a** and **3.12b**), layering a CH_2Cl_2 solution with hexanes at 21 °C (**3.13a$^+$**) or from slow cooling a saturated toluene solution at –20 °C (**3.13b$^+$**). The samples were mounted on MiTeGen polyimide micromounts with a small amount of Paratone *N* oil. X-ray diffraction measurements were made on a Bruker Kappa Axis Apex2 or Bruker-Nonius KappaCCD Apex2 diffractometer at a temperature of 110 K. The data collection strategy involved a number of ω and φ scans, which collected data up to 67.52° (2θ, **3.12a**), 134.74° (2θ, **3.12b**), 46.57° (2θ, **3.13a$^+$**), and 47.124° (2θ, **3.13b$^+$**). The frame integration was performed using SAINT.[72] The resulting raw data was scaled and absorption corrected using a multi-scan averaging of symmetry equivalent data using SADABS.[73]

Structure Solution and Refinement:

The structures were solved by using a dual space methodology using the SHELXT program.[74] All non-hydrogen atoms were obtained from the initial solution for **3.12a**, **3.12b** and **3.13a⁺**. The hydrogen atoms were introduced at idealized positions and were allowed to refine isotropically (**3.12a** and **3.12b)** or to ride on the parent atom (**3.13a⁺**). For **3.13b⁺**, most non-hydrogen atoms were obtained from the initial solution. The remaining atoms were recovered from a difference Fourier map. All of the hydrogen atoms on the cation (**3.13b⁺**) except those bound to C20 were introduced at idealized positions and were allowed to refine isotropically. The structural models were fit to the data using full matrix least-squares based on F^2. The calculated structure factors included corrections for anomalous dispersion from the usual tabulation. The structures were refined using the SHELXL program from the SHELX suite of crystallographic software.[75] The Mercury v3.10.3 software package was used to generate graphical representations of the solid-state structures. Additional data collection and refinement details can be found in Table 3.5

Treatment of Disorders:

For **3.12b**: A difference Fourier map showed that the hydrogen atom positions for methyl group (C20) were disordered over two orientations. This disordered was modelled by assuming an idealized disordered methyl group and fixing the occupancy at 50:50 for the two orientations.

For **3.13a⁺**: The cation is disordered over three orientations. The atoms in the various disordered fragments are denoted by a naming scheme as follows: unprimed names are the major component, the single prime (') denote the second orientation, and the double prime (") denote the third component. The occupancy of these orientations refined to values 0.5377(26), 0.2233(29), and 0.2390(29). The second orientation of the disordered cation can be described as a shift of approximately 0.9 Å and an approximate 180° rotation about a vector co-linear with the B1–C1 direction. The third orientation can be described as an approximate 180° rotation about a vector co-linear with the C2'–C5' direction.

For **3.13b⁺**: The hydrogen atoms bound to methyl group C20 were disordered and were modelled as a second conformation where the hydrogen atom positions were rotated 60º relative to the other set of hydrogen atom positions. The occupancies were allowed to refine and converged to value of 0.50(3). For the final refinement cycles, the occupancy for the methyl disorder was fixed at 0.5000. In addition, the asymmetric unit contains two sites of disordered toluene molecules – one on a general position and the other was in the vicinity of a crystallographic centre of symmetry. The disordered toluene near the centre of symmetry could not be reasonably modelled and was subjected to the SQUEEZE procedure as implemented by the PLATON program.[76] The disordered toluene molecule residing at a general position in the unit cell was modelled using a conventional split atom refinement. The centroids of the aromatic rings differed by 0.49 Å. The methyl groups were rotated by roughly 172º relative to one another. The angle between the two sets of ring atoms was 2.4º.

Table 3.5. X-ray diffraction data collection and refinement details for complexes **3.12a**, **3.12b**, **[3.13a⁺][B(C₆F₅)₄]** and **[3.13b⁺][B(C₆F₅)₄]**.

	3.12a	3.12b	[3.13a⁺][B(C₆F₅)₄]	[3.13b⁺·C₇H₈][B(C₆F₅)₄]
Formula	$C_{20}H_{16}BFN_4O$	$C_{21}H_{18}BFN_4O$	$C_{44}H_{16}B_2F_{20}N_4O$	$C_{52}H_{26}B_2F_{20}N_4O$
FW (g mol⁻¹)	358.18	372.20	1018.23	1124.39
Crystal Habit	Purple Prism	Purple Prism	Purple Prism	Purple Plate
Crystal	Triclinic	Monoclinic	Orthorhombic	Monoclinic
Space Group	P$\bar{1}$	P2₁/c	Pbca	P2₁/c
T (K)	110	110	110	110
λ (Å)	0.71073	1.54178	0.71073	0.71073
a (Å)	8.151(2)	9.0367(10)	20.789(6)	17.113(6)
b (Å)	8.891(2)	13.9481(14)	16.758(6)	20.345(7)
c (Å)	13.504(4)	14.746(2)	22.932(9)	15.711(6)
α (°)	73.052(17)	90	90	90
β (°)	75.953(11)	105.215(5)	90	115.728(10)
γ (°)	68.333(9)	90	90	90
V (Å³)	859.9(4)	1793.5(4)	7989(5)	4928(3)
Z	2	4	8	4
ρ (g cm⁻³)	1.383	1.378	1.693	1.516
μ (cm⁻¹)	0.095	0.766	0.167	0.144
R₁,[a] ωR₂[b] [I >	0.0464,	0.0333,	0.0389, 0.0852	0.0302, 0.0703
R₁, ωR₂ (all	0.0732,	0.0360,	0.0488, 0.0907	0.0478, 0.0785
GOF[c]	1.017	1.029	1.140	1.018

[a]$R_1 = \Sigma(|F_o|-|F_c|)/\Sigma F_o$
[b]$\omega R_2 = [\Sigma(\omega(F_o^2-F_c^2)^2)/\Sigma(\omega F_o^4)]^{1/2}$
[c]$GOF = [\Sigma(\omega(F_o^2-F_c^2)^2)/(\text{No. of reflns.–No. of params.})]^{1/2}$
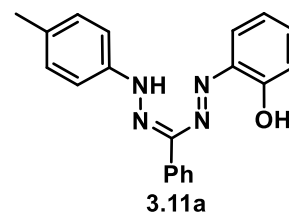
3.4.3   Computational Methodology

All electronic structure calculations were carried out with the *Gaussian* program[68] using the TPSSh functional,[77] def2-TZVP basis set, and the polarizable continuum model of implicit solvation (PCM) by dichloromethane. All geometry optimizations and TDDFT calculations were performed for solvated molecules. The optimized ground-state structures were confirmed by vibrational analysis to be minima on the potential energy surface. The electronic excitation calculations were performed using non-equilibrium solvation (which is the default for single-point TDDFT runs). The UV-vis absorption spectra were artificially broadened using the half-width at half-maximum (HWHM) set to 0.2 eV.

3.4.4   Synthetic Procedures

NMR spectra can be found in the appendix (Fig A3.1 – Fig A3.20).

Formazan 3.11a

In air, *p*-tolylphenylhydrazine hydrochloride (3.00 g, 18.9 mmol) was suspended in MeOH (50 mL) and stirred for 10 min before NEt$_3$ (3.5 g, 4.8 mL 34 mmol) was added. The solution was stirred for 15 min before benzaldehyde (2.1 g, 2.0 mL, 20 mmol) was added dropwise. The pale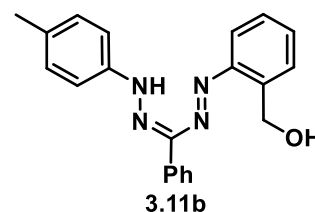-yellow solution was stirred for 1 h. MeOH (100 mL) was added and the mixture was treated with NaOH (2.85 g, 71.3 mmol) and NaOAc (4.05 g, 49.4 mmol). The resulting orange hydrazone-containing solution was cooled to 0 °C for 30 min. In a separate flask, 2-aminophenol (2.49 g, 22.8 mmol) was dissolved in water (25 mL) and concentrated hydrochloric acid (6.6 mL, 79 mmol) was added dropwise before the mixture was cooled to 0 °C. A solution of sodium nitrite (1.73 g, 25.1 mmol) was dissolved in water (10 mL), cooled to 0 °C and then added dropwise to the acidic 2-aminophenol solution. This diazonium salt containing solution was stirred for 10 min and then added dropwise to the orange hydrazone solution. The solution turned dark magenta immediately, and was stirred for 3 h at 0 °C. During this time, large quantities of **3.11a** solid precipitated from solution. The reaction mixture was neutralized with 1 M

HCl (*ca.* 25 mL), and the resulting dark purple precipitate was collected and washed with methanol. The crude solid was purified using flash column chromatography (neutral alumina, ethyl acetate) before volatiles were removed *in vacuo* to afford formazan **3.11a** as a dark purple solid (green reflex). Yield = 3.77 g, 60%. M.p.: 187–189 °C. ^{1}H NMR (399.8 MHz, CDCl$_3$) δ 15.38 (s, 1H, N*H*), 12.68 (s, 1H, O*H*), 7.91 (d, $^3J_{HH}$ = 7.3 Hz, 2H, aryl C*H*), 7.67 (s, 1H, aryl C*H*), 7.45 (t, $^3J_{HH}$ = 7.4 Hz, 2H, aryl C*H*), 7.38 (d, $^3J_{HH}$ = 8.4 Hz, 3H, aryl C*H*), 7.34–7.28 (m, 1H, aryl C*H*), 7.20 (d, $^3J_{HH}$ = 8.4 Hz, 2H, aryl C*H*), 7.10–7.02 (m, 2H, aryl C*H*), 2.37 (s, 3H, C*H$_3$*). ^{13}C{^{1}H} NMR (100.5 MHz, CDCl$_3$) δ 152.7, 141.2, 139.4, 136.6, 136.5, 135.0, 132.2, 130.3, 130.1, 128.8, 128.1, 125.5, 120.4, 118.7, 116.1, 21.2. FT-IR (ATR): 3250 (b), 3031 (w), 2923 (w), 1575 (m), 1506 (m), 1456 (m), 1436 (m), 1201 (m), 1144 (s), 877 (s), 820 (s), 735 (s), 639 (s), 513 (s) cm^{-1}. UV-vis (CH$_2$Cl$_2$): λ$_{max}$ 546 nm (ε = 19,500 M^{-1} cm^{-1}), 307 nm (ε = 20,300 M^{-1} cm^{-1}). Mass Spec. (ESI, −ve mode): exact mass calculated for [C$_{20}$H$_{17}$N$_4$O]$^-$, [M–H]$^-$: 329.1402; exact mass found: 329.1410; difference: +2.4 ppm. Anal. Calcd. (%) for C$_{20}$H$_{18}$N$_4$O: C, 72.71; H, 5.49; N, 16.96. Found: C, 72.38; H, 6.06; N, 17.06.

Formazan 3.11b

In air, *p*-tolylphenylhydrazine hydrochloride (3.96 g, 25.0 mmol) was suspended in MeOH (75 mL) and stirred for 10 min before NEt$_3$ (4.50 g 6.20 mL, 44.4 mmol) was added. The solution was stirred for 15 min before benzaldehyde (2.9 g, 2.8 mL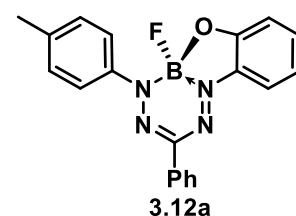, 27 mmol) was then added dropwise. The pale-yellow solution was stirred for 1 h. MeOH (150 mL) was added and the mixture was treated with NaOH (4.00 g, 100 mmol) and NaOAc (5.79g, 70.6 mmol). The resulting orange hydrazone-containing solution was cooled to 0 °C for 30 min. In a separate flask, 2-aminobenzyl alcohol (3.76 g, 30.5 mmol) was dissolved in water (40 mL) and concentrated hydrochloric acid (9.0 mL, 110 mmol) was added dropwise before the flask was cooled to 0 °C. A solution of sodium nitrite (2.42 g, 35.1 mmol) was dissolved in water (15 mL), cooled to 0 °C and then added dropwise to the 2-aminobenzyl alcohol solution. This diazonium salt containing solution was stirred for 10 min and then added dropwise to the orange hydrazone-containing solution. The solution turned dark red immediately, and was

stirred for 3 h at 0 °C. During this time, large quantities of solid **3.11b** precipitated from solution. The reaction mixture was neutralized with 1 M HCl (*ca.* 60 mL), and the resulting dark red precipitate was collected and washed with methanol. The crude solid was purified using column chromatography (silica gel, CH_2Cl_2), before volatiles were removed *in vacuo* and triturated with methanol to afford formazan **3.11b** as a fluffy red solid. Yield = 3.81 g, 43%. M.p.: 183–185 °C. ^1H NMR (399.8 MHz, DMSO-d_6) δ 14.95 (s, 1H, N*H*), 8.11 (d, $^3J_{HH}$ = 7.2 Hz, 2H, aryl C*H*), 8.00–7.94 (m, 3H, aryl C*H*), 7.48 (t, $^3J_{HH}$ = 7.6 Hz, 2H, aryl C*H*), 7.44–7.34 (m, 5H, aryl C*H*), 7.14 (t, $^3J_{HH}$ = 7.9 Hz, 1H, aryl C*H*), 5.65 (t, $^3J_{HH}$ = 5.7 Hz, 1H, O*H*), 4.68 (d, $^3J_{HH}$ = 5.7 Hz, 2H, C*H$_2$*), 2.40 (s, 3H, C*H$_3$*). $^{13}C\{^1H\}$ NMR (100.5 MHz, DMSO-d_6) δ 148.9, 143.3, 141.0, 140.6, 136.9, 130.2, 130.1, 129.0, 128.9, 128.6, 127.7, 125.6, 124.5, 121.0, 114.3, 61.7, 21.1. FT-IR (ATR): 3329 (b), 3181 (w), 3022 (w), 1518 (m), 1230 (m), 1003 (s), 821 (s), 757 (s), 668 (s), 629 (s) cm^{-1}. UV-vis (CH_2Cl_2): λ_{max} 484 nm (ε = 17,800 M^{-1} cm^{-1}), 305 nm (ε = 26,400 M^{-1} cm^{-1}). Mass Spec. (ESI, −ve mode): exact mass calculated for $[C_{21}H_{19}N_4O]^-$, $[M–H]^-$: 343.1559; exact mass found: 343.1569; difference: +2.9 ppm. Anal. Calcd. (%) for $C_{21}H_{20}N_4O$: C, 73.23; H, 5.85; N, 16.27. Found: C, 73.38; H, 6.35; N, 16.75.

BF Formazanate 3.12a

Formazan **3.11a** (1.02 g. 3.09 mmol) was dissolved in dry toluene (100 mL). NEt$_3$ (1.02 g, 1.40 mL, 10.1 mmol) was added and the dark magenta solution was stirred for 10 min. Boron trifluoride diethyl etherate (2.26 g , 2.00 ml, 16.0 mmol) was slowly added, and the solution w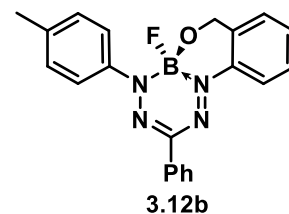as heated at 80 °C for 18 h. The solution gradually turned from magenta to purple during this time. The solution was cooled to 21 °C. and deionized water (20 mL) was added to quench any excess reactive boron-containing species. The solution was transferred to a seperatory funnel and washed with deionized water (3 × 150 mL), dried over MgSO$_4$, gravity filtered and concentrated *in vacuo* to afford the crude BF formazanate **3.12a**. The product was first purified using flash column chromatography (neutral alumina, CH_2Cl_2) and isolated using column chromatography (silica gel, 2:1 hexanes/CH_2Cl_2), where the purple fraction (R_f = 0.64) was collected. The solution was concentrated *in vacuo* and the solids were washed with *n-*

pentane to afford BF formazanate **3.12a** as a dark purple solid. Yield = 0.76 g, 68%. M.p.: 179–181 °C. ^{1}H NMR (399.7 MHz, CDCl$_3$) δ 8.20 (d, $^3J_{HH}$ = 8.6 Hz, 2H, aryl C*H*), 7.91 (d, $^3J_{HH}$ = 8.5 Hz, 2H, aryl C*H*), 7.84 (d, $^3J_{HH}$ = 8.0 Hz, 1H, aryl C*H*), 7.53–7.44 (m, 3H, aryl C*H*), 7.37 (t, $^3J_{HH}$ = 7.8 Hz, 1H, aryl C*H*), 7.30 (d, $^3J_{HH}$ = 8.6 Hz, 2H, aryl C*H*), 7.12 (d, $^3J_{HH}$ = 8.0 Hz, 1H, aryl C*H*), 7.07 (t, $^3J_{HH}$ = 7.7 Hz, 1H, aryl C*H*), 2.42 (s, 3H, C*H$_3$*). ^{11}B{^{1}H} NMR (128.3 MHz, CDCl$_3$) δ 1.1 (d, $^1J_{BF}$ = 36 Hz). ^{13}C{^{1}H} NMR (100.5 MHz, CDCl$_3$) δ 156.4, 150.4, 141.8, 139.8, 133.6, 133.3, 132.5, 130.2, 129.6, 128.9, 126.1, 122.6, 121.7, 116.0, 114.8, 21.5. ^{19}F{^{1}H} NMR (376.1 MHz, CDCl$_3$) δ −153.3 (q, $^1J_{FB}$ = 36 Hz). FT-IR (ATR): 3069 (w), 1602 (m), 1480 (m), 1459 (m), 1392 (s), 1304 (m), 1273 (s), 1225 (m), 1198 (m), 1105 (s), 1004 (s), 988 (s), 844 (m), 809 (m), 752 (s), 674 (m), 667 (s), 561 (s) cm^{-1}. UV-vis (CH$_2$Cl$_2$): λ$_{max}$ 559 nm (ε = 19,900 M^{-1} cm^{-1}), 424 nm (ε = 5,100 M^{-1} cm^{-1}), 319 nm (ε = 24,500 M^{-1} cm^{-1}). Mass Spec. (ESI, −ve mode): exact mass calculated for [C$_{20}$H$_{16}$N$_4$OBF]$^-$, [M]$^-$: 358.1401; exact mass found: 358.1400; difference: −0.3 ppm. Anal. Calcd. (%) for C$_{20}$H$_{16}$N$_4$OBF: C, 67.07; H, 4.50; N, 15.64. Found: C, 66.88; H, 4.79; N, 15.39.

BF Formazanate 3.12b

Formazan **3.11b** (0.501 g. 1.45 mmol) was dissolved in dry toluene (80 mL). NEt$_3$ (0.47 g, 0.65 mL, 4.6 mmol) was added and the dark magenta solution was stirred for 10 min. Boron trifluoride diethyl etherate (1.24 g , 1.10 mL, 8.80 mmol) was slowly added, and the solution was heated at 120 °C for 48 h. The
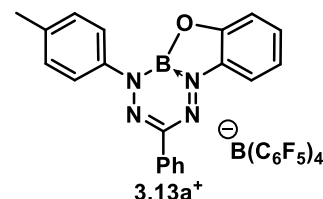

3.12b

solution gradually turned from red to magenta during this time. The solution was cooled to 21 °C. and deionized water (15 mL) was added to quench any excess reactive boron-containing species. The solution was transferred to a seperatory funnel and washed with deionized water (3 × 100 mL), dried over MgSO$_4$, gravity filtered and concentrated *in vacuo* to afford the crude BF formazanate **3.12b**. The product was purified using column chromatography (silica gel, toluene). The magenta solution was concentrated *in vacuo* and the solids were washed with *n*-pentane to afford OBF formazanate **3.12b** as a dark solid (green reflex). Yield = 0.327 g, 61%. M.p.: 208–210 °C. ^{1}H NMR (399.8 MHz, CDCl$_3$) δ 8.19 (d, $^3J_{HH}$ = 8.1 Hz, 1H, aryl C*H*), 8.15 (d, $^3J_{HH}$ = 7.0 Hz, 2H, aryl C*H*), 7.91 (d, $^3J_{HH}$ =

8.5 Hz, 2H, aryl C*H*), 7.47 (m, 3H, aryl C*H*), 7.38 (t, $^3J_{HH}$ = 7.3 Hz, 1H, aryl C*H*), 7.32–7.26 (m, 2H, aryl C*H*), 7.13 (d, $^3J_{HH}$ = 7.5 Hz, 1H, aryl C*H*), 5.27 (d, $^2J_{HH}$ = 14.8 Hz, 1H, diastereotopic C*H₂*), 4.82 (d, $^2J_{HH}$ = 14.8 Hz, 1H, diastereotopic C*H₂*), 2.42 (s, 3H, C*H₃*). ^{11}B{^{1}H} NMR (128 MHz, CDCl₃) δ –0.8 (d, $^1J_{BF}$ = 38 Hz). ^{13}C{^{1}H} NMR (100.5 MHz, CDCl₃) δ 150.0, 141.9, 140.5, 140.1, 133.9, 132.5, 129.8, 129.4, 128.9, 128.8, 128.7, 125.8, 125.7, 123.9, 118.4, 62.4, 21.5. ^{19}F{^{1}H} NMR (376.1 MHz, CDCl₃) δ –156.1 (q, $^1J_{FB}$ = 38 Hz). FT-IR (ATR): 3024 (w), 2959 (w), 1602 (m), 1487 (m), 1457 (m), 1377 (m), 1353 (s), 1276 (s), 1234 (s), 1165 (m), 1068 (m), 981 (s), 923 (s), 877 (s), 791 (w), 763 (s), 696 (s), 666 (s), 572 (s), 540 (s) cm^{-1}. UV-vis (CH₂Cl₂): λ$_{max}$ 530 nm (ε = 20,200 M^{-1} cm^{-1}), 355 nm (ε = 6,400 M^{-1} cm^{-1}), 316 nm (ε = 22,400 M^{-1} cm^{-1}). Mass Spec. (ESI, –ve mode): exact mass calculated for [C₂₁H₁₈N₄OBF]$^-$, [M]$^-$: 372.1558; exact mass found: 372.1558; difference: 0.0 ppm. Anal. Calcd. (%) for C₂₁H₁₈N₄OBF: C, 67.77; H, 4.87; N, 15.05. Found: C, 67.54; H, 5.17; N, 15.25.

Borenium cation 3.13a$^+$

In a vial, freshly prepared [Et₃Si(C₇H₈)][B(C₆F₅)₄] (0.111 g, 0.125 mmol) was dissolved in toluene (2 mL) and stirred for 5 min. In a separate vial, BF Formazanate **3.12a** (0.045 g, 0.13 mmol) was dissolved in toluene (5 mL) and stirred for 5 min. The purple BF Formazanate **3.12a** solution was added dropwise

to the triethylsilylium cation solution over a 5 min period. During the addition, the colour changed from purple to blue. The blue solution was stirred at 21 °C for 1 h before it was concentrated *in vacuo*. The resulting solid was suspended in *n*-pentane (10 mL) and stirred for 15 min. The suspension was filtered and solids were further washed with 3 portions of *n*-pentane (3 × 5 mL) to afford cationic **3.13a$^+$** as a dark blue microcrystalline solid. Yield = 0.101 g, 80%. M.p.: 198–200 °C. ^{1}H NMR (399.8 MHz, CD₂Cl₂) δ 8.46 (t, $^3J_{HH}$ = 7.6 Hz, 3H, aryl C*H*), 8.40 (d, $^3J_{HH}$ = 8.8 Hz, 2H, aryl C*H*), 8.13–8.04 (m, 1H, aryl C*H*), 7.90 (d, $^3J_{HH}$ = 8.7 Hz, 1H, aryl C*H*), 7.82 (t, $^3J_{HH}$ = 8.0 Hz, 1H, aryl C*H*), 7.77–7.67 (m, 3H, aryl C*H*), 7.63 (d, $^3J_{HH}$ = 8.5 Hz, 2H, aryl C*H*), 2.59 (s, 3H, C*H₃*). ^{11}B{^{1}H} NMR (128.3 MHz, CD₂Cl₂) δ 20.1 (s), –16.8 (s). ^{13}C{^{1}H} NMR (100.5 MHz, CD₂Cl₂) δ 154.0, 149.8, 148.7, 147.4, 140.5, 140.0, 139.4, 138.1, 135.6, 133.7, 132.9, 132.1, 130.9, 130.5, 128.7, 128.4, 123.5, 117.6, 117.4, 22.3. ^{19}F{^{1}H} NMR (376.1 MHz, CD₂Cl₂) δ –133.3 (s), –163.7

(t, $^3J_{FF}$ = 19 Hz), −167.6 − −167.7 (m). FT-IR (ATR): 3026 (w), 1635 (m), 1586 (m), 1472 (m), 1351 (m), 1282 (s), 1114 (m), 948 (m), 816 (s), 759 (s), 691 (m), 590 (s) cm^{-1}. Instability in dilute solution prevented collection of UV-vis absorption data for **3.13a$^+$**. Mass Spec. (ESI, +ve mode): exact mass calculated for $[C_{20}H_{16}N_4OB]^+$, $[M]^+$: 339.1417; exact mass found: 339.1415; difference: −0.6 ppm. Anal. Calcd. (%) for $C_{44}H_{16}N_4OB_2F_{20}$: C, 51.90; H, 1.58; N, 5.50. Found: C, 52.10; H, 1.91; N, 5.76.

Borenium cation 3.13b$^+$

In a vial, freshly prepared $[Et_3Si(C_7H_8)][B(C_6F_5)_4]$ (0.098 g 0.11 mmol) was dissolved in toluene (2 mL) and stirred for 5 min. In a separate vial, BF Formazanate **3.12b** (0.041 g, 0.11 mmol) was dissolved in toluene (5 mL) and stirred for 5 min.
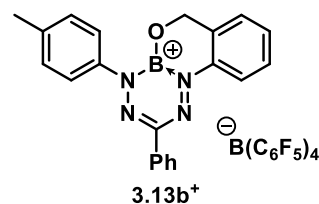
The magenta BF Formazanate **3.12b** solution was added dropwise to the triethylsilylium cation solution over a 5 min period. During the addition, the colour changed from magenta to teal. The teal solution was stirred at 21 °C for 1 h before it was concentrated *in vacuo*. The resulting solid was suspended in *n*-pentane (10 mL) and stirred for 15 min. The suspension was filtered and further washed with 3 portions of *n*-pentane (3 × 5 mL) to afford cationic **3.13b$^+$** as a shiny dark green microcrystalline solid. Yield = 0.098 g, 87%. M.p.: 218–220 °C. ^{1}H NMR (399.8 MHz, CD$_2$Cl$_2$) δ 8.48 (d, $^3J_{HH}$ = 9.1 Hz, 1H, aryl C*H*), 8.29 (d, $^3J_{HH}$ = 7.6 Hz, 2H, aryl C*H*), 8.10 (d, $^3J_{HH}$ = 8.7 Hz, 2H, aryl C*H*), 7.76 (t, $^3J_{HH}$ = 7.5 Hz, 1H, aryl C*H*), 7.71–7.61 (m, 4H, aryl C*H*), 7.51 (d, $^3J_{HH}$ = 8.7 Hz, 2H, aryl C*H*), 7.36 (d, $^3J_{HH}$ = 8.3 Hz, 1H, aryl C*H*), 5.86 (s, 2H, C*H$_2$*), 2.54 (s, 3H, C*H$_3$*). ^{11}B{^{1}H} NMR (128.3 MHz, CD$_2$Cl$_2$) δ 21.2 (s), −16.8 (s). ^{13}C{^{1}H} NMR (101 MHz, CD$_2$Cl$_2$) δ 156.3, 149.9, 147.6, 141.2, 140.0, 138.1, 137.2, 136.2, 135.6, 133.2, 132.0, 131.9, 130.9, 130.3, 130.1, 127.6, 127.2, 124.2, 119.2, 67.6, 22.2. ^{19}F{^{1}H} NMR (376.1 MHz, CD$_2$Cl$_2$) δ −133.2 (s), −163.3 (t, $^3J_{FF}$ = 20.4 Hz), −166.63 − −167.7 (m). FT-IR (ATR): 3032 (w), 1645 (m), 1593 (m), 1511 (m), 1457 (s), 1389 (m), 1273 (m), 1123 (m), 1082 (s), 975 (s), 828 (m), 774 (s), 755 (m), 682 (m), 660 (s), 572 (m) cm^{-1}. UV-vis (CH$_2$Cl$_2$): λ$_{max}$ 650 nm (ε = 8,000 M^{-1} cm^{-1}), 605 nm (ε = 7,100 M^{-1} cm^{-1}), 427 nm (ε = 3,500 M^{-1} cm^{-1}), 309 nm (ε = 3,500 M^{-1} cm^{-1}). Mass Spec. (ESI, +ve mode): exact mass calculated for $[C_{21}H_{18}N_4OB]^+$, $[M]^+$: 353.1574; exact mass found: 353.1574; difference: 0.0 ppm. Anal. Calcd. (%) for $C_{45}H_{18}N_4OB_2F_{20}$: C, 52.36; H, 1.76; N, 5.43. Found: C, 52.56; H, 2.44; N, 5.13.

3.5 References

1.   Huang, Z.; Wang, S.; Dewhurst, R. D.; Ignat'ev, N. V.; Finze, M.; Braunschweig, H. *Angew. Chem. Int. Ed.* **2020**, *59*, 8800–8816.

2.   Turkoglu, G.; Cinar, M. E.; Ozturk, T. *Molecules* **2017**, *22*, 1522.

3.   Zou, S.-J.; Shen, Y.; Xie, F.-M.; Chen, J.-D.; Li, Y.-Q.; Tang, J.-X. *Mater. Chem. Front.* **2020**, *4*, 788–820.

4.   Mellerup, S. K.; Wang, S. *Trends Chem.* **2019**, *1*, 77–89.

5.   Lugovik, K. I.; Eltyshev, A. K.; Suntsova, P. O.; Smoluk, L. T.; Belousova, A. V.; Ulitko, M. V.; Minin, A. S.; Slepukhin, P. A.; Benassi, E.; Belskaya, N. P. *Org. Biomol. Chem.* **2018**, *16*, 5150–5162.

6.   Maar, R. R.; Barbon, S. M.; Sharma, N.; Groom, H.; Luyt, L. G.; Gilroy, J. B. *Chem. Eur. J.* **2015**, *21*, 15589–15599.

7.   Glotzbach, C.; Kauscher, U.; Voskuhl, J.; Kehr, N. S.; Stuart, M. C. A.; Fröhlich, R.; Galla, H. J.; Ravoo, B. J.; Nagura, K.; Saito, S.; Yamaguchi, S.; Würthwein, E.-U. *J. Org. Chem.* **2013**, *78*, 4410–4418.

8.   Mellerup, S. K.; Wang, S. *Chem. Soc. Rev.* **2019**, *48*, 3537–3549.

9.   Pandey, U. P.; Thilagar, P. *Adv. Opt. Mater.* **2020**, *8*, 1902145.

10.   Shimogawa, H.; Yoshikawa, O.; Aramaki, Y.; Murata, M.; Wakamiya, A.; Murata, Y. *Chem. Eur. J.* **2017**, *23*, 3784–3791.

11.   Suenaga, K.; Uemura, K.; Tanaka, K.; Chujo, Y. *Polym. Chem.* **2020**, *11*, 1127–1133.

12.   Sivaev, I. B.; Bregadze, V. I. *Coord. Chem. Rev.* **2014**, *270-271*, 75–88.

13.   Lawson, J. R.; Melen, R. L., Recent developments and applications of Lewis acidic boron reagents. In *Organometallic Chemistry: Volume 41*, The Royal Society of Chemistry: 2017; Vol. 41, p 1–27.

14.   Rao, B.; Kinjo, R. *Chem. Asian J.* **2018**, *13*, 1279–1292.

15.   Fyfe, J. W. B.; Watson, A. J. B. *Chem.* **2017**, *3*, 31–55.

16.   Deloux, L.; Srebnik, M. *Chem. Rev.* **1993**, *93*, 763–784.

17.   Stephan, D. W. *Science* **2016**, *354*, aaf7229.

18.   Stephan, D. W. *Dalton Trans.* **2009**, 3129–3136.

19.   Stephan, D. W.; Erker, G. *Angew. Chem. Int. Ed.* **2015**, *54*, 6400–6441.

20.   Jäkle, F. *Chem. Rev.* **2010**, *110*, 3985–4022.

21.   Wade, C. R.; Broomsgrove, A. E. J.; Aldridge, S.; Gabbaï, F. P. *Chem. Rev.* **2010**, *110*, 3958–3984.

22.   Piers, W. E.; Bourke, S. C.; Conroy, K. D. *Angew. Chem. Int. Ed.* **2005**, *44*, 5016–5036.

23.   De Vries, T. S.; Prokofjevs, A.; Vedejs, E. *Chem. Rev.* **2012**, *112*, 4246–4282.

24.   Franz, D.; Szilvási, T.; Pöthig, A.; Deiser, F.; Inoue, S. *Chem. Eur. J.* **2018**, *24*, 4283–4288.

25.   Maar, R. R.; Katzman, B. D.; Boyle, P. D.; Staroverov, V. N.; Gilroy, J. B. *Angew. Chem. Int. Ed.* **2021**, *60*, 5152–5156.

26.   Adachi, Y.; Arai, F.; Jäkle, F. *Chem. Commun.* **2020**, *56*, 5119–5122.

27.   Radcliffe, J. E.; Dunsford, J. J.; Cid, J.; Fasano, V.; Ingleson, M. J. *Organometallics* **2017**, *36*, 4952–4960.

28.   Yang, W.; Krantz, K. E.; Freeman, L. A.; Dickie, D. A.; Molino, A.; Kaur, A.; Wilson, D. J. D.; Gilliard Jr., R. J. *Chem. Eur. J.* **2019**, *25*, 12512–12516.

29.   Cui, C.; Heilmann-Brohl, J.; Sánchez Perucha, A.; Thomson, M. D.; Roskos, H. G.; Wagner, M.; Jäkle, F. *Macromolecules* **2010**, *43*, 5256–5261.

30.   Hudnall, T. W.; Gabbaï, F. P. *Chem. Commun.* **2008**, 4596–4597.

31.   Marwitz, A. J. V.; Jenkins, J. T.; Zakharov, L. N.; Liu, S.-Y. *Angew. Chem. Int. Ed.* **2010**, *49*, 7444–7447.

32.   Tsurumaki, E.; Hayashi, S.-y.; Tham, F. S.; Reed, C. A.; Osuka, A. *J. Am. Chem. Soc.* **2011**, *133*, 11956–11959.

33.   Matsumoto, T.; Gabbaï, F. P. *Organometallics* **2009**, *28*, 4252–4253.

34.   Sirbu, D.; Benniston, A. C.; Harriman, A. *Org. Lett.* **2017**, *19*, 1626–1629.

35.   Gobo, Y.; Matsuoka, R.; Chiba, Y.; Nakamura, T.; Nabeshima, T. *Tetrahedron Lett.* **2018**, *59*, 4149–4152.

36.   Liu, Y.; Niu, L.-Y.; Liu, X.-L.; Chen, P.-Z.; Yao, Y.-S.; Chen, Y.-Z.; Yang, Q.-Z. *Chem. Eur. J.* **2018**, *24*, 13549–13555.

37. Kubo, Y.; Shimada, T.; Maeda, K.; Hashimoto, Y. *New J. Chem.* **2020**, *44*, 29–37.

38. Chen, N.; Zhang, W.; Chen, S.; Wu, Q.; Yu, C.; Wei, Y.; Xu, Y.; Hao, E.; Jiao, L. *Org. Lett.* **2017**, *19*, 2026–2029.

39. Travieso-Puente, R.; Broekman, J. O. P.; Chang, M.-C.; Demeshko, S.; Meyer, F.; Otten, E. *J. Am. Chem. Soc.* **2016**, *138*, 5503–5506.

40. Protasenko, N. A.; Poddel'sky, A. I.; Bogomyakov, A. S.; Fukin, G. K.; Cherkasov, V. K. *Inorg. Chem.* **2015**, *54*, 6078–6080.

41. Gilroy, J. B.; Patrick, B. O.; McDonald, R.; Hicks, R. G. *Inorg. Chem.* **2008**, *47*, 1287–1294.

42. Maar, R. R.; Rabiee Kenaree, A.; Zhang, R.; Tao, Y.; Katzman, B. D.; Staroverov, V. N.; Ding, Z.; Gilroy, J. B. *Inorg. Chem.* **2017**, *56*, 12436–12447.

43. Maar, R. R.; Catingan, S. D.; Staroverov, V. N.; Gilroy, J. B. *Angew. Chem. Int. Ed.* **2018**, *57*, 9870–9874.

44. Mondol, R.; Otten, E. *Inorg. Chem.* **2019**, *58*, 6344–6355.

45. Buguis, F. L.; Maar, R. R.; Staroverov, V. N.; Gilroy, J. B. *Chem. Eur. J.* **2021**, *27*, 2854–2860.

46. Gilroy, J. B.; Otten, E. *Chem. Soc. Rev.* **2020**, *49*, 85–113.

47. Maar, R. R.; Zhang, R.; Stephens, D. G.; Ding, Z.; Gilroy, J. B. *Angew. Chem. Int. Ed.* **2019**, *58*, 1052–1056.

48. Dhindsa, J. S.; Maar, R. R.; Barbon, S. M.; Olivia Avilés, M.; Powell, Z. K.; Lagugné-Labarthet, F.; Gilroy, J. B. *Chem. Commun.* **2018**, *54*, 6899–6902.

49. Barbon, S. M.; Staroverov, V. N.; Gilroy, J. B. *J. Org. Chem.* **2015**, *80*, 5226–5235.

50. Barbon, S. M.; Price, J. T.; Reinkeluers, P. A.; Gilroy, J. B. *Inorg. Chem.* **2014**, *53*, 10585–10593.

51. Kawano, Y.; Ito, Y.; Ito, S.; Tanaka, K.; Chujo, Y. *Macromolecules* **2021**, *54*, 1934–1942.

52. Chang, M.-C.; Otten, E. *Chem. Commun.* **2014**, *50*, 7431–7433.

53. Chang, M.-C.; Otten, E. *Inorg. Chem.* **2015**, *54*, 8656–8664.

54. Barbon, S. M.; Staroverov, V. N.; Gilroy, J. B. *Angew. Chem. Int. Ed.* **2017**, *56*, 8173–8177.

55. Mondol, R.; Snoeken, D. A.; Chang, M.-C.; Otten, E. *Chem. Commun.* **2017**, *53*, 513–516.

56. Maar, R. R.; Hoffman, N. A.; Staroverov, V. N.; Gilroy, J. B. *Chem. Eur. J.* **2019**, *25*, 11015–11019.

57. Connelly, S. J.; Kaminsky, W.; Heinekey, D. M. *Organometallics* **2013**, *32*, 7478–7481.

58. Bonnier, C.; Piers, W. E.; Parvez, M.; Sorensen, T. S. *Chem. Commun.* **2008**, 4593–4595.

59. Farrell, J. M.; Hatnean, J. A.; Stephan, D. W. *J. Am. Chem. Soc.* **2012**, *134*, 15728–15731.

60. Heitkemper, T.; Sindlinger, C. *Chem. Eur. J.* **2020**, *26*, 11684–11689.

61. Janes, T.; Diskin-Posner, Y.; Milstein, D. *Angew. Chem. Int. Ed.* **2020**, *59*, 4932–4936.

62. Abdalla, J. A. B.; Tirfoin, R. C.; Niu, H.; Aldridge, S. *Chem. Commun.* **2017**, *53*, 5981–5984.

63. Gutmann, V. *Coord. Chem. Rev.* **1976**, *18*, 225–255.

64. Mayer, U.; Gutmann, V.; Gerger, W. *Monatsh. Chem.* **1975**, *106*, 1235–1257.

65. Eisenberger, P.; Crudden, C. M. *Dalton Trans.* **2017**, *46*, 4874–4887.

66. Tseng, H.-C.; Shen, C.-T.; Matsumoto, K.; Shih, D.-N.; Liu, Y.-H.; Peng, S.-M.; Yamaguchi, S.; Lin, Y.-F.; Chiu, C.-W. *Organometallics* **2019**, *38*, 4516–4521.

67. Chiu, C.-W.; Gabbaï, F. P. *J. Am. Chem. Soc.* **2006**, *128*, 14248–14249.

68. Frisch, M. J.; Trucks, G. W.; Schlegel, H. B.; Scuseria, G. E.; Robb, M. A.; Cheeseman, J. R.; Scalmani, G.; Barone, V.; Petersson, G. A.; Nakatsuji, H.; Li, X.; Caricato, M.; Marenich, A. V.; Bloino, J.; Janesko, B. G.; Gomperts, R.; Mennucci, B.; Hratchian, H. P.; Ortiz, J. V.; Izmaylov, A. F.; Sonnenberg, J. L.; Williams; Ding, F.; Lipparini, F.; Egidi, F.; Goings, J.; Peng, B.; Petrone, A.; Henderson, T.; Ranasinghe, D.; Zakrzewski, V. G.; Gao, J.; Rega, N.; Zheng, G.; Liang, W.; Hada, M.; Ehara, M.; Toyota, K.; Fukuda, R.; Hasegawa, J.; Ishida, M.; Nakajima, T.; Honda, Y.; Kitao, O.; Nakai, H.; Vreven, T.; Throssell, K.; Montgomery Jr., J. A.; Peralta, J. E.; Ogliaro, F.; Bearpark, M. J.; Heyd, J. J.; Brothers, E. N.; Kudin, K. N.; Staroverov, V. N.; Keith, T. A.; Kobayashi, R.; Normand, J.; Raghavachari, K.; Rendell, A. P.; Burant, J. C.; Iyengar, S. S.; Tomasi, J.; Cossi, M.; Millam, J. M.; Klene, M.; Adamo, C.; Cammi, R.;

Ochterski, J. W.; Martin, R. L.; Morokuma, K.; Farkas, O.; Foresman, J. B.; Fox, D. J. *Gaussian Development Version, Revision I.13*, Wallingford, CT, 2016.

69. Barbon, S. M.; Reinkeluers, P. A.; Price, J. T.; Staroverov, V. N.; Gilroy, J. B. *Chem. Eur. J.* **2014**, *20*, 11340–11344.

70. Pommerehne, J.; Vestweber, H.; Guss, W.; Mahrt, R. F.; Bässler, H.; Porsch, M.; Daub, J. *Adv. Mater.* **1995**, *7*, 551–554.

71. Cardona, C. M.; Li, W.; Kaifer, A. E.; Stockdale, D.; Bazan, G. C. *Adv. Mater.* **2011**, *23*, 2367–2371.

72. Bruker-AXS, SAINT version 2013.8, **2013**, Bruker-AXS, Madison, WI 53711, USA.

73. Bruker-AXS, SADABS version 2012.1, **2012**, Bruker-AXS, Madison, WI 53711, USA.

74. Sheldrick, G. M. *Acta Cryst.* **2015**, *A71*, 3–8.

75. Sheldrick, G. M. *Acta Cryst.* **2015**, *C71*, 3–8.

76. Spek, A. L. *Acta Cryst.* **2015**, *C71*, 9–18.

77. Staroverov, V. N.; Scuseria, G. E.; Tao, J.; Perdew, J. P. *J. Chem. Phys.* **2003**, *119*, 12129–12137.

Chapter 4

4 Summary, Conclusions and Future Work

4.1 Summary and Conclusions

The work described in this thesis involves the synthesis and characterization of novel cationic boron formazanate complexes. Chapter one provides an overview of recent advances in three-coordinate and cationic boron complexes. Chapter two introduces a series of three and four-coordinate boron cationic and dicationic complexes, where the impact of coordination number, charge and supporting ligands at boron were evaluated for their effect on electronic structure. We found that by increasing the cationic charge in four-coordinate boron formazanate complexes, the low-energy absorption maxima increased in the UV-vis spectra. In addition, by installing a highly planar three-coordinate borenium cation, the low energy absorption could be significantly reduced. Upon investigation of the HOMO, the planar complex allowed for extended π-electron conjugation into the boron-bound phenyl substituent. Finally, it was uncovered that in addition to charge and coordination number, the boron-bound substituent can alter the electronic structure, resulting in electronic transitions containing a degree of charge-transfer character. These results establish methods for the design of optoelectronic molecular materials including cationic (or dicationic) boron fragments that can be applied to π-conjugated heterocycles containing main group elements.
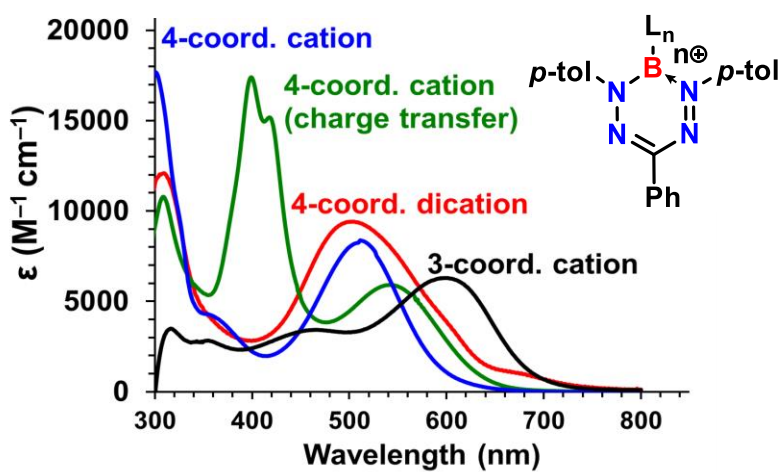
Figure 4.1. Combined UV-vis spectra of several cationic boron formazanate dyes.[1]

Chapter three highlights a new set of BF formazanates and borenium cations supported by an N_2O^{2-} chelating formazanate ligand. The borenium cations offered exceptionally high Lewis acidity (Acceptor Number values >100), which suggest a potential use in catalytic transformations (*e.g.,* hydrosilylation) or anion (*e.g.,* fluoride) sensing. The acceptor properties were further probed using cyclic voltammetry, and we verified that the borenium cation had a markedly reduced first reduction potential, indicating a lowered LUMO energy level. This finding was supported by experimentally estimating the LUMO energies, which confirmed our finding that the introduction of a borenium drastically enhances the electron deficiency. Further investigation of the optical properties revealed a large bathochromic shift between the neutral BF formazanate precursor and the borenium cation, suggesting a narrowed band gap, which was verified using computationally. Surprisingly, the borenium cation was strongly emissive ($\Phi_F = 0.38$) in solution, unlike the neutral BF formazanates in this set. In conclusion, utilization of a borenium cation rendered a highly Lewis acidic, redox-active and fluorescent dye, with a potential use in the design of low band-gap materials and sensory technology.
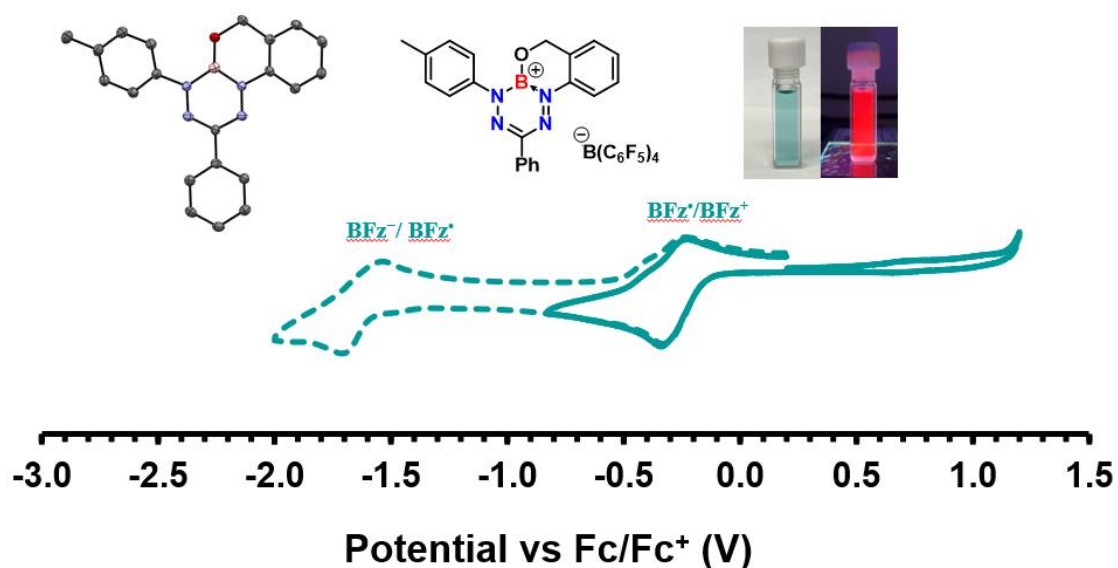
Figure 4.2. Highly planar and Lewis acidic borenium cation with interesting optical and electrochemical properties.

4.2 Future Work

4.2.1 Anion Sensing and Catalytic Transformations

The empty p orbital in three-coordinate cationic boron allows for nucleophiles to interact with the boron atom. Cationic boron atoms typically have increased electrophilicity over neutral three-coordinate boron, making them attractive candidates for anion sensing, specifically fluoride ions.[2, 3] While four-coordinate boronium cationic complexes have shown utility for sensing,[4] to our best knowledge there are no reports of three-coordinate borenium cations used. Borenium cation **4.1**[+] could be an excellent platform for a fluoride ion sensor. The cationic complex is strongly emissive in CH_2Cl_2 solution ($\Phi_F = 0.38$), but the neutral BF formazanate complex precursor was non-emissive. This could be utilized as a fluorescence "turn-off" sensor, where fluoride ions will extinguish emission. Upon addition of an anhydrous fluoride source, such as tetrabutylammonium difluorotriphenyl silicate ([nBu_4N][SiF_2Ph_3]), **4.1**[+] is fluorinated to form BF formazanate **4.2**. Preliminary results show a successful fluorination reaction by ^{1}H NMR spectroscopy. Future work involves titrating various mole fractions of [nBu_4N][SiF_2Ph_3] to monitor the decrease in fluorescence intensity.
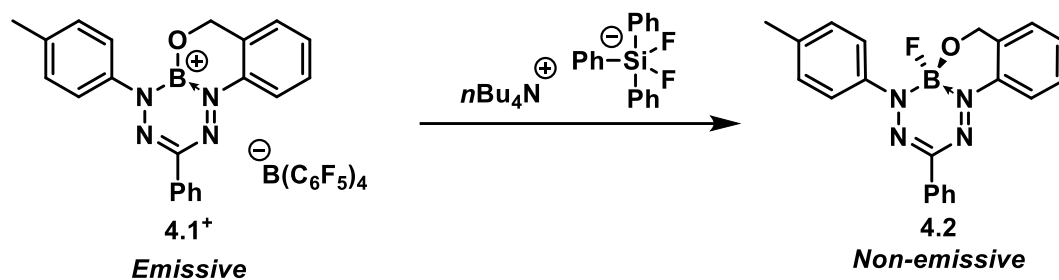
Scheme 4.1. Fluorination of **4.1**[+] using ([nBu_4N][SiF_2Ph_3] to demonstrate utility as a fluoride ion sensor.

4.2.2 Neutral Radical Boron Species Derived from Borenium Cations

Cyclic voltammetry (CV) data shows that borenium cation **4.1**[+] exhibits a relatively high and reversible first reduction potential [$E_{red1} = -0.30$ V], a value close to that of the widely

used ferrocene/ferrocenium redox couple. The CV data and corroborating calculations suggest that **4.1$^+$** could be a platform to allow for the isolation of a stable neutral boron radical complex. The planarity and π-conjugation offered by the complex may allow for delocalization of the radical, increasing the likelihood of stability. In the future, borenium cation **4.1$^+$** will be treated with a mild reducing agent (*e.g.,* decamethylferrocene [Fe(Cp*)$_2$)] in order to isolate neutral radical **4.3$^.$** and unique optical properties are expected.
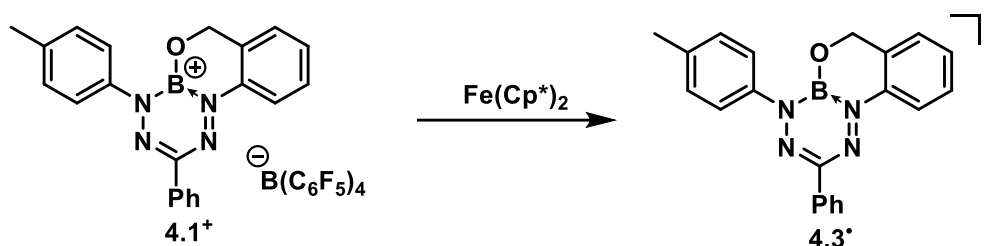
Scheme 4.2. Proposed neutral radical complex derived from borenium cations **4.1$^+$**.

4.2.3   Extending π-conjugation of Borenium Cations

Extension of π-conjugation is well established method for narrowing the HOMO-LUMO gap, which has a drastic effect on the electronic and optical properties of the molecules.[5-7] Recently, the Jäkle group isolated a dimeric cationic boron species via late-stage functionalization.[8] The increased π-conjugation offered lower energy absorption maxima, enhanced fluorescence and increased reduction potentials. The computational studies of the frontier molecular orbitals (HOMO) demonstrated that borenium cation **4.4$^+$**, had an extension of π-conjugation into the boron-bound phenyl substituent (Figure 4.3).[1] Future efforts could be devoted towards synthesizing a phenyl-bridged BF formazanate dimer (**4.5**), which can be treated with one equiv. of [Et$_3$Si(C$_7$H$_8$)][B(C$_6$F$_5$)$_4$] to afford a dicationic complex (**4.6^{2+}**). This transformation would likely drastically lower the absorption maxima and increase reduction potential, because of the extended π-conjugation across two formazanate complexes.
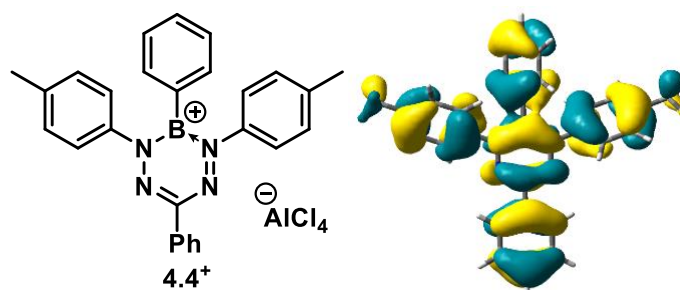
Figure 4.3. Borenium cation **4.4⁺** and computed HOMO.
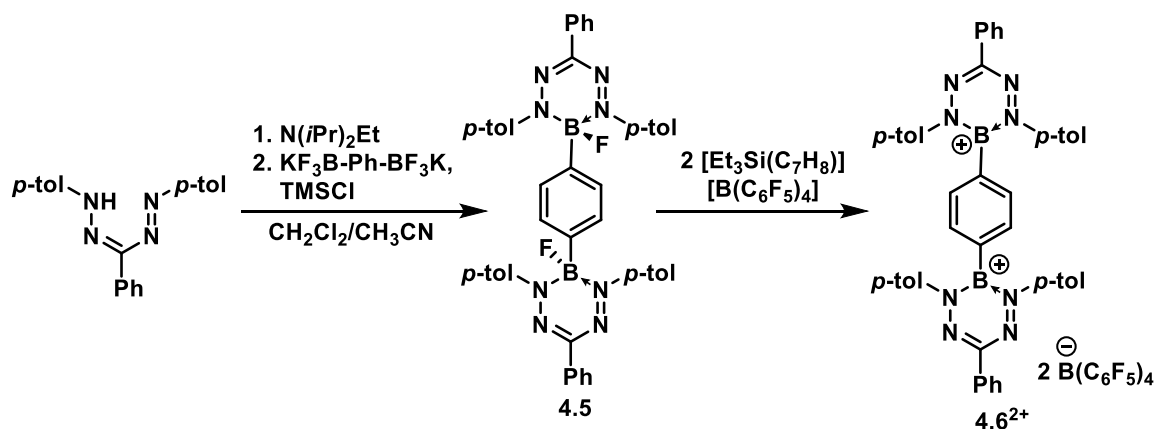
Scheme 4.3. Proposed synthesis of a phenyl bridged dicationic formazanate dimer.

The Gilroy group has made recent advances towards designing near-infrared absorbing and luminescent boron formazanate dyes for molecular materials.[9, 10] Future work is to isolate BPhF formazanate **4.7** containing either a -CN or -Ph substituent. Using Stille coupling, a triphenylamine spacer could be appended on to the *N*-aryl phenyl substituent. Compound **4.8** can be treated with $[Et_3Si(C_7H_8)][B(C_6F_5)_4]$ to afford borenium cation **4.9⁺**. This compound will likely absorb light in the near-infrared region and may be emissive. In addition, there may be charge transfer associated with the low energy absorptions. These features combined pave the way for the design of unique compounds with potential use in molecular materials.
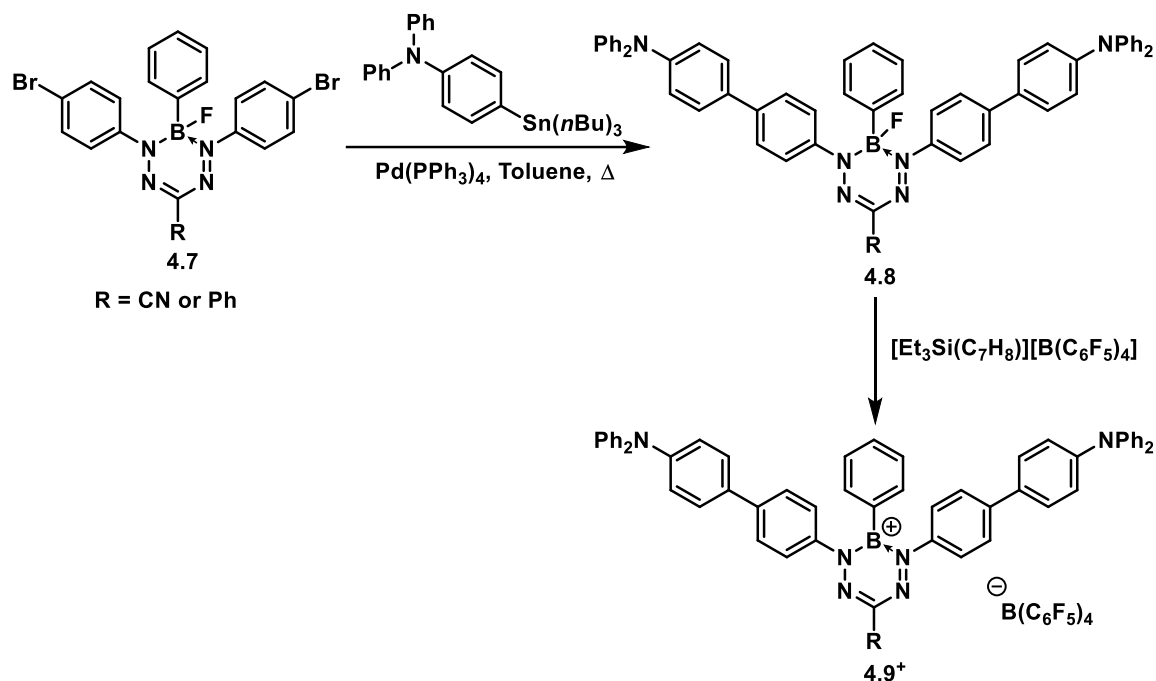
Scheme 4.4. Proposed synthesis of a triphenylamine appended borenium formazanate **4.9⁺**.

4.3 References

1. Maar, R. R.; Katzman, B. D.; Boyle, P. D.; Staroverov, V. N.; Gilroy, J. B. *Angew. Chem. Int. Ed.* **2021**, *60*, 5152–5156.

2. Chiu, C.-W.; Gabbaï, F. P. *J. Am. Chem. Soc.* **2006**, *128*, 14248–14249.

3. Wade, C. R.; Broomsgrove, A. E. J.; Aldridge, S.; Gabbaï, F. P. *Chem. Rev.* **2010**, *110*, 3958–3984.

4. Hudnall, T. W.; Gabbaï, F. P. *Chem. Commun.* **2008**, 4596–4597.

5. Barbon, S. M.; Staroverov, V. N.; Gilroy, J. B. *J. Org. Chem.* **2015**, *80*, 5226–5235.

6. Dhindsa, J. S.; Maar, R. R.; Barbon, S. M.; Olivia Avilés, M.; Powell, Z. K.; Lagugné-Labarthet, F.; Gilroy, J. B. *Chem. Commun.* **2018**, *54*, 6899–6902.

7. Yin, X.; Liu, J.; Jäkle, F. *Chem. Eur. J.* **2021**, *27*, 2973–2986.

8. Adachi, Y.; Arai, F.; Jäkle, F. *Chem. Commun.* **2020**, *56*, 5119–5122.

9.   Buguis, F. L.; Maar, R. R.; Staroverov, V. N.; Gilroy, J. B. *Chem. Eur. J.* **2021**, *27*, 2854–2860.

10.   Maar, R. R.; Zhang, R.; Stephens, D. G.; Ding, Z.; Gilroy, J. B. *Angew. Chem. Int. Ed.* **2019**, *58*, 1052–1056.

Appendices

Appendix A1 Permission to Reuse Copyrighted Material

Permission to reproduce Figure 1.1

This Agreement between University of Western Ontario -- Benjamin Katzman ("You") and Elsevier ("Elsevier") consists of your license details and the terms and conditions provided by Elsevier and Copyright Clearance Center.

License Number	5056561435736
License date	Apr 26, 2021
Licensed Content Publisher	Elsevier
Licensed Content Publication	Trends in Chemistry
Licensed Content Title	Boron-Doped Molecules for Optoelectronics
Licensed Content Author	Soren K. Mellerup,Suning Wang
Licensed Content Date	Apr 1, 2019
Licensed Content Volume	1
Licensed Content Issue	1
Licensed Content Pages	13
Start Page	77
End Page	89
Type of Use	reuse in a thesis/dissertation
Portion	figures/tables/illustrations
Number of figures/tables/illustrations	1
Format	electronic
Are you the author of this Elsevier article?	No
Will you be translating?	No
Title	Cationic Boron Formazanate Complexes
Institution name	University of Western Ontario
Expected presentation date	Jun 2021
Portions	Figure I. in Box 1
Requestor Location	University of Western Ontario 1151 Richmond Street London, ON N6A3K7 Canada Attn: University of Western Ontario

Permission to reproduce figures for Figure 1.2

This Agreement between University of Western Ontario -- Benjamin Katzman ("You") and John Wiley and Sons ("John Wiley and Sons") consists of your license details and the terms and conditions provided by John Wiley and Sons and Copyright Clearance Center.

License Number	5056580069982
License date	Apr 26, 2021
Licensed Content Publisher	John Wiley and Sons
Licensed Content Publication	Chemistry - A European Journal
Licensed Content Title	4,7-Bis[3-(dimesitylboryl)thien-2-yl]benzothiadiazole: Solvato-, Thermo-, and Mechanochromism Based on the Reversible Formation of an Intramolecular B–N Bond
Licensed Content Author	Hiroyuki Shimogawa, Osamu Yoshikawa, Yoshitaka Aramaki, et al
Licensed Content Date	Feb 16, 2017
Licensed Content Volume	23
Licensed Content Issue	15
Licensed Content Pages	8
Type of use	Dissertation/Thesis
Requestor type	University/Academic
Format	Electronic
Portion	Figure/table
Number of figures/tables	1
Will you be translating?	No
Title	Cationic Boron Formazanate Complexes
Institution name	University of Western Ontario
Expected presentation date	Jun 2021

Permission to reproduce Figure 1.3a

Permission to reproduce Figure 1.7

Permission to reproduce Figure 1.9

This Agreement between University of Western Ontario -- Benjamin Katzman ("You") and John Wiley and Sons ("John Wiley and Sons") consists of your license details and the terms and conditions provided by John Wiley and Sons and Copyright Clearance Center.

License Number 5057130821448

License date	Apr 27, 2021
Licensed Content Publisher	John Wiley and Sons
Licensed Content Publication	Chemistry - A European Journal
Licensed Content Title	Stable Borepinium and Borafluorenium Heterocycles: A Reversible Thermochromic "Switch" Based on Boron–Oxygen Interactions
Licensed Content Author	Robert J. Gilliard, David J. D. Wilson, Aishvaryadeep Kaur, et al
Licensed Content Date	Sep 3, 2019
Licensed Content Volume	25
Licensed Content Issue	54
Licensed Content Pages	5
Type of use	Dissertation/Thesis
Requestor type	University/Academic
Format	Electronic
Portion	Figure/table
Number of figures/tables	1
Will you be translating?	No
Title	Cationic Boron Formazanate Complexes
Institution name	University of Western Ontario
Expected presentation date	Jun 2021
Portions	Figure 4c, 4d
	University of Western Ontario 1151 Richmond Street

Permission to reproduce Figure 1.10b

Order Date	27-Apr-2021	Type of Use	Republish in a thesis/dissertation
Order license ID	1114896-1	Publisher	ROYAL SOCIETY OF CHEMISTRY
ISSN	1364-548X	Portion	Chart/graph/table/figure

LICENSED CONTENT

Publication Title	Chemical communications	Country	United Kingdom of Great Britain and Northern Ireland
Author/Editor	Royal Society of Chemistry (Great Britain)	Rightsholder	Royal Society of Chemistry
Date	01/01/1996	Publication Type	e-Journal
Language	English		

REQUEST DETAILS

Portion Type	Chart/graph/table/figure	Distribution	Canada
Number of charts / graphs / tables / figures requested	1	Translation	Original language of publication
Format (select all that apply)	Electronic	Copies for the disabled?	Yes
Who will republish the content?	Academic institution	Minor editing privileges?	Yes
Duration of Use	Life of current edition	Incidental promotional use?	Yes
Lifetime Unit Quantity	Up to 499	Currency	CAD
Rights Requested	Main product		

NEW WORK DETAILS

Title	Cationic Boron Formazanate Complexes	Institution name	University of Western Ontario
Instructor name	Dr. Joe Gilroy	Expected presentation date	2021-06-16

ADDITIONAL DETAILS

Order reference number	N/A	The requesting person / organization to appear on the license	Benjamin Katzman

REUSE CONTENT DETAILS

Title, description or numeric reference of the portion(s)	Figure 2	Title of the article/chapter the portion is from	N/A
Editor of portion(s)	N/A	Author of portion(s)	Royal Society of Chemistry (Great Britain)
Volume of serial or monograph	N/A	Issue, if republishing an article from a serial	N/A
Page or page range of portion	4597	Publication date of portion	2008-08-19

Permission to reproduce figures in Scheme 1.13

Permission to reproduce Figure 1.12

Permission to reproduce Figure 1.13

Permission to reproduce Figure 1.15

Appendix A2 Supporting Information for Chapter 2

8.14
8.12
7.73
7.72
7.50
7.49
7.48
7.46
7.45
7.43
7.42
7.23
7.22
7.20
7.19

2.39

1.99
4.16
2.13
3.19
3.11
4.32

6.00

8 7 6 5 4 3 2 1 0
(ppm)
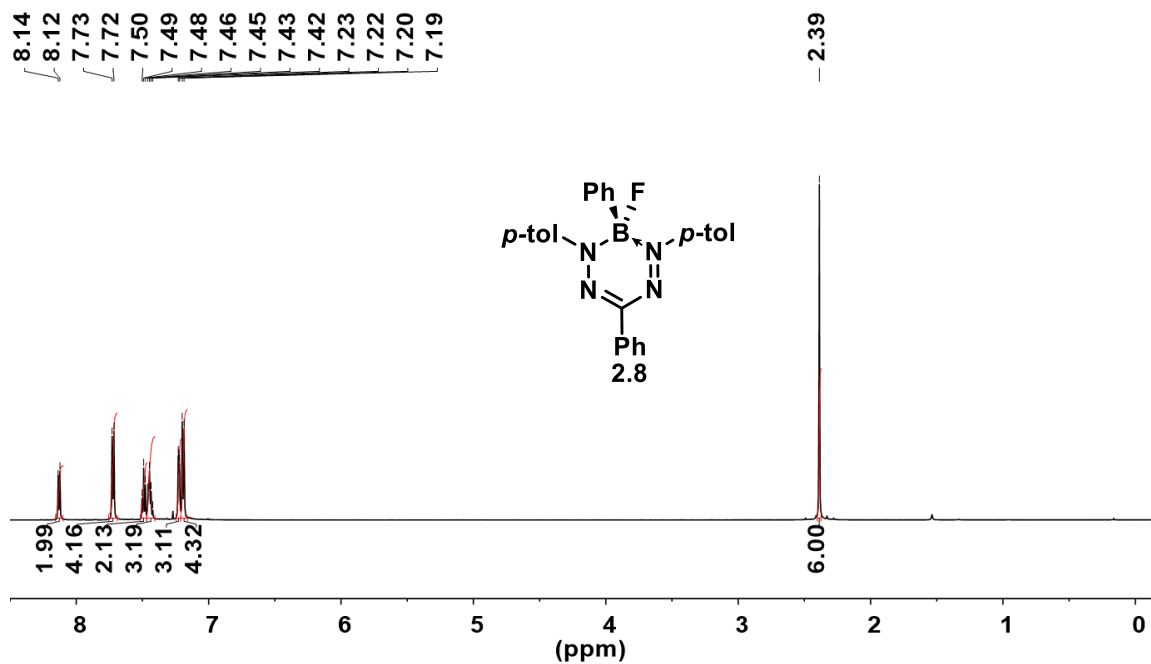
Figure A2.1. ^{1}H NMR spectrum of BPhF formazanate **2.8** recorded in CDCl$_3$.

149.87
142.93
139.28
134.08
132.16
129.23
128.76
128.57
127.81
127.51
125.11
124.23
124.21

21.21

CDCl$_3$

160 140 120 100 80 60 40 20 0
(ppm)
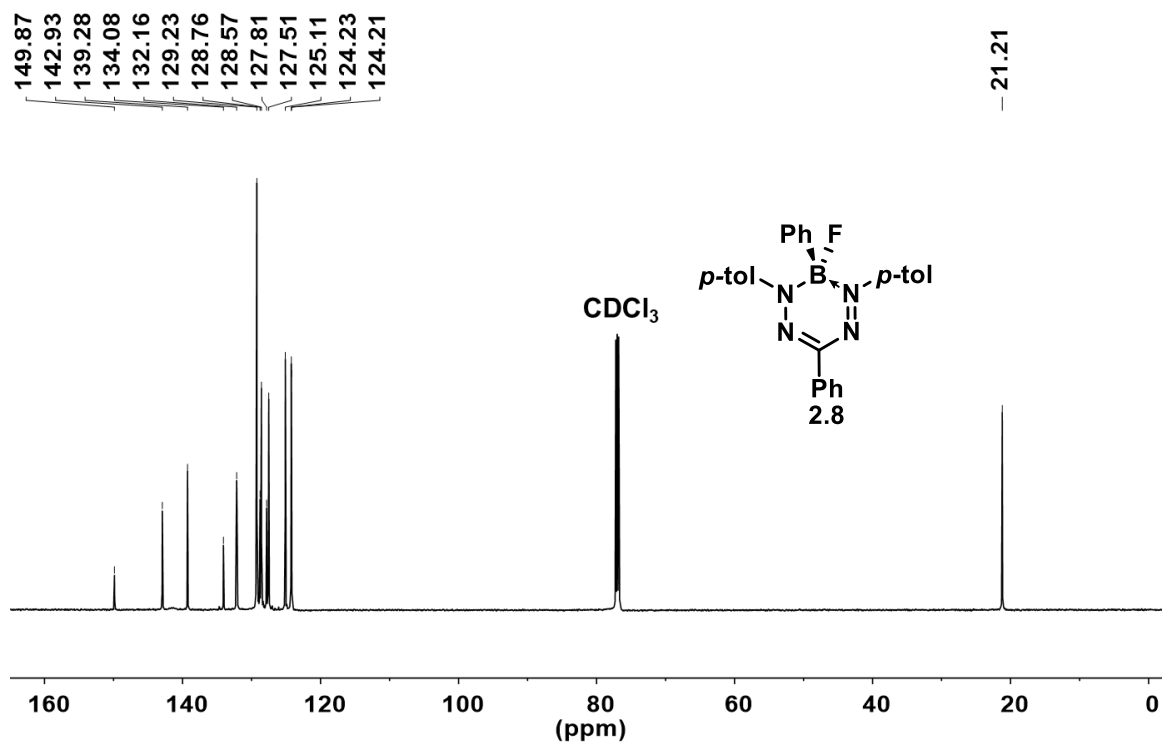
Figure A2.2. ^{13}C{^{1}H} NMR spectrum of BPhF formazanate **2.8** recorded in CDCl$_3$.
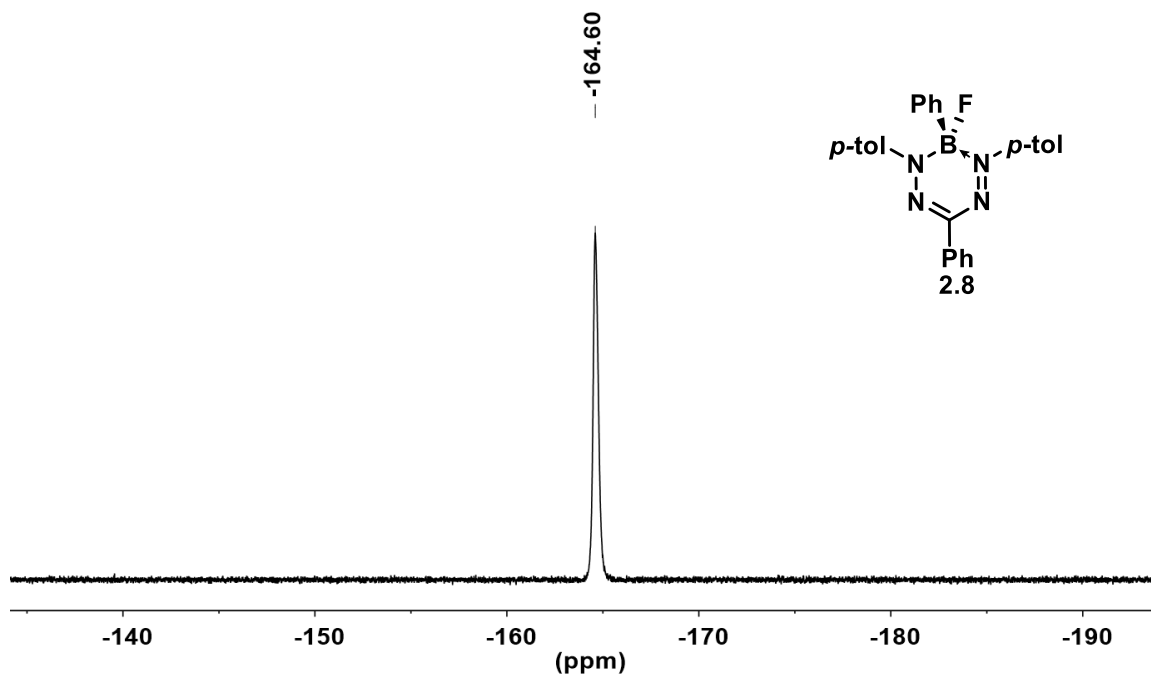
Figure A2.3. $^{19}F\{^1H\}$ NMR spectrum of BPhF formazanate **2.8** recorded in CDCl$_3$.
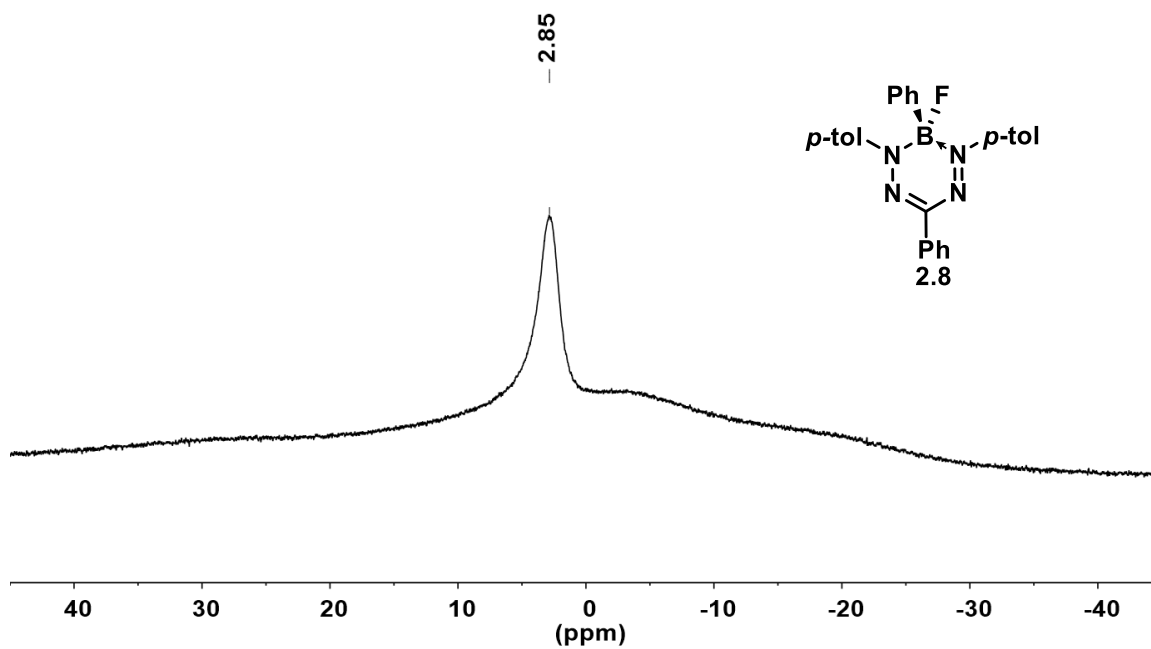
Figure A2.3. $^{11}B\{^1H\}$ NMR spectrum of BPhF formazanate **2.8** recorded in CDCl$_3$.
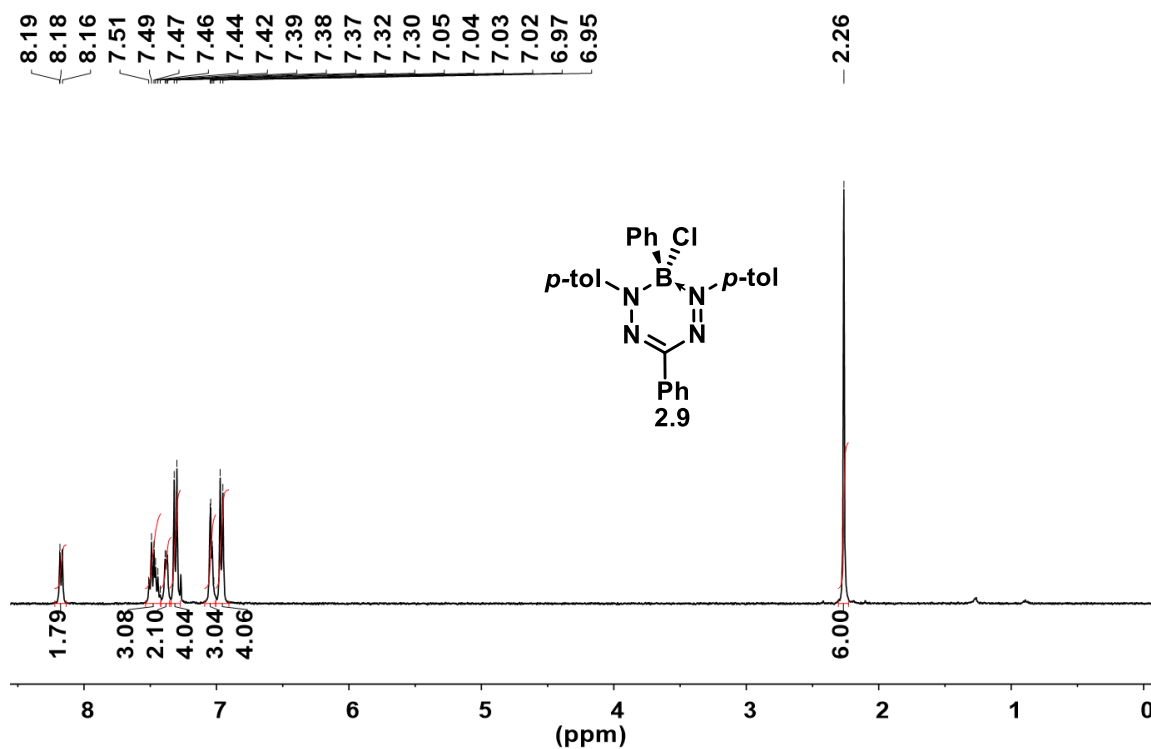
Figure A2.5. ^{1}H NMR spectrum of BPhCl formazanate **2.9** recorded in CDCl$_3$.
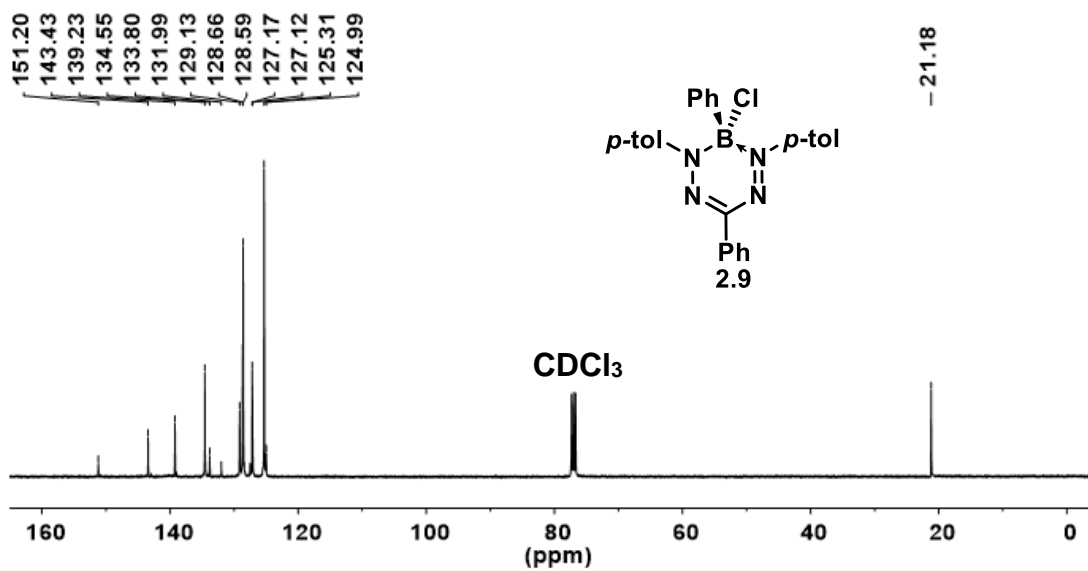
Figure A2.6. ^{13}C{^{1}H} NMR spectrum of BPhCl formazanate **2.9** recorded in CDCl$_3$.
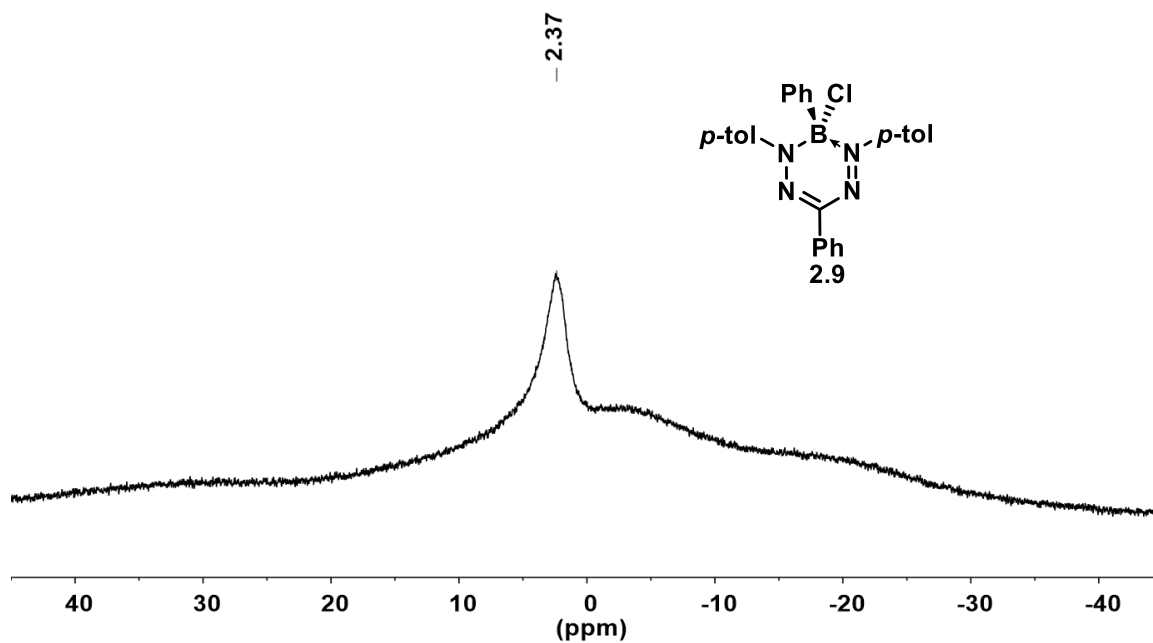
Figure A2.7. ^{11}B{^{1}H} NMR spectrum of BPhCl formazanate **2.9** recorded in CDCl$_3$.
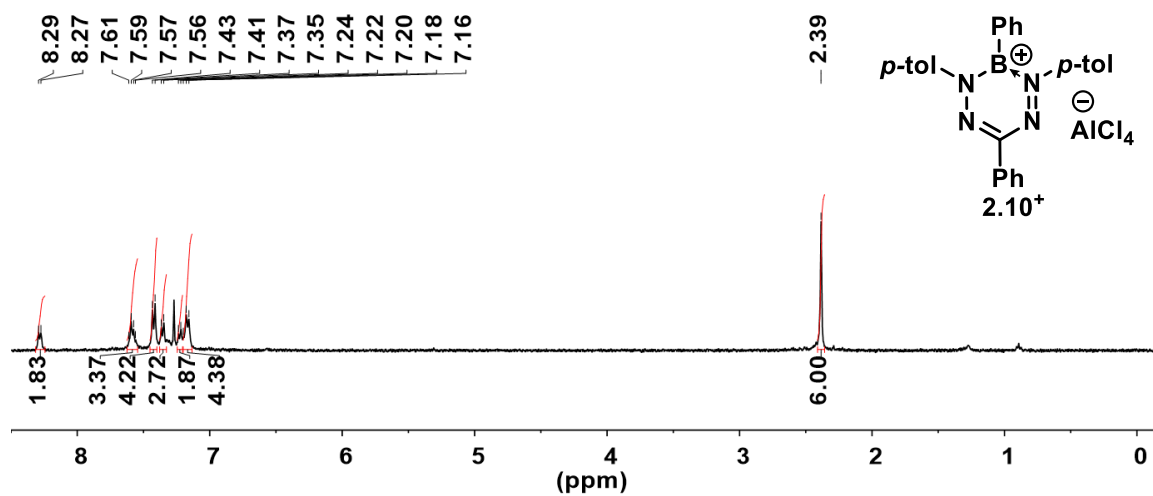
Figure A2.8. ^{1}H NMR spectrum of borenium cation **2.10$^+$** recorded in CDCl$_3$.
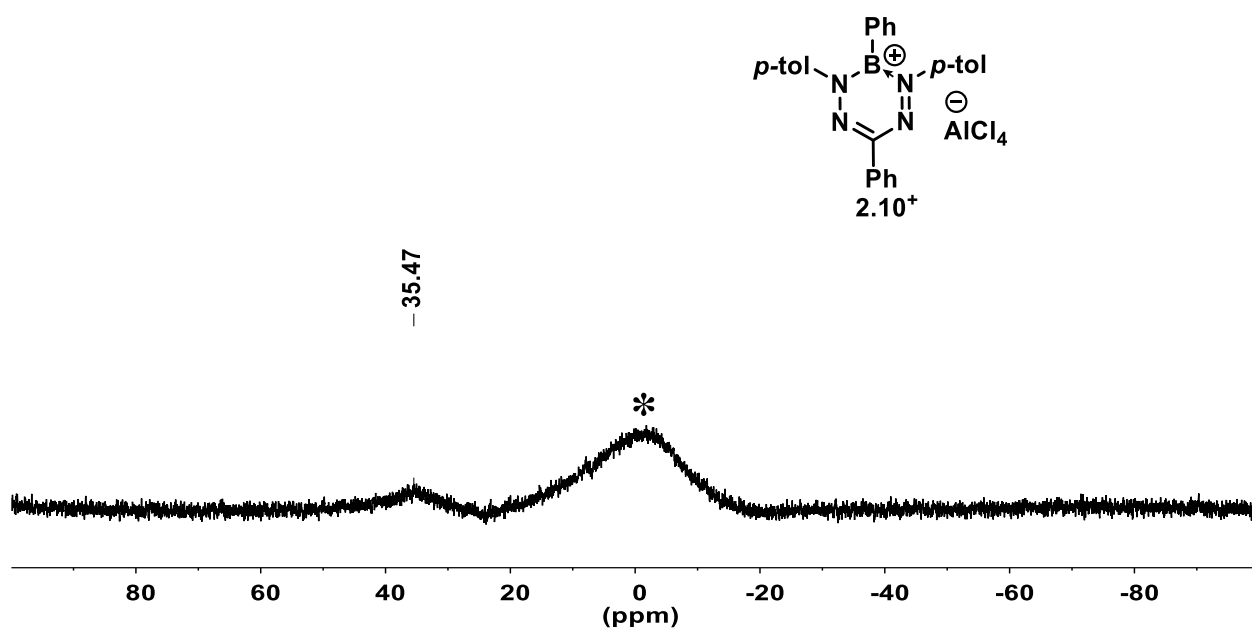
Figure A2.9. $^{11}B\{^1H\}$ NMR spectrum of borenium cation **2.10**$^+$ recorded in CDCl$_3$. The asterisk denotes background signal from the spectrometer probe.
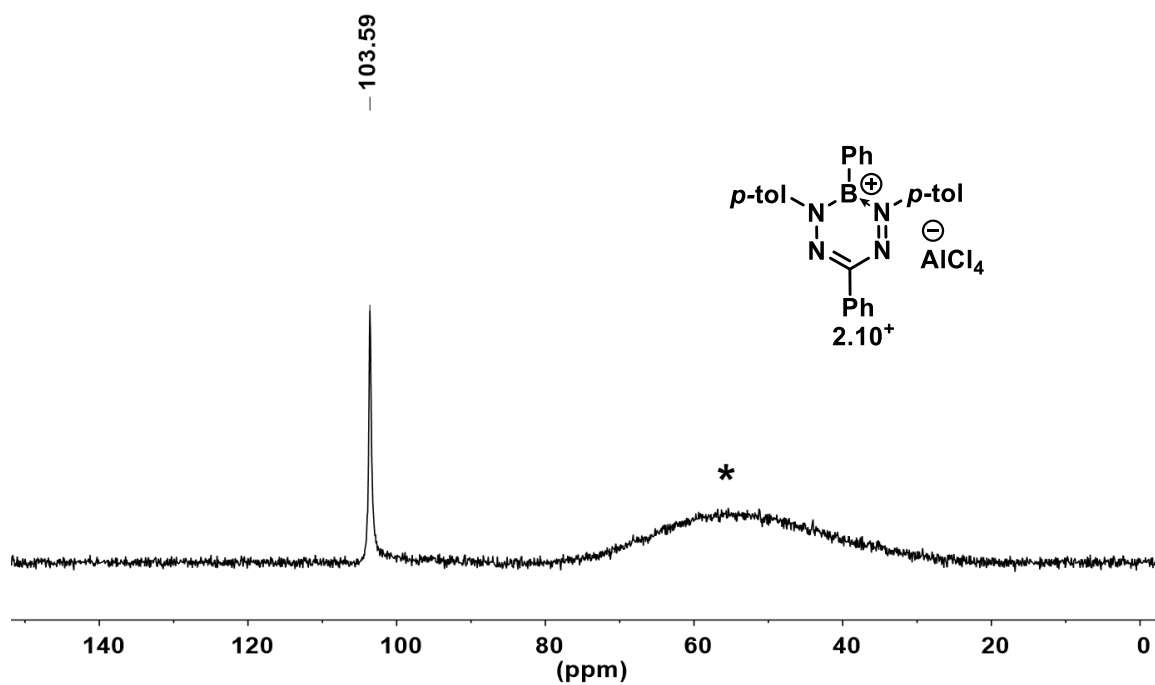
Figure A2.10. $^{27}Al\{^1H\}$ NMR spectrum of borenium cation **2.10**$^+$ recorded in CDCl$_3$. The asterisk denotes background signal from the spectrometer probe.
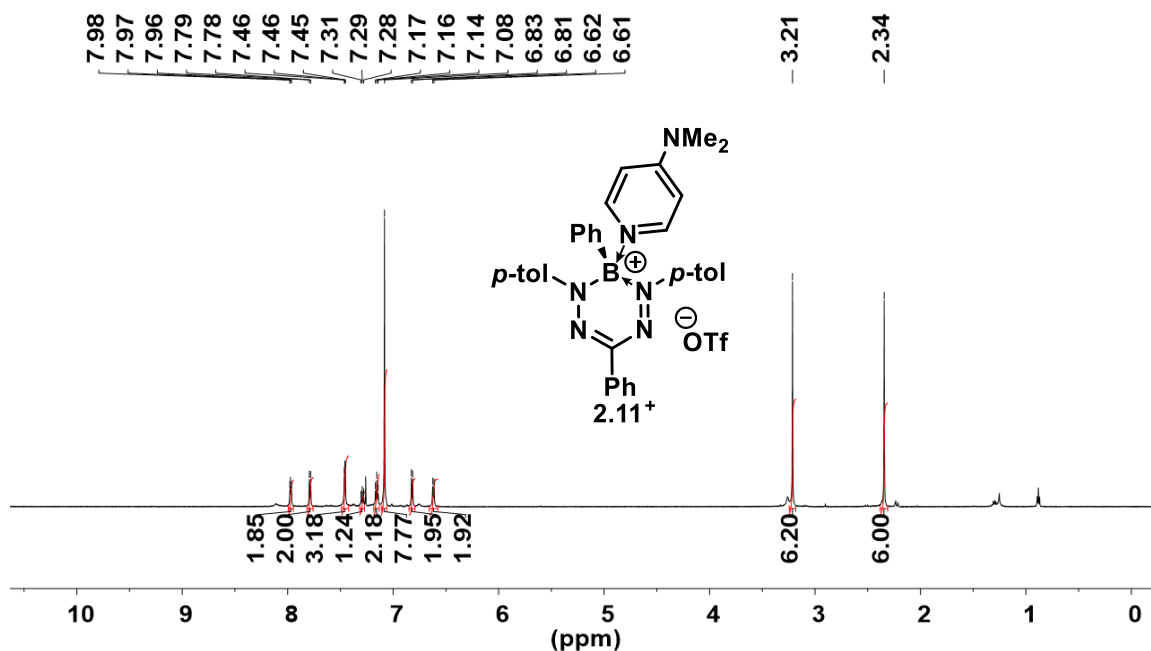
Figure A2.11. ^{1}H NMR spectrum of boronium cation **2.11$^+$** recorded in CDCl$_3$.
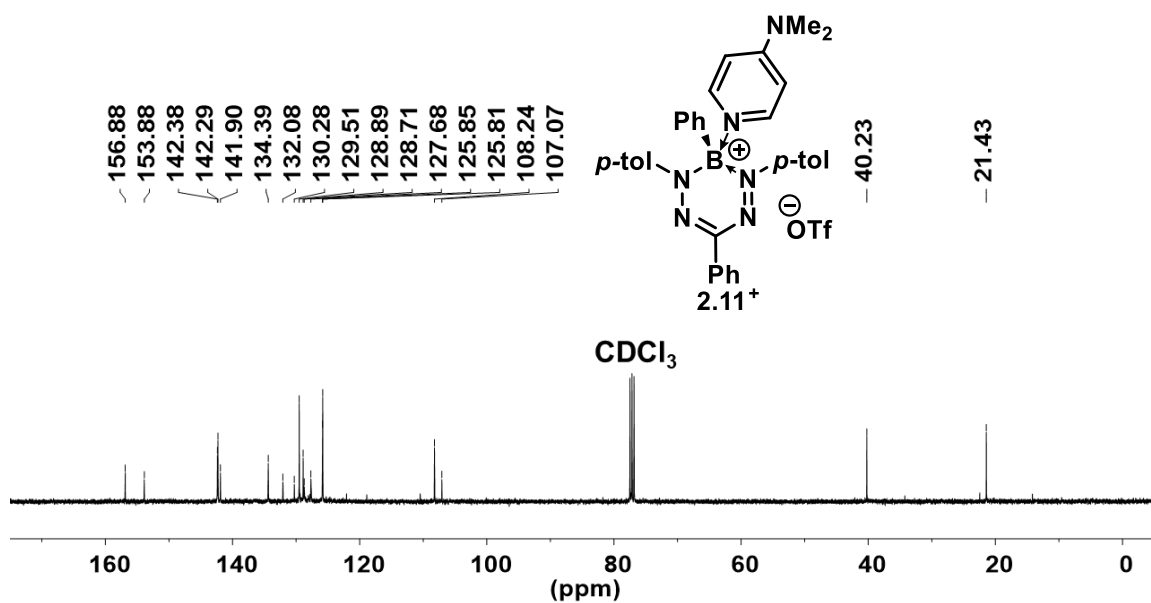
Figure A2.12. ^{13}C{^{1}H} NMR spectrum of boronium cation **2.11$^+$** recorded in CDCl$_3$.
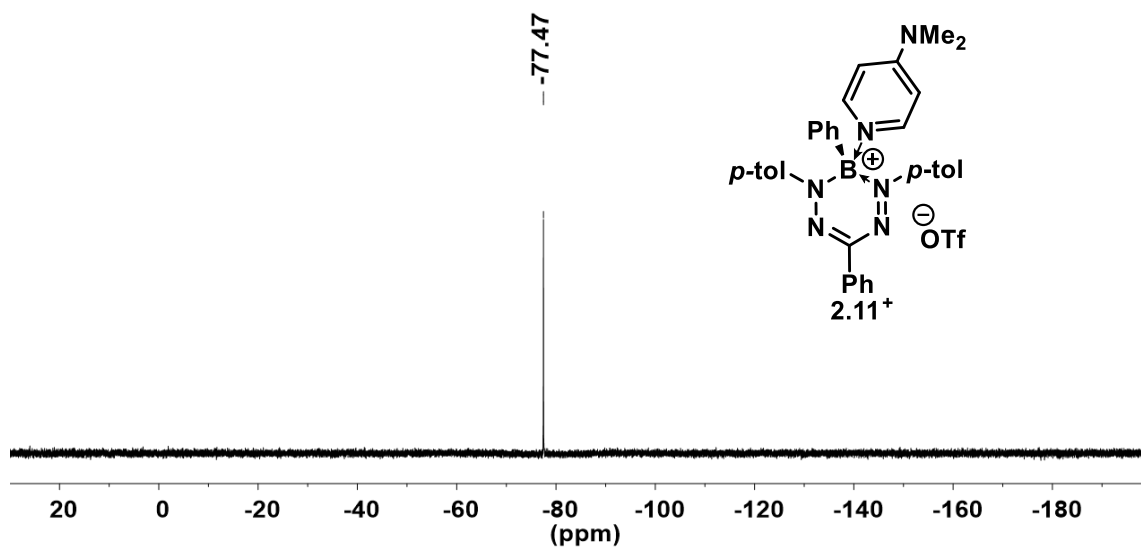
Figure A2.13. ^{19}F{^{1}H} NMR spectrum of boronium cation **2.11$^+$** recorded in CDCl$_3$.
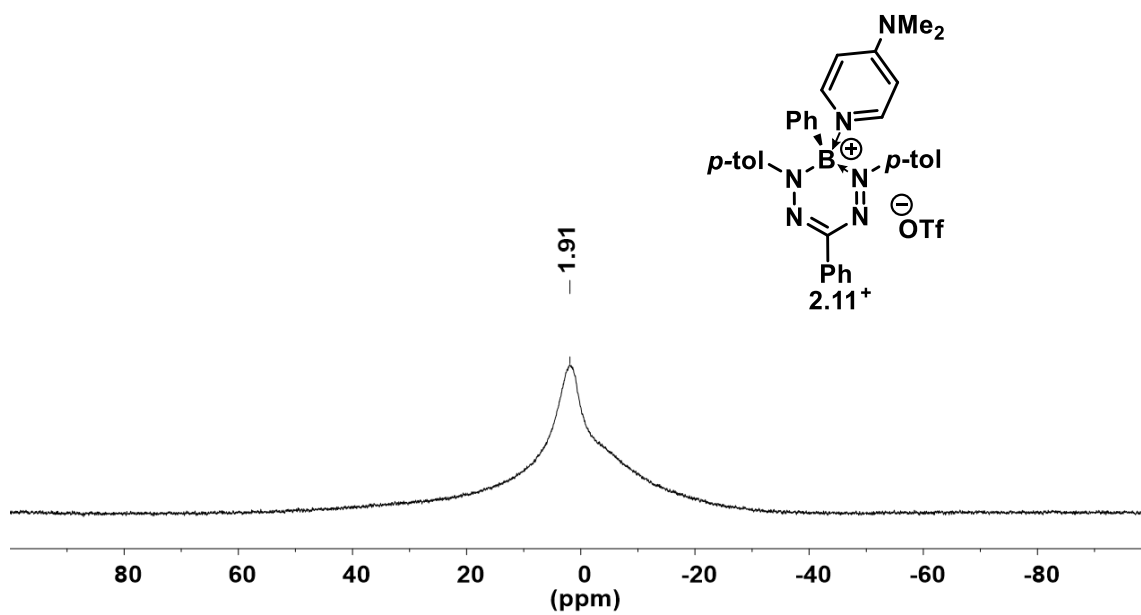
Figure A2.14. ^{11}B{^{1}H} NMR spectrum of boronium cation **2.11$^+$** recorded in CDCl$_3$.
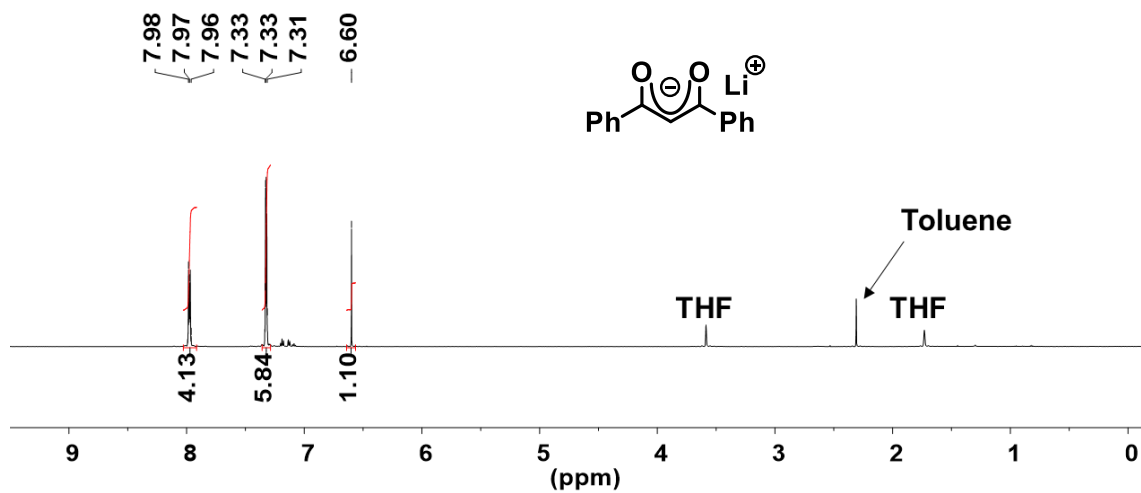
Figure A2.15. ^{1}H NMR spectrum of lithium dibenzoylmethanate recorded in THF-d_8.
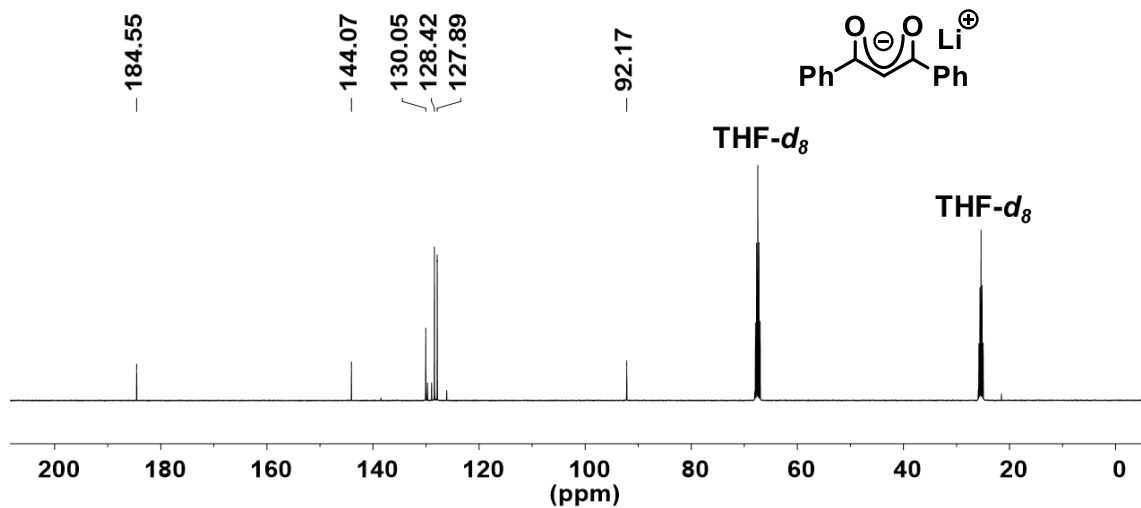
Figure A2.16. ^{13}C{^{1}H} NMR spectrum of lithium dibenzoylmethanate recorded in THF-d_8.
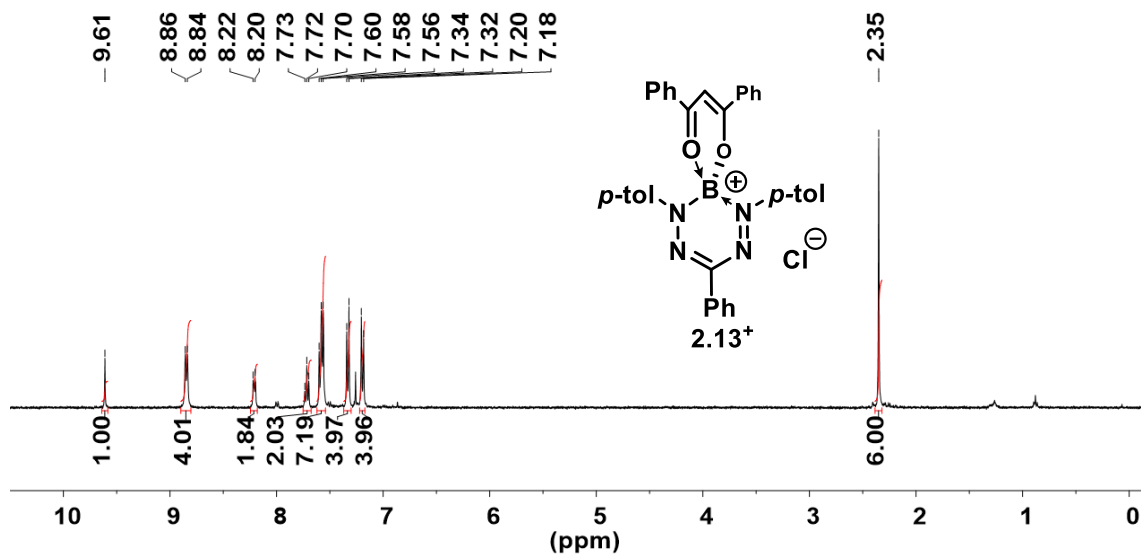
Figure A2.17. ^{1}H NMR spectrum of boronium cation **2.13$^+$** recorded in CDCl$_3$.
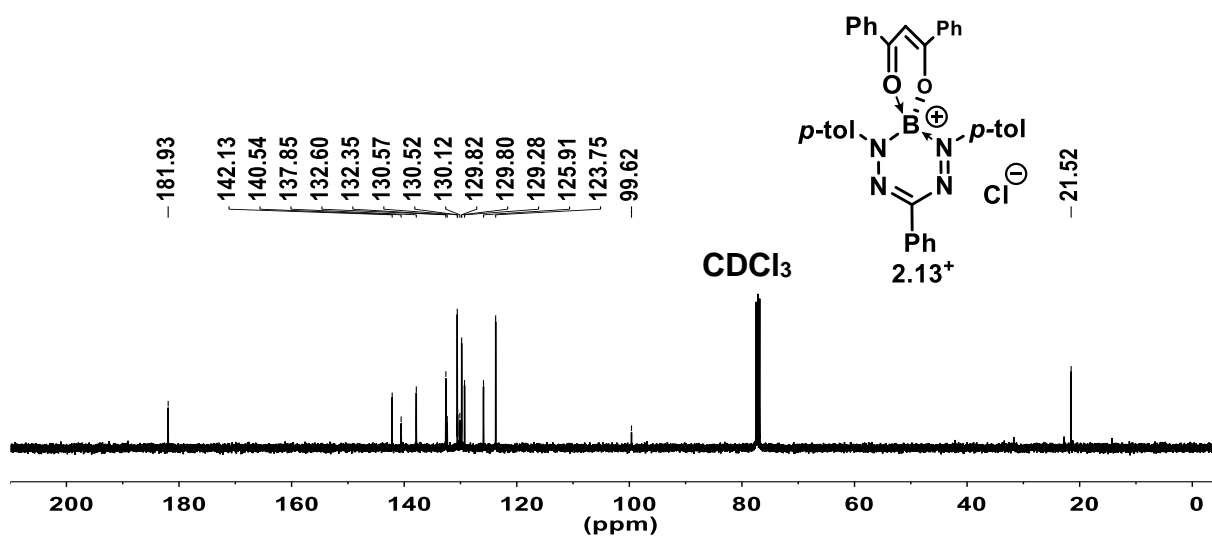
Figure A2.18. ^{13}C{^{1}H} NMR spectrum of boronium cation **2.13$^+$** recorded in CDCl$_3$.
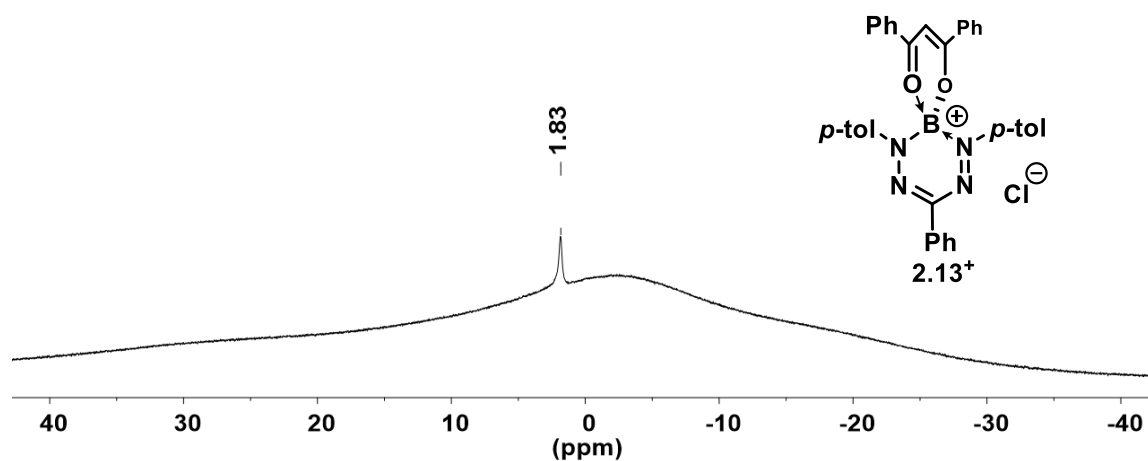
Figure A2.19. $^{11}B\{^1H\}$ NMR spectrum of boronium cation **2.13$^+$** recorded in CDCl$_3$.
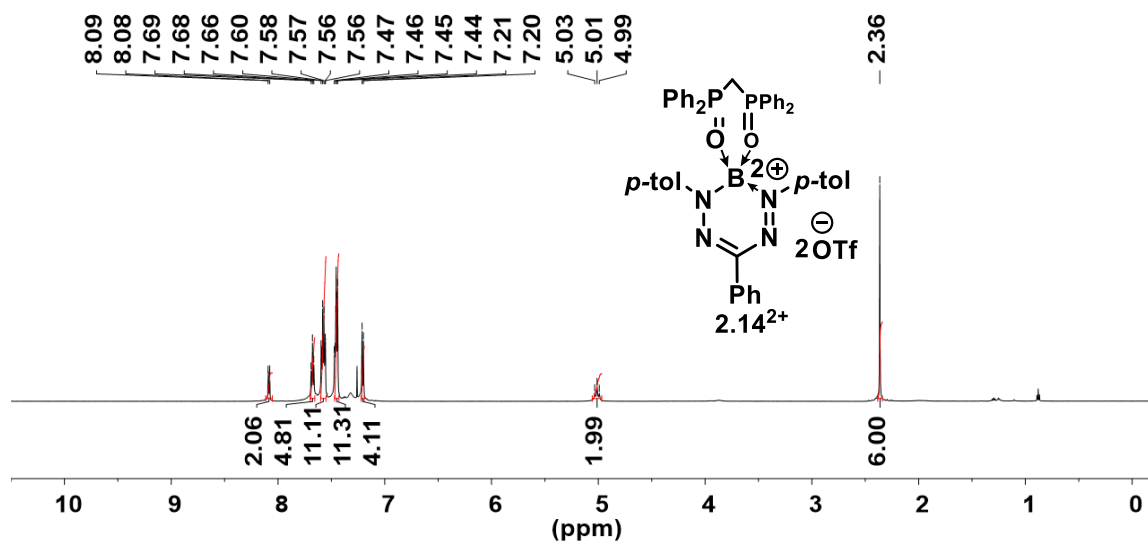
Figure A2.20. ^1H NMR spectrum of boron dication **2.14^{2+}** recorded in CDCl$_3$.
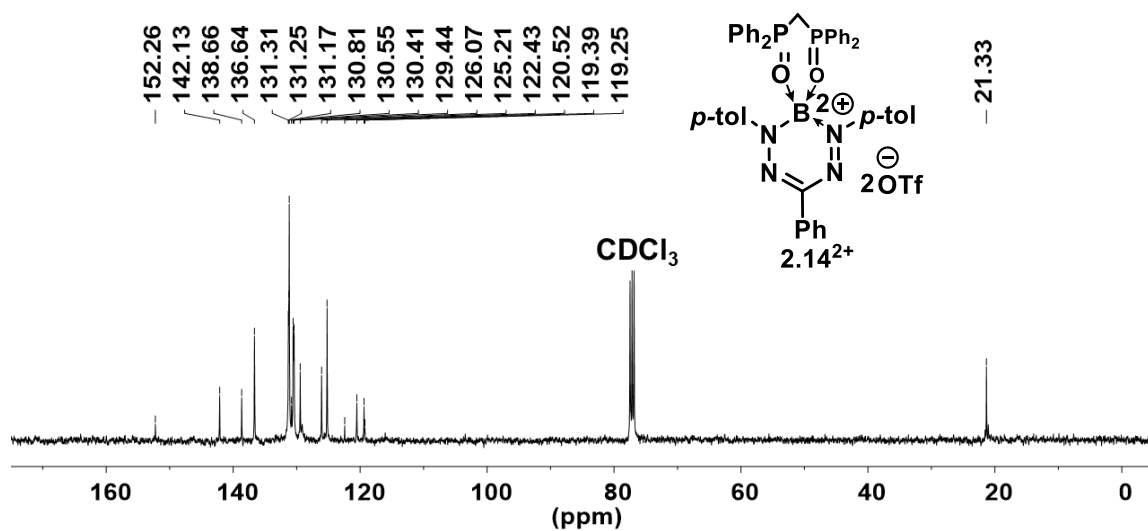
Figure S21. $^{13}C\{^1H\}$ NMR spectrum of boron dication $\textbf{2.14}^{2+}$ recorded in CDCl$_3$.
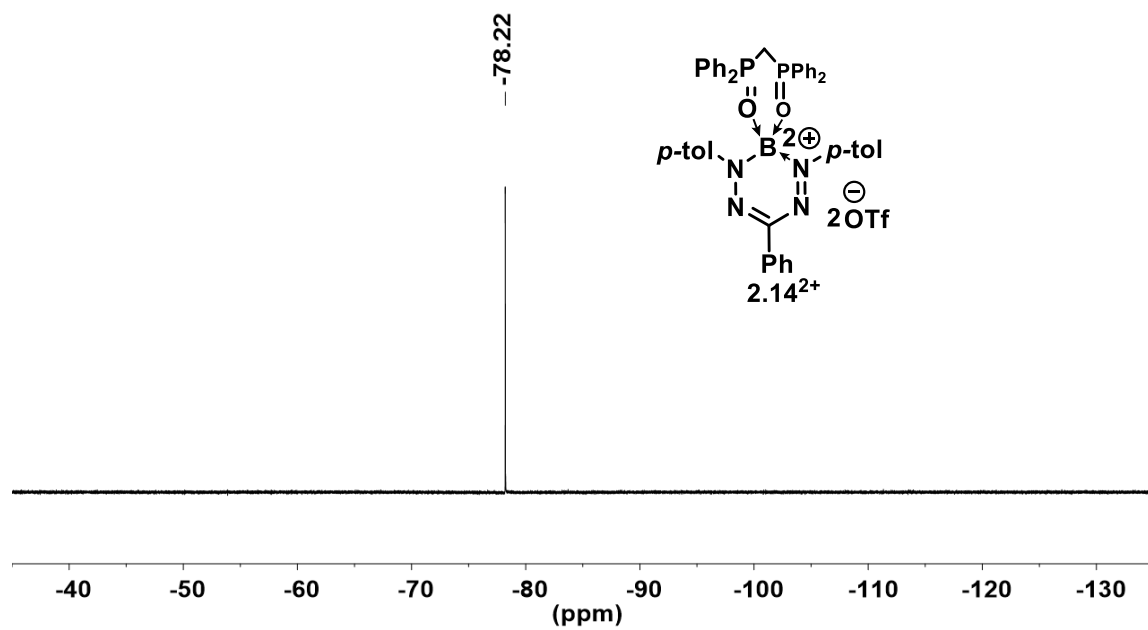
Figure A2.22. $^{19}F\{^1H\}$ NMR spectrum of boron dication $\textbf{2.14}^{2+}$ recorded in CDCl$_3$.
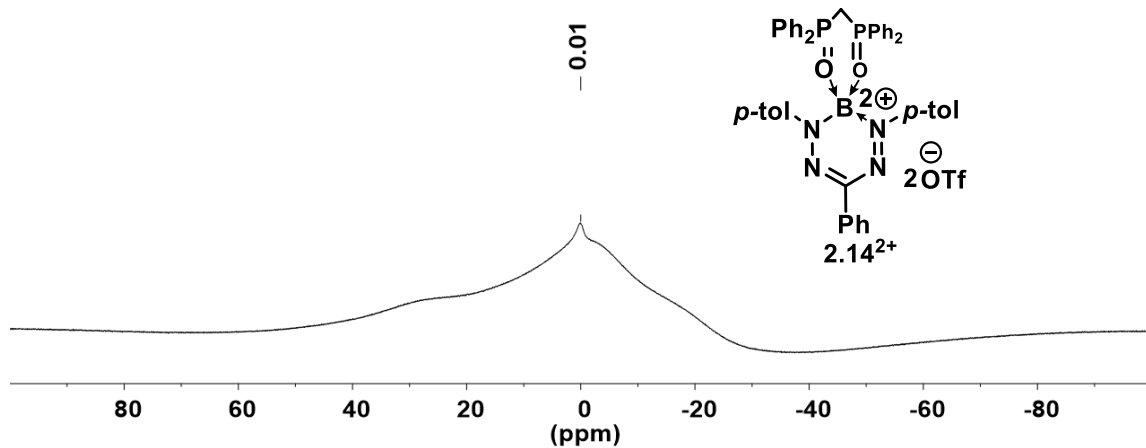
Figure A2.23. $^{11}B\{^1H\}$ NMR spectrum of boron dication **26^{2+}** recorded in CDCl$_3$.
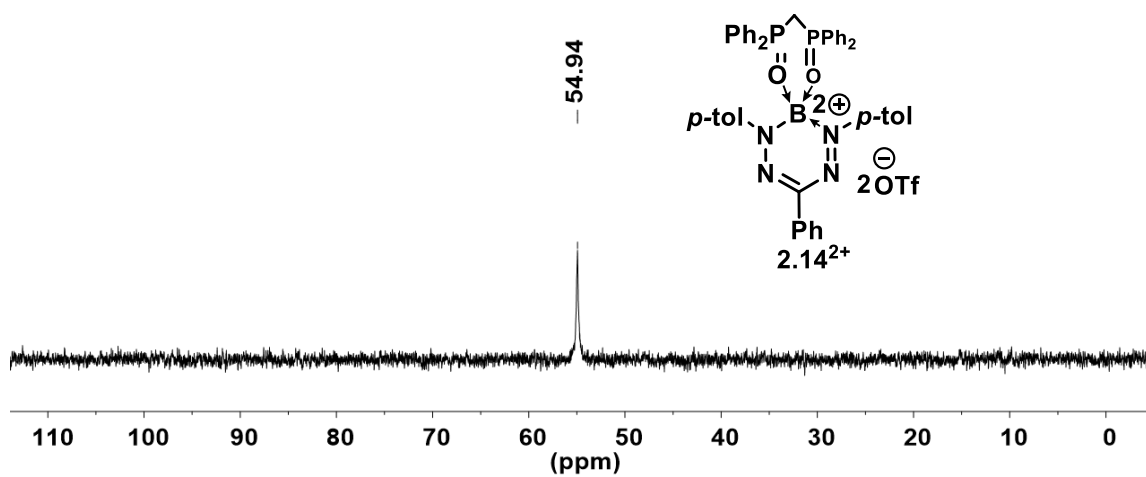
Figure A2.24. $^{31}P\{^1H\}$ NMR spectrum of boron dication **2.14^{2+}** recorded in CDCl$_3$.

OPTIMIZED GEOMETRIES OF COMPOUNDS 2.9−2.11⁺ AND 2.13⁺−2.15

```
# PBE1PBE DGDZVP2 SCF=Tight Int(Grid=UltraFine)
  SCRF(CPCM,Solvent=Toluene)
```

2.9 (C_s)

```
0,1
B      0.436127     0.856428     0.000000
Cl     0.069928     2.719035     0.000000
N     -0.325416     0.232152     1.208611
N     -0.325416     0.232152    -1.208611
N     -1.602212     0.019405     1.177349
N     -1.602212     0.019405    -1.177349
C     -0.147523    -1.244893     3.139532
C     -0.147523    -1.244893    -3.139532
C      0.291175    -0.117149     2.441138
C      0.291175    -0.117149    -2.441138
C      0.435434    -1.573112     4.358877
C      0.435434    -1.573112    -4.358877
C      1.306429     0.681494     2.973942
C      1.306429     0.681494    -2.973942
C      1.458298    -0.789474     4.908767
C      1.458298    -0.789474    -4.908767
C      1.874191     0.343866     4.197365
C      1.874191     0.343866    -4.197365
C      1.998650     0.510764     0.000000
C      2.108262    -1.164695     6.210954
C      2.108262    -1.164695    -6.210954
C     -2.235286     0.088084    -0.000000
C      2.393740    -0.837607     0.000000
C      3.010139     1.479023     0.000000
C     -3.710006     0.011283    -0.000000
C      3.737825    -1.205487     0.000000
C      4.360470     1.122786     0.000000
C     -4.419483    -0.015598     1.208384
C     -4.419483    -0.015598    -1.208384
C      4.730343    -0.222374     0.000000
C     -5.810916    -0.084104     1.206299
C     -5.810916    -0.084104    -1.206299
C     -6.513860    -0.121014    -0.000000
H      0.093596    -2.457445     4.889557
H      0.093596    -2.457445    -4.889557
H     -0.935187    -1.860313     2.718470
H     -0.935187    -1.860313    -2.718470
H      1.445153    -1.780135     6.822715
H      1.445153    -1.780135    -6.822715
```

```
H      1.638528    -1.621071     0.000000
H      1.628438     1.573487     2.450200
H      1.628438     1.573487    -2.450200
H      2.385713    -0.276984     6.784511
H      2.385713    -0.276984    -6.784511
H      2.652127     0.979706     4.610735
H      2.652127     0.979706    -4.610735
H      2.738177     2.531103     0.000000
H      3.024241    -1.738954     6.033474
H      3.024241    -1.738954    -6.033474
H     -3.875012     0.019067     2.145705
H     -3.875012     0.019067    -2.145705
H      4.013222    -2.256320     0.000000
H      5.123912     1.895860     0.000000
H      5.779608    -0.503089     0.000000
H     -6.349096    -0.104603     2.149361
H     -6.349096    -0.104603    -2.149361
H     -7.598515    -0.170427    -0.000000
```

```
# PBE1PBE DGDZVP2 SCF=Tight Int(Grid=UltraFine)
  SCRF(CPCM,Solvent=Toluene)
```

2.10$^+$ (C_2)

```
1,1
B     -0.000000     0.000000    -0.579114
N      0.030439     1.201662     0.245155
N     -0.030439    -1.201662     0.245155
N      0.000723     1.184123     1.554502
N     -0.000723    -1.184123     1.554502
C     -0.000000     0.000000    -2.127783
C      0.000000    -0.000000     2.175046
C      0.000000    -0.000000     3.649868
C     -0.000000     0.000000    -4.937836
C      0.000000    -0.000000     6.444442
C      0.907028     2.848461    -1.351925
C     -0.907028    -2.848461    -1.351925
C      0.179777     1.195417     5.745085
C     -0.179777    -1.195417     5.745085
C      0.179371     1.199200     4.353000
C     -0.179371    -1.199200     4.353000
C      0.931139     4.153817    -1.827914
C     -0.931139    -4.153817    -1.827914
C      0.046283     2.526647    -0.301047
C     -0.046283    -2.526647    -0.301047
C     -1.016077     0.654723    -2.845257
```

```
C      1.016077    -0.654723    -2.845257
C     -1.023372     0.643463    -4.238774
C      1.023372    -0.643463    -4.238774
C      0.095587     5.143732    -1.290905
C     -0.095587    -5.143732    -1.290905
C     -0.779994     3.497013     0.270172
C      0.779994    -3.497013     0.270172
C      0.098384     6.537986    -1.845513
C     -0.098384    -6.537986    -1.845513
C     -0.757260     4.790583    -0.234712
C      0.757260    -4.790583    -0.234712
H     -0.000000     0.000000    -6.023508
H      0.000000    -0.000000     7.529999
H     -1.617752    -4.408889    -2.629473
H      1.617752     4.408889    -2.629473
H      0.323075     2.125456     6.285936
H     -0.323075    -2.125456     6.285936
H      0.322674     2.126647     3.810146
H     -0.322674    -2.126647     3.810146
H     -1.571915    -2.103400    -1.772724
H      1.571915     2.103400    -1.772724
H      1.078232     6.802461    -2.247990
H     -1.078232    -6.802461    -2.247990
H     -1.821571     1.142604    -4.779272
H      1.821571    -1.142604    -4.779272
H     -1.811298     1.174384    -2.317499
H      1.811298    -1.174384    -2.317499
H     -0.177594     7.268882    -1.082963
H      0.177594    -7.268882    -1.082963
H     -1.439910     3.232496     1.089291
H      1.439910    -3.232496     1.089291
H     -0.626991     6.622894    -2.662032
H      0.626991    -6.622894    -2.662032
H     -1.412856     5.539780     0.199042
H      1.412856    -5.539780     0.199042

# PBE1PBE DGDZVP2 SCF=Tight Int(Grid=UltraFine)
  SCRF(CPCM,Solvent=Toluene)
```

2.11⁺ (*C*₁)

```
1,1
B     -0.416325    -0.000579    -0.386341
N     -0.397944    -1.191990     0.617240
N     -0.398548     1.195566     0.611234
N      0.459308     1.174036     1.591510
N      0.460202    -1.165087     1.597087
```

```
N       1.002307     -0.002507     -1.110807
N       4.520602     -0.009853     -3.347271
C       1.039853      0.005433      1.896067
C      -1.283277     -2.302638      0.646703
C      -1.284397      2.305925      0.634445
C      -1.436390     -0.005827     -2.805136
C       1.586756     -1.160935     -1.494854
C       1.593934      1.153508     -1.491052
C      -1.630082     -0.003308     -1.417035
C      -1.714175     -2.799374      1.882433
C      -1.717309      2.808199      1.867217
C      -1.690276      2.927787     -0.549788
C      -1.690550     -2.930340     -0.533988
C       2.187491      0.008140      2.821578
C      -2.543015     -3.911661      1.930109
C      -2.515817     -0.008037     -3.691875
C      -2.547013      3.920103      1.908422
C      -2.515529     -4.048566     -0.468661
C      -2.516123      4.045745     -0.490947
C       2.740776     -1.210915     -2.229979
C       2.748824      1.198604     -2.225180
C       2.744237      1.219187      3.253383
C       2.744756     -1.200289      3.259980
C      -2.961534     -4.557602      0.756763
C      -2.955086     -0.002887     -0.946528
C      -2.964320      4.560172      0.731414
C       3.384735     -0.007486     -2.631451
C      -3.820856     -0.007686     -3.201980
C       3.831853      1.219531      4.123555
C       3.832382     -1.195398      4.130132
C      -3.879619     -5.744221      0.819372
C      -3.883378      5.746384      0.787128
C      -4.037540     -0.005050     -1.821309
C       4.379249      0.013384      4.566650
C       5.133437     -1.268278     -3.745906
C       5.154529      1.245882     -3.720686
H      -0.430989     -0.005975     -3.217825
H       1.097112     -2.075471     -1.181209
H       1.109120      2.070052     -1.175828
H      -1.401329     -2.303979      2.795115
H      -1.405438      2.317301      2.782664
H      -1.360971      2.554524     -1.512140
H      -1.363197     -2.561322     -1.498635
H       2.318913      2.155817      2.909034
H       2.319852     -2.138966      2.920729
H      -2.337356     -0.009971     -4.763147
H      -2.877477     -4.283259      2.894632
```

```
H      -2.883152       4.296033      2.870681
H      -2.816077       4.528363     -1.416520
H      -2.816535      -4.535728     -1.391509
H       3.143651      -2.181813     -2.484871
H      -3.149047      -0.000840      0.123379
H       3.156622       2.167777     -2.478803
H      -3.592973      -6.421861      1.627409
H      -3.597374       6.428858      1.591326
H      -3.875492      -6.300664     -0.119639
H      -3.879563       6.297472     -0.155034
H       4.254606       2.162472      4.456744
H       4.255549      -2.136320      4.468458
H       4.451416      -1.863028     -4.361365
H       4.501020       1.845739     -4.362063
H      -4.662931      -0.009407     -3.887557
H      -4.908705      -5.423486      1.013548
H      -4.912224       5.425945      0.983035
H      -5.050599      -0.004700     -1.430298
H       5.228009       0.015416      5.243576
H       5.434642      -1.857899     -2.874060
H       5.423520       1.832037     -2.836397
H       6.022152      -1.055376     -4.335792
H       6.066223       1.029073     -4.272860



# PBE1PBE DGDZVP2 SCF=Tight Int(Grid=UltraFine)
  SCRF(CPCM,Solvent=Dichloromethane)
```

2.13⁺ (*C_s*)

```
1,1
B       0.000810       0.148111     -0.000000
N       0.612891       0.891641      1.203862
N       0.612891       0.891641     -1.203862
N       0.783663       2.178805      1.175749
N       0.783663       2.178805     -1.175749
O      -1.462026       0.332698     -0.000000
O       0.397726      -1.246214      0.000000
C       2.673801       0.083263     -4.173910
C       2.673801       0.083263      4.173910
C       1.067621       0.246408     -2.384319
C       1.067621       0.246408      2.384319
C      -6.407532       0.451210     -0.000000
C      -3.716157      -0.308132      0.000000
C      -2.303111      -0.672697      0.000000
C       2.237453       0.694803     -3.005623
C       2.237453       0.694803      3.005623
```

```
C      0.341553    -0.809959     2.939918
C      0.341553    -0.809959    -2.939918
C      1.963300    -0.982020    -4.747102
C      1.963300    -0.982020     4.747102
C     -4.070225     1.053159    -0.000000
C     -6.064494    -0.904004     0.000000
C     -5.408097     1.428145    -0.000000
C     -4.728594    -1.284983     0.000000
C      0.789836    -1.409352     4.112371
C      0.789836    -1.409352    -4.112371
C      2.460571    -1.656486     5.993457
C      2.460571    -1.656486    -5.993457
C     -1.835824    -1.988015     0.000000
C     -0.468518    -2.238728     0.000000
C      0.686672     2.811647    -0.000000
C      0.123735    -3.571403     0.000000
C      1.524456    -3.697720     0.000000
C      0.696764     4.288097    -0.000000
C     -0.674220    -4.729939     0.000000
C      2.113288    -4.956270     0.000000
C      0.692220     4.996188     1.209402
C      0.692220     4.996188    -1.209402
C     -0.079994    -5.985326     0.000000
C      1.313316    -6.102047     0.000000
C      0.698537     6.389469     1.207151
C      0.698537     6.389469    -1.207151
C      0.703733     7.092366    -0.000000
H      3.586920     0.433754    -4.646628
H      3.586920     0.433754     4.646628
H     -7.452807     0.744620    -0.000000
H      2.920080    -0.936848     6.674845
H      2.920080    -0.936848    -6.674845
H     -0.593744    -1.137398    -2.499031
H     -0.593744    -1.137398     2.499031
H      2.799030     1.510634    -2.563371
H      2.799030     1.510634     2.563371
H     -3.291979     1.807346    -0.000000
H     -6.841124    -1.661595     0.000000
H      1.651100    -2.168207    -6.517596
H      1.651100    -2.168207     6.517596
H      0.209187    -2.217487    -4.547366
H      0.209187    -2.217487     4.547366
H     -5.675127     2.479874    -0.000000
H     -4.487890    -2.341610     0.000000
H      3.221652    -2.404424     5.745910
H      3.221652    -2.404424    -5.745910
H      2.140951    -2.806655     0.000000
```

```
H    -2.533152    -2.808279     0.000000
H     0.684919     4.452696    -2.147912
H     0.684919     4.452696     2.147912
H    -1.755879    -4.664365     0.000000
H     3.194535    -5.047529     0.000000
H    -0.700326    -6.875424     0.000000
H     0.696827     6.928396     2.149766
H     0.696827     6.928396    -2.149766
H     1.773678    -7.085268     0.000000
H     0.705866     8.178036    -0.000000
```

# PBE1PBE DGDZVP2 SCF=Tight Int(Grid=UltraFine)
  SCRF(CPCM,Solvent=Dichloromethane)

2.14²⁺ (*C*₁)

```
2,1
B     0.141255     0.082449     0.837606
N     0.238026     1.231653     1.844416
N     1.228020    -0.872774     1.359664
N     1.419626     1.721368     2.058131
N     2.396615    -0.348207     1.578361
O    -1.181528    -0.509232     0.721739
O     0.586423     0.665029    -0.466731
P     0.597763    -0.008284    -1.892526
P    -1.992963    -0.787129    -0.615072
C    -0.837964     1.896497     2.498491
C    -0.404862     3.568754    -3.511728
C     1.001055    -6.554141     2.124365
C    -0.841964     3.294153     2.554612
C     0.018362    -2.865682     2.119949
C     1.046542    -5.066302     1.924741
C     0.296900     1.312785    -3.049425
C    -0.167656     2.551641    -2.590440
C    -0.018203    -4.245904     2.310802
C    -1.892090     3.950579     3.182239
C     1.146063    -2.284689     1.539288
C    -0.752182    -1.238563    -1.867790
C    -0.186509     3.347034    -4.872651
C    -1.870205     1.166076     3.088406
C     0.533087     1.087961    -4.412793
C     2.168892    -4.457110     1.341346
C     2.139254    -0.834839    -2.232818
C     0.281035     2.109836    -5.323129
C     3.314817    -0.113781    -1.968140
C    -2.946420     3.240215     3.777301
```

```
C     2.229036    -3.083603     1.153117
C    -2.910857     1.842730     3.721476
C     2.197005    -2.128862    -2.765558
C    -2.602728    -3.460338    -0.223595
C    -4.066978     3.967778     4.463064
C     4.548197    -0.703709    -2.222464
C    -3.098690    -2.152620    -0.339997
C    -3.125718     1.718066    -0.274387
C     2.481610     0.985039     1.694723
C    -2.882795     0.660427    -1.158929
C    -3.488001    -4.505389     0.015195
C     3.439019    -2.702756    -3.028508
C     4.609609    -1.995070    -2.753226
C    -4.471123    -1.893168    -0.219018
C    -3.853648     2.821202    -0.714764
C    -4.856512    -4.249833     0.138621
C    -3.379052     0.694311    -2.472009
C     3.814969     1.611456     1.718151
C    -5.346482    -2.948418     0.023381
C     3.938302     2.995489     1.897890
C    -4.339911     2.863900    -2.021451
C    -4.106313     1.800772    -2.897498
C     4.967116     0.835130     1.533707
C     5.197680     3.590946     1.909009
C     6.224204     1.434767     1.546226
C     6.345093     2.813658     1.735435
H     1.030923    -7.075744     1.162697
H     1.864338    -6.895412     2.702849
H    -1.896990     5.036668     3.206857
H    -0.758941     4.534420    -3.166298
H    -0.343574    -2.214299    -1.590648
H    -0.810632    -2.254459     2.455351
H     3.273693     0.893832    -1.564400
H    -0.036004     3.852084     2.090644
H    -0.330660     2.723564    -1.532036
H     0.093634    -6.857375     2.649042
H    -1.859473     0.082839     3.077539
H    -0.374362     4.143537    -5.585840
H    -0.892814    -4.687386     2.779682
H    -1.217023    -1.332929    -2.851776
H    -1.542833    -3.676414    -0.306862
H     0.916377     0.135335    -4.766380
H    -2.757421     1.685649     0.744939
H     3.009218    -5.070545     1.028439
H    -3.701224     4.483831     5.356344
H     1.298029    -2.693074    -2.990117
H     0.459903     1.945692    -6.380468
```

```
H      3.101284    -2.623600     0.701544
H      5.460101    -0.155769    -2.009691
H     -4.499341     4.727428     3.805910
H     -3.705544     1.266959     4.186463
H     -3.111704    -5.518953     0.104884
H     -4.859403     3.282224     4.767479
H     -4.040670     3.645121    -0.034279
H      3.490444    -3.703099    -3.445039
H     -4.856301    -0.883457    -0.314110
H      3.048547     3.601484     2.031010
H      5.574356    -2.449815    -2.954817
H     -3.215507    -0.127141    -3.162884
H     -5.542857    -5.070304     0.323342
H      4.875900    -0.235626     1.386473
H     -6.409395    -2.754016     0.119060
H     -4.906356     3.725950    -2.359477
H     -4.489062     1.833755    -3.911953
H      5.284203     4.663773     2.051011
H      7.112127     0.825613     1.407513
H      7.325692     3.279416     1.742556
```

# PBE1PBE DGDZVP2 SCF=Tight Int(Grid=UltraFine)
  SCRF(CPCM,Solvent=Dichloromethane)

2.15 (*C_s*)

```
0,1
B      1.172191     0.455876    -0.000000
N     -1.068971     0.035897    -1.188963
N     -1.068971     0.035897     1.188963
N      0.218103     0.138558    -1.239355
N      0.218103     0.138558     1.239355
O      1.597261     1.821885    -0.000000
O      2.330685    -0.371193    -0.000000
C      0.610671     2.833498    -0.000000
C     -1.683433     0.055435     0.000000
C      2.151348    -1.771964    -0.000000
C     -3.162800     0.014507     0.000000
C     -5.975944    -0.058981     0.000000
C     -5.270345    -0.038765     1.205393
C     -5.270345    -0.038765    -1.205393
C     -3.877159    -0.001002    -1.207186
C     -3.877159    -0.001002     1.207186
C      0.772985    -0.028378    -2.535230
C      0.772985    -0.028378     2.535230
C      2.005486     0.553253    -2.850828
```

```
C      2.005486      0.553253      2.850828
C      0.094262     -0.778865     -3.504814
C      0.094262     -0.778865      3.504814
C      2.540258      0.386979      4.125391
C      2.540258      0.386979     -4.125391
C      0.643582     -0.935479     -4.770836
C      0.643582     -0.935479      4.770836
C      1.875569     -0.354440     -5.108897
C      1.875569     -0.354440      5.108897
C      2.449323     -0.518108     -6.488120
C      2.449323     -0.518108      6.488120
H      1.115306      3.802433     -0.000000
H      3.138507     -2.240562     -0.000000
H     -7.061333     -0.086585      0.000000
H      1.608056     -2.117600      0.889943
H      1.608056     -2.117600     -0.889943
H     -0.029851      2.782503      0.891039
H     -0.029851      2.782503     -0.891039
H      2.527136      1.142417     -2.106491
H      2.527136      1.142417      2.106491
H     -3.334946      0.017799     -2.146046
H     -3.334946      0.017799      2.146046
H     -5.807524     -0.050730     -2.149322
H     -5.807524     -0.050730      2.149322
H     -0.850497     -1.246511     -3.252248
H     -0.850497     -1.246511      3.252248
H      3.494892      0.849970      4.359703
H      3.494892      0.849970     -4.359703
H      0.111976     -1.530647     -5.508542
H      0.111976     -1.530647      5.508542
H      3.497798     -0.215743     -6.520651
H      3.497798     -0.215743      6.520651
H      2.377088     -1.556167      6.823912
H      2.377088     -1.556167     -6.823912
H      1.900163      0.094775      7.210999
H      1.900163      0.094775     -7.210999
```

Appendix A3 Supporting Information for Chapter 3
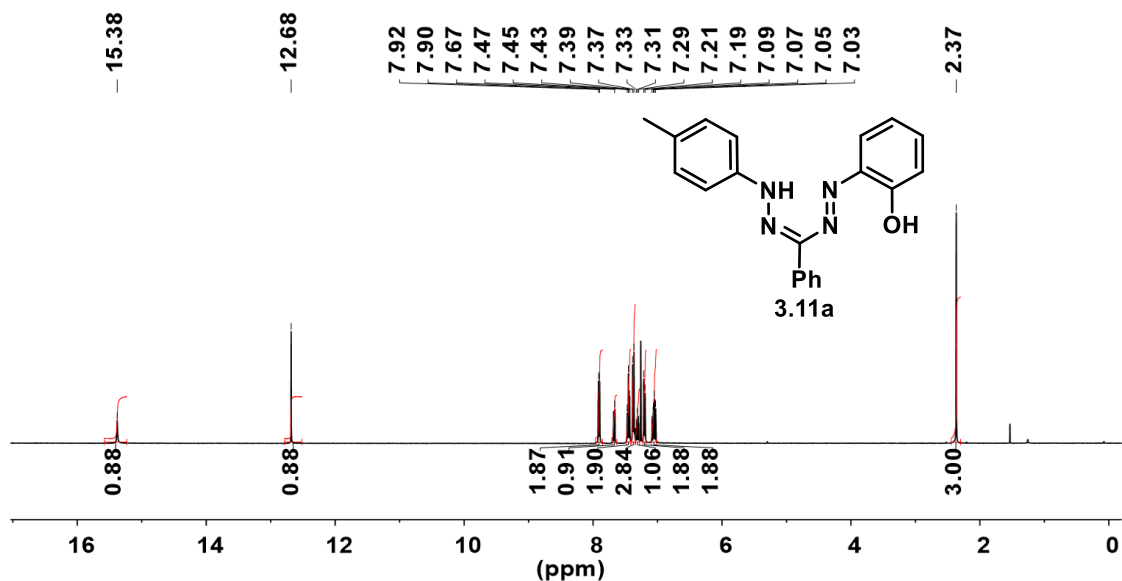
Figure A3.1. ^{1}H NMR spectrum of **3.11a** recorded in CDCl$_3$.
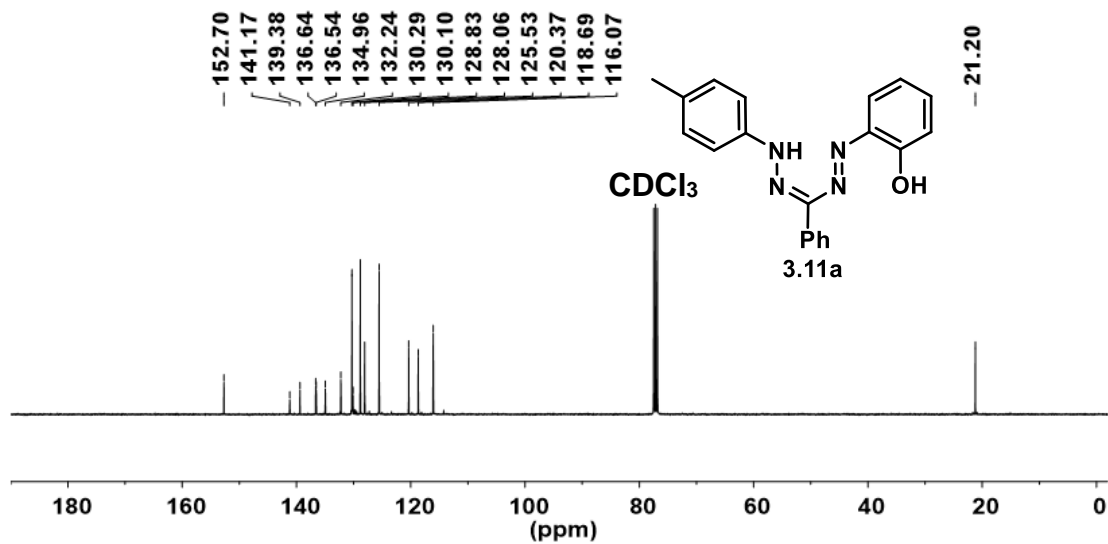
Figure A3.2. ^{13}C{^{1}H} NMR spectrum of **3.11a** recorded in CDCl$_3$.
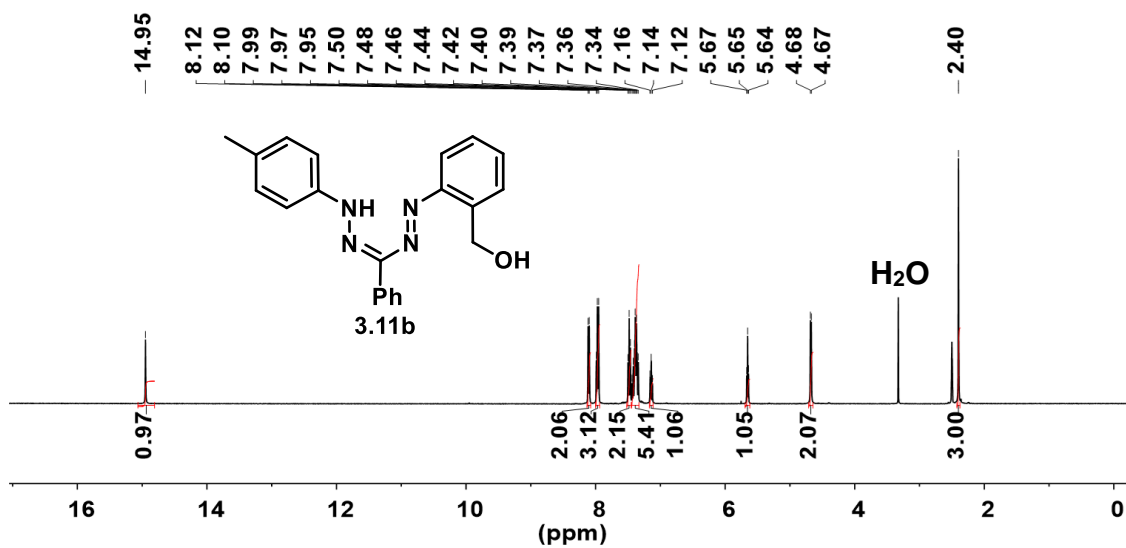
Figure A3.3. ¹H NMR spectrum of **3.11b** recorded in DMSO-d_6.
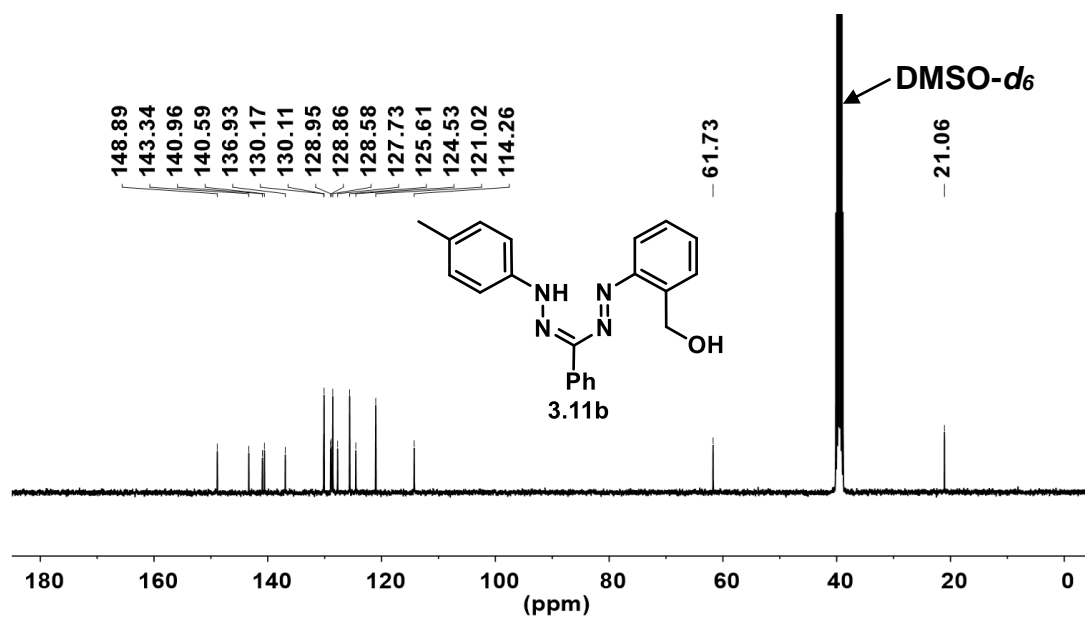
Figure A3.4. ¹³C{¹H} NMR spectrum of **3.11b** recorded in DMSO-d_6.
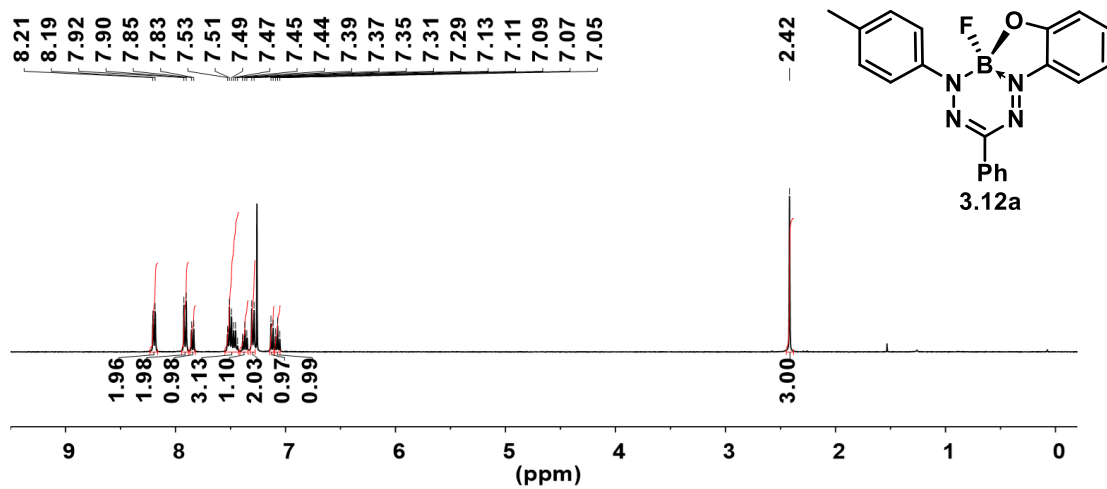
Figure A3.5. ^{1}H NMR spectrum of **3.12a** recorded in CDCl[3].
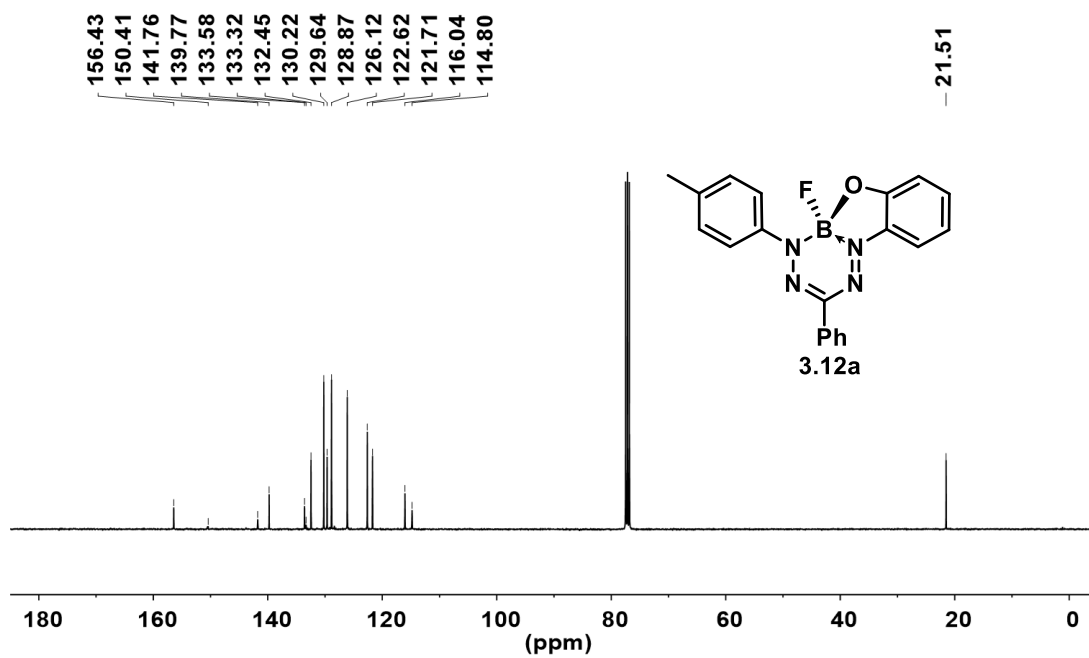
Figure A3.6. ^{13}C{^{1}H} NMR spectrum of **3.12a** recorded in CDCl[3].
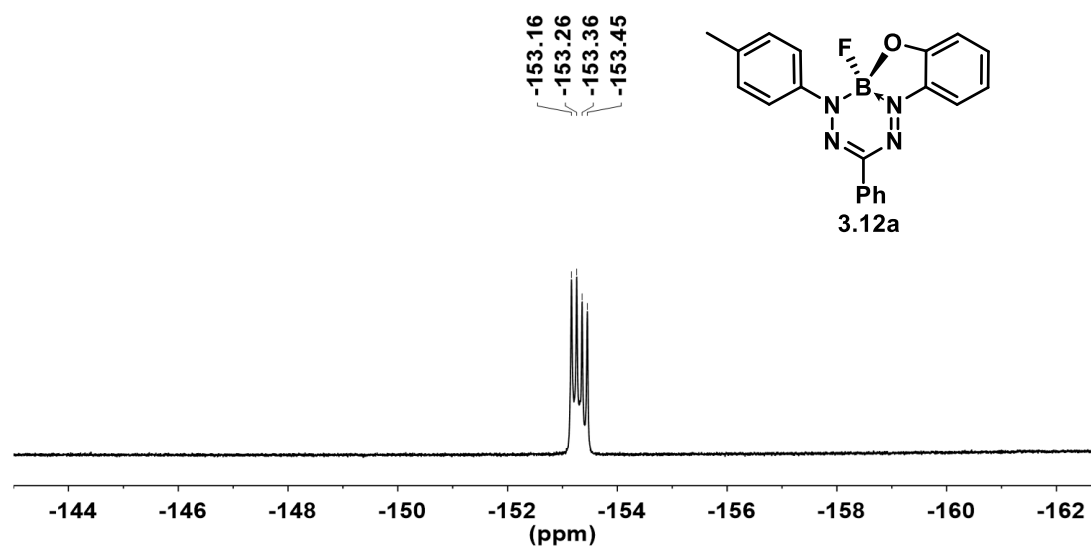
Figure A3.7. $^{19}F\{^{1}H\}$ NMR spectrum of **3.12a** recorded in CDCl$_3$.
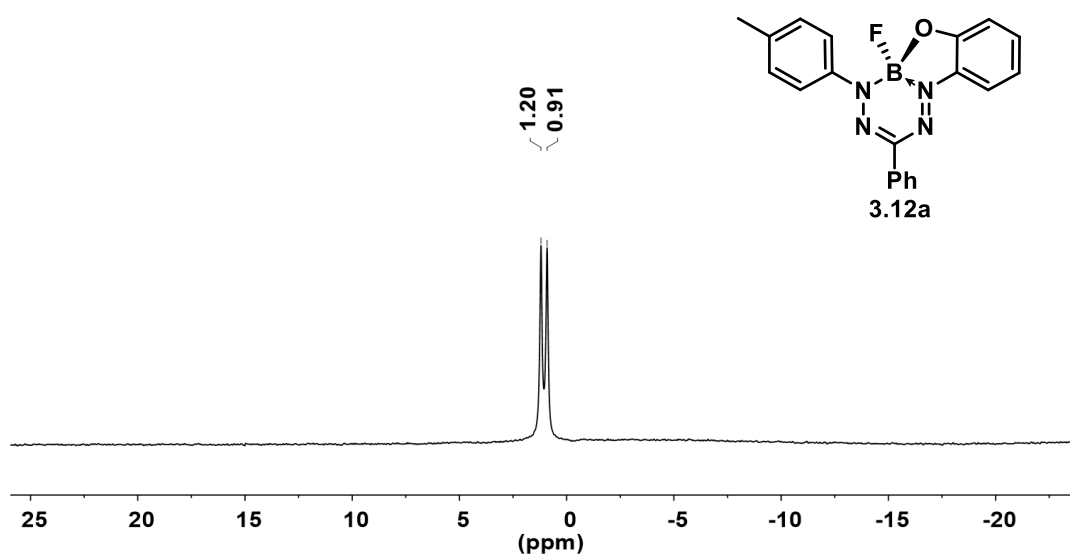
Figure A3.8. $^{11}B\{^{1}H\}$ NMR spectrum of **3.12a** recorded in CDCl$_3$.

Figure A3.9. ^{1}H NMR spectrum of **3.11b** recorded in CDCl$_3$.

Figure A3.10. ^{13}C{^{1}H} NMR spectrum of **3.12b** recorded in CDCl$_3$.
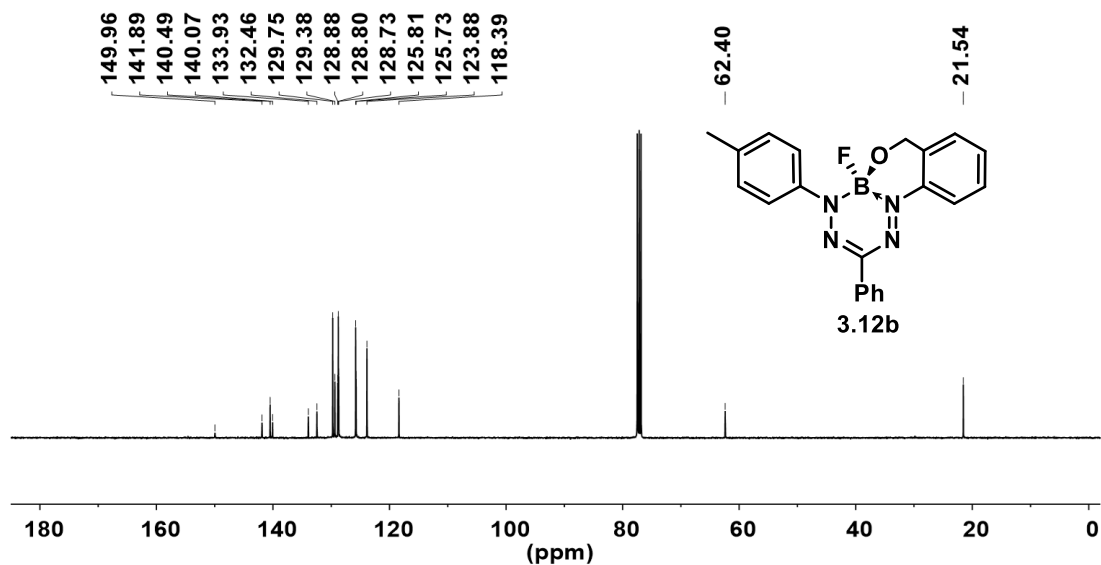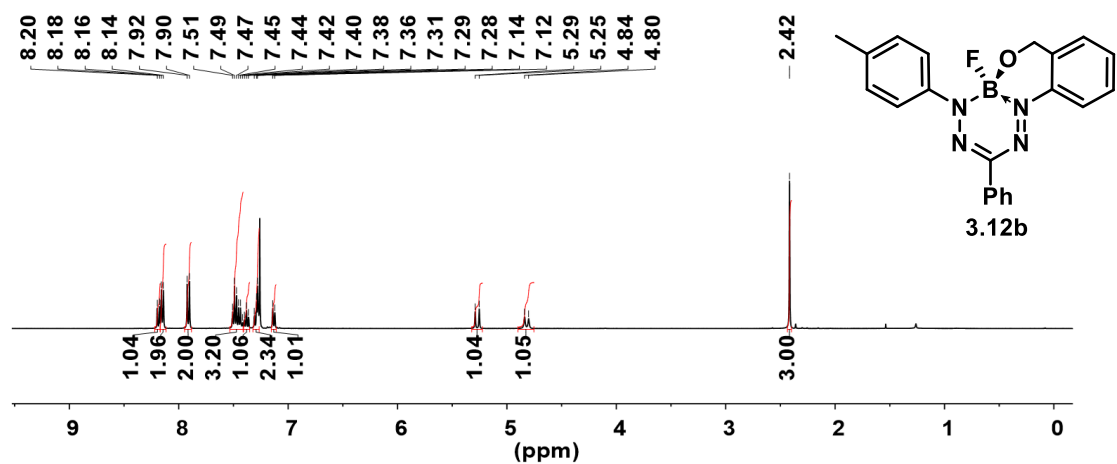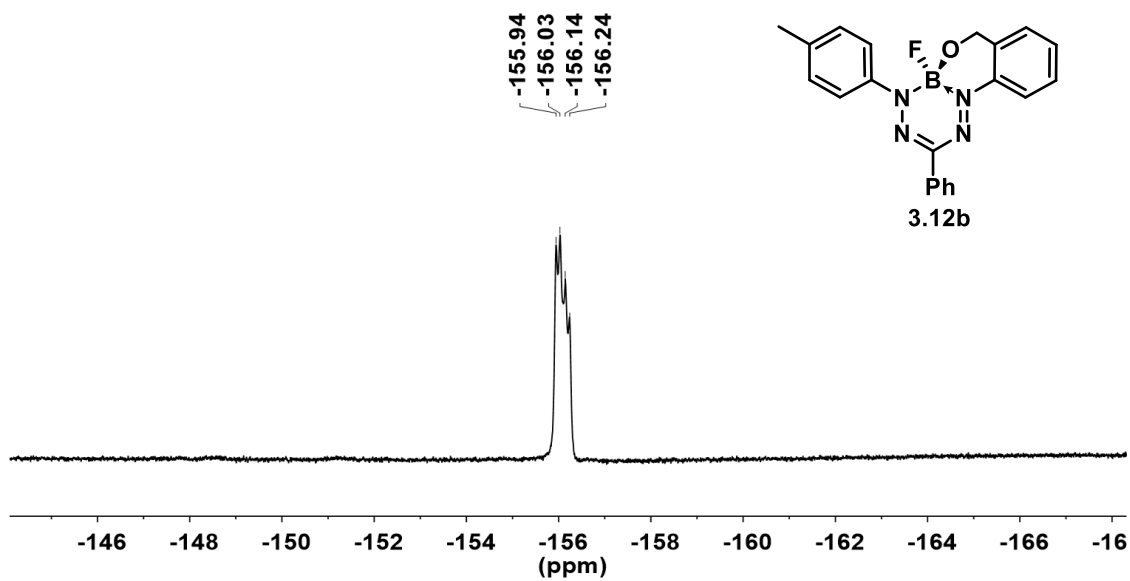
Figure A3.11. $^{19}F\{^1H\}$ NMR spectrum of **3.12b** recorded in CDCl$_3$.
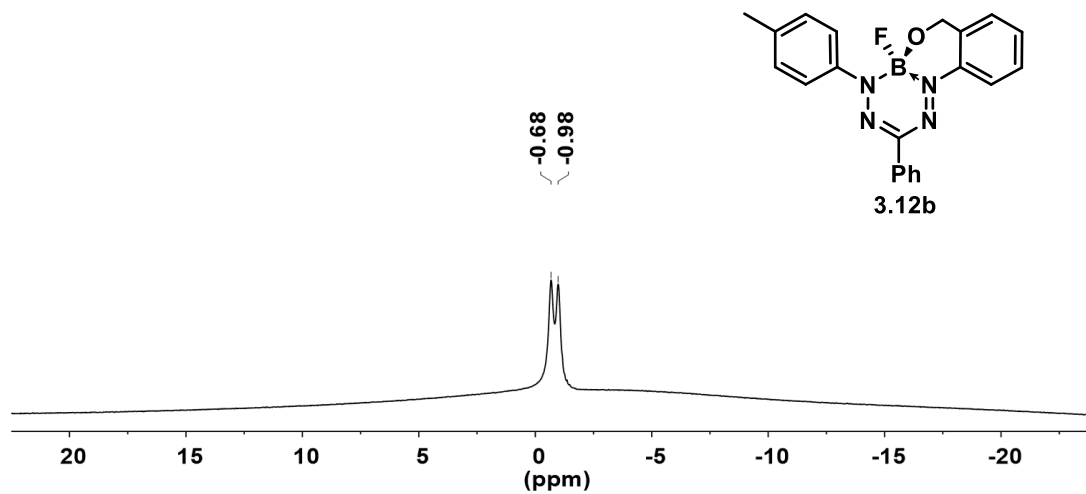
Figure A3.12. $^{11}B\{^1H\}$ NMR spectrum of **3.12b** recorded in CDCl$_3$.

Figure A3.13. ^{1}H NMR spectrum of **3.13a$^+$** recorded in CD$_2$Cl$_2$.

Figure S14. ^{13}C{^{1}H} NMR spectrum of **3.13a$^+$** recorded in CD$_2$Cl$_2$.
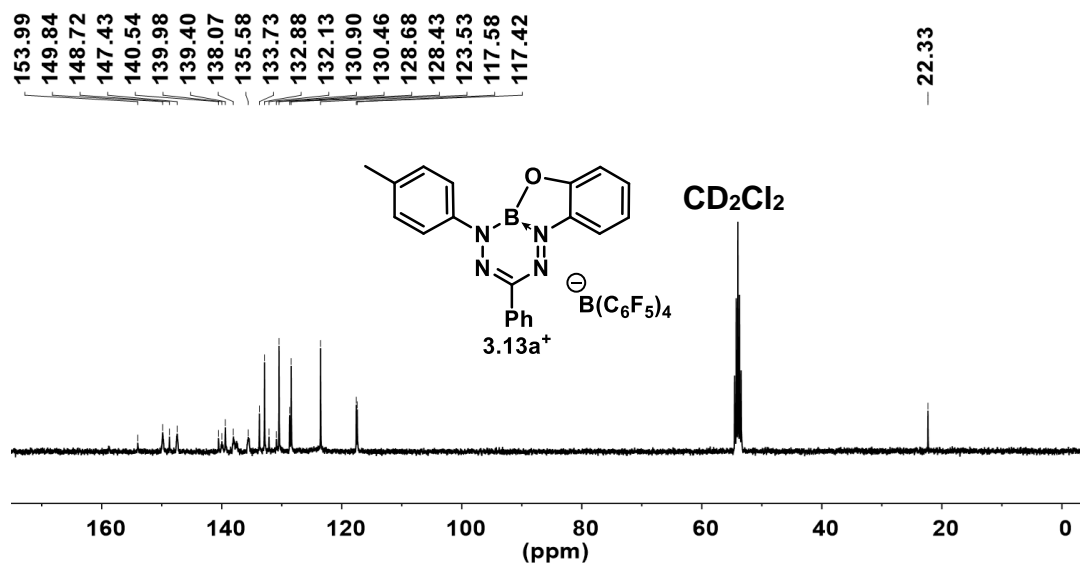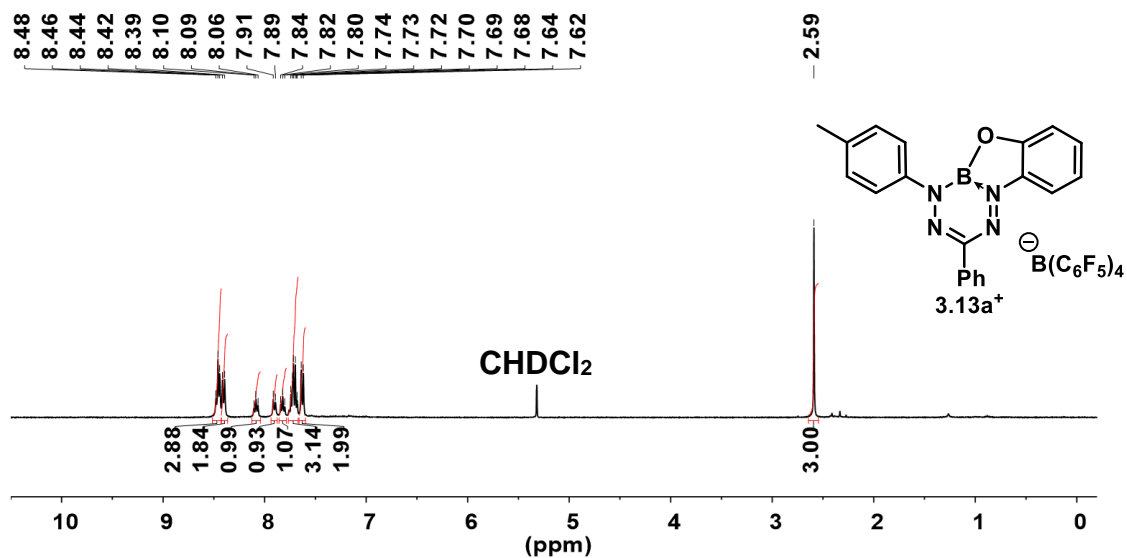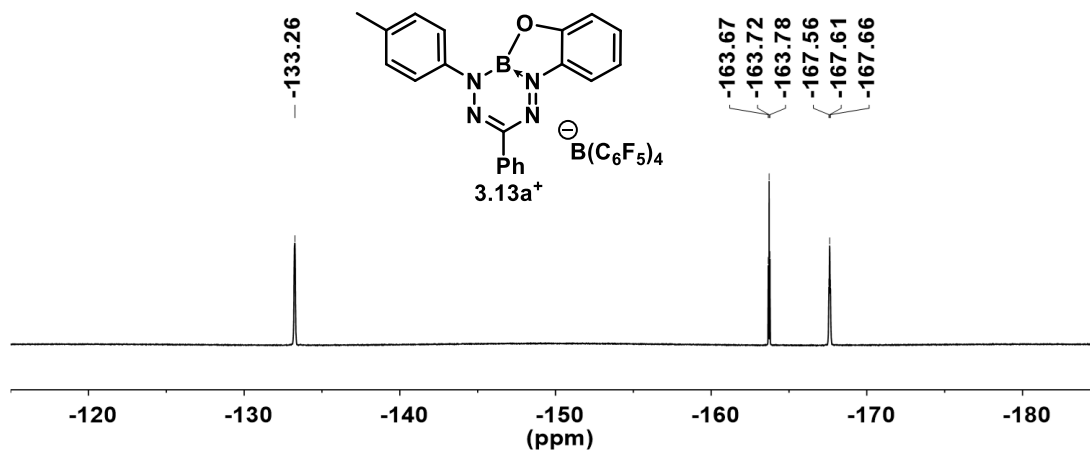
Figure A3.15. $^{19}F\{^1H\}$ NMR spectrum of **3.13a$^+$** recorded in CD$_2$Cl$_2$.

Figure A3.16. $^{11}B\{^1H\}$ NMR spectrum of **3.13a$^+$** recorded in CD$_2$Cl$_2$. The asterisk denotes background signal from the spectrometer probe.

8.49
8.47
8.30
8.28
8.11
8.09
7.78
7.76
7.74
7.70
7.68
7.66
7.66
7.64
7.63
7.62
7.52
7.50
7.37
7.35
5.86

2.54

CHDCl₂

0.99
2.01
2.03
1.06
4.23
2.10
1.06

2.18

3.00

3.13b⁺

B(C₆F₅)₄

9 8 7 6 5 4 3 2 1 0
(ppm)

Figure A3.17. ¹H NMR spectrum of **3.13b⁺** recorded in CD₂Cl₂.

156.28
149.94
147.56
141.21
139.99
138.11
137.21
136.22
135.59
133.23
132.00
131.85
130.87
130.29
130.13
127.60
127.17
124.16
119.16

67.63

22.15

CD₂Cl₂

3.13b⁺

B(C₆F₅)₄

160 140 120 100 80 60 40 20 0
(ppm)

Figure A3.18. ¹³C{¹H} NMR spectrum of **3.13b⁺** recorded in CD₂Cl₂.
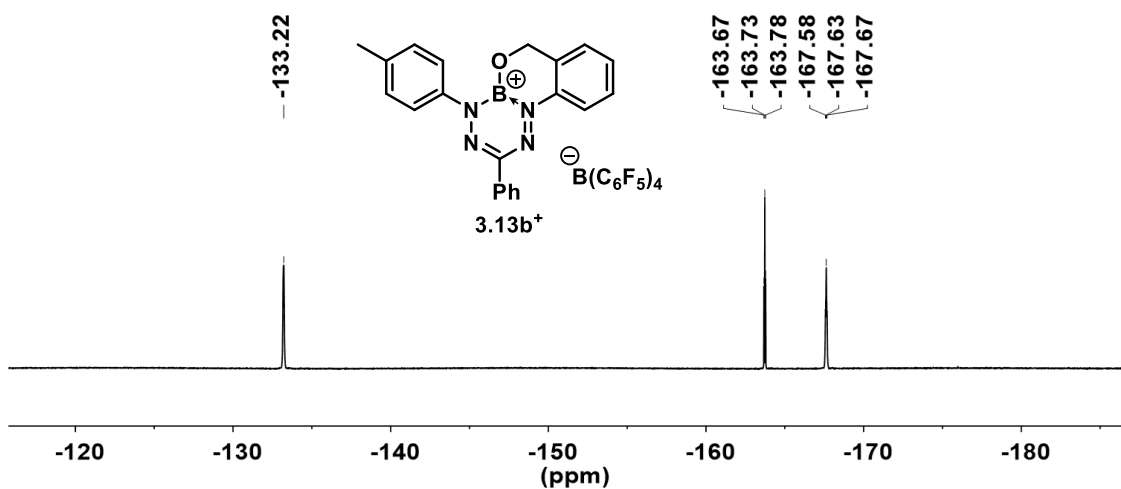
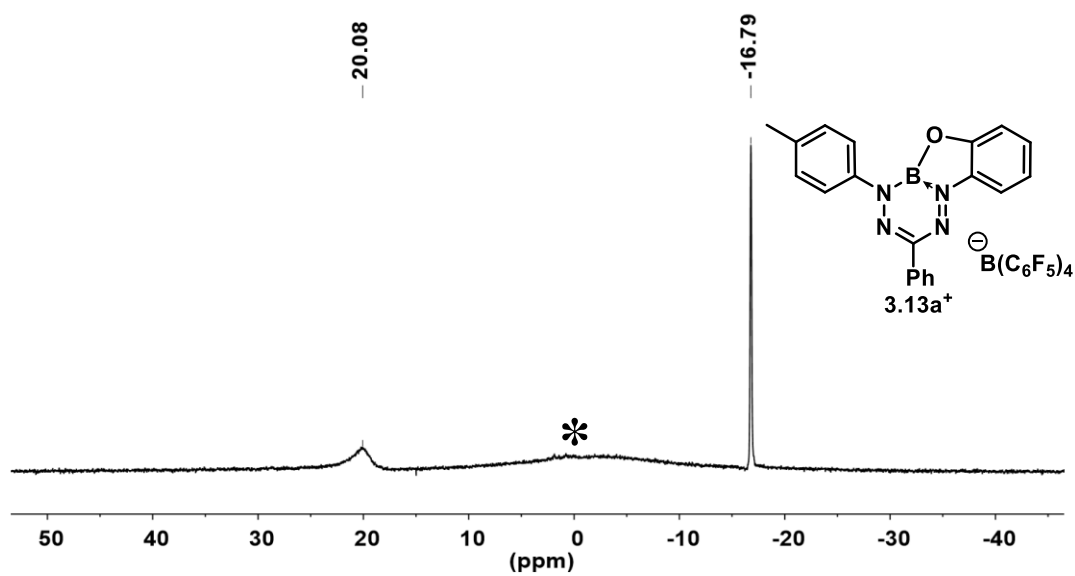**Figure A3.19.** $^{19}F\{^1H\}$ NMR spectrum of **3.13b⁺** recorded in CD_2Cl_2.
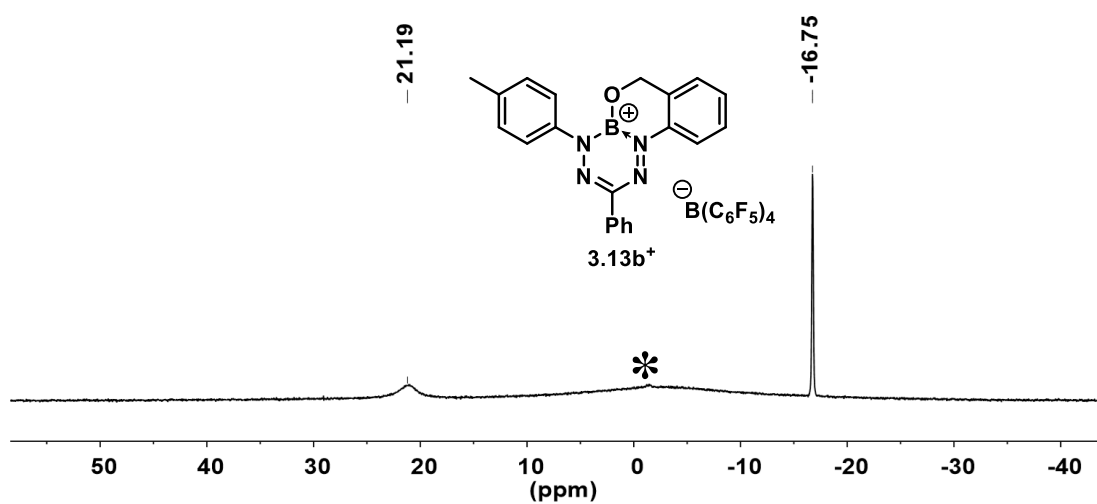
Figure A3.20. $^{11}B\{^1H\}$ NMR spectrum of **3.13b⁺** recorded in CD_2Cl_2. The asterisk denotes background signal from the spectrometer probe.

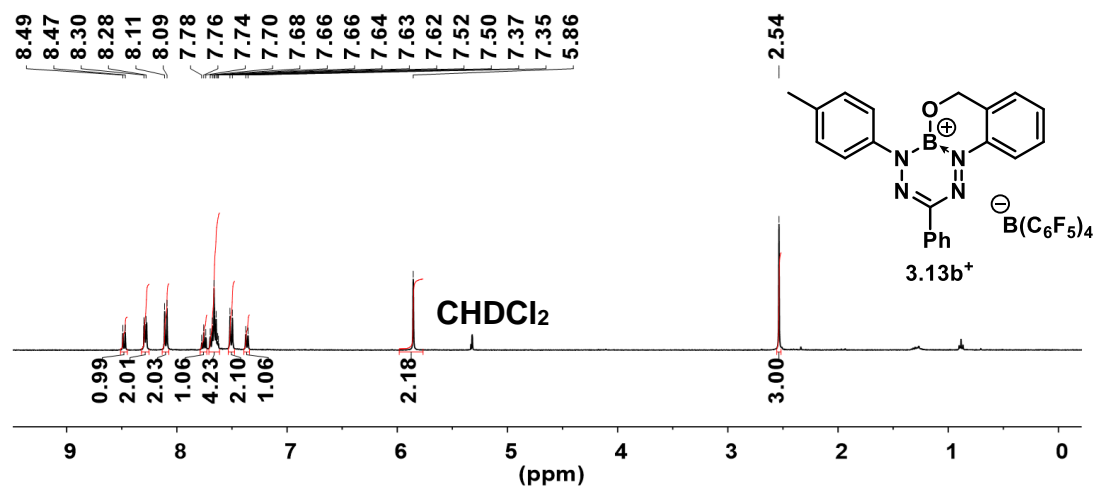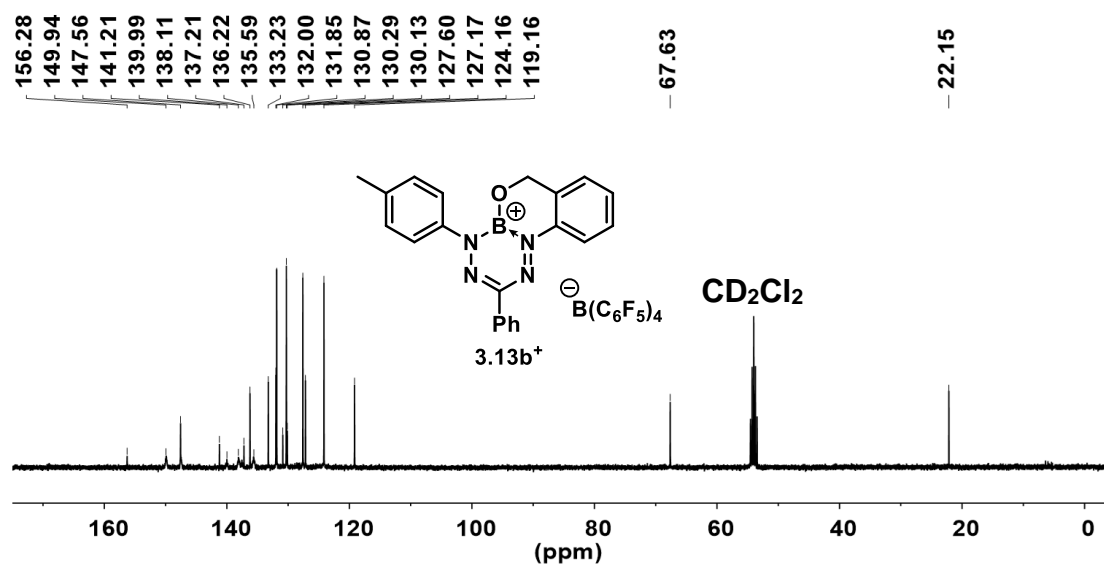**OPTIMIZED GEOMETRIES OF COMPOUNDS 3.12a, 3.12b and 3.13b[+]**

Method: TPSSh/def2-TZVP SCRF(PCM,Solvent=Dichloromethane)

3.12a, ground state (S_0)

0,1

```
C     4.209117    -0.285143    -0.129982
C     3.026963    -1.026397    -0.010387
C     3.102452    -2.424766     0.011397
C     4.331044    -3.064096    -0.101061
C     5.502623    -2.321106    -0.231070
C     5.435332    -0.929807    -0.242631
C     1.727850    -0.339956     0.111425
N     1.704334     1.003755    -0.041504
N     0.577065     1.548691     0.283159
C     0.117764     2.782019    -0.155472
C    -1.251288     2.830943     0.173777
C    -2.013952     3.936821    -0.174732
C    -1.371781     4.980287    -0.839162
C    -0.009179     4.925639    -1.165346
C     0.756759     3.815371    -0.833796
O    -1.701718     1.718839     0.798168
B    -0.554789     0.851773     1.077177
N    -0.540636    -0.555464     0.439804
C    -1.680244    -1.331229     0.121227
C    -2.878431    -1.097521     0.802455
C    -3.993871    -1.869258     0.512848
C    -3.950218    -2.882038    -0.451255
C    -2.742767    -3.093104    -1.127274
C    -1.617423    -2.330973    -0.853381
C    -5.158489    -3.730790    -0.739260
F    -0.282203     0.756468     2.438640
N     0.622425    -1.093852     0.157421
H    -2.935239    -0.325693     1.559081
H    -4.917279    -1.682420     1.050353
H    -2.686935    -3.860818    -1.891799
H    -0.693053    -2.493446    -1.391839
H    -3.068414     3.980640     0.066606
H    -1.944575     5.858698    -1.112815
H     0.449890     5.758576    -1.683300
H     1.808275     3.749772    -1.082422
H     2.193859    -3.003983     0.116799
H     4.373893    -4.147246    -0.083619
H     6.460207    -2.822055    -0.315187
H     6.341818    -0.342529    -0.335853
H     4.160740     0.796542    -0.134460
H    -5.175068    -4.610422    -0.086747
```

```
H      -5.153892     -4.088282     -1.770670
H      -6.082593     -3.176404     -0.565193
```

3.12b, ground state (S$_0$)

0,1

```
C       3.803619     -1.658092     -0.093734
C       2.452033     -2.016092     -0.014746
C       2.107575     -3.373326     -0.040710
C       3.092511     -4.346431     -0.161226
C       4.434414     -3.983102     -0.251639
C       4.784463     -2.635079     -0.214973
C       1.412665     -0.979472      0.119475
N       1.773893      0.304594     -0.017974
N       0.879526      1.197565      0.292342
C       1.084058      2.522393     -0.147197
C      -0.049052      3.347286     -0.190670
C       0.103322      4.664798     -0.610392
C       1.353075      5.151683     -0.983804
C       2.468952      4.315656     -0.939536
C       2.342036      2.998015     -0.523422
C      -1.385819      2.752842      0.162627
O      -1.281060      1.870854      1.274230
B      -0.337275      0.824350      1.192270
N      -0.790975     -0.511949      0.459450
C      -2.117509     -0.872762      0.115316
C      -3.187121     -0.399620      0.880335
C      -4.481750     -0.784456      0.557612
C      -4.745378     -1.632018     -0.522053
C      -3.658386     -2.094810     -1.275169
C      -2.359626     -1.723610     -0.968883
C      -6.153848     -2.018781     -0.882571
F       0.111805      0.445697      2.460805
N       0.127354     -1.375475      0.138329
H      -3.003105      0.249965      1.724247
H      -5.304503     -0.423463      1.165381
H      -3.835348     -2.751488     -2.120512
H      -1.527335     -2.078763     -1.562584
H      -0.765792      5.312873     -0.647095
H       1.458716      6.181867     -1.302653
H       3.443696      4.695210     -1.222393
H       3.198224      2.338494     -0.477231
H       1.065679     -3.658424      0.033104
H       2.810604     -5.393087     -0.181442
H       5.201185     -4.743959     -0.341850
H       5.826567     -2.342438     -0.276027
```

```
H      4.079200    -0.611524    -0.058068
H     -6.835765    -1.851276    -0.047449
H     -6.212003    -3.069495    -1.175659
H     -6.512490    -1.425044    -1.729986
H     -2.093058     3.538154     0.432754
H     -1.795854     2.219249    -0.707833
```

3.13b⁺, ground state (S₀)

```
1,1
B     -0.010889    -1.204164     0.053718
O     -0.313138    -2.500520     0.161820
N     -1.008049    -0.138689    -0.027554
N     -0.647115     1.126825    -0.038213
N      1.664494     0.559871    -0.017544
N      1.355702    -0.712850     0.020574
C      0.653388     1.438297    -0.019085
C     -2.417630    -0.362362    -0.017741
C     -2.951805    -1.515067    -0.596635
H     -2.309874    -2.250666    -1.058983
C     -4.328055    -1.692002    -0.601514
H     -4.741285    -2.580036    -1.065743
C     -5.187695    -0.751190    -0.027770
C     -4.622720     0.394725     0.552942
H     -5.267851     1.132789     1.016220
C     -3.255993     0.598950     0.557737
H     -2.827618     1.480259     1.015208
C      2.421565    -1.652747    -0.005426
C      2.102586    -3.009261     0.145639
C      3.141995    -3.935152     0.100619
H      2.916092    -4.989440     0.213759
C      4.455744    -3.523451    -0.083756
H      5.249350    -4.259655    -0.116540
C      4.753043    -2.167264    -0.233300
H      5.776071    -1.846568    -0.383946
C      3.739116    -1.227216    -0.197692
H      3.945702    -0.174058    -0.322392
C      1.001933     2.873403    -0.024611
C      0.019886     3.837827    -0.279425
H     -0.997347     3.527380    -0.479539
C      0.352436     5.186760    -0.283440
H     -0.413375     5.926072    -0.486249
C      1.662529     5.587951    -0.032632
H      1.918807     6.640901    -0.036107
C      2.642109     4.631196     0.222690
H      3.662340     4.937062     0.422022
C      2.317340     3.280355     0.226675
```

```
H      3.079204     2.539249     0.430312
C     -6.675703    -0.954360    -0.025784
H     -6.946694    -1.908924    -0.476993
H     -7.174048    -0.155039    -0.582154
H     -7.068897    -0.928033     0.994232
C      0.700734    -3.497295     0.393637
H      0.466848    -4.335830    -0.262804
H      0.588090    -3.829171     1.428935
```

Curriculum Vitae

Name: Benjamin Katzman

Post-secondary Education and Degrees:

University of Western Ontario
London, Ontario, Canada
2015-2019 B.Sc. (Hons)

University of Western Ontario
London, Ontario, Canada
2019-2021 M.Sc.

Honours and Awards:

Lipson-Baines Award in Chemistry, 2021

Natural Sciences and Engineering Research Council (NSERC) Canadian Graduate Scholarship-Masters (CGS-M), 2020–2021

Ontario Graduate Scholarship (OGS), 2020–2021

Andrew E. Scott Gold Medal & Prize, 2019

Third place Oral Presentation Inorganic Chemistry: Southern Ontario Undergraduate Student Chemistry Conference (SOUSCC), 2019

Chemistry Alumni Scholarship, 2018

Chemistry Class of 1950 Scholarship, 2017

Related Work Experience

Teaching Assistant – Chem 3371F and 1302B
University of Western Ontario
2019 – 2020

Publications:

1. Maar, R. R.[‡]; **Katzman, B. D.**[‡]; Boyle, P. D.; Staroverov, V.N.; Gilroy, J.B. Cationic Boron Formazanate Dyes. *Angew. Chem. Int. Ed.* **2021**, *60*, 5152–5156. ([‡] = shared first authorship)

2. Katzman, B.D.; Traum, P.; Medline, P.B. New Histologic Finding of Amyloid Insulin Bodies at an Injection Site in a Patient With Diabetes. *Am. J. Dermatopathol*. **2018**, *40*, 527–530

3. Maar, R. R.; Rabiee Kenaree, A.; Zhang, R.; Tao, Y.; **Katzman, B. D.**; Staroverov, V.N.; Ding, Z.; Gilroy, J. B. Aluminum Complexes of $N_2O_2{}^{3-}$ Formazanate Ligands Supported by Phosphine Oxide Donors. *Inorg. Chem.* **2017**, *56*, 12436–12447.

Presentations:

1. Oral Presentation (International): **Katzman, B.D.**; Maar, R.R.; Boyle, P.B.; Staroverov, V.N.; Gilroy, J.B. *Electronic Structure Modulation in Cationic Boron Formazanate Complexes.* ACS Spring 2021, April 5–16, Online.

2. Poster Presentation (Regional): **Katzman, B.D.**; Gilroy, J.B.; Hudson, R.H. E. *Synthesis and Characterization of Nucleobase Containing Boron Difluoride Formazanate Conjugates.* Physical Organic Minisymposium (POMS), Toronto, ON, Nov 1–3, 2019

3. Oral Presentation (Regional): **Katzman, B.D.**; Gilroy, J.B.; Hudson, R.H. E. *Synthesis and Characterization of Nucleobase Containing Boron Difluoride Formazanate Conjugates.* Southern Ontario Undergraduate Chemistry Conference (SOUSCC), Toronto, ON, Mar 30, 2019.

Course Work:

Crystallography I (9541A) – 93%

Advanced Medicinal Chemistry (9713R) – 95%

Advanced Polymer Chemistry II (9663S) – 89%